Doctoral Dissertation
Doctoral Program in Energetics (32th Cycle)

Gas network modelling for a multi-gas system

Marco Cavana
* * * * * *

Supervisors
Prof. Pierluigi Leone, Supervisor
Prof. Gianfranco Chicco, Co-Supervisor

Doctoral Examination Committee:

Prof. Adrianus Johannes Maria van Wijk,   *Referee,*   *Delft University of Technology*

Prof. Luis Miguel Romeo Giménez,   *Referee,*   *University of Zaragoza*

Politecnico di Torino
April 30th, 2020

I hereby declare that, the contents and organisation of this dissertation constitute my own original work and does not compromise in any way the rights of third parties, including those relating to the security of personal data.

………………………………......

Marco Cavana

Turin, April 30th, 2020

Summary

In the framework of the energy transition towards a decarbonized energy system, the role of natural gas sector is controversial but appears to be crucial for the successful achievement of the future environmental goals, in terms of sustainability, affordability and security.

The renewable gases inclusion within the gas infrastructure appears to be a promising option. Renewable gases are a range of low net-carbon-emissions fuel gases such as biomethane and hydrogen. The most influent institutions in the framework of future energy scenarios studies have lately considered them as a viable option for the decarbonisation of energy intensive sectors and as a way to add flexibility and diversification to the energy system.

However, the impact of their injection within the current gas infrastructure needs to be evaluated by means of suitable simulation tools. This work is devoted to the development of a versatile gas network model and its application on a number of sample cases regarding biomethane and hydrogen grid injection.

A fluid-dynamic transient and multi-component modelling tool of the gas network has been developed for the purpose. It may be easily applied either to high-pressure transmission networks or local distribution ones thanks to the choice of a wide-range equation of state for natural gas mixtures (GERG-2008). Not only is the model sensitive to the gas chemical composition, but it also can perform quality tracking.

A number of case studies addressing the injection of biomethane and hydrogen within the current infrastructure have been performed focusing in particular on the local distribution gas networks. The aim was both to show the capabilities of the model and to address some common issues of distributed injection practices.

As for the biomethane injection case, a local medium-pressure distribution infrastructure has been considered for the evaluation of the impacts and the criticalities of the practice. The strong mismatch between biomethane production and times of low gas consumption may induce to the curtailment of the injections. Innovative strategies of network management such as modulating pressure and

linepack storage have been simulated to enhance the biomethane receiving potential, taking advantage of the transient feature of the newly developed model.

As for hydrogen, the impacts on the gas quality perturbation and its distribution throughout the network has been evaluated thanks to the multi-gas and quality tracking features of the model. Furthermore, multiple injections of hydrogen have been tested. Critical operating conditions have been obtained and time-dependent hydrogen acceptability maps have been produced on the basis of gas network operational constraints, so to provide hydrogen acceptability profiles to be matched with possible future productions.

At last, a sample case study of power and gas sector coupling by means of power-to-hydrogen and grid injection pathway has also been addressed. The aim was to evaluate whether and how much the gas network is available to receive power from the electricity infrastructure surplus on-demand, in order to relax its critical operations. The results shows that the seasonal variations of natural gas consumptions and seasonal production form renewable such as solar may anyway limit the potentialities of the sector coupling. However, hydrogen acceptability limits have also an important role in determining the viability of similar integration strategies.

As a general result, the work aims at underline both potentialities and criticalities that the gas sector (with special focus on the local, distribution level) will have to address in the near future by offering suitable tools and innovative methodologies to analyse future scenarios based on a multi-gas system.

Acknowledgements

This final dissertation marks the end of almost four years of advanced education and research at the Department of Energy of Politecnico di Torino.

Time has come to wrap up almost four years of advanced education and research. Or maybe more.

My mind is coming back to that moment at the new Bologna high-speed train station when I hopped on my train towards… here. No clear plans were on my mind but something brought me in Turin back then, in September 2013. The same thing that attracted me to Alma Mater Studiorum in Bologna.

That mysterious force was, and still is, Energy. What moves everything and everyone.

We, as human beings, have learnt how to handle this power by creating an infrastructure that resembles more and more a living being. And we can really tell it right now, in this very peculiar historical moment, when all the interconnections have been undermined.

Energy would be lost without a suitable infrastructure able to drive its flow.

This is the deep rationale that gave me the passion, the enthusiasm and the perseverance to address a PhD in Energetics, focusing on gas networks.

Networks are indeed the infrastructures that hold the world together these days. Being them material or immaterial. In fact, no one is isolated thus any achievement comes along with a number of interconnections which form one's own personal network and to which owe a thanks.

I would like first to thank Pierluigi to accept me as its first PhD, for having inspired me in pursuing the studies and the research towards the network infrastructures and the gas network ones in particular, when few had started to look into them as a possible carrier of renewables. And I must also thank him for both his presence and his absence, which I realized where both a proof of trust you gave to me and which I had to preserve (back then and for the future). I can barely believe that nowadays everyone is talking about renewable gases and I am really thankful and proud of the results we reached in this work.

Secondly, I would like to thank my co-supervisor prof. Gianfranco Chicco for his knowledge on the electrical side of the energy infrastructure and his kind attitude towards my needs, especially when they were the last minute ones. I really hope these collaborations between the two sides of the department will go on and tight up in the very near future.

Most of the immaterial network, which have been created along this PhD, would not be possible without the kind attentions of Ing. Luciano Baratto form ANIGAS, who introduced the entire research group and me to the most important players in the Italian framework of gas distribution and transmission networks. His interest on my research has been fundamental for me to grow in this field and motivated me to persist in the efforts.

However, the whole passion about the research environment and the gas networks would not have grown if it were not for the beautiful experience I lived at Risø DTU National Laboratory for Sustainable Energy. There I moved my first steps in the world of research supervised by Prof. Allan Schrøder Pedersen in the perfect environment where to grow inspirations about PhD, surrounded by nature, renewable energy and young passionate researchers. Our interconnection have never been down, so I would like to thank Ilaria, Alessia and Anna which where there when I submitted my application to the PhD in Turin. Sara and Cati, to have shared our visiting student status and the final times as undergraduate students. Filippo to have co-habited our wonderful house (Risø 33) and to have become great friends. Kosova who has never refused to give me shelter. Simon, Alexandra, Peyman, Đorđije and Kristina his wife, Kristina, Steven, Katrine, Fabrizio and Claudia, Venkat and Morgan. You "sons of Risø" have all been so inspirational to me.

But once having become a PhD student, the Energy Department have been my new working environment and new reference persons quickly emerged from… my office. Thanks to Marta and Domenico to have accepted me in our tiny, (very) warm and not-so-cosy office. Thank you to have shared a lot of laughs, to continue to advise me, to support me during my concerns, to have always been a step ahead of me so that I could learn from you and most of all to recognize and expand the enthusiasm in me.

Almost 11 years have gone since I stepped in the world of university and about 13 years more of school, which I must say, I enjoyed a lot. Almost a quarter of a century I have spent learning so let me spend a few words more to say some thanks to the ones which were there since the beginning, to those I met along the journey, to the ones that got away and the ones are by my side now.

This long and enjoyable journey would not be possible with the incessant and enthusiastic support of my parents: my dad Giuseppe and my mum Giuseppina. To dad I owe the relentless curiosity, to mum the empathy in addressing things. I feel as I was born and have been grown as a lucky combination of the two of you. Could some good school marks and prizes pay back all the effort and all the energy you put on me?

Not only parents but also all my family network have been my solid infrastructure where to take the fuels for my outcomes. Firstly, the very ancient roots, the grandparents. Thanks to the nonno Bruno's meekness and the deep heart of nonna Agar who have always waited for me and offered me the warmest shelter. The simplest things, the ones that take you grounded are the most precious ones. You are not here anymore but still always present in me. Thanks to the ones who are still here instead, nonno Mario and nonna Rosanna. In particular, thanks to his never-ending persistency and passion for his job: only a tireless worker can reach for his aims. And thanks to her patience and her acceptance and capability to stay a step back while keeping everything together, my growth too. Passion, hard work, resolution and attitude always pay you back, no matter if you are standing the front or the last rows.

To complete the family portrait I cannot leave behind my two crazy aunts Patrizia and Elisabetta: your endless energy and smiles always reminds me to look for the good and keep myself up. Thanks to Armando and Marco too, my patient uncles. And to Mauro… every family needs a "bad guy" to understand that "good and bad" are just useless judgments form other people's opinion. Thanks to Alessandro my elder cousin and his wife Sara to have always been a source of example and inspiration. Thanks to my little cousin Silvia: I saw you growing up while I had my head on books… It has been hard for me too to keep you away from me thus I will always be grateful to your earlier understanding. Last but not least, thanks to Andrea, the smallest one of the family: you took this role when I was ready (more than ready) to leave it. And even if our time together is scarce, you are always happy when I am around.

"Friends are the family you choose" someone said. Well either I am unconsciously good to choose them or I have been lucky enough to meet the right persons without having to choose. I owe to all my friends all the time they had to wait for me, from an answer to my physical presence. Your patience is a fairly

good measurement of the friendship that binds us. What is more, you have always kept me grounded without dismissing me.

So thank you to Sara's empathy and awareness, Alexandre's courage, Mattia's presence, Pasquale's mindfulness, Chiara's pragmatism, Matteo's readiness, Anna's tenacity, Giorgia's friendliness, Alice's meekness, Alessia's kindness, Andrea's calmness, Daniele's intellectualism, Mario's yearning, Fabio's hardworking attitude, Tommy's craziness and Maria's presence and absence.

Thanks to Marty, my other PhD student friend: we shared joys and sorrows of this employment. Thanks to Mony and to her tough, determined and shiny temperament. Thanks to all the friends from Penzale: Kekko and Ilaria, Fede, Bea, Rossi, Chiara and Michele. You have always been there when I came back home, ready to organize some party.

Thanks to Ashkan, my "outsider" friend and Alona his girlfriend. You brought that international spirit to my small-town world which helped me open my mind up. Thanks to Cate, the one that firstly introduced me to the university world. Thank you for your strict affection with whom you are still trying to educate me.

The first times at Energy Engineering lectures at the Alma Mater in Bologna made me feel a little bit misplaced. No matter what, it took very few weeks to tight up with some of my dearest university mates: Chiara and Alessandra. You have always been helpful to me and I feel our time together was too short.

That feeling acted as a fundamental driver to take one last deep dive within the university world choosing to move to the Politecnico. It took two days for me to meet some of the most important persons of my later years: Felice and Stefania which, together with Chiara, Francesco C. , Paolo, Francesco S, Ale and Davide, formed my family in Turin. Thanks to Francesco C. my very first lecture-mate, with whom we shared the earliest struggles of our Politecnico times. Thanks to Chiara, whose sensitivity, kindness and big heart brought some human feelings along the curses and the exams. Thanks to Stefania, a sort of sister I have never had. We took the most from our time together at university to go on with the best of ourselves later on until now. We both know we can always count on each other. Thanks to Felice, a sort of brother I have never had. We are different but so close to each other. I am grateful to have you around when I most needed a friend. Harsh time kept us together and what I took from you, I give you back and vice versa. Now we know we are always ready to support one another.

If it was not for Felice, I would not even imagine the existence of the person I found to be my soul mate. This is Giulia and to her I must acknowledge the recovery of my deep and true self-confidence while keep growing in my self-understanding and self-awareness. You made me find my direction again, with unconditional love, support and commitment. I love you.

Contents

Symbols

Variables

		Unit of measurement
A	Pipeline cross-sectional area	$[\,m^2\,]$
$(\,b_h, b_{h+1}\,)$	Gas batch limits positions	$[\,m\,]$
c	Speed of sound	$[\,m/s\,]$
c	Lineic capacitance	$[F/m]$
c_v	Specific isochoric heat capacity	$\left[\dfrac{J}{kg\ K}\right]$
C	Courant–Friedrichs–Lewy number	$[-]$
$\mathcal{C}$	Line capacitance	$[F]$
D	Pipeline diameter	$[\,m\,]$
dx	Infinitesimal length	$[\,m\,]$
E_{th}	Calorific equivalent of the outgoing gas flow rate (thermal loads)	$[\,W\,]$
g	Gravitational acceleration	$[\,m/s^2\,]$
$G_{0,AM1.5}$	Standard global irradiance for air mass AM=1.5	$[\,kWh/m^2\,]$
G	Global irradiance on the panel plane	$[\,kWh/m^2\,]$
h	Elevation	$[\,m\,]$
HHV	Higher Heating Value	$[\,MJ/kg\,]$ or $[\,MJ/Sm^3\,]$

$\underline{I}$	Line current phasor	[A]
$\underline{I}_{ext}$	Nodal current phasor	[A]
l	Edge section length	[m]
l_e	Corrected pipe section length	[m]
ℓ	Lineic inductance	[H/m]
L	Pipeline length	[m]
$\mathcal{L}$	Line inductance	[H]
LP	Linepack	[kg]
$\dot{m}$	Mass flow rate	[kg/s]
$\dot{m}_{ext}$	mass flow rate (exchanged with outer environment at one node)	[kg/s]
p	Pressure	[Pa] or [bar_g] or [atm]
P	Quadratic pressure	[Pa^2]
$\mathcal{P}$	Electrical active power	[W]
PR	Performance ratio	[%] or [−]
$\dot{Q}$	Heat flux	[W]
Q	Electrical reactive power	[VAr]
r	Lineic resistance	[Ω/m]
R	Specific gas constant	$\left[\dfrac{J}{kg\ K}\right]$
R_I	Inertial hydraulic resistance	$\left[\dfrac{kg}{m^2\ s^3}\right]$
R_F	Fluid-dynamic hydraulic resistance	$\left[\dfrac{1}{m^2\ s^2}\right]$
$\mathcal{R}$	Line resistance	[Ω]
Re	Reynolds number	[−]
$\underline{S}$	Complex power	[VA]
t	Time	[s]
T	Temperature	[K] or [$°C$]
v	Velocity	[m/s]

V	Geometrical volume	$[\,m^3\,]$
$\underline{V}$	Nodal voltage phasor	$[\,V\,]$
$w_{(c)}$	Mass fraction of cth chemical species	$[\,w/w\,]$ or $[\,\%_{w/w}\,]$
$[w]$	Gas chemical composition – mass fraction	$[\,w/w\,]$ or $[\,\%_{w/w}\,]$
$y_{(c)}$	Molar composition of cth chemical species	$[\,mol/mol\,]$ or $[\,\%_{mol/mol}\,]$
$[y]$	Gas chemical composition – molar	$[\,mol/mol\,]$ or $[\,\%_{mol/mol}\,]$
Z	Compressibility factor	$[-]$
α	Reduced Helmholtz free energy	$[-]$
δ	Reduced density	$[-]$
ΔP	Corrected quadratic pressure	$[\,Pa^2\,]$
Δt	Time step	$[\,s\,]$
Δx	Space discretization	$[\,m\,]$
ε	Roughness	$[\,m\,]$
ϵ	Relative error	$[\,\%\,]$
η_{HHV}	Hydrogen conversion efficiency of the electrolyzer (higher heating value based)	$[\,\%\,]$ or $[-]$
ϑ	Pipeline inclination	$[\,°\,]$
λ	Friction factor	$[-]$
μ	Dynamic viscosity	$\left[\dfrac{kg}{m\,s}\right]$
ρ	Density	$[\,kg/m^3\,]$
τ	Inverse of the reduced temperature	$[-]$
ϕ	Accumulation term coefficient in continuity equation	$[\,m\,]$

Indices, vectors and matrices

		dimensionality
b	Number of branches	
h	Generic gas batch	
i	Generic node index	
i^*	Generic junction node index	
j	Generic branch section index	
J	Generic pipeline between junctions index	
n	Number of nodes	
t	Generic time step	
$\mathcal{E}$	Set of edges/branches	
$\mathcal{G}$	Oriented graph	
$\mathcal{V}$	Set of vertices/nodes	
$\mathbf{A}$	Incidence matrix	($n \times b$)
$\mathbf{A_g}$	Modified incidence matrix (gravitational term)	($n \times b$)
$\mathbf{E_{th}}$	Vector of calorific equivalent of outgoing gas flow rate (thermal loads)	($n \times 1$)
$\mathbf{I}$	Identity matrix	($n \times n$)
$\underline{\mathbf{I}}$	Vector of line current (phasor)	($n \times 1$)
$\underline{\mathbf{I}}_{ext}$	Vector of nodal currents (phasor)	($n \times 1$)
$\dot{\mathbf{m}}$	Vector of branch mass flow rates	($b \times 1$)
$\dot{\mathbf{m}}_{ext}$	Vector of nodal mass flow rates exchanged with outer environment	($n \times 1$)
$\mathbf{p}$	Vector of nodal pressures	($n \times 1$)
$\boldsymbol{\mathcal{P}}_{loss}$	Vector of Joule power losses	($b \times 1$)
$\mathbf{R}$	Linearized hydraulic resistance diagonal matrix	($b \times b$)
$\boldsymbol{\mathcal{R}}$	Diagonal matrix of electrical resistance	($b \times b$)
$\mathbf{R_F}$	Fluid-dynamic hydraulic resistance diagonal matrix	($b \times b$)

$\mathbf{R_I}$	Inertial hydraulic resistance diagonal matrix	$(b \times b)$
$\underline{S}$	Vector of complex power (phasor)	$(n \times 1)$
$\underline{V}$	Vector of nodal voltage (phasor)	$(b \times 1)$
$\mathbf{\Phi}$	Diagonal matrix of accumulation term coefficients	$(n \times n)$

Abbreviations

	Definition
AGA	American Gas Association
BFS	Backward Forward Sweep method
BWR	Benedict-Webb-Rubin equation of state
BWRS	Benedict-Webb-Rubin-Starling equation of state
CCS	Carbon Capture and Sequestration/Storage
CCU	Carbon Capture and Utilization
CEN	European Committee for Standardization
CNG	Compressed Natural Gas
COP	Conference of the Parties
DHW	Domestic Hot Water
DSO	Distribution System Operator
EBA	European Biogas Association
ENTSO-E	European Network of Transmission System Operators for Electricity
ENTSOG	European Network of Transmission System Operators for Gas
E-RES	Electric Renewable Energy Sources
FRS	Final Reduction Station
GERG	Groupe Europeen de Recherches Gazières
GERG	European Gas Research Group

HHV	Higher Heating Value
HV/MV	High Voltage / Medium Voltage
IEA	International Energy Agency
JRC	Joint Research Center
KCL	Kirchhoff's Current Law
LNG	Liquefied Natural Gas
LPG	Liquefied Petroleum Gas or Liquid Petroleum Gas
M/R	Metering and Reduction station
NG	Natural Gas
NREL	National Renewable Energy Laboratory
PDE	Partial Differential Equation
PEM	Proton Exchange Membrane
PR	Peng Robison equation of state
PV	Photovoltaic
RD	Relative Density
RES	Renewable Energy Sources
RK	Redlich-Kwong equation of state
SNG	Substitute Natural Gas or Synthetic Natural Gas
SRK	Soave-Redlich-Kwong Equation of state
STP	Standard Temperature and Pressure
TRL	Technology Readiness Level
TYNDP	Ten Year Network Developement Plan
V-RES	Variable Renewable Energy Sources
WI	Wobbe Index

List of Tables

List of Figures

Chapter 1

Introduction

1.1   The gas infrastructure in today's energy system

The origins of the gas utilisation as a public service dates back to more or less 200 years ago, when the so-called manufactured gas started to be employed for lightning purposes, both for streets lightning and for household lightning as a valid alternative to candles or oil lamps. The first utility ever created for this purpose was the "Gas Light and Coke Company", settled in London in 1812. From there, during 1820s, many other cities throughout England and Europe started the business, too, laying the foundation to the European gas infrastructure, starting from a local and distribution level. These systems were not interconnected and they were mainly based on gas production facilities (gas works) within the cities, where manufactured gas was produced from the gasification of coal (mainly) or other solid fuels. This gas, also known as "coal gas", "town gas" or "water gas" was thus very different from the gas used in today's systems being a mixture of hydrogen, carbon monoxide, methane, ethylene and other light hydrocarbons as well as carbon dioxide and nitrogen. Today it would commonly be referred to as synthetic gas or syngas. Of course, the gas was soon employed not only for lightning purposes but also for heating and cooking ones, which would have turned out to be the main final uses after the spreading of the electricity infrastructure, which occurred at least 60 years later the first gas utilities.

The discoveries of the natural gas fields during the first half of the 20th century and the growing energy needs after the World War II cause a systematic fuel switching and set the conditions for the development of the continental-wide

infrastructure for the transmission of natural gas, completing the evolution of one of the backbones of today's energy system.

According to the latest statistics of International Energy Agency (IEA) on the total primary energy supply trends for the period 1990-2015 [1], the natural gas supply to the energy system grew by 77 % on absolute terms, with respect to the 1990 level. In relative terms, though, it increased its role within the overall energy system by only 2.7%, partially replacing oil and nuclear which, instead, decreased. At present (2017), around 41% of the total natural gas produced worldwide is employed for the power generation. Within this sector, natural gas as a source accounts for about the 24% of the electricity generation. The remaining 59% of the worldwide natural gas production directly feeds the final consumptions. Among these natural gas final consumptions, the industrial sector accounts for the 37.7%, the residential sector for the 29.2%, the tertiary sector for 12.6% and the transport one accounts for about the 7% (the rest is employed in non-energy use).

Natural gas is then directly employed as an energy supply among all the final consumption sectors, together with electricity and other sources. As for the industrial sector, the natural gas contribution to the final consumption is about 20%, while in the transport sector its share is only 4 %. Regarding the residential sector, in which it is mainly used for space heating, domestic hot water production and cooking, the natural gas contribution to the final energy needs is 21% on a worldwide level. However, this figure is very sensitive to the context in which these residential users are located. For instance, in The Netherlands, this share peaks 71%, in Italy it is set to 53%, while in the US and in Germany, it is equal 43% and the 39% respectively. On the other hand, it may be almost null as in the case of the African continent but also of Sweden and Iceland.

These figures aims at showing how pervasive the presence of the natural gas is in the today's energy system, in which it is employed not only for the power generation but also to produce heat and provide other services such as mobility.

The figures about the presence of natural gas in the residential sector provides with some twofold information. On the one hand, natural gas is an optional commodity to satisfy the final energy needs of the residential sector; on the other hand, it is a commonly preferred option among the countries that have a well-established and widespread infrastructure.

Today's gas network is an interconnected and complex infrastructure at a continental level, able to transport natural gas from the gas production fields to the areas of consumption by travelling even thousands of kilometres. With the development of Liquefied Natural Gas technology and markets in the past few decades, the interconnection between separated networks have made it possible, aiming at the creation of a global infrastructure and market. The high-pressure transport of natural gas is driven by compression stations disseminated all along the infrastructure in order to compensate the pressure losses by re-boosting the gas

pressure. Gas infrastructure has a hierarchical structure organized on different pressure levels: the major continental corridors that are operated at the highest pressure levels feeds lower pressure levels that have a national or regional extension. From these levels, local distribution infrastructures receives the gas which is distributed to even lower pressure gas mains which directly feed the final costumers' systems. The passage from a hierarchical level to the subsequent one foresees a gas reduction step which is performed at the gas reduction (and often metering) stations. At the national or regional level of the networks, these points are often the gas station that feeds an urban area (also addressed as city-gates) or that feeds a major industrial customer. Until this point, the gas network infrastructure does not differ too much from the electrical one. However, the gas sector has some peculiarity that are much harder to find on the power infrastructure, thanks to the intrinsic physical properties of the transported energy carrier. A peculiar component of the gas network are in fact the storage facilities. They mainly consist in underground storages within depleted gas fields, aquifers, salt caverns or any geological underground formation that is fit for the purpose. The availability of such huge volumes, together with the compressibility of the fuel gas, make it possible to counterbalance the mismatch between gas demand and availability of supply, counterbalancing the remarkable seasonal variation of the thermal load as well as allow the system to accept minor mismatches between the forecasting of the demand and the programming of the supply. What is more, the volume of the whole gas system itself may act, to some extent, as a gas storage buffer, as it contains fuel gas under pressure. The amount of gas that is stored within the geometrical volume of the gas infrastructure is defined as "linepack" and it is given by multiplying the geometrical volume of the pipes with the density of the gas at the pressure and temperature condition within the pipes themselves.

These features of the gas network allow the entire system to follow dynamics that are much slower than the ones of the power sector. This aspect has an implication on the modelling strategies of the operations of the different infrastructures: transient phenomena of the power grids are of the order of milliseconds, so in the case of power flow simulations of the network in normal operating conditions, the steady state model perfectly suits. On the other hand, gas networks have much slower dynamics thus transient modelling tools are often required to have a consistent simulations of the infrastructure, especially if quality-tracking features are to be implemented.

The slower dynamics of the gas network play a crucial role in the determination of the fundamental position that the gas sector has within the energy system. On a merely technical point of view, the natural gas infrastructure is able to provide an available, reliable and highly controllable source of energy. This has an implication in the energy transition towards a decarbonised energy system. During the earlier stage of this transition, which have been carried out for the past two decades, the natural gas utilisation seen an extraordinary growth

especially among the most relevant world's economies, mainly committed to the substitution of oil and coal fossil resources. This trend is clearly visible in the European and North American past trends [2], while it has just started in China, where the gas sector has grown by an impressive 18% in 2018 only [3].

However, the higher decarbonisation goals which have been set by the Paris Agreement [4] pushed further the commitments and the efforts needed towards zero-net carbon society at 2050. In this context the whole gas sector has been placed a controversial position, raising doubt on its beneficial role to sustain the long-term transition and posing the dilemma whether it is convenient and fruitful to invest on the reinforcement of the sector or not, in order to avoid the so-called "carbon lock-in" situation [5],[6]. A clear picture of the role of the existing energy infrastructure and its future development have a fundamental role in the definition of the roadmaps for the energy transition.

1.2   The role of the gas network in the energy transition

With European Directive 2018/2001/EC [7] the European Union updates its efforts on energy transition towards a more sustainable energy system for the decade 2020-2030. The agreed binding targets have been set to achieve at least 32% of the EU's gross final consumption supplied by renewables, in line with the European Union's commitments expressed at COP21. The directive is a part of the broader initiative "Clean Energy for all Europeans" that completes the EU-2030 targets fixing the CO_2 reduction goal to 45 % and the efficiency improvement goal to 32.5 % with respect to 1990 levels. The initiative is a step of the decarbonization process laid by the Energy Roadmap 2050 [8].

As it is well known, these ambitious programs will have significant impacts not only on the energy system, but also at economic, institutional and societal levels. A collection of a number of impact assessment studies concerning the energy scenarios implementing the 2030 goals is given in [9]. Most scenarios agrees that the general RES goal of around 30 % corresponds to a share of renewables on the electricity sector equal to 50 %, thus implying significant impacts on the electricity system. The deployment of Variable Renewable Energy Sources (V-RES) such as solar and wind has already changed the traditional electrical system paradigm both in terms of the management of geographical distributed and smaller size V-RES plants and in terms of solving production-consumption mismatches. As the planned energy transition measures develop further, these mentioned issues will be more and more critical, asking for additional flexibility.

Flexibility within the power system may come from different sources such as the presence of a suitable fleet of back-up power plants, the setting up of Demand-Response strategies, enhanced grid interconnections and energy storage solutions

[10]. At the moment, it is difficult to determine which of the options will have the prominent role. Energy systems optimization models and scenarios still strive to disentangle the different options so to determine a ranking among the flexibility solutions. They often strongly depend strongly on the dynamic evolution of the system: for instance in [9] it is reported that grid expansion may be the most cost effective solution in order to enhance the flexibility of the electric system. Nonetheless, in case of a fast increase of E-RES within the energy system (as it is the case following the roadmaps), then the implementation of storage systems may be more effective. This has to deal with the inertia related to the planning and the actual renovation rate of an infrastructural asset.

Not only does the higher amount of V-RES in the power system have to deal with the issues of the storability of the renewable energy when mismatches occurs, it may also affect the stability of the system itself, undermining the energy supply security. These stability issues are related to the higher sensitivity of the power system towards sudden or unexpected events that may cause the cut-off of significant portions of the generation capacity. Under these circumstances, faster and more significant frequency deviations may happen because of a too low overall physical inertia connected to the system, as a consequence of high level of renewables connected. In this context, the term "physical inertia" refers to the inertia which is associated with the rotational kinetic energy of traditional synchronous generators and which provides an actual inertia against the frequency variations as well. When higher fractions of wind and solar power plants replace traditional power plants based on synchronous generators, the inertia of the power system gets lower, because wind and solar are interfaced with the network by means of electronic-based converter systems (with no inertia).

Critical situation related to the lack of inertia within the power transmission system have already been observed. The so called "Black System" event in South Australia is one of the best example [11]. As concluded in this government report [12], in the clean energy target scenarios, a minimum amount of inertia must be granted to the system in order to run it in a secure way.

These issues about the lack of utility level suitable storage systems and concerning the need of suitable back-up and reserve power plants are severe barriers against a strong uptake of a renewable based and electrified future energy system. The picture may get even worst if sectors such as the transport, the heating and the industrial ones are to be electrified. The amount of electricity required and the added consumption pattern would inevitably put the power sector under excessive stressful conditions for which substantial investment would be needed. In the meanwhile, a great effort towards a disinvestment from the gas sector should happen which results to be even less credible, given the actual trends.

Indeed natural gas sector finds itself in a controversial position, being considered as one of the key enablers of the energy transition in the short run, but

with several scenarios that foresee a necessary phasing out to meet longer-term goals of deep decarbonisation. On the other hand, today's gas network plays a unique role for the distributed delivery of heat for domestic and industrial use, as the today's infrastructure is able to deliver twice as much energy as the power one. Its substitution may not be as easy as it seems [13], [14], [15].

The role of the existing energy infrastructures and its future development have a fundamental role in the definition of the roadmaps for the energy transition. This complex co-evolutionary process has hardly been modelled in future energy scenarios models until the most recent years. The multi-sectorial and multi-vector approach is clearly emerging both from the methodologies and form the results of the latest World Energy Outlook (2019) by IEA [16], in which the role of the gas sector and its future evolution is further address in a dedicated section and it is clearly stated throughout the document. Similarly, the need of sector coupling for an integrated planning of energy infrastructure has also been perceived as fundamental by the European Network of Transmission System Operators for Electricity and Gas (ENTSO-E and ENTSOG), which have recently practiced it. For the first time in 2018, the Ten Year Network Developement Plan 2018 (TYNDP-2018) [17] was built on energy scenarios jointly agreed, showing an actual interest in building the so called "hybrid energy infrastructure" through a fully sector coupling. A very similar commitment is emerging at the distribution system level, as it is clearly stated in [18] and [19]. At a transmission level, the effort has been repeated for the TYNDP-2020 [20]. Interestingly, in these long terms scenario studies, the Paris Agreement targets have been set thus determining clear constraints on the decarbonization goals both on gas and on electricity sector, following a top-down approach. It is stated that the power sector must be carbon neutral by 2040 while all the other sector should comply with this goal by 2050. In this context the sector coupling is considered as a key approach to reach the targets, together with the coal-to-natural gas switch for the decarbonization of the power sector and the promotion of higher share of renewable gases for the greening of the gas sector. Astonishingly, it is also stated that by 2050 hydrogen may become as important as today's methane as an energy vector in gaseous form. In fact, natural gas-hydrogen blends (sometimes referred to as H_2-NG) contribute to lower the carbon footprint of the whole gas sector value-chain ("greening of the gas network" [21]). It is framed within the broader context of renewable gas injection (i.e. bio-methane [22], synthetic natural gas [23], hydrogen…), a practice that, by 2050, appears to be more economically convenient than 100% electrification according to recent studies, with annual savings ranging between 8 and 138 billion € per year [24],[25],[26],[27]. On a more technical basis, the white paper by the Sustainable Gas Institute (2017) [28] presents a comprehensive study on the various options for a greener gas network.

1.2.1 Renewable Gases

Indeed, the future of the gas infrastrucure and of its whole value chain seems to consists in a transition towards a multi-gas system able to integrate (or literally to blend) higher fraction of renewable gases.

In [29], renewable gases are defined as "a range of low net carbon emissions gas energy fuels" thus the term refers to any fuel gas which does not come directly from a fossil origin and whose use in the energy system grants a reduction of greenhouse gases emissions. Thus, biogas, biomethane, syngas, hydrogen and synthetic natural gas (SNG) all belong to this category. Among these, biomethane and hydrogen appears to be the most promising.

Biomethane

Biogas, biomethane and syngas may be seen as a family of the renewable gas originated by a solid matrix that undergoes a gasification process. When this process involves bio-chemical reactions such as during anaerobic digestion, biogas is produced. When the gasification consists in a higher temperature thermo-chemical transformation such as the pyrolysis, then syngas is obtained. What makes these gases "green" is their organic origins. In fact, the raw materials that feeds these processes are usually wastes from agricultural or breeding activity, forestry and the organic fraction of municipal solid wastes or wastewaters and sludge. In order to enhance the productivity of these plants it is common to provide higher quality organic matter in input such as crops that have been grew for the purpose thus called energy crops. These aspects may undermine the sustainability of the biogas value chain, even though some overall positive implications on the agro-energy sector are to be recognized. Syngas, which generally comes from the gasification of wood, may also be obtained from the gasification of coal.

Both biogas and syngas are generally lower calorific value gases with biogas being a mixture of methane and carbon dioxide and syngas a mixture of hydrogen and carbon monoxide. Biomethane, instead, is characterized by a step forward: it is the result of the upgrading of the biogas form anaerobic digestion. The upgrading process consists in the separation of methane and carbon dioxide so to obtain a fuel gas that has barely the same quality of the gas within the pipeline.

The whole biogas sector has known its first and biggest expansion during the first two decades of the 21st century when it was produced in order to generate electrical energy. As of 2018, the total installed capacity in Europe reached 11 GW_e and about 18,200 plants which produce about 63,500 GWh_e on annual basis [30]. The deep decarbonisation programmes and the growing interest towards the green gases pushed this sector to the production of biomethane instead, with countries such as Germany and United Kingdom leading in Europe. At present

(2019), 610 biomethane plants are currently in operation in Europe, producing almost 22,800 GWh of energy in chemical form on annual basis.

Along with the development of the production of biomethane, its access to the existing gas infrastructure has been tackled, with a remarkable effort in the upgrading and the adaptation of the regulatory framework and technical standards, which, however, sometimes slowed the development down. On the other hand, the issue of network acceptability of an "unconventional" source of gas intersects with a remarkable number of issue throughout many sectors, from the preservation of technical integrity and operability of the infrastructure to correct energy accounting and billing and to the correct interoperability of an interconnected system. In fact, in view of the EU Directives 2003/55/EC and 2009/28/EC (common market for natural gas and promotion of renewable energy), the European Commission established the following two mandates: M/400 EN [31] on gas quality standardization and M/475 EN [32] on standardization on bio-methane. Both of them were assigned to CEN (European Committee for Standardization). The one concerning biomethane ended with the promulgation of the EN 16723 standard [33] only in 2016, when countries such as Italy directly implemented it within its internal technical norm body [34], settling the premises for the development of the sector. This in fact occurred few years later and it is now growing rapidly [35] thanks to a well-structured incentives scheme [36].

Biomethane injection within the existing natural gas infrastructure is not a very critical point in the context of renewable gas inclusion within the system, provided that a deep cleaning from contaminants (mainly halogens acids and sulphur-based compounds) is performed along with CO_2 removal. However, some issues are already well known and some others may arise as the sector grows. The slightly different calorific value in countries like Germany requires LPG addition according to the national standard [37] or, alternatively, the implementation by the Distribution System Operators of quality tracking systems to manage different gas qualities within smaller and confined areas [38]. The distribution level of the gas network may furtherly be invested in the near future by an increasing amount of connection requests which may soon saturate the acceptability limits of renewable gas inclusion, mainly caused by the limited capacity of these portions of infrastructure and highly seasonal consumption patterns. Part of this work is devoted to the analysis of these scenarios and the testing of some possible countermeasures.

Hydrogen

Hydrogen is not an energy source but is an energy vector, as it cannot be found in nature but it has to be produced somehow. It is then necessary to clarify

some concerns about its sustainability. The same concerns may be applied to the SNG as well since it is also produced starting form hydrogen. In fact, depending on its production pathways, hydrogen may be more or less sustainable. Hydrogen is defined as "grey" when it is produced form steam reforming thus splitting the molecules of methane and releasing CO_2 in the atmosphere. It is named "blue" when the same production process is followed by Carbon Capture and Sequestration (CCS) and/or Utilization (CCU), thus setting to zero the carbon dioxide emissions. At last, the hydrogen is classified as "green" when it is produced by electrolysis powered by electricity (or renewable electricity in the strictest sense). Of course in view of the energy transition, the most interesting option are the blue and the green one, the latter providing the missing link for a complete integration between power and gas sector. On the other hand, blue hydrogen may be an effective initiator of a hydrogen or hydrogen-blends economy, easing the market penetration of electrolyzers and power-to-gas facilities.

In the framework of an integrated system, electrolyzers and power-to-gas solution in general are gaining interest as an unconventional electricity storage option, besides traditional and well established options such as pumped hydro, batteries. In fact, they consist in the production of a fuel gas (hydrogen or more rarely methane) using surplus energy from renewables as energy input, thus fixing the energy excess within chemical bonds, producing a commodity or an energy vector that is alternative and more easily storable than electricity. In particular, hydrogen has been getting renovated attention in the last years as key enabler for the energy transition [39]. As an energy vector, crucial is the opportunity that hydrogen offers to avoid the requirements for instantaneous supply-demand balancing. According to [40], hydrogen can play a major role in decarbonizing the energy system thanks to its versatility of use: in transportation, electricity and heating provision, storage and grid services and as a commodity for industrial applications. Even though most of the hydrogen applications are featured with a low TRL and their uptake is considered to happen no earlier than a few decades because of the absence of an economy of scale, hydrogen is gaining a serious industrial interest among natural gas sector stakeholders (please refer "innovative project platform" on hydrogen on ENTSOG website [41]). The practice of hydrogen production through power-to-gas and subsequent blending within the already existent gas infrastructure is an example of electricity-gas sector coupling [42] and it is considered an innovative and effective decarbonisation option.

However, a number of technical aspect should be adressed because of the considerably different properties hydrogen have with respect to natural gas. An extensive review of the opportunities and the criticalities of hydrogen admixture within the current gas infrastructure is given in [43]. In [44] maximum values of admissible hydrogen concentrations are given for a number of different areas of the overall gas system. No major issues should be met up to concentration of 15

%, even though in presence of CNG fuelling station or gas turbines the limit may need to be 1 % or lower. Concerning users' appliances, the ones commercialised in Europe since the '90s under the Gas Appliances Directive (Gas Appliances Regulation as for 2019 [45]) should be able to withstand hydrogen molar fraction up to 23 % according to the testing procedures they have to undergo (according to [46]). Hydrogen blending has thus a very different and non-negligible impact of the various levels of the gas sector and all the literature and the stakeholders agrees that additional research is to be pursued. This also reflects at regulatory level, with the attempts towards the harmonization of the national natural gas quality requirements at european level (M/400 EN [31]). The M/400 EN focuses specifically on gases belonging to "second family - group H" (according to the classification set in UNI-EN 437 [47]), the type of gas transmitted through all Europe. In [48], a cross country review on gas quality legislation has been produced by the CEN technical committee in charge. It is worth mentioning that the higher heating value (also referred to as gross calorific value), the relative density and the Wobbe index[1] are the most common indicators, together with hydrocarbon condensation point and water dew point. Interestingly, limits on single chemical species are infrequent, apart from the ones on sulphur and its compounds.

However, it is still struggling in its more general harmonization procedure. In fact, the latest achievement of CEN technical committee is the publication of the norm EN 16726:2019 [49] on standardisation of gas quality (group H). Here the case of hydrogen injection is mentioned in an informative annex, reporting the results already presented in [44] and concluding with the impossibility of setting a common limiting value for hydrogen in the European infrastructure and recommending a case by case analysis.

The Wobbe Index is defined as the ratio between the fuel gas heating value (higher or lower) and the square root of its relative density

$$WI = HHV/\sqrt{RD}$$

Where the relative density of a gas is the ratio of the density of the gas to the density of the air both calculated at standard pressure and temperature conditions.

In this work: normal conditions [$T_n = 273.15\ K$, $p_n = 101,325\ Pa$];
Standard conditions [$T_{STD} = 288.15\ K$, $p_{STD} = 101,325\ Pa$];

1.3   Motivation & Research Question

The uncertainties and the barriers discussed in the previous paragraph, together with the increased interest on the decarbonisation of a crucial sector such as the natural gas one justify the interest towards the modelling activities on gas network simulation under transient and multicomponent premises. In fact, while the effort towards the creation of simulators able to follow the dynamics of the natural gas system dates more or less back to the early 80s [50], the assumption of considering a variable gas quality took place only more recently motivated by the growth of wider international interconnection brought by LNG and renewable gas uptake.

Earlier works on these aspects are [51] and [52] which performed assessment of the impact of distributed injection of renewable gas on distribution system infrastructures. These works, as well as [21] make use of steady state equations of the fluid-dynamic and apply them to networks topology. A peculiarity of [21] is the ability to cope with different pressure levels of the network thanks to the implementation of non-pipelines devices such as reduction stations and compressors. In addition, it is sensitive to the different chemical compositions of the natural gas by means of a suitable equation of state. An example of hydrogen blending on a real case regional gas network was performed and its potential assessed on the basis of constrained molar fraction of hydrogen.

In [53] and [54] the fluid-dynamic of a transmission pipeline trunk with an hydrogen injection points is modelled under transient flow assumptions and considering a defined hydrogen molar fraction. In the first case, the assumption of constant delivered mass flow rate between the non-injection and the injection case is considered highlighting the effect of reduced energy delivery to the costumers due to the lower heating value of hydrogen. In the second, the assumption of constant energy delivered is considered. These works interestingly extend the gas quality analysis to the transient network cases; however, they limit their focus on single pipelines belonging to the transmission system.

Advanced modelling works on the same field have been presented more recently in [55] and [56], with very detailed description of the thermo-fluid-dynamic behavior of the gas flowing within a single pipeline, under conditions of variable gas quality.

The modelling of sectorial coupling through the integration of gas and power systems needs instead a co-simulation framework, where also the electricity network is to be modelled. In this context [57], [58], and [59] are all inspiring example of co-simulation of an integrated gas and electricity systems. However, they all focus on the transmission level of the power and the natural gas systems. [57] solves an integrated optimization problem to obtain optimal scheduling of the whole energy system. In [58] and [59] optimal power flow for a national power transmission system is solved considering the possibility to use P2G as an

effective option to store otherwise curtailed renewable energy. Subsequently, the impact of hydrogen injection on the transmission pipeline system has been evaluated, with different admissible hydrogen concentration limits. However, a strong assumption is made on the way the hydrogen spread all over the network upon injection.

The present work aims at provide a gas infrastructure simulation tool oriented to the simulation of network gas infrastructure with interconnected topology. It is based on transient fluid-dynamic equations in order to be suitable for simulating operational evolution of the entire infrastructure. In addition to that, a pipeline based gas quality tracking methodology is embedded into the model end extended to the whole topology in order to perform network based gas quality tracking. These feature will be useful to run simulations over scenario of distributed and possibly multiple renewable gas injection (namely biomethane and hydrogen), with focus to the distribution infrastructure.

The research question that animated the current project is the following:

In the framework of the transition of the transition of the energy infrastructures towards a fully coupled future, in which also the gas network infrastructure will be invested by a wave of renewable molecules, which are the impacts of these unconventional gas on the current infrastructure operations?
Which real potentialities the infrastructure is able to offer to the energy system?
Which are the bottleneck and the barriers that needs to be faced and how to overcome them?

By means of this tools, the main dynamics related to the distributed injection and blending practices such as quality perturbation transport and diffusion within the infrastructure, pressure level and linepack variations, gas velocity deviations can be simulated and analysed in order to check whether the constraint on safe operation conditions of the gas network are observed. What is more, injection potentials, capacity limits and innovative strategies to push forward some operational constraint can be defined.

Chapter 2

Transient Gas Network Model

2.1 Governing Equations

The flow of a fluid along a pipeline is described starting from the conservation laws of mass, momentum and energy together with a closure relation describing the thermodynamic state of the fluid itself.

In the case of a fluid flowing through a pipeline, the problem is commonly approximated as one dimensional, being the longitudinal dimension of the pipes L (length) much greater than their diameter D, thus averaging the flow parameters over the cross-sectional area of each pipe. Referring to a pipeline section with infinitesimal length dx and cross-sectional area A, the conservation laws result in a set of partial differential equation (PDEs) as follows:

Conservation of Mass

$$\frac{\partial \rho}{\partial t} + \frac{\partial (\rho v)}{\partial x} = 0 \tag{2.1}$$

where: ρ is the gas density [kg/m^3] and v is the gas velocity velocity [m/s]

Conservation of Momentum

$$\frac{\partial (\rho v)}{\partial t} + \frac{\partial (\rho v^2)}{\partial x} + \frac{\partial p}{\partial x} + \frac{\lambda \rho v |v|}{2D} + \rho g sin\vartheta = 0 \tag{2.2}$$

where: p is the gas pressure [Pa], λ is the friction factor [-], D the pipeline diameter [m], g the gravitational acceleration [m/s^2] and ϑ the pipe inclination [°].

Conservation of Energy

$$\frac{\partial}{\partial t}\left[\left(c_v T + \frac{1}{2}v^2\right)\rho A\right] + \frac{\partial}{\partial x}\left[\left(c_v T + \frac{p}{\rho} + \frac{1}{2}v^2\right)\rho v A\right] + \rho v A g \sin\vartheta = \dot{Q} \qquad (2.3)$$

where c_v is the specific isochoric heat capacity [J/kg/K], A the pipeline section area [m^2], T the gas temperature [K] and $\dot{Q}$ is the heat flux exchanged towards the external environment [W].

This set of three conservation equations displays four unknowns of the thermo-fluid-dynamic state of the gas: pressure p, temperature T, density ρ and velocity v. Thus, a closure relation needs to be adopted, this being the equation of state for real gases, which relates pressure, temperature and density.

Equation of State for Real Gas

$$\frac{p}{\rho} = Z\,R\,T \qquad (2.4)$$

where R [J/kg/K] is the specific gas constant and $Z = Z(p, T, [y])$ is the compressibility factor, a function of pressure, temperature and gas composition $[y]$, which accounts for the deviation from the ideal gas behaviour of a real gas. The literature about the natural gas sector collects a number of different relations for the determination of the compressibility factor, thus defining several different options for the choice of the proper equation of state, depending on either the temperature-pressure ranges or the type and composition of the gas of interest.

Besides the real gas equation of state, another relation is necessary for the determination of the friction factor λ in the fourth term of equation (2.2). This is the hydraulic resistance term and it is derived from the Darcy-Weisbach relation for the frictional shear stress. In this way, it is possible to relate the pressure loss due to friction phenomena to the velocity or the mass flow within the pipe through a quadratic relation. In general terms, the friction factor is a function of the flow regime (defined by the Reynolds number Re) and the relative roughness (ε/D) of the pipe:

$$\lambda = f(Re, \varepsilon/D) \qquad (2.5)$$

In the following sections, a brief overview on the choice of the friction factor relation and the equation of state for the current model is give.

2.1.1 Friction factor

The friction factor takes into account the interaction between the fluid flow and the pipe wall and it is mainly determined by means of semi-empirical

correlations, which relate the pipeline inner wall roughness ε, the pipeline diameter D and the flow regime of the fluid. The flow regime is determined according to the Reynolds number, a dimensionless ratio of inertial forces to viscous forces within a fluid, defined in this way:

$$Re = \frac{\rho v D}{\mu} \tag{2.6}$$

where ρ is the fluid density, v the velocity, D the inner diameter and μ the dynamic viscosity of the fluid [kg/m/s].

The accurate prediction of the friction factor is very important within the oil and gas industry in order to obtain a correct estimation of the pressure losses and thus the capacity of transport of the pipelines and their related operating costs [60]. This justifies the abundant literature on the correlations for the friction factor [61], which are usually given with different relations according to the flow regime.

For $Re < 2300$, the flow is laminar and the friction factor λ is always determined following explicit and linear relation:

$$\lambda = \frac{64}{Re} \qquad if\ Re < 2000 \tag{2.7}$$

For $Re > 3400$, the flow is in a turbulent regime. In this region, the flow can undergo three different sub-regimes: in the case of very small values of relative roughness ε/D, the pipe can be considered as smooth so the friction factor is independent of ε/D; the flow is defined as completely smooth turbulent and the friction factor is given by the Prandtl's correlation [62]. For higher ε/D it is possible to see a transition from a region of non-fully developed turbulent regime to the one of fully developed turbulent regime. The first occurs at lower Reynolds numbers and the friction factor is still sensitive to the Re (monotonically decreasing while Re increases); in the second region, the friction factor shows an asymptotic behaviour with respect to increasing Re (it depends only to the relative roughness ε/D of the pipe). A friction factor formulation for this completely rough turbulent regime was first given by Nikuradse in [63].
In the turbulent region, the friction factor is determined by means of a number of semi-empirical correlations. The most commonly used is the Colebrook-White correlation [64], even though it dates back to 1939. It was obtained by fitting the data of experimental studies, with particular focus on the transition of the fluid flow from the non-fully to the fully turbulent regime.

$$\frac{1}{\sqrt{\lambda}} = -2\log\left(\frac{2.51}{Re\sqrt{\lambda}} + \frac{\varepsilon}{3.71\,D}\right) \qquad if\ Re > 3400 \qquad (2.8)$$

It can be noted that the expression is composed of two additive terms, each representing the contribution of the two different flow regimes: in fact, as the Reynolds number increases, the first term, related to the smooth turbulent flow, becomes negligible giving to the friction factor the asymptotical behaviour typical of the fully developed turbulent region (Nikuradse formula).

One of the main drawbacks of the Colebrook-White relation is that it is an implicit relation in λ, thus requiring a recursive procedure that may end up being computationally daunting. For this reason, a number of explicit approximation of Eq.(2.8) are given and commonly used in the literature such as the one by Hofer [65] or the ones listed in [61].

Recently, the suitability of the Colebrook-White equation for gas pipeline application has been questioned by some authors such as Langelandsvik et al. [66], who in [67] showed that the friction factor undergoes a more abrupt transition from the smooth to the fully developed regime. In this sense, the European Gas Research Group (GERG) suggested the following modified version of the Eq.(2.8):

$$\frac{1}{\sqrt{\lambda}} = -\frac{2}{n}\log\left(\left(\frac{1.499}{Re\sqrt{\lambda}}\right)^{0.942\,n} + \left(\frac{\varepsilon}{3.71\,D}\right)^{n}\right) \qquad if\ Re > 3400 \qquad (2.9)$$

in which n can be tuned in order to control the transition shape, with $n = 1$ corresponding to the Colebrook-White relation. However, Eq.(2.9) is still an implicit formula, with fewer application and explicit approximation available up to now, to the author's knowledge.

A common limitation of Eq.(2.8) and Eq.(2.9) consists in the fact that they are valid only in the turbulent regime. Even though the correlation for the laminar regime is simple and well known (Eq.(2.7)), according to the friction factor theory based on the Colebrook-White experience, there is a gap in the ability to define a friction factor value for the transitional regime between laminar and turbulent flow, corresponding to Reynolds number within $2000 \div 3400$. Aiming at building a gas network simulation tool that is able to handle conditions for which the mass flow may be very low, it is of interest to rely on a unified formulation, which can guarantee the continuity of the friction factor function with respect to the Reynolds number, form the laminar regime to the fully turbulent one. In this sense, most of the academic works devoted to the purpose is based on the data from Nikuradse experiments [63] who was able to register the friction factor values for the transition regime, in contrast to the Colebrook-White experiment.

To be noted that for the Nikuradse experiment, the roughness was artificially controlled while for the other, commercial pipes were used.

In [68], Cheng uses an interpolation approach to derive the following explicit formula for the determination of the friction factor, valid for any value of the Reynolds number

$$\frac{1}{\lambda} = \left(\frac{Re}{64}\right)^{\alpha} \left(1.8 \log \frac{Re}{6.8}\right)^{2(1-\alpha)\beta} \left(2.0 \log \frac{3.7\,D}{\varepsilon}\right)^{2(1-\alpha)(1-\beta)} \tag{2.10}$$

with:

$$\alpha = \frac{1}{1 + \left(\frac{Re}{2720}\right)^{9}}$$

$$\beta = \frac{1}{1 + \left(\frac{Re}{160\,\frac{D}{\varepsilon}}\right)^{2}}$$

This formula follows the inflectional behavior of the experimental data from Nikuradse experiment with an improved accuracy and provides a function for the laminar-turbulent transition. What is more, the computation of the friction factor requires a little computational burden being the formula explicit.

An alternative explicit formula has more recently been proposed by the European Joint Research Center (JRC) in [69] that is based on the use of switching formulas. Thanks to them, it is possible to guarantee the continuity in the transition regions thanks to a smooth mathematical switch between the different formulas that are valid within the different intervals of Reynolds number. The formulation is given in the following general expression:

$$\lambda = (1 - f_1)(a) + (f_1 - f_3)(c_1) + y_2(c_3) \tag{2.11}$$

where f_i are the switching functions and a, c_1, c_3 the interchangeable expression of the friction factor for the laminar, the smooth turbulent and fully developed turbulent flow respectively. This structure gives flexibility to the unified expression because it is possible to use all the formulations for the friction factor available in literature.

In Figure 1 a comparison between the four discussed friction factor formulas spanning from the laminar regime to the fully developed turbulent one is given, for common relative roughness values.
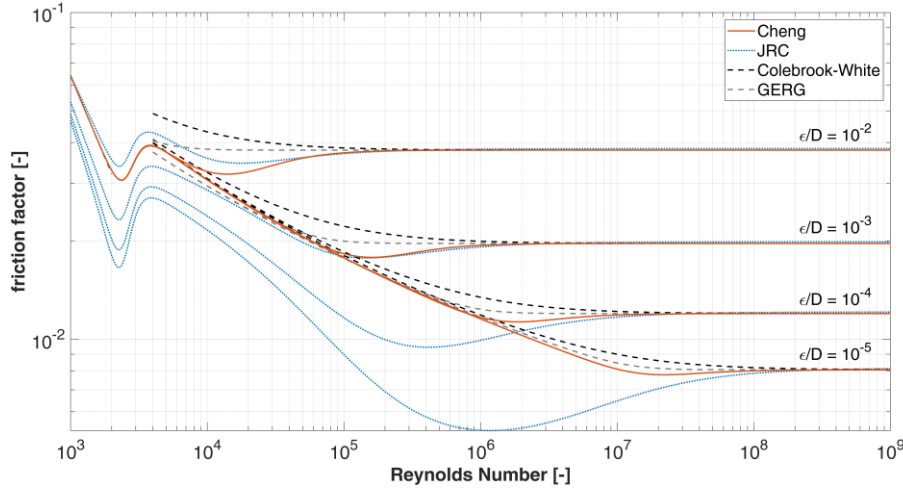
Figure 1 – Comparison among different friction factor correlations on the Moody Diagram (friction factor as a function of Reynolds number, for different values of relative roughness).

It is possible to note that Colebrook-White and GERG expressions are not defined for values of Reynolds between 2000 and 3400, while the other two displays continuity. While GERG shows a more abrupt transition between the non-fully developed and fully developed turbulent flow, the Cheng equation considers also the inflectional behavior observed by Nikuradse. The JRC formulation seems to amplify this inflection as the relative roughness ε/D decreases. However, by means of the JRC approach, many different curves can be adopted, by tuning the choice of the best-fitting correlation according to specific experimental evidences.

For the sake of the gas network simulations in this present work, the Cheng correlation has been chosen as the most suitable one. It provides a unified formulation able to a better representation of the transitional regions while keeping close to the traditional and well-referenced Colebrook-White equation, commonly used in the gas sector. What is more, the explicit formulation reduces significantly the computational burden.

2.1.2 Equation of State

In the framework of gas network modelling, the equation of state is a fundamental closure relation that links together the thermo-hydraulic quantities for the definition of the thermodynamic state of the gas. It allows, in fact, expressing the density as a function of pressure and temperature thus reducing the number of unknowns from the system of conservation equations. The common strategy that is followed when dealing with gas pipeline or network modelling is to refer to the equation of state in its most general form: the universal gas law (i.e.

Eq. (2.4)). The equation of state in such form allows an easy formulation of the relationship between state variables to be integrated in the system of conservation equations while transferring the complexity and the specificity of the chosen equation of state to the determination of the compressibility factor *Z*.

In the natural gas industry, the choice of the gas equation of state is a well-known issue, which relates not only with the operational aspect of any gas transmission operator (physical simulation and balancing of the infrastructure), but also with financial and legal aspects related to the gas supply and its metering (custody transfer). Depending on the application, different requirements and constraints on the equation of state type and accuracy are requested. In [70], a collection of different equations of state which are usually employed in the gas industry are reviewed and commented from the point of view of the industrial interest. In general, from a mathematical point of view, equation of states can be classified into three main groups: the cubic equations of states, the virial equations of state and the multi-parameter equations of state.

The cubic equations of state mainly originates from successive modifications and improvement of the Van der Waals equation form. The "cubic" attribute comes from the fact that the molar volume can be expressed as a cubic function. The widely use Peng-Robinson (PR) [71] and its modifications as well as the Redlich-Kwong (RK) [72] and the Soave-Redlich-Kwong (SRK) [73] all belongs to this group. They are relatively easy to implement, but their simple structure causes a few limitations. In particular, they are not suitable in the supercritical and liquid regions, where the densities are higher and a third order expression cannot provide a well replication of the density behaviour [70]. Extensions to multicomponent gases may be obtained by integrating proper mixing rules that are correlation between molar fractions and thermo-dynamic properties. A collection of mixing rules are available here [74].

The virial equations of states originates instead from the virial expansion of the compressibility factor in a polynomial function of order *n* of density or volume, according to this form:

$$Z = \frac{p}{RT\rho} = A + B\rho + C\rho^2 + \cdots$$

Each coefficient may be determined on the basis of further polynomial fitting of experimental data, both for pure substances and for mixtures. An example of a widely used virial equation for natural gas mixture comes from the GERG-88 series [75], a second order formula that is truncated after the third term. It was developed for the calculation of compressibility factor of natural gas considered as a mixture [76]. The virial coefficients are second order polynomial functions of the temperature and depends on the molar fraction of the mixture. In particular,

the second virial coefficient is related to the binary mixtures while the third one is related to the tertiary mixtures. The equation is available in a master or standard (simplified) version; the standard version sGERG-88 is still considered as an international standard for the compressibility factor calculation by the ISO 12213-3 [77], where a detailed description of the methodology and all the coefficients are provided.

Virial equations, allowing higher order expression are able to overcome some of the limitations of the cubic equations as discussed above such as the inaccuracies when dense phase is approached.

However, a further step towards accurate properties prediction over a wide range of conditions is taken by adding to the virial expansion an exponential term as it was first done by Benedict, Webb and Rubin in their BWR equations ([78] and [79] for a generalization to mixtures), subsequently modified by Starling (BWRS) [80]. The hybrid form of this equation is also used by Starling et al. in [81] order to build the AGA-8 equation of state proposed by the American Gas Association, one of the most widely used in the gas industry as it is also an ISO standard [82]. It is explicit in the compression factor and it can be used for natural gas mixtures with up to 21 components. Similarly, to GERG-88, two different methodology are given: a detailed estimation and a gross estimation, whether the gas composition is accurately known or not. As it can be inferred, the aim to broaden the applicability condition of any equation of state leads to consider the composition as a further variable according to which determining the fluid properties. This calls for the need of generalizing the coefficient formulation according to the varying gas composition, thus integrating in the calculation appropriate mixing rules generating the so-called "compositional equation of states", which are properties calculation methodologies rather than simple equations. The reason why AGA-8 and sGERG-88 are considered as ISO standards is that they provide a thorough methodology for the determination of the properties of natural gas for a wide-range of temperature, pressure and chemical composition. To be noted that according to [82], the AGA-8 methodology is to be used for pipeline-quality gases; similarly in in [77] the ranges of application of sGERG-88 are limited to 12 MPa and gas quality close to the conventional one (for instance, hydrogen content should be less than 10 %$_{mol}$).

According to [83], the most common equations used among the system operators in America and Europe are the AGA-8 equation and the sGERG-88 which, in fact, appear frequently among the academic literature too.

The most recent advancement in the framework of wide-range equations of state for natural gas mixtures is given by the GERG-2004 [84] and GERG-2008 [85] equations of state. They differ from the previous methodologies, which were based on volumetric equation of state, because they are based on an equation of state in its fundamental form instead (i.e. a relationship between density, temperature and Helmholtz free energy). They belong to the family of multi-

parameter equations of state and both are explicit in the reduced Helmholtz free energy, expressed as in the following:

$$\alpha(\delta, \tau, [y]) = \alpha^0(\rho, T, [y]) + \alpha^r(\delta, \tau, [y]) \qquad (2.12)$$

where α^0 represent the ideal gas behaviour of the fluid and α^r is the residual part. The quantity α is the reduced Helmholtz free energy, while δ and τ are the reduced density and the inverse of the reduced temperature respectively. These reduced quantities are defined as follows:

$$\alpha = \frac{a(T,p,[y])}{RT} ; \qquad\qquad \delta = \frac{\rho}{\rho_{cr}([y])} ; \qquad\qquad \tau = \frac{T_{cr}([y])}{T} ;$$

with ρ_{cr} and T_{cr} being the critical density and the critical temperature.

As it can be noted, the reduced Helmholtz free energy is a function of temperature, density and composition of the mixture. Both the equations are based on a multi-fluid approximation: the only difference between the two GERG equations lies in the number of considered components: GERG-2008 results as an extended version of the GERG-2004 including 21 typical natural gas component: all the alkanes hydrocarbons up to the *n*-decane, nitrogen, carbon dioxide, carbon monoxide, hydrogen, oxygen, water, hydrogen sulphide, helium and argon.

A thorough explanation of the methodology of GERG-2008 is given in [85], where the comparison with other very common equations of state (AGA-8 and PR) is also given. In [85], the ranges of applicability in terms of pressure, temperature and also composition are given, making this equation one of the most versatile in terms of unconventional natural gas composition, being able to model hydrogen rich natural gases.

The high flexibility of GERG-2008 equation in handling higher molar fraction of unconventional component within the natural gas mixture and its very wide range of applicability led the author to choose it as closure relation for the multi-component model of the gas network. One of the aim of the model here described is in fact the simulation of gas network scenarios with unconventional gas injection, such as hydrogen, thus the need of a flexible equation of state over the gas composition is fundamental. In addition, its recentness and its novelty, together with the fact that it has recently been included as an ISO standard [86] for the calculation of the properties of the natural gas and other similar mixtures together makes it even more attractive for a newly developed network model. In [86] is clearly stated that the method can be applied to wider ranges of temperature, pressure and composition with no increase of uncertainty with respect to AGA-8.

The GERG-2008 equation of state is incorporated within the network model by means of the determination of the compressibility factor $Z = Z(p, T, [y])$, as a function of the local pressure, temperature and gas composition (expressed in molar fraction):

$$Z = \frac{p(\delta, \tau)}{\rho RT} = 1 - \alpha_\delta^r \qquad (2.13)$$

Where α_δ^r is the derivative of the residual of the Helmholtz free energy in its reduced form with respect to the reduced density:

$$\alpha_\delta^r = \left. \frac{\partial \alpha^r}{\partial \delta} \right|_\tau$$

For a complete and detailed description of all the formulas please refer to the original paper from Kunz et al. [85].

Academic and industrial research have produced a considerable number of equations of state for gases, each with its strengths and weakness: some are easier to implement and fast in computation but are less adequate to be applied to wide ranges conditions or multi-composition cases. Of course, benchmarks and comparisons among the different equations and methods are treated in literature according to the field of application. Concerning the pipeline modelling, several sensitivity analysis on the choice of the gas equation of state are addressed in order to quantify the impact it may have on the pressure or mass flow predictions. In [83], the AGA-8, the BWR and the SRK equations are applied to model the same section of transmission pipeline operated at around 7 MPa. It is concluded that no relevant differences can be observed in the pressure and mass flow rates calculation. The choice of the equation of state has an influence on the linepack estimation instead, with maximum differences among the equations of 0.23 %. To similar conclusion got [87], in which GERG-2004 was compared to a SRK type of equation and a non-negligible difference in the linepack evaluation was obtained. GERG-2004 was considered also in [88],[89] where a comparison of the already mentioned equations was performed over a wider range of pressure. It was demonstrated that at higher pressures (> 10 MPa), most of the equations of state behave differently as the limit of their applicability is approached. The most performing equation in this study is said to be the GERG-2004, which is stated to be valid up to 30 MPa.

The most recent works on multi-component gas flow modelling for applications in the field of unconventional gas blending have used sGERG-88 [21] and GERG-2004 [87], [56],[55].

2.2   Simplifying assumptions

When modelling gas network infrastructures, a large number of interconnected pipelines are considered, thus increasing the computational effort for the solution of the complete set of PDEs as previously presented. It is then reasonable to simplify the system of equations by neglecting some of the terms that are non-relevant under the normal operating conditions of gas transport systems. There is a wide literature on the simplification process of gas pipeline transport equations and about the estimation of the magnitude of errors that these approximations bring to the simulation results ([90],[91],[92]). Most of these references converge in the following assumptions:

1. Isothermal problem
   The changes in the gas temperature are assumed to be negligible in space and time. This means to neglect the Joule-Thomson effect and any thermal exchange with the environment since the gas is assumed to be in thermal equilibrium with the surroundings (usually ground or sea). Consequently, the temperature of the gas is set equal to the temperature of the surrounding environment.
   In the real-life operation of a pipeline, the major sources of temperature deviation may come from compression stations and pressure regulator stations or they may be common for gas transport pipelines that are characterized by long distances and different surrounding conditions (i.e. on-shore and offshore transport). However, they are commonly equipped with, respectively, gas coolers and pre-heaters to compensate for the temperature variation caused by the thermodynamic transformation. Other sources for thermal variation of the gas, which happen along the pipeline, are the Joule-Thomson effect that is linked to the pressure drop the gas undergoes while flowing through a pipe and the thermal exchange with the surrounding environment. However, in normal operating conditions, the slow velocity of the gas and the stability of the temperature of the surrounding environment (pipeline are usually buried few meters underground) allows the thermal equilibrium so that assuming the temperature of the gas equal to a constant value of the surrounding temperature is reasonable.
   An in-depth discussion on the deviations on pressure prediction introduced by the isothermal assumption is made by Osiadacz et al. in [92]. In the worst scenario, the pressure at the outlet end of a transmission pipeline (about 120-km long) results overestimated by 1% in the isothermal case with respect to the non-isothermal one.
   This assumption allows a considerable simplification of the PDEs system since it is possible to neglect completely the Energy Equation, thus

reducing the number of equations and unknowns. Furthermore, it is possible to express the isothermal speed of sound c by means of the state equation through the following relation:

$$\frac{p}{\rho} = c^2 = Z R T \tag{2.14}$$

2. Creeping motion

Gas networks for transport and distribution of natural gas are designed so to keep the gas velocity below the maximum value between 10 and 25 m/s. Due to the these relatively small velocities, the influence of the convective term in the momentum equation – second term of Eq. (2.2) – is smaller compared to the others and can easily be ignored [50]. In fact, this can be easily inferred from the comparison between the magnitude of the convective term and the pressure term, both being partial spatial derivatives, under the typical operating condition of a pipeline.

From Eq. (2.2) it is possible to extract the following:

$$\frac{\partial(\rho v^2)}{\partial x} + \frac{\partial p}{\partial x} = \frac{\partial}{\partial x}[\rho v^2 + p] = \frac{\partial}{\partial x}\left[p\left(1 + \frac{v^2}{c^2}\right)\right]$$

In the case of maximum flow velocity $v = 25$ m/s, assuming a flow of pure methane at $p = 50$ bar and $T = 15$ °C, with a resulting speed of sound $c = 428$ m/s, the comparison results in:

$$\frac{\partial}{\partial x}\left[p\left(1 + \frac{v^2}{c^2}\right)\right] = \frac{\partial}{\partial x}\left[p\left(1 + \frac{25^2}{428^2}\right)\right] = \frac{\partial}{\partial x}\left[p\left(1 + \frac{25^2}{428^2}\right)\right]$$

$$= [p(1 + 3.41 \cdot 10^{-3})] \approx \frac{\partial p}{\partial x}$$

proving that the influence of the convective term is at least three order of magnitude smaller than the pressure one.

2.3   Network description

The gas infrastructure, as well as the electricity grid and many others commodities and civil infrastructures have the structure of a network, being a set of physically interconnected elements. Graph theory is a powerful mathematical tool in the framework of the analysis, the simulation and the optimization of network-like systems. In fact, any network can be described as a directed graph. In mathematical term, a graph is an ordered pair $\mathcal{G} = (\mathcal{V}, \mathcal{E})$ where $\mathcal{V}$ is a set of elements called vertices (or nodes) and $\mathcal{E}$ an ordered set of vertex pairs called directed edges (or directed branch). Therefore, in a physical network representation, a directed edge represents any element of the network connecting an inlet and an outlet node with a defined direction. The vertices are most of the times the interconnections between two or more contiguous edges with the exception of those edges which start (or end) from (in) one peripheral node.

In the framework of network modelling and simulation, one of the most effective way to represent a directed graph in a computational useful way is by means of its incidence matrix:

$$\mathbf{A} = \left[a_{i,j} \right]^{n \times b}, \qquad a_{i,j} = \begin{cases} +1, & \text{node } i \text{ is the inlet of edge } j \\ -1, & \text{node } i \text{ is the outlet of edge } j \\ 0, & \text{node } i \text{ and edge } j \text{ have no connections} \end{cases} \qquad (2.15)$$

where n is the number of nodes and b is the number of edges.

The incidence matrix stores the entire topology of the network (i.e. all the information about the interconnections between vertices). From a computational point of view, it allows expressing in an algebraic form the relations between nodal and edges quantities. These quantities are represented as column vectors of dimensionality ($n \times 1$) and ($b \times 1$).

In the gas network application, the pipelines are the most common pieces of the infrastructure to be modelled as directed edges. Others elements are resistors, compressors, regulators and valves. Resistors are the general representation of any device that causes a local pressure drop. Together with the pipelines, they are referred to as the "passive elements" because they generates pressure drops as a consequence of the gas flowing through them. Compressor stations, pressure regulation stations and valves are considered as active elements since their behaviour and/or operating status may be imposed from the external by means of an operating variable. Concerning to the nodes, they are not only the interconnections between the network elements, but they are also the points in which gas fluxes are exchanged with the external environment.

Thus, three main types of nodes can be defined, along with a sign convention:

- injection nodes: supply points in which gas enters the network $\dot{m}_{ext} < 0$;
- consumption nodes: in which gas exits the network, $\dot{m}_{ext} > 0$;
- junctions: no gas exchange, $\dot{m}_{ext} = 0$.

According to the convention adopted, $\dot{m}_{ext}$ can be defined as the nodal load (i.e. the gas consumption).

In the framework of gas network simulations, the entire set of pipelines and nodes equations will be solved by means of an algebraic problem that is built starting from the topological information stored in the incidence matrix. The main variables describing the status of the network are the nodal pressures and the nodal loads:

$$\boldsymbol{p} = \begin{pmatrix} p_1 \\ p_2 \\ \vdots \\ p_i \\ \vdots \\ p_n \end{pmatrix} \qquad \dot{\boldsymbol{m}}_{ext} = \begin{pmatrix} \dot{m}_{ext\,1} \\ \dot{m}_{ext\,2} \\ \vdots \\ \dot{m}_{ext\,i} \\ \vdots \\ \dot{m}_{ext\,n} \end{pmatrix}$$

and the edges' mass flows:

$$\dot{\boldsymbol{m}} = \begin{pmatrix} \dot{m}_1 \\ \dot{m}_2 \\ \vdots \\ \dot{m}_j \\ \vdots \\ \dot{m}_b \end{pmatrix}$$

whose sign is positive if the gas flow direction is from the inlet to the outlet node.

2.4 Pipeline equation derivation

The simplifying assumptions previously mentioned reduces the set of PDE to a coupled pressure-velocity-density problem made of two equations in three unknowns: pressure p, velocity v, density ρ. By means of Eq. (2.14) the number of unknowns may be reduced to two. In order to derive a proper pipeline equation, it is convenient to substitute the velocity v with the mass flow rate $\dot{m}$ by means of the following relation:

$$\dot{m} = \rho v A \qquad (2.16)$$

In this way, the pipeline equation relates the main operational variables of a duct: pressure and gas flow.

The simplified system of equations may be re-written as follows:

$$\frac{1}{c^2}\frac{\partial p}{\partial t} + \frac{1}{A}\frac{\partial \dot{m}}{\partial x} = 0 \qquad (2.17)$$

$$\frac{1}{A}\frac{\partial \dot{m}}{\partial t} + \frac{\partial p}{\partial x} + \frac{\lambda c^2}{2DA^2 p}\dot{m}|\dot{m}| + \frac{g sin\alpha}{c^2}p = 0 \qquad (2.18)$$

The derivation of a pipeline equation consists in the deduction of a relation between the pressure drops along the pipe as a function of the mass flow rates. Rewriting the momentum equation (Eq. (2.18)) as follows

$$\frac{\partial p}{\partial x} = -\frac{1}{A}\frac{\partial \dot{m}}{\partial t} - \frac{\lambda c^2}{2DA^2 p}\dot{m}|\dot{m}| - \frac{g sin\alpha}{c^2}p \qquad (2.19)$$

it is possible to obtain a differential expression of the pressure drops along a pipeline as a composition of several terms such as:

- inertia, related to the time derivative of the mass flow, accounting for the forces which oppose the flow acceleration direction;
- hydraulic resistance accounting for the friction which is quadratically proportional to the mass flow and it oppose the mass flow direction;
- gravitational resistance accounting for the pressure losses due to gravity if the pipeline has an inclination α.

In the form of Eq. (2.19), the pressure drops equation displays non-linearity both on mass flow and on pressure. Some further elaborations are required to get to a linearized form, which is suitable for network modelling purpose.

First, the non-linearity associated with the pressure can be avoided by performing a substitution of variable such as $P = p^2$, thus referring to the quadratic pressure, obtaining:

$$\frac{\partial P}{\partial x} + \frac{2gsin\alpha}{c^2}P = -\frac{2\,p}{A}\frac{\partial \dot{m}}{\partial t} - \frac{\lambda c^2}{DA^2}\dot{m}|\dot{m}| \tag{2.20}$$

The presence of the time and spatial derivatives requires the adoption of integration strategies. Regarding the integration of the spatial derivative, Eq. (2.20) can be considered as a linear and non-homogeneous differential equation of first order provided that the coefficients of the right hand side are averaged over the pipe section $\Delta x = l$, so to be constant with respect to the x. Assuming this approximation, the equation is solved analytically yielding to the following pipeline equation.

$$P_{in} - P_{out}e^{s_j} = \frac{2\,\bar{p}_j\,l_{e_j}}{A_j}\frac{\partial \dot{m}_j}{\partial t} + \frac{\lambda_j\,\overline{c^2}_j\,l_{e_j}}{D_jA_j^2}\,\dot{m}_j|\dot{m}_j| \tag{2.21}$$

with:

$$l_{e_j} = \begin{cases} l_j\,, & h_{in} = h_{out} \\ \dfrac{e^{s_j}-1}{s_j}\,l_j\,, & h_{in} \neq h_{out} \end{cases} \qquad\qquad s_j = \frac{2g(h_{out}-h_{in})}{\overline{c^2}_j}$$

Where subscripts *in* and *out* stand for the inlet and the outlet sections of the generic j^{th} pipe. In order to account for the gravitational contribution, the "effective length" l_e is defined as the corrected length of the pipeline section in case of non-horizontal pipelines (whose slope is defined by the elevation difference $(h_{out} - h_{in})$ of their ends.

The averaged quantities, which make the analytical solution possible, are calculated starting from the computed value of the average pressure $\bar{p}$ as expressed in [93] and here reported:

$$\bar{p} = \frac{p_{in}^2 + p_{in}p_{out} + p_{out}^2}{p_{in} + p_{out}}$$

And in turn:

$$\overline{c^2} = Z(\bar{p}, T, [y])RT$$

Eq. (2.21) has now the form of an ordinary differential equation in which the time derivative can be treated by means of an implicit finite different scheme for the approximation the inertia term, leading to the following expression:

$$P_{in}^{t+1} - P_{out}^{t+1} e^s = \frac{2\,\overline{p^{t+1}}\,l_e}{A\,\Delta t}(\dot{m}^{t+1} - \dot{m}^t) + \frac{\lambda\,\overline{c^2}\,l_e}{DA^2}\dot{m}^{t+1}|\dot{m}^{t+1}| \qquad (2.22)$$

This scheme is a single-step backward differentiation formula also known as backward Euler method. It is one of the most common and basic numerical method for the solution of ordinary differential equations with first-order convergence and fully implicit feature, so to guarantee stability for large time steps, as reported in [94] and in [95].

The integrated form of the pipeline equation is finally given in a more concise form as follows

$$\Delta P^{\,t+1} = R_I \cdot (\dot{m}^{\,t+1} - \dot{m}^{\,t}) + R_F \cdot \dot{m}^{\,t+1}|\dot{m}^{\,t+1}| \qquad (2.23)$$

with ΔP representing the corrected and quadratic pressure drop as defined here

$$\Delta P^{\,t+1} = P_{in}^{t+1} - P_{out}^{t+1} e^s \;;$$

And the coefficients of the right hand side grouped in two resistance coefficients:

$$R_I = \frac{2\,\overline{p^{t+1}}\,l_e}{A\,\Delta t}\;; \qquad\qquad R_F = \frac{\lambda\,\overline{c^2}\,l_e}{DA^2} = \frac{16\,\lambda\,\overline{c^2}\,l_e}{\pi^2 D^5}\;;$$

The two terms in the right hand side of the Eq. (2.23) represent the two physical phenomena contributing to the pressure variation along the pipeline. The first (subscript I) is the inertia contribution, that is proportional to the mass flow variation during the time interval Δt. The second is the fluid-dynamic friction (subscript F) within the pipe, quadratically proportional to the fluid velocity (and thus the mass flow).

Eq. (2.23) is the most general version for the transient flow of gas through a pipeline, under the simplifying assumptions previously mentioned. Some authors [96] further simplify the problem neglecting the inertia term for those cases in which the transient behaviour is slow i.e. the mass flow variation per unit of time is small. Nevertheless, either the inertia term is neglected or not, the quadratic relation between pressure drop (also expressed as quadratic difference) and mass

flow brings an unavoidable non-linearity to the pipeline equation, which needs to be treated properly in order to set up an algebraic problem to be suitable for network simulations.

Linearization of the pipeline equation

The quadratic pressure drop equation as expressed in Eq.(2.23) is a parabolic function of the mass flow. In order to be included in an algorithm for the network simulation, it has to be linearized. In general, the linearization technique means that any curve is approximated with a tangent line touching the curve at a specific point. Therefore, considering the generic pipe j and assuming the linearization point as $\left(\Delta P_j^{t+1}, \dot{m}_j^{t+1}\right)$, the application of the linearization formula leads to the following expression:

$$\Delta P_j^{t+1\,(k+1)} - \Delta P_j^{t+1\,(k)} = \left.\frac{d\Delta P_j^{t+1\,(k)}}{d\,\dot{m}_j^{t+1\,(k)}}\right|^{(k)} \left(\dot{m}_j^{t+1\,(t+1)} - \dot{m}_j^{t+1\,(k)}\right)$$

from which, solving the derivative of the pressure drop Eq.(2.23), it is possible to obtain the final expression:

$$\Delta P_j^{t+1\,(k+1)} - \left(2R_F \cdot \left|\dot{m}_j^{t+1\,(k)}\right| + R_I\right) \dot{m}_j^{t+1\,(k+1)} =$$

$$= -R_F \cdot \left|\dot{m}_j^{t+1\,(k)}\right| \dot{m}_j^{t+1\,(k)} - R_I \dot{m}_j^{t\,(k)}$$

(2.24)

This method was presented in [97] for the steady state case and generalized for the application to the transient equation in [96].

In the end, in order to refer to the normal pressure drop Δp rather than the corrected-square pressure drop ΔP, the Eq. (2.23) and its linearized version (2.24) which are generally applied to the pipeline j, shall be divided by $(p_{in} + p_{out}e^{s/2})$.

2.5 Nodal mass balance

The pressure drop equation cannot be solved without knowing the mass flow rates flowing along the corresponding pipeline. Thus, a nodal mass balance equation is derived from the continuity equation, in order to obtain a closed problem. Unlike the case of pipeline equation derivation, where the control volume was the pipeline, in this case, the continuity equation is applied around the junctions between pipelines in its integral form. The mass balance between inflows and outflows should be equal to the variation of the gas quantity stored within the nodal volume as a consequence of pressure variation. In Figure 2 a schematic of a general junction for the definition of the nodal volume is given in order to clarify the boundaries of each control volume.
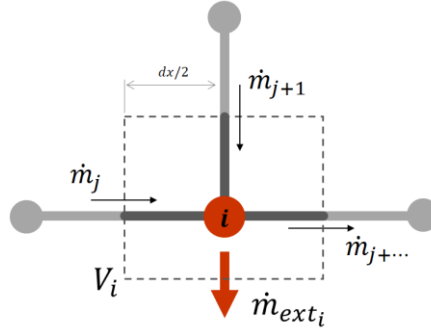
Figure 2 – Scheme of a general junction between pipelines and consumption node.

The continuity equation (2.17) is integrated over the control volume:

$$\int_{CV_i} \frac{1}{c^2}\frac{\partial p}{\partial t} + \frac{1}{A}\frac{\partial \dot{m}}{\partial x}\ dV\ = 0$$

obtaining

$$\frac{1}{c^2}\frac{\partial p_i}{\partial t}V_i + \int_{CV_i} \frac{1}{A}\frac{\partial \dot{m}}{\partial x}\ dV\ = 0$$

The second term can be simplified by the application of the Gauss-Green Theorem so that

$$\int_{CV_i} \frac{1}{A}\frac{\partial \dot{m}}{\partial x}\ dV\ = \int_{\partial(CV_i)} \frac{1}{A}\dot{m}\ dA$$

then the integral on the boundary of the control volume is turned in the following discrete summation

$$\int_{\partial(CV_i)} \frac{1}{A} \dot{m} \, dA = \sum_j a_{i,j} \frac{1}{A_j} \dot{m}_j A_j$$

The integral form for the continuity equation, applied to the ith node, is thus obtained:

$$\frac{V_i}{c^2} \frac{dp_i}{dt} = -\sum_j a_{i,j} \dot{m}_j - \dot{m}_{ext_i} \qquad (2.25)$$

with:

$$V_i = \frac{\pi}{8} \sum_j D_j^2 \, \Delta x_j \ ;$$

that is the geometrical volume of the ith node.

In the formulation of Eq. (2.25), the left hand side corresponds to the balance among the inward and outward mass flows. The coefficient $a_{i,j}$ is the one of the incidence matrix as defined in (2.15). Reading the incidence matrix by rows it is possible to retrieve retrieving the following information related to the ith node:

$$a_{i,j} = \begin{cases} +1, & \text{edge } j \text{ is outgoing to node } i \\ -1, & \text{edge } j \text{ is incoming from node } i \\ 0\,, & \text{edge } j \text{ has no connections with node } i \end{cases}$$

In agreement with this sign convention, mass exchanges with external are considered in the last term of the right hand side, in order to complete the balance. Since the problem is transient and it concerns a compressible fluid, imbalances between inlets and outlets of the control volume occurs. The right hand side represent the gas accumulation within the geometrical volume V_i, which correspond to a nodal pressure variation in time.

Eq. (2.25) is now an ordinary differential equation, which will be translated into an algebraic one applying the backward Euler method, in analogy with the procedure followed for Eq.(2.21), resulting in the following equation:

$$\frac{V_i}{c^2 \, \Delta t} \left(p_i^{t+1} - p_i^t \right) = -\sum_j a_{i,j} \dot{m}_j^{\,t+1} - \dot{m}_{ext_i}^{t+1} \qquad (2.26)$$

that is valid for each ith node of the network.

While pressure p_i^{t+1} and mass flow $\dot{m}_j^{\,t+1}$ are the unknowns of the problem, the mass flows exchanged with the external environment $\dot{m}_{ext_i}^{t+1}$ are boundary conditions to be provided to the problem.

2.6   System of Equations

2.6.1   Matrix form of momentum and continuity equations

The linearized pressure drop equation (2.24) and the nodal mass balance (2.26) in their discretised forms the system of algebraic equations to be solved in order to obtain the nodal pressures and the mass flows through each pipeline. it can be noted that, from a spatial discretisation point of view, a staggered grid setting has been in fact adopted: pressures are defined at the ends of the pipelines (i.e. nodes of the network) while mass flows are related to the pipelines themselves (the edges of the network), so the "points" between a two nodes.

The matrix representation of the network topology explained in section 2.3 is useful to give a matrix representation of both the pipeline and the nodal equations, so to reach a full algebraic representation of the system of equations for the simulation of the complete network.

The pipeline-linearized equation (2.24) for the whole network becomes:

$$\mathbf{A_g^t}\, P^{t+1\,(k+1)} - \mathbf{R}\, \dot{m}^{t+1\,(k+1)} = -\,\mathbf{R_F}\big(\big|\,\dot{m}^{t+1\,(k)}\big| \circ \dot{m}^{t+1\,(k)}\big) - \mathbf{R_I}\, \dot{m}^{t\,(k)} \qquad (2.27)$$

where $\mathbf{R}$, $\mathbf{R_F}$ and $\mathbf{R_I}$ are the ($b \times b$) square diagonal matrices whose general elements (j,j) are the coefficients of Eq.(2.24) corresponding to the jth pipe. To be noted that the operator $\circ$ stands for the element-wise product. The matrix $\mathbf{A_g}$ is a modified version of the incidence matrix $\mathbf{A}$ in order to take into account the gravitational term, and it is defined as follows:

$$\mathbf{A_g} = \big[a_{g_{i,j}}\big]^{n \times b},\ a_{g_{i,j}} = \begin{cases} +1, & \text{node } i \text{ is the inlet of edge } j \\ -e^{s_j}, & \text{node } i \text{ is the outlet of edge } j \\ 0, & \text{node } i \text{ and edge } j \text{ have no connections} \end{cases}$$

However, this equation refers to the corrected-square pressures. In order to refer to the vector of nodal pressures $\boldsymbol{p}$, the whole equation has to be divided by ($p_{in} + p_{out}e^{s/2}$) for each pipeline j. A matrix $\mathbf{A_g'}$ can be defined in analogy to the matrix $\mathbf{A_g}$, considering that all the non-zero elements will be positive. Then an element-by-element ratio can be performed between the matrices in Eq.(2.27) and $\mathbf{A_g}$ (excluding the zero elements) in order to obtain the modified versions of the matrices that forms the set of equations for the pipeline elements of the network:

$$\mathbf{A'_g^t} \, p^{t+1\,(k+1)} - \mathbf{R'} \, \dot{m}^{t+1\,(k+1)} = -\mathbf{R'_F}\left(\left|\dot{m}^{t+1\,(k)}\right| \circ \dot{m}^{t+1\,(k)}\right) - \mathbf{R'_I} \, \dot{m}^{n\,(k)} \qquad (2.28)$$

It is worth noting that the right hand side of Eq.(2.28) is the known term of the equation, and it is composed of the "old" mass flow $\dot{m}^{t\,(k)}$, belonging to the previous timestep, and of the "tentative new" mass flow $\dot{m}^{t+1\,(k)}$, originated from the iterative procedure for the solution of the linearized version of the pipeline equation.

In order to solve the fluid-dynamic model of the network, another set of equation is necessary. This second set of algebraic equations comes from the generalization to the whole network of the nodal mass balance (Eq.(2.26)) whose matrix form results in:

$$\mathbf{\Phi} p^{t+1} + \mathbf{A} \, \dot{m}^{t+1} + \mathbf{I} \, \dot{m}_{ext}{}^{t+1} = \mathbf{\Phi} p^{t} \qquad (2.29)$$

where $\mathbf{I}$ is the identity matrix and $\mathbf{\Phi}$ a diagonal matrix defined as follows:

$$\mathbf{\Phi} = \left[\phi_{i,i}\right]^{n \times n}, \phi_{i,i} = \frac{V_i}{c_i^2 \, \Delta t}$$

The algebraic system formed by Eq.(2.28) and Eq.(2.29) accounts for $b + n$ equations with $b + n + n$ unknowns, these being:

- b mass flow rates for each pipe;
- n pressures for each node;
- n mass flow rates exchanged with the external environment.

An additional set of n equation needs to be provided. This set of equation is in fact representative of the n boundaries conditions, which needs to be specified at any nodes of the network.

2.6.2 Boundary conditions

As it was already anticipated in section 2.3, each node of the network is an interface towards the external of the network control volume.

Junction nodes have no mass exchanges with the external of the network and its pressure is determined by the fluid-dynamic equilibrium of the system. Thus, these nodes are assigned with an external mass flow set point equal to zero for each time step of the simulation.

All the other nodes that are connected with any facilities (i.e. entry stations, LNG terminals, storages, exit stations, consumption facility…) are assigned with the control mode of the corresponding facility. In general, either the exchanged mass flow (also called nodal load) or the nodal pressure is the controlled variable of any external facility and so will be provided as a boundary condition each time step of the simulation. In case of "pressure controlled node", a pressure set point function $p_{set_i}(t)$ is known and its value is given for any time step $t + 1$. The nodal load $\dot{m}_{ext_i}(t)$ will result from the calculations. On the contrary, for the "gas flow controlled nodes", a nodal load function $\dot{m}_{ext_i}(t)$ is known and its value is assigned for any time step $t + 1$, with the corresponding nodal pressure $p_i(t)$ calculated accordingly.

A general linear equation can be written in order to include all the possible cases of nodal control modes, which acts as boundary condition assignment in terms of mathematical formalization of the problem. The equation, in its scalar form results as:

$$k_{p,i}\, p_i^{t+1} + \; k_{m,i}\, \dot{m}_i^{t+1} = \beta_i^{t+1} \qquad\qquad (2.30)$$

where the coefficients $k_{p,i}$ and $k_{m,i}$ assume either value 0 or 1 according to the control mode of the ith node, and β_i^{t+1} is the set point value of pressure or exchanged mass flow for the time step $t + 1$.

This equation is valid for the n node thus providing the set of equations that were missing.

The following table sums up the possible nodal control mode and the corresponding boundary equations that originates.

Table 1 – Summary table for nodal possible control modes and corresponding boundary equations.

Control mode	Equation	coefficients
pressure	$p_i(t) = p_{set_i}(t)$	$k_{p,i} = 1, \; k_{m,i} = 0, \; \beta_i = p_{set_i}$
mass flow	$\dot{m}_{ext_i}(t) = \dot{m}_{set_i}(t)$	$k_{p,i} = 0, \; k_{m,i} = 1, \; \beta_i = \dot{m}_{set_i}$
junction/no flow	$\dot{m}_{ext_i}(t) = 0$	$k_{p,i} = 0, \; k_{m,i} = 1, \; \beta_i = 0$

2.6.3 Complete problem set-up and solution

The fluid-dynamic model of a complete gas network under non-steady state assumptions is given in the form of a linear matrix equation, which is the result of

the composition of the pipeline equation Eq.(2.28) and the nodal balance equation Eq.(2.29), together with the matrix version of Eq.(2.30) which includes all the boundary conditions of the problem. The complete problem takes the following form:

$$
\begin{pmatrix} \boldsymbol{\Phi} & \mathbf{A} & \mathbf{I} \\ \mathbf{A'_g^t} & -\mathbf{R'} & \mathbf{0} \\ \mathbf{K_p} & \mathbf{0} & \mathbf{K_m} \end{pmatrix} \begin{pmatrix} p^{t+1} \\ \dot{m}^{t+1} \\ \dot{m}_{ext}^{t+1} \end{pmatrix} = \begin{pmatrix} \phi\, p^{t} \\ r \\ \beta \end{pmatrix}
\tag{2.31}
$$

where the first row represents the n nodal balance equations, the second is the set of b pipeline equations with r as the vector of known terms of the linearized equations (2.28) and the last row collects the n boundary condition equations, with β as the vector of pressures or mass flows set points.

Knowing the state of the network at time step t, it is possible to compute the nodal pressures, pipeline mass flows and the nodal mass flows injected/withdrawn at time step $t+1$, according to the set points at the boundaries, thus defining the subsequent state of the network. Repeating this operation for the whole simulation interval, the evolution in time of the gas network is simulated. It is worth noting that, even though the complete problem in Eq.(2.31) has the form of an algebraic system of equations, the computation of the gas network state at time step $t+1$ is performed by means of an iterative procedure. The need for an iterative procedure originates from the linearization approach in order to simplify the non-linearity of the momentum equation. In fact, the coefficients of matrices $\boldsymbol{\Phi}$, $\mathbf{A'_g^t}$, $\mathbf{R'}$ all depend on the unknown pressures and the mass flows. For this reason, each time step is solved assuming an initial tentative state of the network (k) (see notation of Eq.(2.24),(2.28)) which allows for the definition of all the coefficients of the matrices of the problem (2.31). The solution of Eq.(2.31) provides a new state of the network $(k+1)$ which is calculated on the basis of the correct boundary conditions at $t+1$ but with coefficients coming from the tentative state (k) – often assumed equal to the previous time step t – and with a linear version of a non-linear relation. Is thus necessary to check for the approximation errors by means of the evaluation of the residuals: the solution of the $(k+1)^{th}$ iteration $(p, \dot{m}, \dot{m}_{ext})^{t+1\,(k+1)}$ is substituted within the continuity equation and the momentum equation in order to evaluate the residuals, defined by these formulas:

Momentum equation residuals:

$$
\boldsymbol{Res_{mom}} = \mathbf{A'_g^t}\, p^{k+1} - \left[\mathbf{R'_I} \cdot \left(\dot{m}^{k+1} - \dot{m}^{t} \right) + \mathbf{R'_F} \cdot \dot{m}^{k+1} \left| \dot{m}^{k+1} \right| \right]
\tag{2.32}
$$

Continuity equation residuals:

$$Res_{cont} = \mathbf{\Phi}p^{k+1} + \mathbf{A}\,\dot{m}^{k+1} + \mathbf{I}\,\dot{m}_{ext}{}^{k+1} - \mathbf{\Phi}p^t \tag{2.33}$$

When the solution of the problem is exact, both the residuals of the momentum and the continuity equation are equal to zero. On the contrary, during the iterative process, the residuals will be other than zero so that a convergence criterion must be adopted.

One of the most common convergence criterion refers to the Euclidean norm of the residual vectors. Most stringently, one can refer to the maximum value among the elements of the vectors Res_{mom} and Res_{cont}.
Referring to the more common Euclidean norm approach, once computed the two norms for the momentum and the continuity equation, the maximum value is selected and compared against a set tolerance $toll = (10^{-3} \div 10^{-8})$.

$$\max(\,\|Res_{mom}\|\,,\|Res_{cont}\|\,): \begin{cases} \leq toll\,, & \text{converged solution} \\ > toll, & \text{not converged solution} \end{cases}$$

when the residuals are greater than the tolerance, the iterative procedure goes on with a further solution of Eq.(2.31), in which the $(k + 1)^{th}$ solution is taken as the new tentative network state, which defines the problem in order to compute the subsequent state. This iterative algorithm is repeated until the convergence is reached. In the majority of cases, the convergence is reached within five iterations but it is very sensitive to the magnitude of the changes of the boundary conditions between two time steps. Smooth functions of time at the boundary conditions ease the convergence of the solution.

While building the algorithm for the fluid-dynamic solution of the network, it is fundamental to set a maximum number of possible iteration $(k_{\max})$ for the solution of the linearized problem. This number may be changed along with the tolerance *toll* according to the feature of the network problem and the admissible computational burden.

In case of non-converging computations, which show oscillatory behaviour, a possible solution to improve convergence is the use of under-relaxation technique. This is a common technique to suppress the oscillations and help the convergence of iterative linear methods. Referring to a general linear problem $\mathbf{A}x = b$ in which $x^{(k+1)}$ is the solution from the kth iteration, the tentative solution used for the re-definition of the problem at the $(k + 1)^{th}$ iteration when using under-relaxation will not be $x^{(k+1)}$ but:

$$x^{*(k+1)} = \omega\,x^{(k+1)} + (1 - \omega)x^{(k)}$$

with $\omega \in [0,1]$ that is called relaxation coefficient and its optimal value is to be determined case by case.

In this way, the convergence properties of the problem may be restored, though the convergence rate will slow down.

The convergence of the fluid-dynamic problem within the same time step brings to the computation of the fluid-dynamic state of the gas network for the current time step, enabling the computation for the following ones. This temporal sequence calls for the need of an initial condition for which everything about the gas network is already known and given. This is usually not the case so that a computation strategy for the definition of an initial condition is needed.

2.7 Initial condition definition – SIMPLE gas

In the framework of transient gas network modeling, it is nearly impossible to get the exact knowledge of the state of the network at the beginning of a simulation because the conditions of imbalance of each portion of the network are hardly known. For this reason it is a very common assumption to start with a steady state initial condition, which can be calculated more easily starting from the knowledge of the boundary conditions.

In case of a tree-shaped network, the calculation of the initial stationary state is straightforward once all the gas flow rates of the withdrawal nodes $\dot{m}^*_{ext}$ are known and one value for the pressure at the gas inlet node is known. All the mass flows $\dot{m}$ within each pipe can be computed form the steady-state version of the continuity equation:

$$\mathbf{A}^* \dot{m} + \dot{m}^*_{ext} = \mathbf{0} \quad \rightarrow \quad \dot{m} = -\mathbf{A}^{*-1} \cdot \dot{m}^*_{ext} \tag{2.34}$$

where $\mathbf{A}^*$ is a square matrix ($b \times b$) originated from the incidence matrix of the tree-shaped network, without the line that corresponds to the node with the given pressure. Once the pipeline mass flows $\dot{m}$ are known, they can be used to calculate the corrected-square pressure drop vector P employing the steady state version for the momentum equation:

$$\Delta P = \mathbf{A}^t P = \mathbf{R_F} \cdot (\dot{m} \circ |\dot{m}|) \tag{2.35}$$

then, all the unknown nodal pressure p^* may be obtained by the square root of:

$$P^* = (\mathbf{A}^{*\mathbf{t}})^{-1} \Delta P + P_{set} \tag{2.36}$$

However, the general topology of any network system is not tree-shaped but rather displays looped structures.

In the case of looped networks, the determination of the pipeline mass flows $\dot{m}$ is not possible anymore by the application of Eq.(2.34) because the modified incidence matrix is not a square matrix anymore, making its inversion impossible. From a mathematical point of view, there are infinite sets of pipeline flows configurations that satisfy the given boundary conditions $\dot{m}_{ext}^*$, because in the presence of loops, there are multiple possible way for the gas to reach an outlet. From a physical point of view, given a set of $\dot{m}_{ext}^*$, the fluxes within the network cannot be univocally determined with the mass balance equation only because the way the mass flow splits in a loop depends on the hydraulic resistance of each set of pipes in the loop, which depends in turn on the mass flow rates themselves. In analogy, the nodal pressures are determined by the pressure drops along each pipeline, which are a quadratic function of the mass flows that are, in turn, driven by the pressure gradients. In shorter terms, there is a pressure-velocity coupling between the continuity and the momentum equations that needs to be treated with a proper iterative algorithm. In [98], implicit pressure-correction methods are said to be effective for the steady state solution of pressure-velocity or pressure-velocity-density coupled problems (i.e. incompressible and compressible problems). Among the methods that are discussed, the SIMPLE algorithm is described for the incompressible flow cases. It is the acronym for Semi-Implicit Method for Pressure-Linked Equations and its algorithm was first proposed in [99] for incompressible problems. In [100] a SIMPLE based algorithm is proposed for the solution of the fluid-dynamics of district heating networks. Concerning the compressible case, a version of the SIMPLE algorithm is already present in literature as described in [101]. However, in the following section a specific version for the gas network case is given, as a modification of the algorithm described in [100].

For the computation of the steady state of a compressible fluid network, the continuity equation is the same as the one for the incompressible network case:

$$\mathbf{A}\,\dot{m} + \dot{m}_{ext} = 0 \tag{2.37}$$

While the momentum equation has the following form:

$$\Delta P = \mathbf{A}^{\mathbf{t}}P = \mathbf{R_F} \cdot (\dot{m} \circ |\dot{m}|) \tag{2.35}$$

where P is the vector of the square nodal pressure ($P_i = p_i^2$) and the $\mathbf{R_F}$ is the diagonal matrix of the fluid-dynamic resistances as defined along with Eq.(2.23). Thus, the only difference versus the incompressible version of the equation is the use of squared pressures. The squared pressure term originates form the fact that the coefficient of the hydraulic resistance term depends on the fluid density, and thus, on the pressure by means of the equation of state, as it can be seen in Eq.(2.19). However, the use of squared pressures allows Eq.(2.35) to preserve the same structure as the momentum equation of the incompressible case so that all the steps of the SIMPLE method and its algorithm are directly applicable to the compressible network case.

The SIMPLE algorithm consists in an iterative procedure based on a "guess-and-correct" approach on the pressure. The algorithm starts with a nodal pressure vector guess $\boldsymbol{p}^{*\,2} = \boldsymbol{P}^*$ that allows for the calculation of the corresponding "guessed" vector for the pipeline mass flow $\dot{\boldsymbol{m}}^*$. In order to do so, Eq.(2.35) must be rewritten in a pseudo-linear form as follows:

$$\Delta P = \mathbf{A^t} P = \mathbf{R_{FM}}(\dot{m}) \cdot \dot{m} \quad \rightarrow \quad \dot{m} = Y\, \mathbf{A^t} P \qquad (2.38)$$

where $Y = Y(\dot{m}) = \mathbf{R_{FM}^{-1}}(\dot{m})$ is defined as the pseudo-conductance matrix and it is the inverse of the hydraulic resistance matrix. Being matrix $\mathbf{R_{FM}}$ a diagonal matrix, its inverse is a diagonal matrix whose diagonal elements are the reciprocal of the hydraulic resistances. This form of the momentum equation is defined as pseudo-linear because the quadratic term of the mass flows has been split and partially incorporated into the coefficient of the algebraic problem matrix. For this reason, the solution of Eq.(2.38) needs a dedicated numerical procedure for non-linear equations (e.g. the fixed-point method).

If the guessed vector $\boldsymbol{P}^*$ is known, it is possible to obtain:

$$\dot{m}^* = Y^* \, \mathbf{A^t} P^* \qquad (2.39)$$

The rationale of any guess-and-correct method is the determination of the corrections to apply to the guessed value, in order to converge to the exact solution. Therefore, rather than compute pressures and mass flows, it is of interest to compute their correction:

$$P' = P - P^* \; ; \qquad\qquad \dot{m}' = \dot{m} - \dot{m}^* \; ;$$

by means of the following equation, obtained from the difference between Eqs.(2.38) and (2.39):

$$\dot{m} - \dot{m}^* = Y \, \mathbf{A^t} P - Y^* \, \mathbf{A^t} P^*$$

In order to get a linear equation, an approximation is needed: the difference between the two pseudo-conductance matrices is assumed to be negligible ($Y = Y^*$). This leads to:

$$\dot{m} - \dot{m}^* = Y^* \, \mathbf{A^t}(P - P^*) \quad \rightarrow \quad \dot{m}' = Y^* \, \mathbf{A^t} \, P' \tag{2.40}$$

which links the pressure correction to the mass flow correction. A relation for the pressure correction P' in function of the guessed value P^* and the related $\dot{m}^*$ is obtained by rewriting the continuity equation (2.37) using the definition of $\dot{m}'$ and substituting Eq.(2.40):

$$\mathbf{A} \, \dot{m}' = -\mathbf{A} \, \dot{m}^* - \dot{m}_{ext} \quad \rightarrow \quad \mathbf{A} \, Y^* \, \mathbf{A^t} \, P' = -\mathbf{A} \, \dot{m}^* - \dot{m}_{ext}$$

resulting in:

$$\mathbf{H} \, P' = \gamma \tag{2.41}$$

with:

$$H = \mathbf{A} \, Y^* \, \mathbf{A^t} \; ; \qquad\qquad \gamma = -\mathbf{A} \, \dot{m}^* - \dot{m}_{ext} \; ;$$

Eq.(2.41) is the core of the SIMPLE algorithm, allowing the calculation of the corrections starting from the guessed values from the previous iteration step. For a complete discussion on the SIMPLE algorithm, it is worth underling that the algebraic problem in Eq.(2.41) has to be modified so to include the boundary condition on nodal pressure: the node in which the pressure is exactly defined will have a pressure correction $P' = 0$. It is essential that this condition be implemented in Eq.(2.41). So, once P' is determined, also $\dot{m}'$ can be computed with Eq.(2.40) and the new guessed values of pressures and mass flows may be calculated and provided to the next iteration step. It is worth mentioning that the corrections obtained by means of this method are often too large to guarantee stable computations. This is why under-relaxation strategies for the determination of $P^{*(new)}$ and $\dot{m}^{*(new)}$ are employed:

$$P^{*(new)} = P^* - \omega_P \, P' \; ; \qquad\qquad \dot{m}^{*(new)} = \dot{m}^* - \omega_m \, \dot{m}' \; ;$$

with ω_P and ω_m between 0 and 1. For under-relaxation factors close to one, the stability of the calculation is guaranteed but its convergence is considerably lowered down. An optimum relation between the factors may be derived following [102]. The slow convergence rate is one of the main drawbacks of the SIMPLE algorithm. On the other hand, it is a robust scheme, allowing getting a solution even though the initial guess on the pressures is very far from its correct value.

Now that all the equations have been described, a flow chart of the algorithm is given in Figure 3 in order to sum up the complete SIMPLE approach.
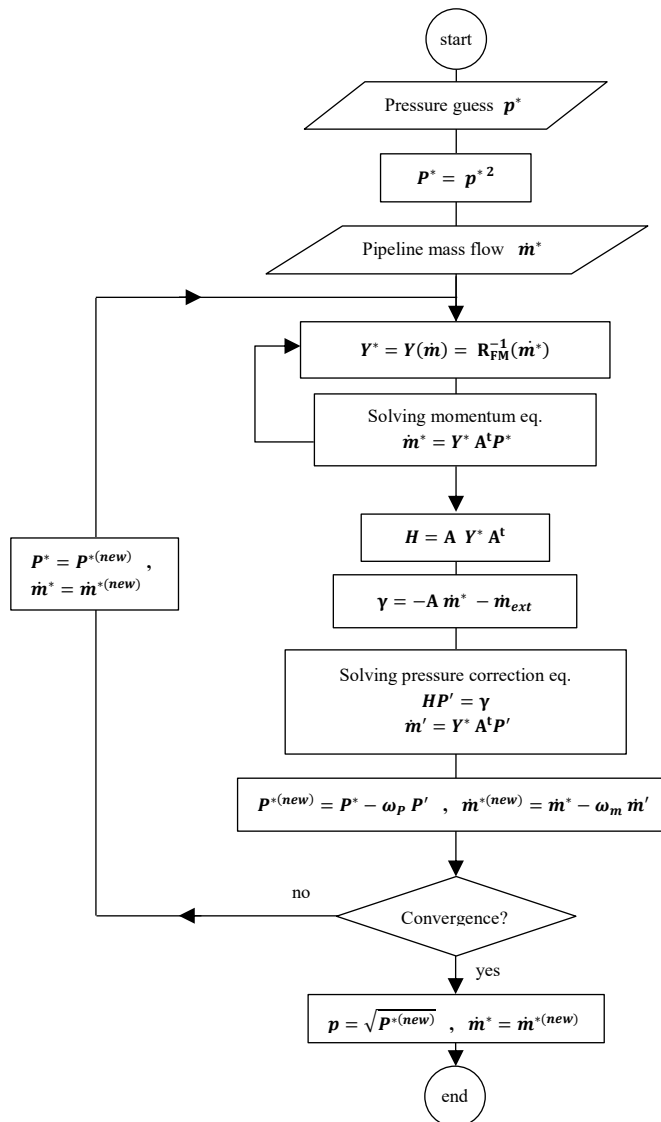
Figure 3 – Flow chart of the SIMPLE method for the calculation of the steady state initial conditions of the network

2.8   Multi-Component feature

The technological innovation brought about by the plans for the energy transition towards renewables has affected the gas sector too, in the recent years. Not only is the natural gas infrastructure considered to gain a fundamental role in complementing the renewable energy sources whenever they may be unavailable, but it will also have to host at least a fraction of renewable sources too. This means to allow alternative fuel gases such as bio-methane, syngas, synthetic natural gas (SNG) and hydrogen to be injected and blended along the gas network. The natural gas system is thus likely to be shifted towards a "multi-gas" system, able to handle gases whose chemical composition may considerably differ from the common local quality requirements. This implies that all what concerns the gas quality management, tracking and simulation is gaining more and more attention among the gas stakeholders. Indeed, this trend has started since the development of liquefied natural gas (LNG) facilities and markets, which allowed the admission of uncommon natural gas within gas networks that have always been run relying on the very well known gas qualities from the neighboring gas fields.

The algorithm of the transient fluid-dynamic gas network model described in the previous sections is complemented by a quality tracking section, extending the model to a multi-component one. The mathematical formulation based on mass and momentum conservation laws, as formulated by Eqs (2.1) and (2.2), needs to be complemented by the equation for the transport of any physical quantity, in this case, the molar composition $y_{(c)}$ of the cth element:

$$\frac{\partial y_{(c)}}{\partial t} + v\frac{\partial y_{(c)}}{\partial x} + D_x\frac{\partial^2 y_{(c)}}{\partial x^2} + \frac{1}{r}\frac{\partial}{\partial x}\left(rD_r\frac{\partial y_{(c)}}{\partial r} \right) = S \tag{2.42}$$

The version of the transport equation above is the most complete form, where besides the advective term $v\frac{\partial y_{(c)}}{\partial x}$, the axial and the radial diffusion terms are included, as well as the source term S.

In case of transport within pipelines, the problem is advection-dominated since diffusion coefficients are smaller by two orders of magnitude at least: in fact, bulk velocity v is often of the order of [m/s] while diffusion coefficients are always expressed in [cm/s]. What is more, the molecular diffusion coefficient is proportional to the inverse of the pressure [103].

For these reasons, only the following simplified formula is considered:

$$\frac{\partial y_{(c)}}{\partial t} + v\frac{\partial y_{(c)}}{\partial x} = 0 \tag{2.43}$$

in which the generation term S was set to zero because no generation is expected in the pipeline transport case. Eq.(2.43) is a first order PDE in time and space.

The solution for the transport problem is possible only by means of numerical approaches. A number of them have already been tested on natural gas quality tracking problems and they have been discussed in the technical literature.
In [104], two alternative methods have been compared: an upwind finite difference scheme in its implicit version and an explicit random choice method. The upwind finite difference is a common numerical method for the solution of advection-based problems. The spatial dimension is divided into a proper mesh and the derivative is approximated as a finite difference computed on the mesh points. It is in fact a first-order backward- or forward-difference approximation scheme, depending on the flow direction: assuming the velocity $v > 0$ then upwinding is obtained applying a backward difference scheme as follows:

$$\frac{\partial y_{(c)_i}}{\partial t} + v_i \frac{y_{(c)_i} - y_{(c)_{i-1}}}{\Delta x} = 0 \tag{2.44}$$

The time derivative is then approximated by means of the backward Euler differentiation formula, so to obtain a fully implicit scheme:

$$\frac{y_{(c)_i}^{t+1} - y_{(c)_i}^t}{\Delta t} + v_i^{t+1} \frac{y_{(c)_i}^{t+1} - y_{(c)_{i-1}}^{t+1}}{\Delta x} = 0 \tag{2.45}$$

In the field of quality tracking problems, this approach is the most recurrent, either the aim is to transport the gas composition or some gas features [105] or both [55]. More precisely, the spatial differentiation formulas that were chosen in [55] are more complex, higher order schemes which nonetheless relies on upwinding. For transport problems, the upwind feature, together with the choice of implicit methods for time differentiation, grants the stability of the solution for any choice of Δt and Δx as it is discussed in [106]. This turns out to be untrue for explicit methods, which may become unstable or conditionally stable. In the case of explicit upwind scheme, in order to have stability, the choice of Δt is bounded to the value of Δx and viceversa. The stability is granted if:

$$C = v \frac{\Delta t}{\Delta x} \leq C_{max}$$

where C is known as "Courant–Friedrichs–Lewy number" and $C_{max} = 1$ in case of explicit methods. This means that for a given Δx, the Δt cannot be deliberately large, which may turn out to be a limiting condition in pipeline simulations.

However, as pointed out in [104] and also experienced by the author, upwind-based methods are affected by severe numerical diffusion, especially if large gradients of the computed variable are to be transported along. This means that sharp changes in gas composition are smoothed out while translated along the spatial direction. This phenomenon is also observed and discussed in [56].

Numerical diffusion may be avoided using the second method analyzed in [104], called explicit random choice method and originally presented in [107] as a numerical method for the solution of nonlinear hyperbolic systems. Even though it is an explicit method, no stability restrictions such as the CFL condition are imposed (Courant–Friedrichs–Lewy). It is not based on integration formulas but rather on the solution of the Riemann problem followed by the construction of the piecewise constant random choice solution, by sampling the sequence of Riemann solutions. In this way, the shape of the spatial profile of the transported quantity is preserved. However, it has been noticed that the coupling of the sharp changes in the gas quality and the hydraulic problem solver causes oscillations on the computation of fluid-dynamic variables.

A total different approach for the pipeline simulation oriented to quality tracking is presented in [108], where it is performed a switch in the coordinate system according to which the conservation equations have been defined. The conservation equations for mass, momentum and energy (Eqs. (2.1) – (2.3)), as defined in section 2.1, are in fact expressed in Eulerian coordinates that is a system of coordinates fixed with the observer in which the fluid particles flows in and out. This generates all the first-order advective terms in the formulation of the equations, which generate the above-mentioned issues. Referring instead to the Lagrangian approach, the system of coordinates is integral with a control volume of the fluid, moving along with it, so all the advective related terms disappear. Each control volume should have invariant mass and composition, while the density changes according to the expansion or the compression of the volume itself. It is in [88] that a quality tracking method based on the Lagrangian approach is explained and applied. In [56], Chaczykowski uses the same method referring to it as the "batch method". More in details, a fully implicit finite difference method is applied to the conservation equations for the solution of the thermo-fluid-dynamic problem. The transport equation is then solved using two different methods, namely an implicit scheme and the "batch method", in order to perform a comparison between them and benchmarking the numerical results against field data from a number of real pipelines. It is found that, in terms of the determination of transport times (i.e. the moment in which a quality variation reaches the end of the pipeline), batch tracking is slightly better than the implicit method, but the figures are very similar. However, the implicit method is affected by numerical diffusion, smearing the sharp changes in composition and loosing much of the details of the known inlet composition profile. This issue is totally overcome using the batch method, which consists, in practice, in a rigid

translation of the composition profiles given at the inlet. This becomes quite clear after the detailed explanation of the method.

A "batch" is a volume of the fluid where the composition (or any other transported quantity) is assumed constant. This fluid element is defined by the coordinates of its starting point and its ending point. The position of the batch is given by means of the position of these points (b_h, b_{h+1}) in the Eulerian system of coordinates. The tracking method in the Lagrangian approach consists in the determination of the new position of each batch's limits at every time step:

$$b_h^{t+1} = b_h^t + v_j^t \, \Delta t \qquad (2.46)$$

Where v_j is the gas velocity in the jth pipe element, which have been computed from the solution of the hydraulic problem. This pipe element is delimited, instead, by the mesh points $x_{i,J}$ and $x_{i+1,J}$ that are fixed to the pipeline and corresponds to the points of the discretization mesh of the hydraulic problem. A set of pipe element between two junction nodes (nodes at which more than two branches are connected) belongs to the same pipeline J.

Whenever:

$$x_{i,J} \le b_h^t < x_{i+1,J}$$

the point b_h is translated with velocity v_j, as in equation (2.46). At the moment when b_h gets out of the interval it means that the batch has completely flowed out the pipeline element, and the velocity computed in the adjoining element mesh should be computed. The graphical representation in Figure 4 is given for clarification.
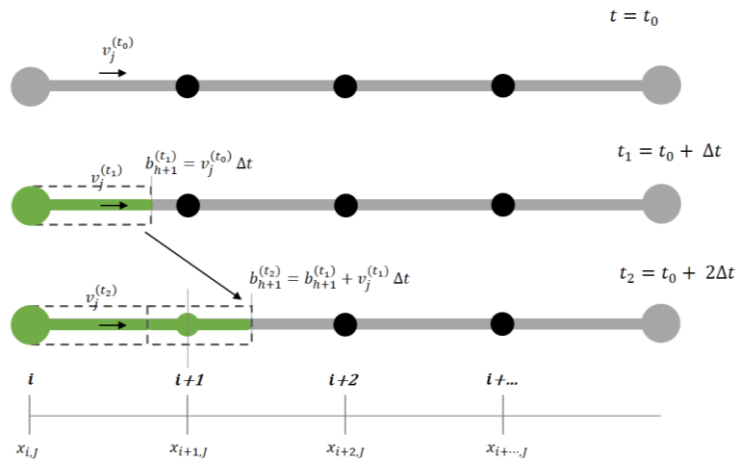
Figure 4 – Graphical representation of batch tracking method principle

When the computation of all the new positions of the batches is completed, the batch tracking algorithm needs to provide a sampling section in order to update the set of information about the composition (or other transported quantity) of the gas at the fixed mesh nodes, according to the following rule:

$$\left[y_{(c)}\right]_{i,J}^{t+1} = \left[y_{(c)}\right]_h \qquad if \qquad b_h^{t+1} \leq x_{i,J} < b_{h+1}^{t+1}$$

For any new time step $t + 1$, the gas composition vector at the sampling point i of the pipe J is the one of the batch h if the position of the sampling point $x_{i,J}$ lies within the gas batch.

The assignment of a composition value to the pipe elements is also important in the integration of the batch-tracking algorithm with the hydraulic model, since many gas properties are defined on the pipe element rather than the junctions.

Different approaches may be considered: either the composition of the element inlet node is assigned to the whole pipe, or average or weighted average approaches are applied.

It is important to highlight that, even if the batch tracking method has the advantage of avoiding numerical diffusion thus preserving the shape of gas quality variation, it is affected by propagating errors in the computation of the batch translation. Eq.(2.46) is in fact an application of a dead reckoning technique: each new position of the batch ends b_h^{t+1} is determined starting from b_h^t, which is computed, in turn, in a similar way. The errors are therefore cumulative and grows as the time.

The batch-tracking algorithm is perfectly suited for the quality tracking along a single pipeline structure. When dealing with more complex topological structures such as networks, it may lose its effectiveness because batches loses their definitions as the fluid mixes up or it is split at junctions. A specific set of equations are needed in order to complement the batch tracking with the mixing phenomena at junctions. For this reason, they are defined at junction nodes i^*, where more than two branches are connected. The set of pipe sections j between two contiguous junction nodes i^* defines a pipeline J (pipeline between two junctions).

This system of equations mainly consists in the application, at each junction i^*, of the continuity equation in the form of Eq.(2.26) for each component c of the composition vector $[w]_i$, expressed in mass fraction:

$$\left[\sum_j a^+_{i^*,j} \dot{m}_j^{t+1} + \dot{m}^{(+)t+1}_{ext_{i^*}} + \frac{V_{i^*}}{c^2\,\Delta t}\left(p_{i^*}^{t+1} - p_{i^*}^t\right)\right]\cdot\left[w_{(c)}\right]_{i^*} =$$

(2.47)

$$= -\sum_j a^-_{i^*,j}\,\dot{m}_j^{t+1}\cdot\left[w_{(c)}\right]_j - \dot{m}^{(-)t+1}_{ext_{i^*}}\cdot\left[w_{(c)}\right]_{ext_{i^*}}$$

where:

$$a^+_{i^*,j} = \begin{cases} +1, & \text{edge } j \text{ is outgoing from junction node } i^* \\ 0, & \text{edge } j \text{ is incoming to junction node } i^* \\ 0, & \text{edge } j \text{ has no connections with junction node } i^* \end{cases}$$

that is the generic element of the matrix $\mathbf{A}^+$;

$\dot{m}^{(+)t+1}_{ext_{i^*}}$ is the withdrawn gas flow from junction node i^*;

$$a^-_{i^*,j} = \begin{cases} 0, & \text{edge } j \text{ is outgoing from junction node } i^* \\ -1, & \text{edge } j \text{ is incoming to junction node } i^* \\ 0, & \text{edge } j \text{ has no connections with junction node } i^* \end{cases}$$

that is the generic element of the matrix $\mathbf{A}^-$;

$\dot{m}^{(-)t+1}_{ext_{i^*}}$ is the injected gas flow in junction node i^*;
and:

$\left[w_{(c)}\right]_{i^*}$ is the mass fraction of the component c at the junction node i^*; it is the unknown of the equation, resulting from the perfect mixing of the incoming fluxes.

$\left[w_{(c)}\right]_j$ is the mass fraction of the component c at all the adjoining nodes that are connected to the junction node i^* through the jth pipe.

$\left[w_{(c)}\right]_{ext_{i^*}}$ is the mass fraction of the component c within the mass flux that is injected from outside in the network.

Under a perfect mixing assumption, the mass fraction of component c that originates at junction node i^* is given by this following relation:

$$\left[w_{(c)}\right]_{i^*} = \frac{-\sum_j a^-_{i^*,j}\,\dot{m}_j^{t+1}\cdot\left[w_{(c)}\right]_j - \dot{m}^{(-)t+1}_{ext_{i^*}}\cdot\left[w_{(c)}\right]_{ext_{i^*}}}{\sum_j a^+_{i^*,j}\,\dot{m}_j^{t+1} + \dot{m}^{(+)t+1}_{ext_{i^*}} + \frac{V_{i^*}}{c^2\,\Delta t}\left(p_{i^*}^{t+1} - p_{i^*}^t\right)}$$

(2.48)

This last formula can be rewritten in a proper matrix form on the basis of the given definitions of the special incidence matrices ($\mathbf{A}^+$, $\mathbf{A}^-$).

Thus, combining the nodal mixing equation and the batch tracking approach in the same algorithm it is possible to extend the gas quality tracking from a

simple pipeline to complex network structures. For each new time step, the composition resulting from the mixing at each junction node of the gas network is considered as the first batch that is inserted into the downstream pipeline. The subsequent batch-tracking module of the algorithm, applied to each pipeline, is then devoted to translate each gas batch along the pipelines, updating the gas composition at their end node. A flow chart of the quality tracking section is given in Figure 5
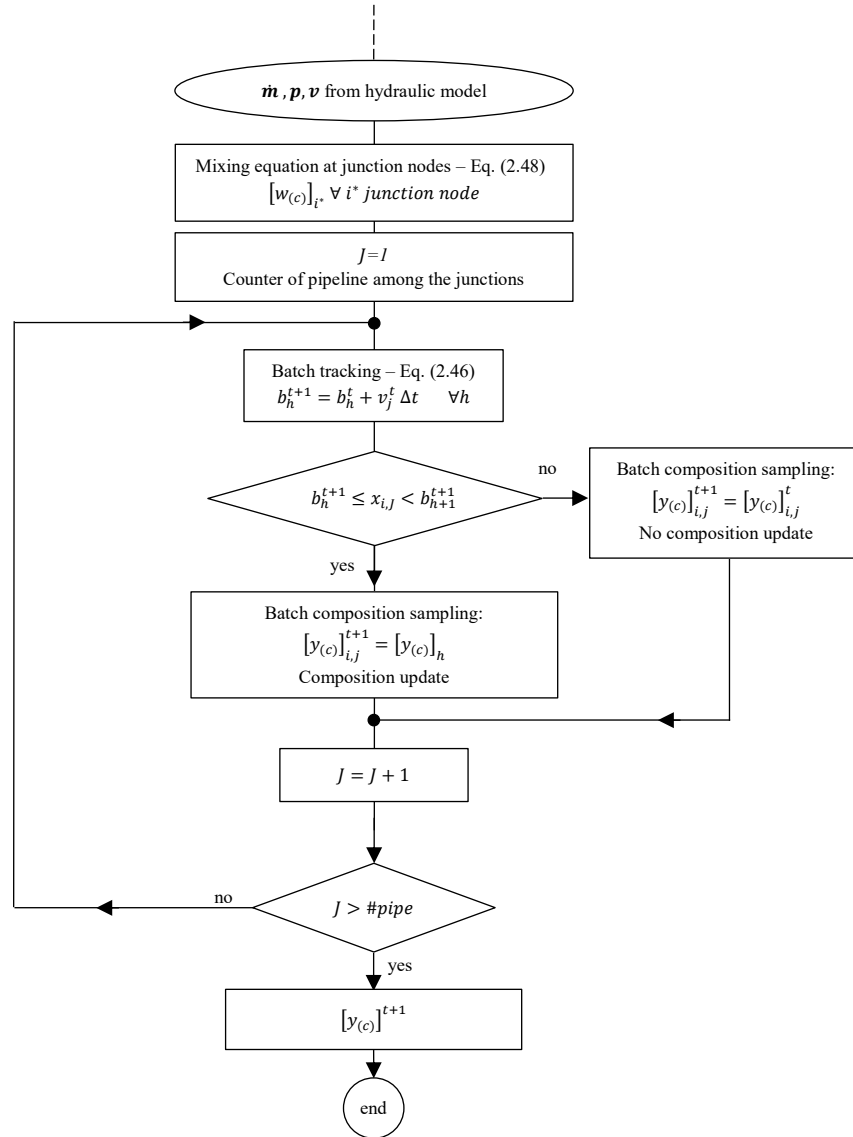
Figure 5 – Flow chart scheme of the quality tracking section of the gas network model.

2.9   Algorithm

In order to develop a simulation framework able to solve a transient model of a natural gas network with gas quality tracking, all the computational sections described in this chapter have been integrated in a single algorithm that is described by the flowchart in Figure 6. It is composed of two main parts: the transient hydraulic model and the gas quality section. These two cores are nested within an iterative computational cycle because of the interdependency between the hydraulic status of the network and the gas composition: properties in the hydraulic model depends on the gas composition flowing through each part of the network. On the other hand, the modifications of the gas quality depends on the fluid-dynamic status of the network that is a result of the hydraulic solver part. Thus, an iterative procedure is needed in order to get the convergence of the results.
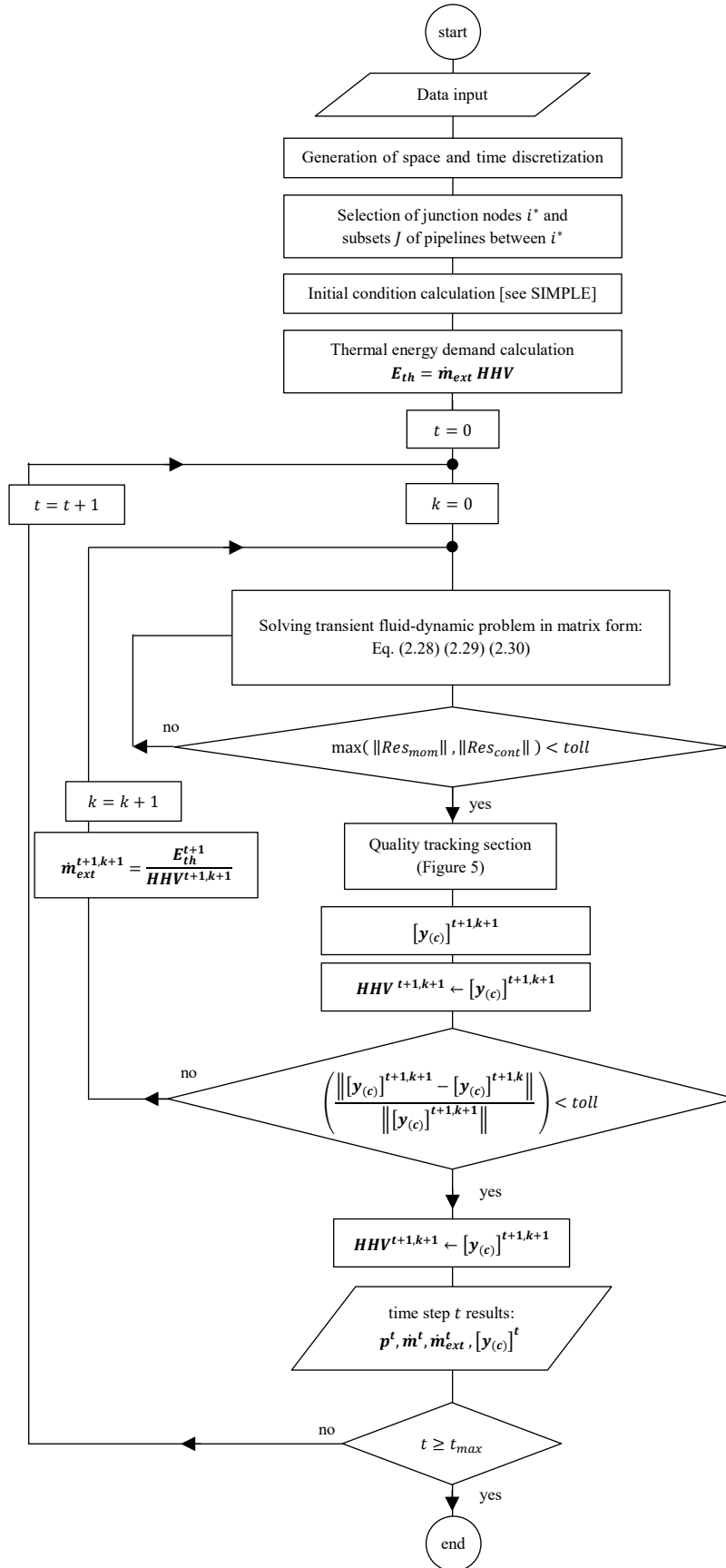
Figure 6 – Synthetic flow chart of the complete architecture of the algorithm for gas network simulation under transient and multi-component conditions.

2.10 Model Validation

The transient and multi-component fluid-dynamic model of the gas network presented in this work is validated in the following sections.

Firstly, the hydraulic part is evaluated on a simple test network that is recurrent in the literature ([109],[110],[90],[111],[112],[113] and [96]). Results have been compared to check the correct behavior of the fluid-dynamic algorithm and evaluate possible differences originated from the variations of the model. Since not all the information about the natural gas of the test case are provided (e.g. the gas composition), a sensitivity analysis is also performed. The effect on the pressure prediction of the different friction factor formulas is also investigated.

In a second step, the quality tracking section of the model has been evaluated by comparison with an analogous model in literature, presented in [56], where the model results have been tested on experimental data.

2.10.1 Fluid-dynamic validation

A triangular gas network, as first introduced in [109], has been taken as a sample network for the fluid-dynamic model validation. Results have been benchmarked with the ones obtained by [109], [110], and [96] where results from the commercial software SIMONE [114] are also provided and here reported as a further benchmark.

The network topology is depicted in Figure 7. The gas enters the system from node 1, in which a pressure set point is given, while nodes 2 and 3 are both consumption nodes.
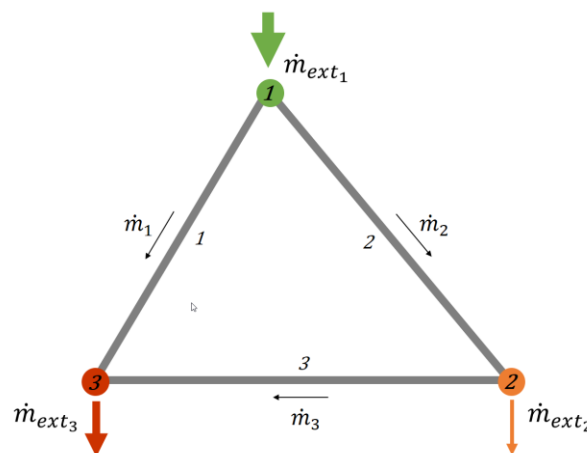
Figure 7 – Topology of the triangular network used for the validation of the model

The network technical data are given in Table 2. The pipeline roughness ε is assumed to be equal to 0.012 mm as in [96], being a typical value for the transport pipelines.

Table 2 – Network topology and technical data.

Pipe	Inlet node	Outlet node	Diameter [mm]	Length [km]	Roughness [mm]	N° sections
1	1	3	600	80	0.012	1
2	1	2	600	90	0.012	1
3	2	3	600	100	0.012	1

Concerning the gas properties, the relative density is approximately 0.6 according to all the sources. Only [110] and [90] specify that the fluid density ρ is 0.7165 kg/m^3 at STP (T = 273.15 K and p = 1 atm) which is exactly equal to the density of pure methane. No sources specify the reference gas composition, thus leaving to the multi-component model here presented some degrees of uncertainty, which will be investigated through a sensitivity analysis. Similarly, the friction factor is estimated in different ways among the different references: [109] and [110] do not take into account the pipeline roughness while in [96], the Hofer approximation of the Colebrook-White correlation is used in order to rely on an explicit formula. The behavior of the model using different friction factor formulas is also investigated in this section.

On an operational side, the gas temperature is assumed constant and equal to 5 °C (T_g = 278.15 K), as all the reference gas model are isothermal ones. As for the boundary conditions, the pressure set point at node 1 is kept constant at 50 bar (see Figure 8.a) while the consumption nodes 2 and 3 follows the consumption profiles given in Figure 8.b.
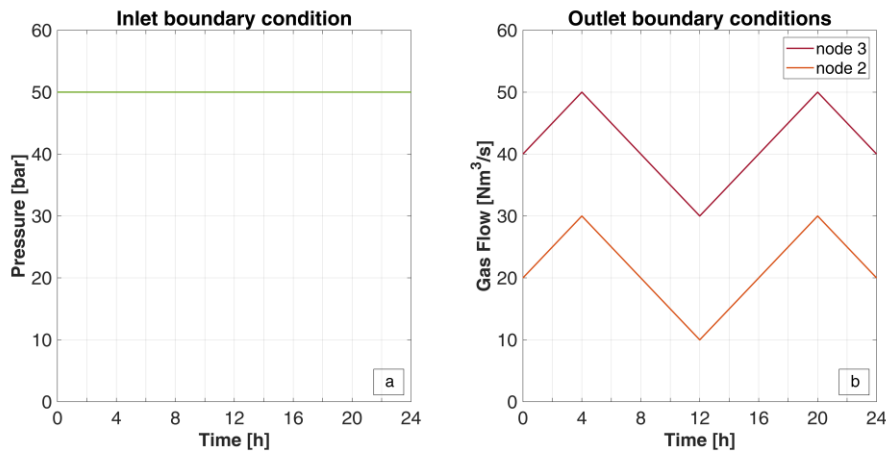
Figure 8 – Boundary conditions for the simulation of the triangular network. a) pressure set point at the inlet node; b) gas withdrawal profiles for the gas consumption node.
Reference conditions are set to T = 273.15 K and p = 1.01325 bar .

At last, space and time discretization are assumed equal to the ones in reference [96], in order to have a fair comparison between the results: the pipes are discretized considering just one section per pipe (the pipe itself), while in [109] and [110] pipelines are discretized in 10 and 5 segments respectively. Concerning the time discretization, a $\Delta t = 180$ s is considered and the total simulation interval lasts 24 h. In the next sections, the sensitivity analysis on the Δx and the Δt is also addressed.

Validation on literature results

In this first round of validation, the model was run using as friction factor formula the implicit version of the Colebrook-White as presented in Eq. (2.8), in order to be as close as possible to the assumption in [96]. Following this rationale, the fluid properties of the natural gas were defined by choosing a gas mixture with the following composition:

Table 3 – Natural gas composition chosen for the validation against the literature data.

Inlet node	CH$_4$ [%$_{mol}$]	N$_2$ [%$_{mol}$]	CO$_2$ [%$_{mol}$]	C$_2$H$_6$ [%$_{mol}$]	C$_3$H$_8$ [%$_{mol}$]	Higher C [%$_{mol}$]
1	92.8	0.9	1.2	4.2	0.9	0

which gives a Relative Density exactly equal to 0.6. However, the fluid density differs from the one declared in [90] and [110], being equal to 0.77 kg/Nm^3.

The pressure prediction results are given in Figure 9 for both the consumption nodes and they are compared to the pressure profiles resulting from the model in literature.
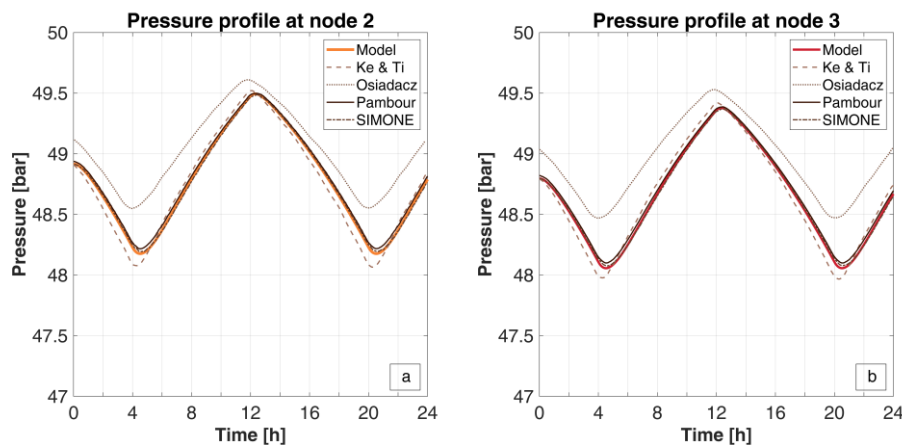
Figure 9 – Comparison between the computed pressures at node 2 (a) and 3 (b) and the results from literature.

It is possible to see how the pressure at the demand nodes follows the consumption profiles with a little delay, by decreasing its value whenever the gas withdrawal increases and vice versa. The results are very similar to the ones obtained by Pambour [96] and its reference results from the software SIMONE, as one could expect, since the computational architecture is very similar. The minor differences may be given by the choice of a different equation of state that have been employed (GERG-2008 rather than the Papay formula [115]) and of the friction factor formula. The different assumptions on the friction factor calculation in [109] and [110] are probably the main reason for the major differences in the pressure prediction. Anyway, the mean deviation on pressure prediction for both the nodes is well below 1% for any of the references taken from the literature. Detailed results are given in the following Table 4.

Table 4 – Summarizing table of the relative mean deviation [%] of the outlet pressures predicted by the current model from the benchmarks in literature.

Node	Ke & Ti [%]	Osiadacz [%]	Pambour [%]	SIMONE [%]
2	0.14	0.53	0.06	0.02
3	0.14	0.61	0.06	0.02

Concerning the mass flow prediction, either along the pipelines and at the injection node (node 1), no results are available from reference [109] and [110], so only the data from [96] have been considered as benchmark.

In Figure 10.a, the average mass flows along the pipelines of the network are displayed. One should refer to these quantities as "average" because no pipelines were discretized in subsections, so each pipeline is associated with a single value of mass flow, rather than a profile along the space dimension.
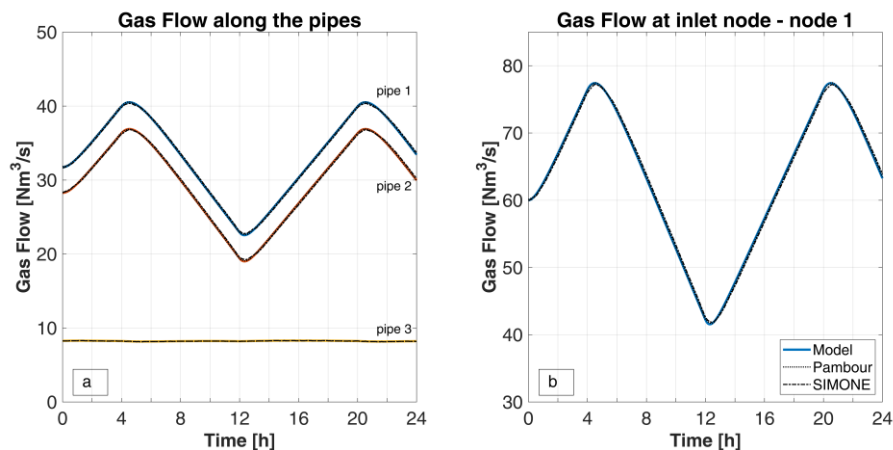
Figure 10 – Comparison between the computed gas flows along the pipelines (a) and at the inlet node (b) and the results from literature.

From the test case results, it is possible to note that the fluctuations of the gas consumption reflects on the mass flow of the two pipelines directly connected to the entry node. Pipeline 3, which connects the two consumption nodes, does not show these high fluctuations but rather acts as a balancing buffer for the gas supply to the consumption nodes. Its fluctuations are almost negligible because the gas consumption pattern is followed instead by the calculated mass flow from the supply node, which is pressure controlled at a constant pressure of 50 bar. This profile is given in Figure 10.b, where the delayed response of the supply node to the demand ones can be observed, if compared to the profiles given in Figure 8.b. In this case too, the deviations are marginal (less than 1%). Detailed results are given in the following Table 5

Table 5 – Summarizing table of the relative mean deviation [%] of the gas flows computed by the current model from the benchmarks in literature.

benchmark	Pipeline 1	Pipeline 2	Pipeline 3	Inlet node
Pambour [%]	0.2	0.2	0.2	0.6
SIMONE [%]	0.5	0.6	0.2	1.2

The transient feature of the model are best represented in Figure 11, where the variation of the total linepack is provided. The linepack consists in the amount of gas that is stored within the geometrical volume of the network or of any portion of it (i.e. pipelines or section of pipelines). It is calculated by means of the following formula, valid for any edges j of the network:

$$LP_j = \frac{A}{c^2} \int_{x=0}^{x=l} p \, dx \Bigg|_j = \frac{\bar{p}_j}{c_j^2} V_{geom_j} \qquad [kg] \qquad (2.49)$$

The amount of gas that is stored depends on the local density of the gas, thus it depends mainly on the pressure level of the pipes and also on the temperature of the gas. As the pressures varies according to the variation at users' node, caused by the consumption pattern, the linepack varies as well, offering a buffer of gas which is readily available to provide or store gas whenever an imbalance between inlet and outlet occurs. The way the linepack varies is well displayed in Figure 11, where the results of the current model are similar to the results from Pambour's model and not so different form the ones form the SIMONE software. The deviation are around 0.5 % and 1 % respectively. It is worth noting that the main difference originates at the beginning of the simulation (thus the steady state). This is probably due to the differences in the determination of the fluid density, which depends on the choice of the chemical composition and of the equation of

state. An investigation on the effect on the linepack caused by the different chemical compositions is presented in one of following sections.
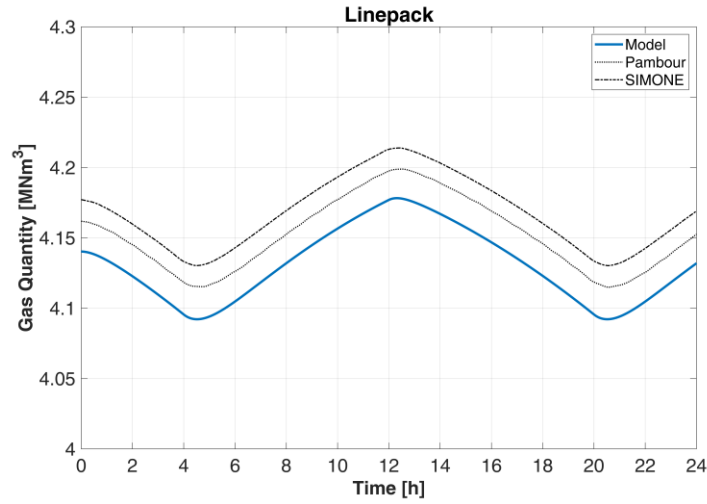
Figure 11 – Variation of the overall linepack of the triangular network

At last, the balance between the gas inflows and outflows is reported in Figure 12 and compared with results from [96]. This further indicator represents the time derivative of the linepack that means the rate of change of the gas stored in the geometrical volume of the network. Together with the linepack diagram, these figures show the buffering properties of a compressible fluid network.
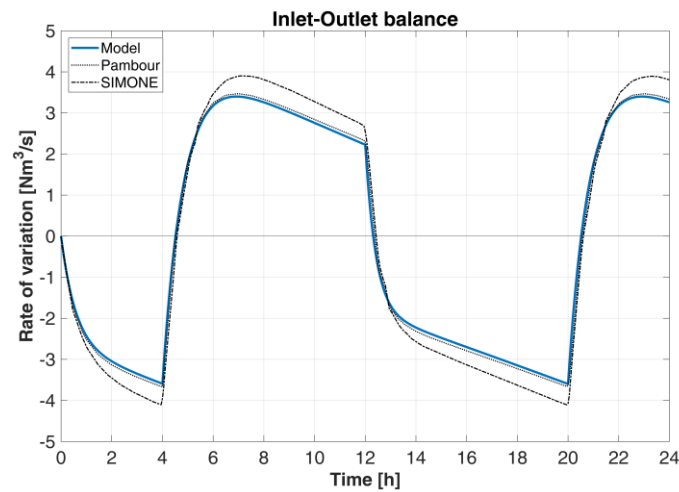
Figure 12 – Rate of variation of the amount of gas stored in the linepack of the network caused by the imbalances between inlet and outlet flows.

Effect of the friction factor formula

A second round of model validation was performed changing the friction factor formula in order to check the acceptability of the results and the impact of the friction factor choice, especially on the pressure prediction at the outlet nodes. The implicit Colebrook-White formulation has been substituted with the explicit Cheng formulation (Eq(2.10)), which is valid throughout all flow regimes.

Pressure prediction results are given in Figure 13 (a and b) for both the outlet nodes, together with the results from literature and from the previous trial using the Colebrook-White.
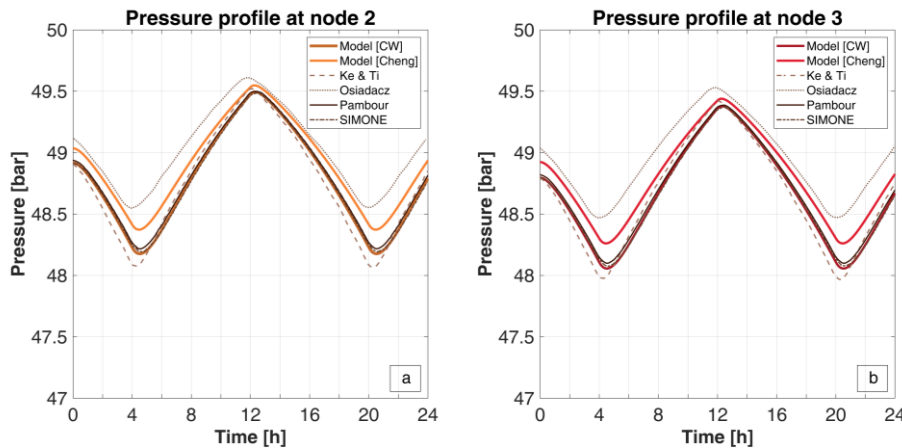
Figure 13 – Effect of the friction factor formula on the outlet pressure prediction: comparison between the computed pressures with the two different friction factor formula and the results from literature. a) pressure at node 2; b) pressure at node 3.

The pressures calculated using the Cheng formula results higher than the one calculated with the Colebrook-White version: the deviation is 0.3% on average. This is in line with what is depicted in Figure 1: the current test conditions correspond to a relative roughness $\varepsilon/D = 2\cdot10^{-5}$ and a Reynolds number around 4 $\div$ $5\cdot10^6$. This is the region where the Cheng friction factor and the Colebrook-White one differ the most, with the Cheng factor being lower. Thus, the results are justified. Even though the pressures calculated in this case deviates more from the ones resulting from [96] and [110], while approaching the results from [109], their average deviation is still well below 1%, making the Cheng formula a valid alternative in the choice of the friction factor correlation.

The differences on the pressure computation reflects also on the calculation of the mass flow rates, both along the pipelines and at the inlet node. The average deviations with respect to the pipeline mass flows do not exceed 1 % while for the mass flow at node 1, the deviation is slightly higher but still within 2 %. To be noted that the benchmark for the mass flow computations is only reference [96] in which the Hofer version of Colebrook-White relation has been used.

Interestingly, the choice of the friction factor has an impact also on the linepack variation as it can be observed in Figure 14. The linepack profile

associated to the Cheng friction factor is higher than the one associated to the Colebrook-White case. The curve is shifted upwards since the initial steady state as the pressure level is, on average, higher (due to the lower pressure losses). It is also worth noting that the new linepack curve does not run parallel to the ones from reference anymore, probably due to different choice of the friction factor formula.
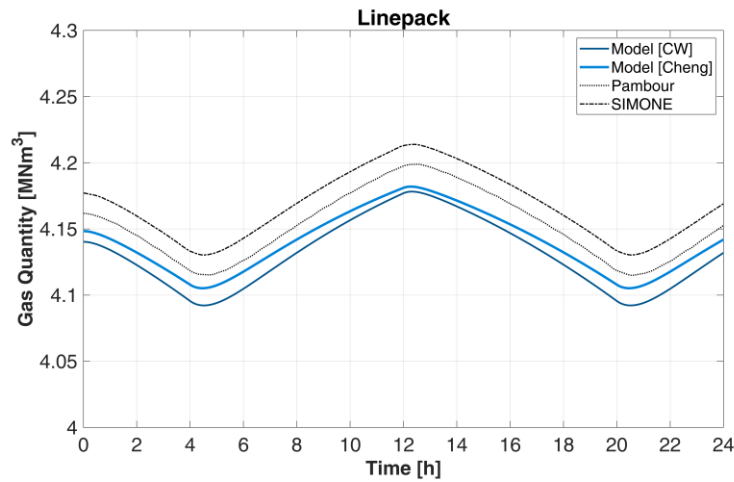
Figure 14 – Effect of the friction factor formula on the estimation of the variation of the overall linepack.

Effect of the Gas Composition

Since the composition of the natural gas considered in the references is not univocally determined it is of interest to investigate the effect of the choice of different gas qualities on the fluid-dynamic results. This is even more important considering that the model presented in this work is based on a multi-component feature so that is sensitive to the precise gas composition, by means of the GERG-2008 equation of state.

The model has been tested with a total of five different compositions: three typical European gas qualities have been considered and compared with the case of pure methane and with the case of the "guessed" gas mixture that was used for the previous speculations. The main features of the test gases are summarized in the Table 6.

Table 6 – Natural gas composition chosen for the investigation on the effect of the composition on the model. Data on the compositions from [116] except for "guessed" one.

Natural Gas type	CH_4 [% mol]	N_2 [% mol]	CO_2 [% mol]	C_2H_6 [% mol]	C_3H_8 [% mol]	C_4^+ [% mol]	Density [kg/Nm^3]	Relative Density
Nord Sea	90.81	1.91	1.32	4.73	0.82	0.41	0.7923	0.6132
Panigallia LNG	90.15	0.70	0.00	7.81	1.07	0.27	0.7881	0.6100
"guessed"	92.8	0.9	1.2	4.2	0.9	0	0.7751	0.6000
Russian	95.58	0.71	0.30	2.47	0.69	0.25	0.7545	0.5840
Methane	100	0	0	0	0	0	0.7165	0.5553

The comparison between the results and the references has been limited to the data from [96]. For this reason, the chosen friction factor formula is the Colebrook-White.

Pressure prediction results are presented in Figure 15 for both node 2 and 3. As it can be seen, the model is sensitive to the different gas qualities even though the pressure predictions result very similar and close to each other. This is wanted because the aim of this validation section is twofold: testing the model sensitivity to the gas composition while looking for the gas mixture that gives the best approximation of the results from literature (in which the Relative Density was provided as the only gas quality indicator).
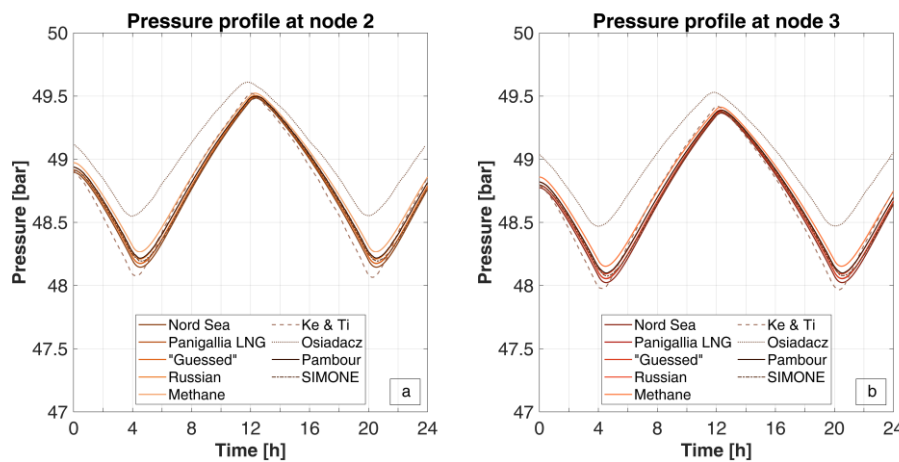
Figure 15 – Effect of the different gas composition on the outlet pressure prediction: comparison between the computed pressures with the five different gas quality and the results from literature. a) pressure at node 2; b) pressure at node 3.

As a general comment, it is possible to note that for both nodes, the lower the density of the gas, the higher the outlet pressure.

On the other hand, by comparing the average deviations of the different gas mixtures with respect to the results form Pambour [96] simulations and SIMONE software computations, it results that the Russian gas best approximate the

Pambour's curve while the Panigallia LNG gas best agrees with the SIMONE's one. In any case, the differences among all the average deviations are minimal, being all below 0.1% anyways. Similar observations may be done on the mass flows predictions.

The speculation around the role of the gas composition is more interesting when addressing the evaluation of the linepack evolution, as depicted in Figure 16. Depending on the gas composition, the overall network linepack deviates from the reference values between –2.2 % to + 0.7 %. To be noted that the different profiles all looks parallel. Thus, the differences are originated already at the beginning of the simulation, at the steady state initial condition, implying that the linepack is very much sensitive, of course, to the gas composition which affects the gas density at the operational pressure and temperature conditions. It is worth noting how the LNG gas is the one giving the highest estimation of the linepack even though its relative density is not the highest one. This is possible because at the operational conditions, it is the gas with the highest density.
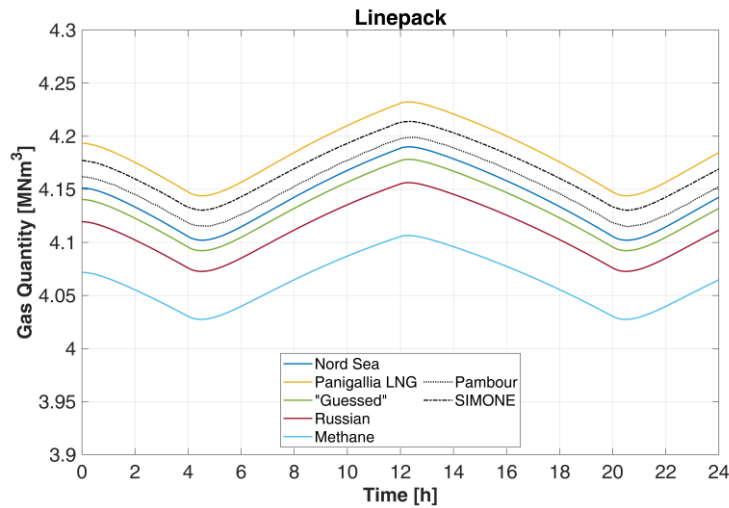
Figure 16 – Effect of the natural gas composition on the estimation of the variation of the overall linepack.

Sensitivity to the choice of Δt and Δx

To complete the validation of the model, a sensitivity analysis with respect to the space and time discretization choice is addressed in this section, in order check the computational behavior of the model.

As for the behavior of the solution with respect to the spatial grid, starting from the validation set up described in the previous sections, with a time step dt = 180 s and a only one section for each pipeline, the problem was solved increasing the number of the pipeline sections to 10 and 100. The latter case was considered

as the reference solution (the "exact" solution) to which compare the others. The errors where computed following this formula:

$$rel.\ err_{\%} = \frac{\|\chi_{trial} - \chi_{exact}\|}{\|\chi_{exact}\|} \cdot 100 \qquad (2.50)$$

where χ_{trial} is the generic quantity computed with a certain dx or dt.
The behavior of the relative error with respect to the dx size is given in Figure 17 for all the major fluid-dynamic quantities discussed before. As it can be noted, the solution improves with a second order slope for all the analyzed quantities. It is worth noting that, in any case, the errors are always lower the threshold of 1% for any of the analyzed variable.
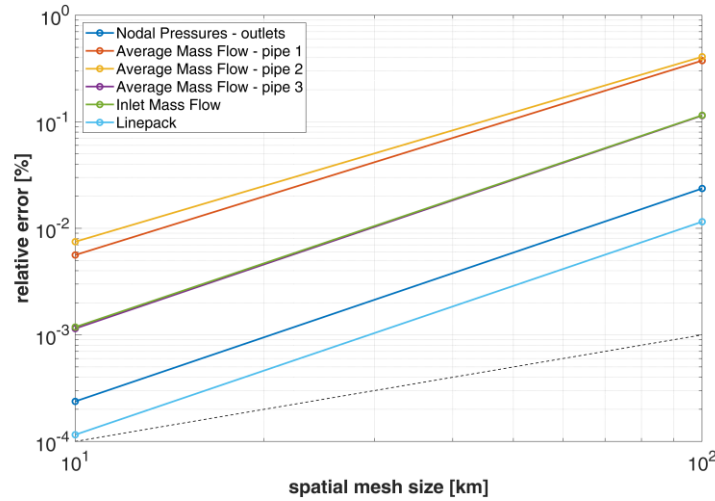
Figure 17 – Sensitivity analysis of the solution of the hydraulic network problem with respect to the spatial grid size. The dashed line indicates the 1st order slope.

Concerning the sensitivity of the solution with respect to the time discretization, the test case with the coarsest spatial grid was simulated with time steps ranging from 60 s to 3600 s (1 hour), over the timeframe of one day. The case with $dt = 60$ s was taken as the reference solution for the comparisons and the errors were computed following Eq.(2.50). Results are given in Figure 18 where it can be noted that the solution improves with a first order slope for all the analyzed quantities. With respect to the errors related to the spatial mesh, the ones related with time discretization are higher, thus the model is more sensible to improvement in time discretization. On the basis of these results, the choice of small time step (less than 1 hour) is to be preferred. This choice also depends on the rate of change of the boundary conditions of each specific modelling case.
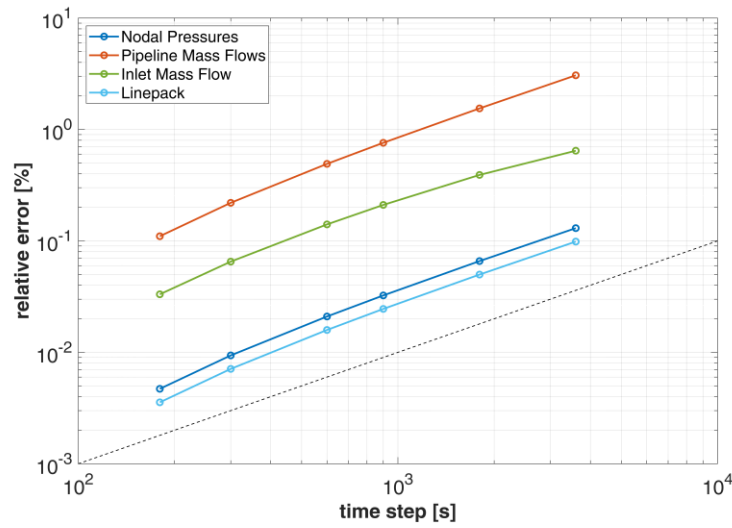
Figure 18 – Sensitivity analysis of the solution of the hydraulic network problem with respect to the time step choice. The dashed line indicates the 1st order slope.

2.10.2 Quality tracking validation

The quality tracking feature of the current model was validated by applying it to one of the validation cases reported in [56], where the batch method and the implicit method for the tracking of gas composition were benchmarked against real data.

A single pipeline belonging to the Polish gas transmission system was chosen. It is an 81.5 km-long onshore line, with an inner diameter of 693.8 mm (28 inches), which connects an underground storage facility to the rest of the network. No compressors are present on the line. The line was chosen because it is equipped with gas flow meters and gas composition measurement units at both ends, so to provide all the field data for the validation. In Figure 19, the measured quantities used as boundary conditions for the validation test are depicted. The outlet gas flow rate is given for all the time steps, while the pressure is always defined at the inlet node. The gas composition should be fully provided at the inlet node, for any time step of the simulation. In Figure 19.c, the temporal evolution of the concentration of ethane is given, as it is considered as the tracer-gas for the evaluation of the quality tracking capability. Data are available both at the inlet node (as a boundary condition) and at the outlet node (to have the benchmark term). As for the other gas components, no information were made available by the authors. Similarly, assumptions about the inner roughness of the pipeline and about the gas temperature or the ground temperature were omitted.
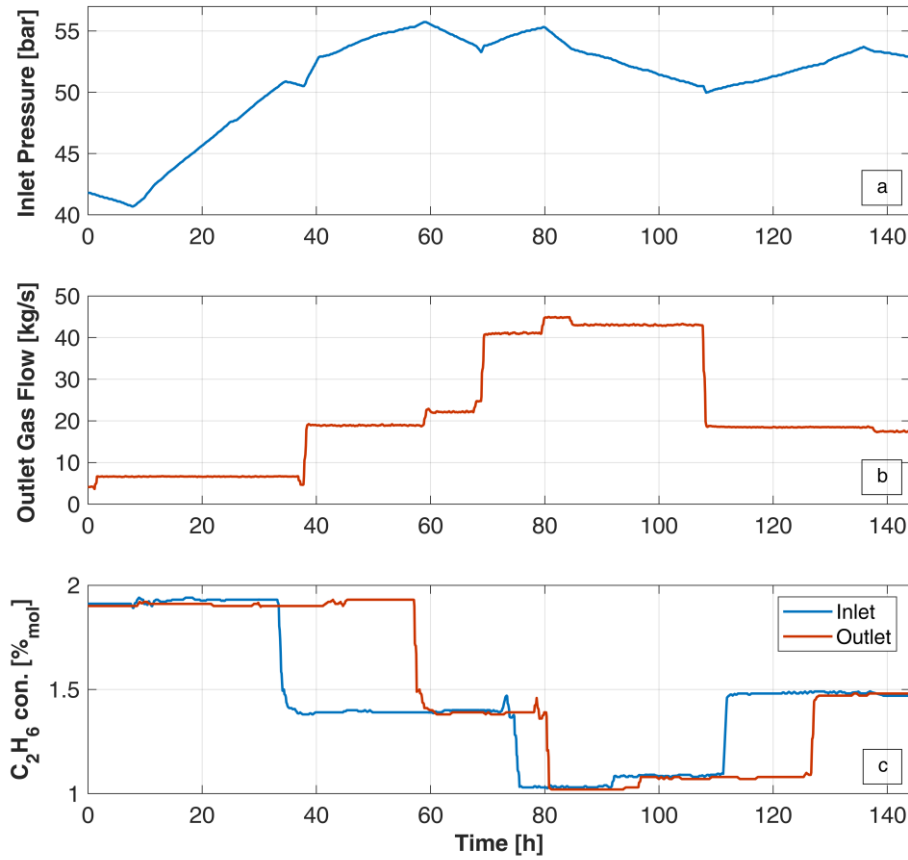
Figure 19 – Measured quantities for the quality tracking validation as available from [56], used as boundary condition to the numerical problem; a) inlet pressure profile; b) outlet gas demand; c) molar concentration of the ethane at the two ends of the pipeline, considered as the tracer gas for the quality tracking validation

In order to run the simulation, an inner roughness of $\varepsilon = 0.012$ mm and a gas temperature of 5 °C were assumed, considering the gas always in thermal equilibrium with the surrounding ground. On the numerical side, the simulation was run dividing the pipeline in 80 sections, so to have a space discretization of around 1 km. As for the time step, the choice was 5 min and the whole simulation concerns 6 days in total. These assumption are the same as in [56] so to have a fair comparison.

The result of the current model benchmarking against the field data available in literature is given in Figure 20, where the profile of the molar concentration of ethane measured at the pipeline outlet is compared to the calculated profile.
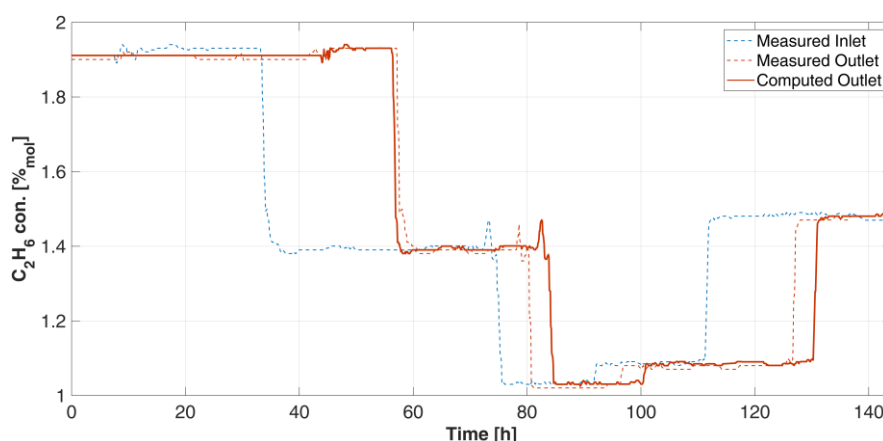
Figure 20 – Comparison between the computed (solid orange line) and the measured (dashed orange line) composition profile of ethane at the outlet. The measured composition profile at the inlet node is also given for an estimation of the variations of arrival times.

As a first general comment, it is worth noting that all the major steep changes in the composition profile, which appears at the inlet node, have been well replicated at the outlet. This would not have happened if the Euler implicit scheme had been applied. Thus, no numerical diffusion phenomena are introduced. In order to quantify the accuracy of the calculated profile with respect to the field measurements, it was chosen to refer to the arrival time of the composition perturbation to the end of the pipeline. In particular, the three major step variation are focused. As it can be seen, the model is able to predict closely the arrival time of the first concentration step: the difference between the estimated arrival time of the model and the measured arrival time is about 50 minutes. In terms of accuracy, this time mismatch should be compared to the measured value of the transportation time, that is, for this case, equal to about 24 hours. This gives an error on the calculated transportation time of about 3.5 %. As for the others two steps, the model delays in the calculation of the arrival time of about 4 hours and 3.5 hours respectively, with grater relevance on the transportation time errors given that, especially for the second step, the transport time is lower, due to higher mass flow rates.

The batch-tracking model, as mentioned in section 2.8, cumulates some inaccuracies as the elapsed time grows, since it is based on a dead-reckoning technique for the computations of the batch position. However, this error source cannot explain the behavior of the errors of the addressed cases. The motivation for the computed mismatch may be originated instead form the isothermicity assumption of the current model. In fact, errors on the transportation time comes from errors on the estimation of the gas velocity, which depends on the gas flow rate and on the density, which is, in turn, a function of the temperature. A sensitivity analysis on the gas temperature showed that transportation times are affected by the choice of the temperature as it is shown in Figure 21. In general, computed transport time reduces as the assumed temperature is higher.

Specifically, transportation times are reduced by between 30 minutes to 1 hour every 10 °C of temperature increase, depending to the velocity and pressure fields. This improves the prediction for the second and the third composition step, while it worsen the first one.
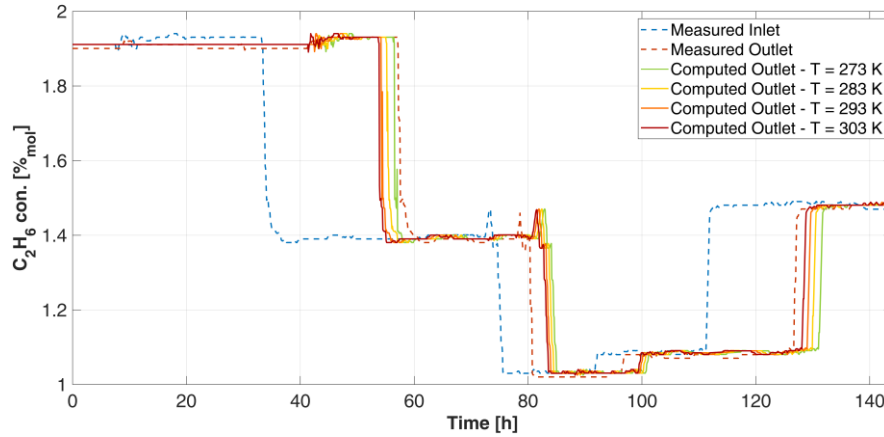
Figure 21 – Influence of the gas temperature on the estimation of the outlet profile of the molar fraction of ethane.

It is important to underline that the model presented and benchmarked in [56] is a non-isothermal one, thus solving the hydraulic problem taking into account the energy equation too, in order to consider the effect on the fluid-dynamic of the changing inlet temperature and the thermal interaction between the gas and the ground. It is likely that over the 6 days of the simulation, the gas temperature within the pipe varies because of the thermal interaction with the ground and a varying temperature at the pipe inlet, thus reducing the transport times with respect to the isothermal case. However the author does not know this temperature pattern.

In conclusion, the quality tracking part of the gas network algorithm gave satisfactory results in terms of composition profile replicability, avoiding the non-physical diffusion effects that were encountered in other algorithms in the literature. This is considered as an important feature when trying to extend the quality tracking exercise from a single pipeline case, to a network case, where fluxes admix together and unphysical composition profiles may spread all over the infrastructure.

Considering the lack of information on the thermal status of the pipeline and of the inlet gas, as well as on the pipeline inner roughness assumptions, the estimations of the transport times are also satisfactory, provided that the assumption of isothermicity could be applied to the whole infrastructure all over the timeframe of the simulations.

2.11 Conclusions

A fluid-dynamic model for the simulation of gas network with complex topology has been proposed in this chapter and is the tool that will be used to perform studies of the impact of renewable gas injection and blending within the current gas infrastructure.

For this reason, the model needs to be based on transient fluid-dynamic equations and has to feature a quality tracking section. What is more, the choice of the equation of state must be so that the gas composition variations should be detected and accounted for.

On the basis of the validation procedure against literature results and the numerical analysis on the spatial mesh and on the time discretization, the whole model architecture gives satisfactory results, both concerning the fluid-dynamic section and for the quality-tracking feature.

Considering the advanced characteristics of the equation of state that have been chosen (GERG-2008) the current model can be applied either to high-pressure transmission level infrastructure or to lower-pressure distribution grids. The sensitivity to the composition of up to 21 typical components of the natural gas make it versatile for the modelling of natural gas with uncommon composition such as higher content of hydrogen or CO_2. For gas network operating conditions far from the phase transitions of its higher hydrocarbon and its main components, this model can be considered suitable for any modelling scenario, including cases almost pure hydrogen in blending contexts.

As for the quality tracking feature, given the batch-based tracking method, the presence of any components which is carried around at the same velocity of the bulk fluid can be traced (either it is one of the 21 considered by the equation of state or any impurities or trace compound). The extension of this method to a complex and interconnected set of pipelines may bring sometimes to non-convergence or inexact solutions which takes place when very low velocities and flow direction variations occurs within some pipes.

In the next three chapters, the model will be applied on three case studies regarding distribution system infrastructure in which biomethane and hydrogen is injected in order to show the model potentialities in tackling specific issues related to the injection practices.

Chapter 3

Biomethane injection at distribution level

3.1   Introduction

According to the European Biogas Association's (EBA) Statistical Report 2018 [117], bioenergy in Europe has known its major expansion almost a decade ago with the number of installed plants multiplied by a factor of 3 between 2009 and 2016, and with Germany, UK and Italy as leading countries as biogas producers [118]. Within the Italian context, the biogas production chain has rapidly grown since 2008 in the direction of electricity production, thanks to a very favorable feed-in tariff [119] that brought to the rise of a huge number of small scale ($< 1MW_e$) biogas power plants, largely fed by energy crops [120]. This policy has helped to bring the Italian energy system to reach the European goals of the 20-20-20 program for what concerns renewable share in the electric power production and the global energy system. However, concerning the goals on the penetration of renewables in the transport sector, Italy is still lagging behind the goals of 10 % of bio-fuels in the entire transport sector [121]. This is why these later years, Italian policy has strongly committed towards the promotion of biomethane production and injection into the natural gas infrastructure.

Biomethane is defined as a fuel gas produced from biomass whose properties are comparable to the ones of natural gas [122]. At present, it is mostly produced from the upgrading process of biogas produced by anaerobic digestion. In fact, the

biogas from anaerobic digestion contains between $30 \div 60$ % of CO_2 together with smaller amounts (traces) of contaminants such as hydrogen sulfide and ammonia that have to be cleaned out. While the biogas cleaning is performed anyways to make the gas exploitable, the upgrading phase is peculiar to the biomethane production and consists in the separation of the CO_2 form the biogas, so to obtain a high-methane gas (more than 95%). In order to be allowed in the natural gas value chain, the biomethane is in fact required to have quality parameters within the same range of the fossil natural gas usually transported by the network.

The gas system is in fact a highly interconnected system at national and continental level, which is mainly based on a widespread network infrastructure. A relative small amount of fossil gas fields and sources (such as LNG terminals), which delivers most of the natural gas, are connected to the industrial and residential customers by means of the gas network. In the past, the management of the gas quality has already been a tackled issue, because different gas field may delivers different gas quality. Sometimes, the difference is so high that two different infrastructure are run. This is mainly the case of The Netherlands and a portion of Germany infrastructure, where a low calorific value network runs from the Dutch domestic fields (Groningen and the north see ones) to feed mainly households users and an high calorific value network feeds the industrial ones. According to this rationale, any gas fed appliance is tested and commissioned to work safely and efficiently on specified gas quality ranges, assuming a certain stability of the natural gas type.

In the past few decades, with the growth of LNG facilities, gas quality management issues started to rise again. The problem is becoming even more urgent since the biomethane sector started to develop.

Biomethane plants may be considered as a distributed and renewable source of natural gas. Its injection within the current infrastructure appears to be the straightforward and most sustainable practice to contribute at the greening of the gas sector. However it is, to some extent, a revolutionary challenge for a sector whose state of the art has been settled since years.

In order to start the exploitation of biomethane, national and European technical regulation and standards were needed. At the European level, the European Commission assigned to CEN (European Committee for Standardization) the mandate M/475 EN [32] on standardization of biomethane injection criteria. It ended with the promulgation of the EN 16723 standard [33], directly implemented in Italy in the technical standard UNI/TR 11537:2016 [34]. While the European standard [33] states generally that biomethane has to comply with the typical ranges of the fuel gases which belongs to group H (higher heating value fuel gas), the national standards set more stringent and specific limits on compounds that are not usually present in the natural gas but may appear in traces in the biomethane. For example, according to the Italian technical norm, compounds such as hydrogen sulfide, ammonia, halogens may have negative

impacts on the infrastructure and thus they have to be limited and continuously monitored. In case of non-compliance, any injection should be immediately stopped. In Germany, instead, the limits are different according to the type of gas network targeted by the injection [123]. Furthermore, in order to limit the impacts on the gas quality of the distributed gas, the system operators are often required to add a certain amount of LPG in order to increase the heating value, creating a gas with identical calorific properties of the one within the pipes, so to avoid any billing issues [124]. This is said to be an expensive part of the biomehtane upgrading and conditioning and it may be avoided by means of the adoption by the system operators of suitable quality tracking systems in order to comply with accuracy requirements in billing processes. This is particularly impactful on the business of Distribution System Operators (DSOs), which use to operate local and lower pressure portions of the infrastructure, which never had to deal with "unconventional" distributed sources of gas.

Not only did biomethane introduce the quality management challenge at all the levels of the natural gas infrastructure, but it also brought about the issues of the mismatch between production and consumption, especially on the lower pressure level of the infrastructure where portion of the network insists on local areas characterized by seasonal and limited consumptions.

Concerning the European gas infrastructure, definitions of distribution level and transmission level may varies from country to country. Most of the times, it is defined as transmission infrastructures the set of pipelines that have a national relevance, carrying the gas from border to border thus being a part of the continental infrastructure. The distinction is also often made based on the operator that is in charge of the management of the infrastructure itself. This aspect, in particular, generates unclear and non-unique definitions especially for the distribution level, which may be regulated and operated differently throughout Europe. For instance, for what concerns the Italian situation, one single Transmission System Operator (Snam) is in charge of the national gas corridors and the directly connected regional branching. Instead, Distribution System Operators (DSOs) have in charge the lower-pressure networks, usually serving cities and smaller industrial areas, at a pressure level lower than 5 bar$_g$. For historical reasons, the number of Italian DSO is almost 500, while other countries such as Denmark, The Netherlands have a much smaller number. In Denmark and Germany, the DSOs usually run also higher-pressure portion of the network, insisting on greater areas. For the sake of precision in terms, in this work, the portion of the gas infrastructure characterized by lower operating pressure and serving a well-defined cluster of users will be addressed as "distribution network".

The biomethane injection into these confined portions of gas infrastructure is not a very common practice. In fact, most distribution systems serve urban areas whose consumptions are characterized by a strong seasonality. This may undermine the acceptability of any distributed source of biomethane, which is

instead quite steady in its production. Thus, even though distribution infrastructure may be located closer to the biomethane production plants and would not require any further gas compression, they are often discarded as injection option. The injection into higher-pressure transportation pipelines is then preferred even if it is more expensive, because it guarantees the access of the whole production, with no risk of curtailment due to production-consumption mismatch.

These mismatch issues at local level are well known to the system operators and they are faced differently by each country or by each system operator. The adopted solutions depends on the current status of biomethane grid injection and on the way the entire gas system is managed.

In Italy, the biomethane sector is at its early stage, even though it has known a remarkable expansion since 2018. Most of the plants that are currently injecting biomethane within the infrastructure are connected to the regional transmission lines, which are portions of the high-pressure transmission network, operated by Snam. At present (April 2020), the number of biomethane plant which have been authorized for the injection are 20. Among these, just three of them are already injecting at distribution level. Each distribution system operator (DSO) is entitled to follow its own procedures to evaluate the acceptability of biomethane injection requests. However, most gas DSO associations have published common guidelines which are concerned to guarantee the safety operation of the infrastructure [125]. In this sense, it is required that the biomethane injection point can never become the only gas feeding point of the distribution network. The network should always be fed by the traditional reduction station too, in order to guarantee the continuity of the service. Consequently, any innovative network management strategies, such as bi-directional gas reduction-and-metering stations and linepack buffering are excluded. Considering the strong seasonality of consumption in most of the areas served by distribution networks, these restrictions limit considerably the biomethane receiving potential of lower pressure infrastructures, with DSOs which may curtail biomethane injection during the late-spring and summertime months.
Circumstances are different in other countries in Europe.

In Denmark, for instance, the limited capacity of distribution networks have been solved by adopting probably the most straightforward solution: returning the excess biomethane production to higher pressure transmission level by means of compression stations, thus inverting the usual gas flow on demand (so called: bi-directional reduction and metering stations). The return plants must also be equipped with a proper de-odorization section since the gas in the transmission lines cannot contain any odorant. According to the latest system plan by Energinet (the Danish TSO) [126], two gas return plants were already in operation and three more were in a planning phase as of 2018. Interestingly, as detailed in [127], for one of the already operating plants, an additional connection with a nearby

distribution network which used to be separated was also planned, in order to distribute the biomethane throughout a greater consumption area.

Such solutions are conceptually simple and technically feasible even though they add capital costs to the injection projects. However, they require a very good level of coordination between the different parties of the gas network value chain as well as updates to the regulatory framework. These institutional aspects may act as a barrier to the early implement of these measures.

As for The Netherlands, the main Transmission System Operator (Gasunie) is taking part in *Projectgroep Groen Gas*, a working group of the Association of Energy Network Operators (*Netbeheer Nederland*) aimed to developing pilot projects to improve the biomethane acceptability within the current infrastructure. Among these, the case of bi-directional gas receiving stations is addressed too, together with more innovative projects aimed at generating a buffering storage capacity within the network itself. The latter, appears to be one of the less impacting solution in terms of capital expenditures, as it deals with the way the network is operated.

In this chapter, the transient and multi-component gas network model presented in Chapter 2 is applied to a real gas distribution infrastructure which has a limited receiving capacity of biomethane. An overview of the area is given, with a focus on the adopted method for the determination of the gas hourly consumption profiles. The impacts of biomethane injection under the business-as-usual scenario are assessed and discussed. In this scenario, the biomethane is always accepted because it is limited to the times of the year when consumptions are higher than production. The impact from the point of view of the hydraulic rearrangement of the network and from the point of view of the gas quality deviations are studied considering the effect of the choice of different injection point. Subsequently, the model is applied to situations of exceeding production (and thus curtailed injection) in order to assess the criticalities and to test, by means of simulations, scenarios of short-term gas storage within the network linepack in order to avoid or minimize the biomethane curtailment while operating the network within its technical limits.

3.2 Methodology

This chapter is devoted to the verification of the admissibility of a distributed source of biomethane into a low-pressure infrastructure (i.e. a municipal gas infrastructure).

A real municipal gas network was considered, thanks to the availability of data from a previous collaboration with a Distribution System Operator (DSO) [128]. The complete set of technical information about the grid is known together with the yearly gas consumption of each costumer. In the area, a biogas-based power plant is also located allowing for the construction of a possible scenario that consists in the conversion of the existing plant to a biomethane one, injecting its production in the distribution grid.

The complete network topology has been simplified. The current distribution network consists of two levels of pressure:

- a lower pressure level, highly meshed, which reaches most of the users in the most densely populated areas (the proper urban network);
- a higher-pressure level (up to 5 bar_g) which distributes the gas from the city-gate booths (the connection to the regional high-pressure network) to the secondary pressure reduction substations, which feed the lower level networks and most of the industrial users.

When assessing the biomethane receiving potential of a network, it is reasonable to limit the investigation to the higher-pressure portion of the infrastructure as it is the target for the possible connection. Lower levels of the network have too low pressures and a very limited capacity both in terms of volumes and in terms of overall consumption.

Consequently, a spatial clustering of the scattered users is performed, allocating most of the costumer to the nearest secondary substation.

In order to evaluate the feasibility of the biomethane injection within the distribution grid, a profiling of the yearly consumption of the users is needed, with, at least, an hourly time resolution. This is necessary in order to evaluate the receiving capacity of the gas network according to the overall gas consumption pattern, the operating pressure set points and the maximum operating pressure.

Once the biomethane production potential is known, the receiving potential of the network and its limits are assessed.

A preliminary analysis "out of the fluid-dynamic" is performed to check major bottlenecks caused by the mismatch between biomethane availability and consumption patterns. The relevant seasonality of the gas consumption throughout the year is usually a barrier against the biomethane acceptability during warmer months. By means of gas consumption duration curves, it is possible to evaluate the occurrence of biomethane curtailments.

For the times of the year when the biomethane is acceptable within the grid, a "business as usual" fluid-dynamic verification of the gas network is carried out by means of the application of the gas model described in Chapter 2. In particular, the day characterized by the maximum hourly gas consumption (January 17th) was selected. In order to evaluate the effects on the fluid-dynamic of the injection point location, different simulations have been performed and compared. These results are also commented from the point of view of the quality perturbations induced by the injection and blending of the biomethane within the network.

A similar network test is performed for the times of the year when biomethane exceeds the gas consumption of the area. In particular, the day with the minimum hourly consumption rate was considered (August 18th). The gas network has been simulated introducing a peculiar working condition, which required an implementation of a conditional boundary condition at the primary gas receiving station (city gate reduction station).

In fact, no reverse-flows of the gas receiving station are accepted because no re-compression stations are installed at that point. Thus under the circumstances of production-consumption mismatch, and more specifically, in case of abundant gas injected, gas accumulation occurs, increasing the pressure level of the whole network.

From the point of view of the computational model, when gas pressure becomes higher than the set-point value given at the pressure-controlled node (usually the inlet), an inversion of the gas flow happens at this node. This is in fact the only possible solution in order to comply with the pressure constraint of the boundary condition. Given that this is considered to be a non-realistic situation (at least for what concerns the Italian context), the network model has been adapted as follows. When the pressure field is so to imply an inversion at the city-gate, a change in the boundary condition is assumed, shifting from a pressure-control to a mass flow control, which is set to zero.

Thus, the following conditional boundary condition at the city-gate reduction station is given:

$$\begin{cases} p(i,t) = p_{set_i}(t) & if\ p_{set_i}(t) > p\,(i+1,t) \\ \dot{m}_{ext}(i,t) = 0 & if\ p_{set_i}(t) \le p\,(i+1,t) \end{cases} \qquad \forall\, t \qquad (3.1)$$

where i is the city-gate reduction station node and $i+1$ is the adjacent node. Referring to the boundary condition equation discussed in section 2.6.2 – Eq. (2.30), the coefficients will be modified as follows:

$$\begin{cases} k_{p,i} = 1, & k_{m,i} = 0, & \beta_i = p_{set_i}(t) & if\ p_{set_i}(t) > p\,(i+1,t) \\ k_{p,i} = 0, & k_{m,i} = 1, & \beta_i = 0 & if\ p_{set_i}(t) \le p\,(i+1,t) \end{cases} \qquad (3.2)$$

The case of gas accumulation within the linepack is thus considered and the measures for the improvement of linepack storage are tested.

At first, the pressure level set point is lowered by 1-bar steps, so to unlock linepack capacity, considering as the maximum acceptable linepack value, the one generated by a network that is set to 5 bar_g as operating pressure.

For each cases, the hydraulic verification of the network is performed for both the non-injection and the injection case. The first verification is needed to grant that nodal pressure does not drop below a minimum value. The second verification checks the gas accumulation curve and the network saturation time.

In a second phase, a reduction on the injected biomethane is imposed in order to modify the gas accumulation curve so to determine the proper balance among biometane injection, gas consumption and linepack accumulation, which guarantees the network to operate within its limits.

The injection scenario determined by means of this analysis, is then verified on a sequence of critical summer days, in which modifications of the pressure set points are also simulated in order to set up the case of modulating inlet pressures.

3.3 Case study description

The fluid-dynamic and multi-component transient model was applied on a real gas distribution network asset, serving a small urban and rural area located in the northern Italy. In the next sections, a description of the area, the gas consumption and its profiling is provided as well as a description of the network asset.

3.3.1 Area Description

The area served by the distribution corresponds to a small municipality composed of two urban agglomerations, three industrial areas and rural areas surrounding these major consumption centers. It covers a surface of 29 km^2 with a population of approximately 6,500 inhabitants. The total number of active gas meters in the area is equal to 3,262, of which 94% are classified as residential or tertiary users' gas meters while the remaining 6% are classified as industrial users' ones. The annual gas consumption of the area is equal to 8.25 MSm^3. Despite the proportions of the gas meters, the industrial users contribute to the 59% of the annual gas consumption of the whole area while the remaining 41% is imputable to the residential and tertiary sector. A summary of this information is given in the pie chart of Figure 22.
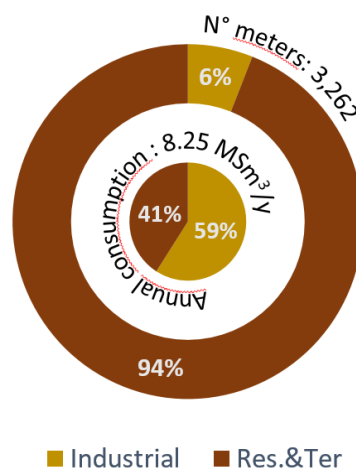
Figure 22 – Composition of gas customers and distribution of the yearly gas consumption between the registered user types.

3.3.2 Bioenergy availability

In the rural area, a biogas power plant of $1MW_e$ is present. Its location is given by the star in Figure 23. The electricity production is obtained by means of the combustion of about 12,000 Sm^3/d of biogas from dedicated crops. The composition of the biogas is 52 % of methane and 48 % of carbon dioxide.

In view to test the potentialities of a transient and multi-component simulation of the gas network, the bioenergy availability of the area is assumed to be shifted from the power production towards the production of biomethane. Given the biomethane flow rate, its injection within the distribution network infrastructure is evaluated by means of the gas network model.

Assuming a constant biogas production rate and an ideal upgrading process, the possible biomethane production rate downstream the upgrading section is 6,240 Sm^3/d corresponding to 260 Sm^3/h. This is the biomethane injection flow rate to be verified with the model, under different gas network working conditions.
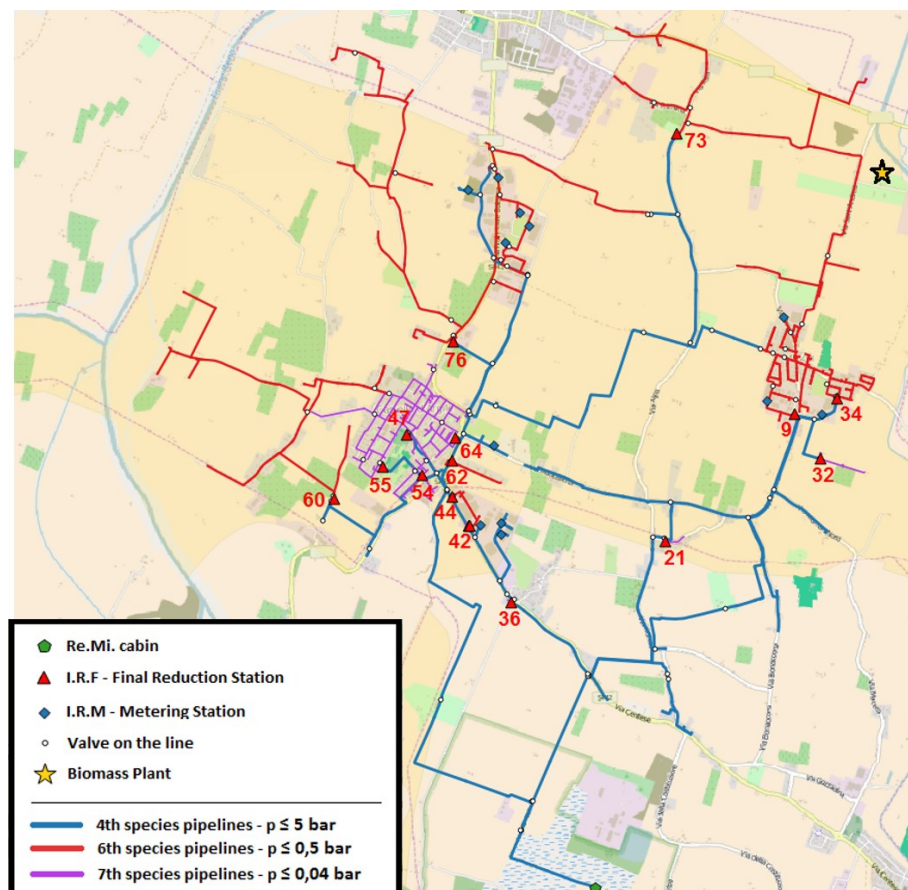
Figure 23 – Geographical layout of the whole gas distribution infrastructure.
The primary reduction station is depicted by the green pentagon in the bottom part of the map; the final reduction stations are depicted by red triangles (urban booths) or blue squares (industrial users); the pipelines belonging to the different pressure levels of the network are represented in different colors; the star indicates the position of the biomass power plant.

3.4 Data Pre-processing

3.4.1 Network features and schematization

As it is possible to see from Figure 23, the gas distribution network is fed by a single city-gate booth that is directly connected to the regional transport facility. In the city-gate booth, the gas is generally preheated in order to have its pressure reduced to the distribution network operating condition by means of a reduction valve. The pre-heating is required in order to avoid the condensation of the higher hydrocarbons or the formation of the methane clathrate, as a consequence of the sudden temperature drop caused by the Joule-Thomson effect.

The current network works on two pressure levels, with three different maximum operating pressures. At the city gate, the gas is set at constant pressure of 5 bar_g (maximum operating pressure for the medium pressure ducts – blue lines in Figure 23).

The medium pressure network serves the lower pressure levels by means of 15 final reduction stations (red triangles) that reduce gas pressure either to 0.5 bar_g (red lines) or to 0.04 bar_g (violet lines). These networks are highly meshed, usually following the layout of the streets of the urban areas in order to provide gas directly to the majority of residential/tertiary users and some of the industrial ones, especially if they are clustered within the urban or industrial areas. The remaining industrial users and a few of the residential ones, located in the rural areas, are directly connected to the medium pressure infrastructure (the blue squares indicates industrial reduction and metering booths).

For the sake of the modeling activity in this work, only the higher-pressure level of the gas network is simulated, consisting in the blue lines depicted in Figure 23. The schematic topology of the gas network is given in Figure 24.

The nodes represented by dots are the consumption points of the gas infrastructure (the numbering reflects the one in Figure 23 for the final reduction stations). Most of the single users are then clustered and the related gas consumption is allocated to the nearest final reduction station. The two triangles indicates the gas entry points. The yellow triangle represents the city gate, from which the fossil natural gas enters the network. The green one represents the biomethane injection node. This node has been chosen as the injection one being the nearest to the biogas plant.

It is worth underling that Figure 24 represents just the structure of the gas network in terms of connections between pipelines, thus the branch lengths are not representatives of the pipeline lengths. In terms of topology, the network is weakly meshed due to the presence of two loops. This is a common design feature of medium-pressure distribution gas network.
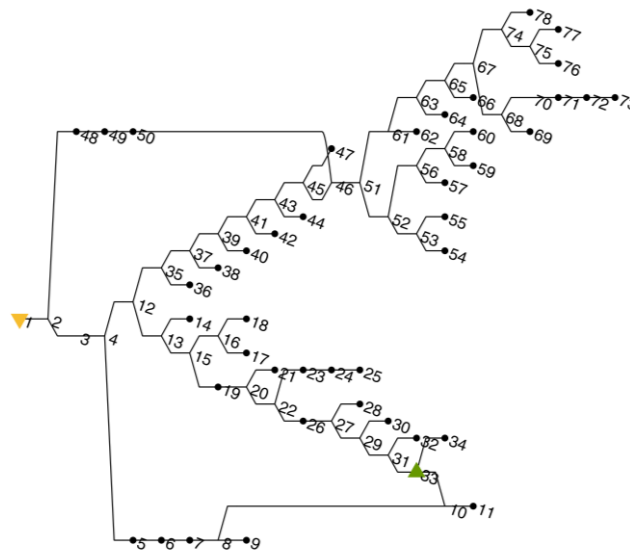
Figure 24 – Medium pressure topology of the gas distribution network.

This level of the gas infrastructure has a total length of about 34 km and it is made of pipelines with nominal diameter ranging from 25 mm to 280 mm. The total geometrical volume of the system of pipeline is about 250 m^3.

3.4.2 Gas Consumption profiling

In order to carry out a fluid-dynamic simulation of the gas network, the gas consumption rates of all the connected users have to be known with a suitable time resolution.

The availability of metered gas consumption data at time resolutions higher than the daily or the yearly base is very uncommon among the distribution system operators (DSOs), especially for households' final costumers. This is due to the lack of smart and telemetered gas counters. Usually, DSOs collects gas consumption data for each users on an annual basis and then applies a profiling procedure for billing purposes. This procedure is regulated by the Italian energy authority through resolution 229/2012 [129].

Within this resolution, the natural gas users are classified in seven categories according to the final use of the gas. Five out of seven refers to residential or tertiary users, with natural gas utilization ranging from cooking and/or domestic hot water (DHW) production only to space heating and to space cooling and possible combinations. The remaining two categories refers to industrial use, with natural gas utilization for technological purpose only or for technological purpose and space heating. For the sake of clarity, Table 7 summarizes the gas usage categories.

Table 7 – Gas usage categories according to [129]

Code	description	seasonality
C1	Space heating	yes
C2	Cooking and/or DHW	no
C3	Space heating + cooking and/or DHW	yes
C4	Space cooling and conditioning	no
C5	Space conditioning and heating	yes
T1	Technological use	no
T2	Technological + space heating	yes

For each of these gas usage categories, three additional withdrawal classes are assigned, depending on the weekly frequency of the use of gas (Table 8).

Table 8 – Class of withdrawal according to [129]

Code	Withdrawal days
1	7 days per week
2	6 days per week (excluding Sundays and national holidays)
3	5 days per week (excluding Saturdays, Sundays and national holidays)

Gas use categories and withdrawal classes are assigned in order to profile the annual gas consumption of each user throughout the year, on a daily basis.

Resolution 229/2012 specifies also the modality of the annual profiling procedure, providing a formula based on coefficients that are updated year by year, depending on the current calendar. The matrix of coefficient is also different according to the climate zone in which the area is located. In Figure 25 the result of the profiling procedure is given. Together with the daily gas consumption of the area, the biomethane daily availability is also given in order to compare consumption data with the injection source.
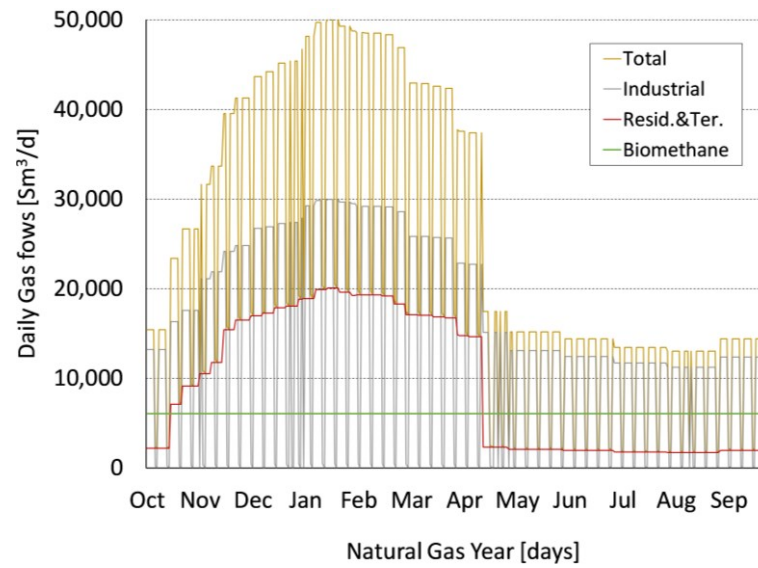
Figure 25 – Annual gas consumption profile and biomethane production on a daily basis [129]

The calculated daily gas consumption profiles are not suitable for a dynamic modeling of the gas network, being the characteristic time of the transient phenomena of the gas less than a day. For this reason, for each gas usage category present in the case study here addressed, a set of daily gas consumption profiles have been proposed and here reported in Figure 26. The profiles are the hourly fraction of the total daily consumption. The hourly profile of each user is obtained multiplying the daily consumption with the profile corresponding to the user category.
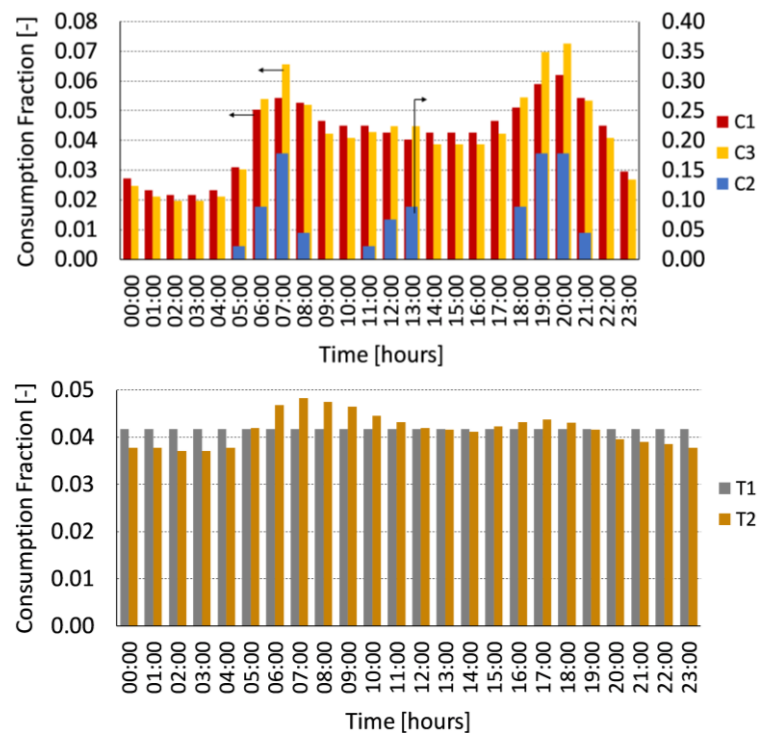
Figure 26 – Daily gas consumption profiles for the residential and tertiary users (above) and industrial users (below)

Higher time resolution (i.e. every 15-min) can be obtained by a linear interpolation of the hourly profile.

3.5 Biomethane injection – business-as-usual scenario

In this section, the impacts of biomethane injection within gas distribution infrastructure are considered. The case study described in the previous section is used to evaluate the acceptability of the biomethane that is possible to produce from the redesign of the already existent biogas power plant.

The biomethane acceptability limits are set by the current business-as-usual scenario, following the guidelines from the Italian DSOs associations [125]. The fluid-dynamic impacts on the network are evaluated by means of the application of the gas network model to the non-injection and the injection scenarios. The gas quality perturbation consequent to the biomethane injection is discussed.

3.5.1 Preliminary production-consumption analysis

The major (and most frequent) issue that may arise when injecting biomethane into a distribution grid comes from the mismatch between a constant production and the variable nature of the gas consumption. Particularly critical is the non-heating season, when gas consumption may drop to about $25 \div 30$ % of the winter peak (or even less), as it is already visible in Figure 25. Additionally, the consumption variations between weekdays and weekends may also turn critical, depending on the share of the industrial gas users within the area.

In Figure 27, the year-round total gas consumption on hourly base, as obtained applying the procedure of section 3.4.2, is compared to the hourly biomethane production.
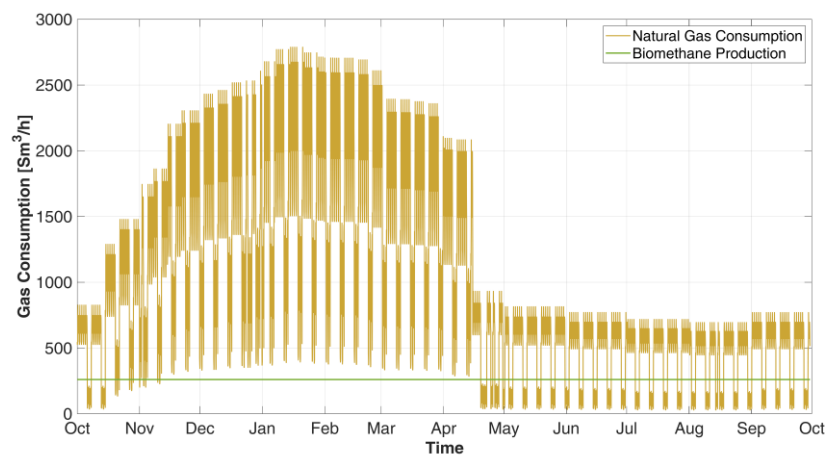
Figure 27 – Overall natural gas consumption profile on an hourly base for the entire year in comparison with the biomethane production rate that is available in the area.

As it is possible to note, the biomethane production is not always acceptable within the infrastructure. In fact, the biomethane production is completely absorbed by the overall gas consumption during most of the heating season (which formally starts on October 15th and ends on April 14th), while it is always exceeding the consumption during the weekends of the non-heating season.

Considering that distribution gas networks are usually managed in a passive way so that the inward gas flow rate at the primary reduction station is the result of the balancing of the overall gas demand of the area, whenever the production exceeds the overall consumption, the biomethane cannot be accepted in injection and it is cut-off the grid. This circumstance, otherwise, would imply the accumulation of gas within the pipeline and it cannot be handled by most of DSOs at present (it is also excluded by the guidelines [125]).

Under this business-as-usual approach, only a fraction of the yearly produced biomethane can be accepted in the network. This value can be retrieved from the following duration curves (Figure 28), which displays the allowable biomethane under two different assumptions.
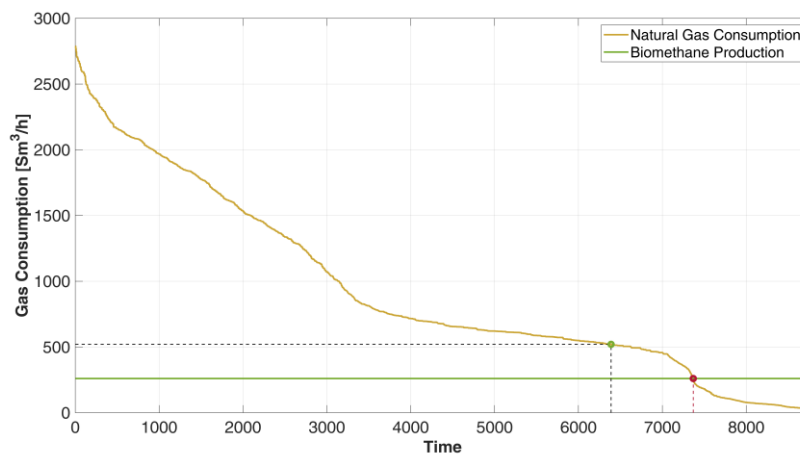
Figure 28 – Natural gas consumption duration curves for the whole area and biomethane production rate for the estimation of the injection curtailment criteria. Loose criteria: acceptability until biomethane injection equals the consumption (red dot). Strict criteria: acceptability until the biomethane injection is equal to the fossil-natural gas inflow (green dot)

The red dot and dashed line define the maximum amount of hours of biomethane acceptability under the least stringent constraint according to which the biomethane is always accepted provided that consumptions are higher or equal to the production. However, most DSOs may want to keep a safety-margin which basically consists in keeping the traditional city-gate reduction station always in operation, avoiding that the whole network would be fed exclusively by the biomethane injection [125]. This has a twofold purpose: on the one hand, it is a preventive measure in case of unexpected lower consumption rates; on the other, it prevents possible gas shortages in case the biomethane injection is stopped because of gas quality deviations or unplanned stop of the production.

A good rule of thumb is to consider that the traditional reduction station should provide at least half of the total gas consumption. This may result in a reduction of the accepted injection rate or, as for the case of Figure 28, the reduction of the timespan of acceptability of the whole production (green dot and black dashed lines). The obtained results are summarized in the following table (Table 9).

Table 9 – Results of the preliminary production-consumption analysis in the business-as-usual injection scenario under two different curtailment assumptions

Curtailment criteria	Yearly injection [MSm^3]	# hours	%
loose	1.91	7 369	84.1
strict	1.66	6 389	72.9

3.5.2 Verification of the network and fluid-dynamic impacts

When a certain amount of biomethane is allowed to a distribution network, a verification of the fluid-dynamic status of the network is required. Most often, this simulation is performed by means of steady-state network models which are applied to the worst-case scenario, that is, under a fluid-dynamic point of view, when the gas consumption rate is the maximum.

When managing a fully passive network (i.e. without compressors), the DSO has to guarantee to each downstream node of the network a sufficient pressure level: modifications on the gas fluxes throughout the network may increase in an unacceptable way the pressure drops along some pipes. Furthermore, the speed of the gas within each pipeline needs also to be kept within a limit. In the case of lower pressure network (local distribution networks) these limits are set by the technical standard UNI 9165 [130] and are reported in Table 10.

Table 10 – Fluid-dynamic operational limits for medium pressure (4th species) distribution networks

Parameter	Units	Range
pressure	bar$_g$	1.5 ÷ 5
gas velocity	m/s	< 25

In this case, a fluid-dynamic verification of the network was performed using the transient model presented in Chapter 2. The day with maximum gas consumption was considered and set as the simulation timeframe. The results

from the injection case were compared to the base case scenario where biomethane injection is not present. Results are given in the following sections.

When performing a fluid dynamic simulation of a gas network, at least one nodal pressure has to be fixed. In correspondence of the node at fixed pressure, the gas flow rate exchanged with the external environment is calculated accordingly. Under normal operating conditions, the pressure set point is fixed at the city gate of the gas network so that pressures throughout the network are determined according to the pressure drops along the pipelines and the gas inlet flux is determined by the summation of the all gas consumption contributions and the variation of the linepack.

Since the model is sensitive to the gas composition, the gas properties may change accordingly along the network. For instance, the gas heating value can change thus resulting in a different thermal power output at the consumption nodes. In this case, to account for this effect and to avoid possible power scarcity at the users, the assumption of maintaining the power demand satisfied is considered, as it is done in other references [21,54]. This implies that the network constraints at the loads are given in thermal power terms, converting the known gas consumption profiles into power demand profiles by means of the higher heating value of the fossil natural gas that is currently distributed (HHV_{NG} = 54.68 MJ/kg). Starting from the so calculated thermal loads, the mass flow rate that is requested at each outlet node is re-assessed using the local higher heating value, which depends on the composition that is expected at each node. This step is necessary because the hydraulic model is based on mass flows rather than energy fluxes. Each time the composition at the outlet nodes changes, the outlet mass flow rates needs to be updated and the fluid-dynamic re-assessed.

Under distributed biomethane injection, the pressure condition is still kept at the city gate boundary while the biomethane injection node is modeled as "negative" consumption node, thus a node with a fixed and net gas flows inwards the network. The pressure will be determined accordingly.

The current gas network is operated with a city-gate pressure set point at 5 bar_g . All the other nodes are assigned with an updated value of thermal equivalent gas consumption every 15 minutes. The injection node is assigned with a negative thermal equivalent gas consumption (thus a gas injection) which corresponds to 260 Sm^3/h of biomethane (HHV_{bio} = 51.23 MJ/kg). This injection is constant throughout the whole simulation period.

Fluid-dynamics impact of the biomethane injection

The results of the fluid-dynamic verification of the network are displayed in Figure 29, in terms of the evolution of the nodal pressure throughout the network. The node sequence is represented along the *x*-axis, giving the complete picture of the pressure field of the network. The time evolution of the pressure field is given

along the perpendicular direction, along the time axis (y-axis). To be noted that the node sequence is useful to give the complete and synthetic information for the whole network but information about complex connections (i.e. non-sequential) and about the network topology is sometimes lost. Thus, when sudden increase of the pressure are observed, it means a sequence of adjacent pipe has ended and the current node is connected to another series.

Figure 29.a reports the results of the base case scenario that consists in the gas network with no distributed injection, working under maximum consumption conditions Figure 29.b displays instead the fluid-dynamic verification of the gas network in case of injection of the whole biomethane production. In this figure, the pressure profile of the injection node (node 33) is highlighted in green.

It can be observed that the pressure variations throughout the day, in any point of the network remains within the operating pressure range [1.5 ÷ 5] bar$_g$.
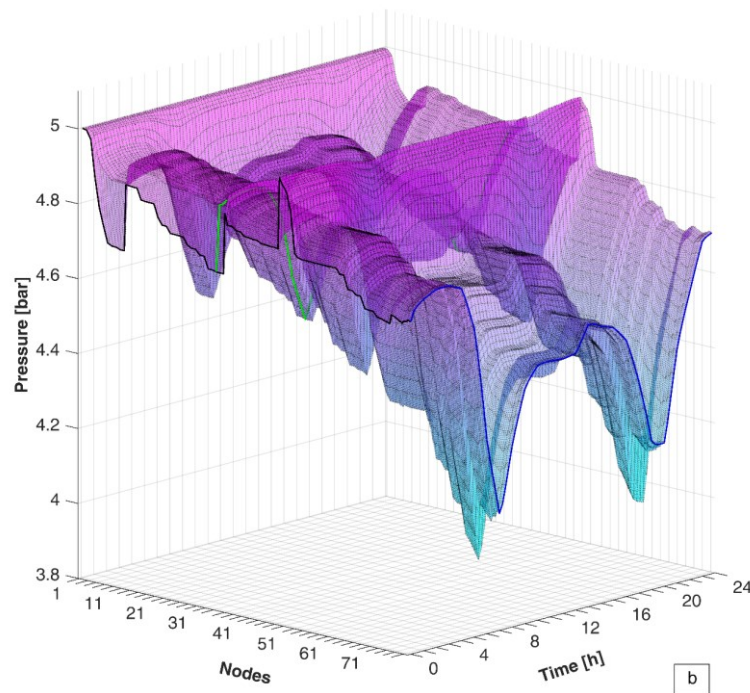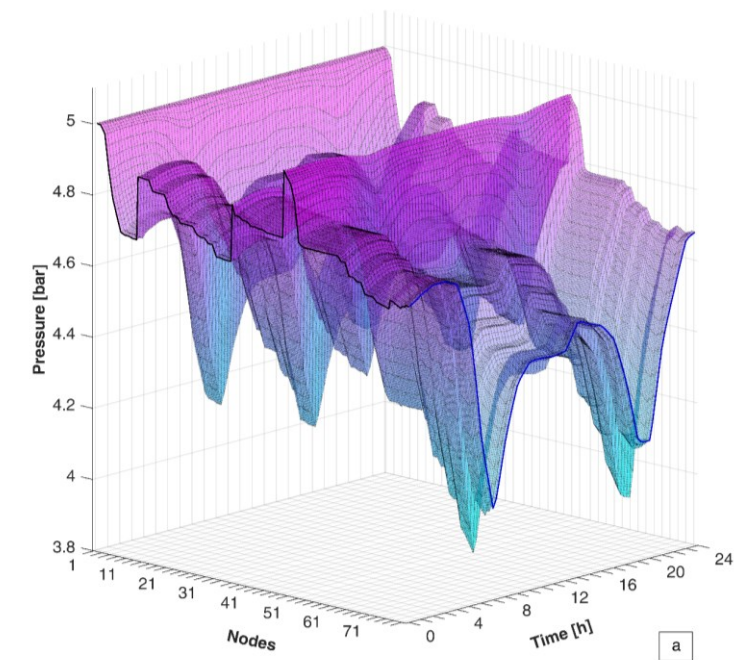
Figure 29 – Time evolution of the nodal pressure field throughout the network during the day of maximum consumption (Jan.17th) under the following scenarios: a) baseline scenario: no injection of biomethane; b) biomethane injection at node 33. The pressure evolution at the injection node is highlighted in green. The nodal pressure field is represented following the numbering sequence of the nodes, thus topological information about network connections are sometimes lost. A sudden increase of the pressure means that the previous sequence of nodes has ended and the node is connected to a previous one, with higher pressure. Along the perpendicular direction (y-axis) the time dependence is reported. The blue border of the surface highlights the pressure time pattern. The black border is intended to highlight the nodal pressure sequence. A similar pattern as the one in the following figure may be recognized.

What is more, from a comparison between the two figures, it is possible to note that, in the case of biomethane injection, the nodal pressures set to higher values than the ones in the base case scenario. The difference is more relevant for those nodes that are closer to the traditional reduction station. This is a consequence of the partial substitution of fossil natural gas by the injected biomethane. In fact, having a second source of gas, nearer to some of the users, reduces the overall gas request to the city gate and the gas flows along the pipelines which are the topological roots of the network (i.e. which carries the total gas consumption of the network). In this way, pressure drops along the pipeline located upstream the injection node are reduced, allowing for higher nodal pressure throughout the network.

In order to have a clearer picture of the difference in the nodal pressures between the two scenarios, Figure 30 is given. For the sake of clarity, couples of nodal pressure sequences, one for the base case (solid lines) and one for the injection case (dashed lines), are displayed for six different hours of the day, sampled every four hours.
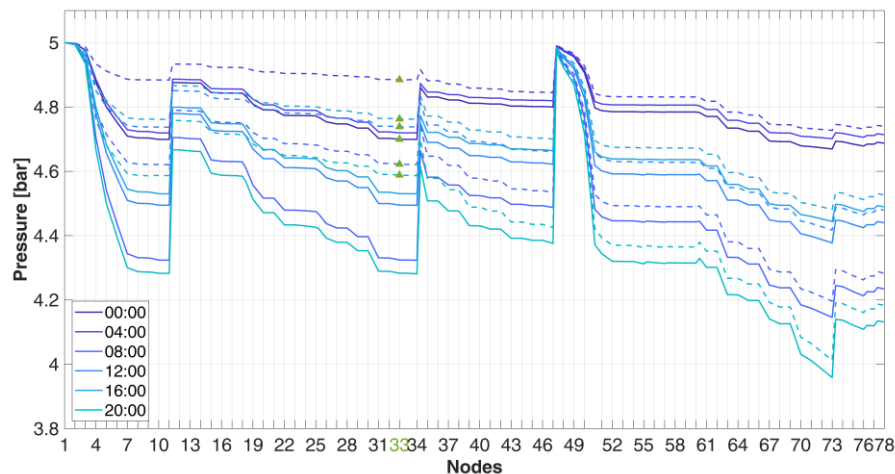
Figure 30 – Impact of biomethane injection on pressure profiles: comparison of the complete nodal pressure sequences between non-injection and injection scenario, for a selection of hours (every 4 hours). Solid lines: non-injection scenario; Dashed lines: injection scenario. The green triangle highlight the nodal pressure of the injection node.

Lines having the same color corresponds to the same hour; the lighter the color, the later the hour.

By means of Figure 30 it is possible to have a direct comparison of the pressure changes caused by the biomethane injection. The dashed lines are always higher than the corresponding solid ones, meaning that the overall pressure level of the network not only is preserved, but it is also increased, with no risk of insufficient pressure at the far ends of the network. This is a consequence of the peripheral position of the injection node. The presence of an additional source of gas located

downstream the main entry point and the main gas collectors allows the upstream part of the network to provide less natural gas, because a portion of the grid is served by the additional source. A decrease of the gas request at the traditional and main gas supply implies less gas fluxes along the pipeline and so lower velocity and lower pressure drops. This occurrence can be observed analyzing the different behavior that the nodal pressure deviations have upstream and downstream the injection node (node 33). The nodal pressure deviation observed in the first part of the network is remarkably higher than the one of the downstream nodes, which is more or less constant. A graphical representation of the nodal pressure deviation is given in the first bar plot of Figure 31. The quantities represented in there are the deviations of the generic quantity χ with respect to the base case scenario, calculated element-by-element according to this formula:

$$\boldsymbol{rel.\,err}_{\chi_\%} = \left.\frac{\chi_{inj.case}(i,t) - \chi_{base\,case}(i,t)}{\chi_{base\,case}(i,t)}\right|_t \cdot 100 \quad \forall\, i^{th} node\ or\ pipe \qquad (3.3)$$

The bar plots in Figure 31 refers to (from the top to the bottom) the nodal pressures, the pipeline mass flows, the pipeline velocity and the pressure drop (pipeline referred). These values are referred to a specific time of the simulation (t = 20:00). The deviations of the nodal pressures (blue bars) originates from the redistribution of the mass flows among the pipelines, as it is possible to see in the orange bar plot, which shows the deviations of the mass flows along each pipe. Branch 33, which is the first branch downstream the injection point, undergoes the highest impact, carrying almost all the injected mass flow. A small portion flows through branch 34, which is a direct connection to an outlet node (user node). This branch has its gas flow constrained to the user demand, thus the slight increase that is possible to note is due to a combination between the higher gas demand (consequent to the variation in the heating value – biomethane has lower heating value than fossil natural gas in this case) and the fluid-dynamic rearrangement of the network. Similar observations may be applied to branch 10. Most of the upstream branches (1 ÷ 31) reports instead negative or null mass flow deviations. Negative mass flow deviations are observed at the root pipelines (1 ÷ 4) and along the pipeline sequences that compose the loops. Null mass flow deviations regards branches directly connected to outlet nodes, which do not undergo gas quality variations. Interestingly, there is a whole subnetwork which is not affected at all by the biomethane injection: it is the tree-shaped network starting from node 51: the biomethane does not reach these portion of the network so the gas quality remains constant and equal to the one of the fossil natural gas. This implies no variations in the gas demand and in the gas flows throughout the pipelines, meaning that the velocity remains the same (see yellow bar plot) and thus pressure drops too (purple bar plot). The nodal pressure deviation (blue bar plot) is then

constant and positive throughout these downstream nodes, showing an increase of the pressure in this part of the network, as a consequence of the higher pressure level at node 51, originated by the fluid-dynamic rearrangement after the injection.

As for the velocity field modifications, even though the velocity deviation can reach more than +75% (as it is depicted in Figure 31), it does not affect the correct operation of the network. In fact, the overall maximum velocity in the case of biomethane injection is equal to 10.4 m/s resulting lower than the base case scenario (in which it is equal to 10.5 m/s).
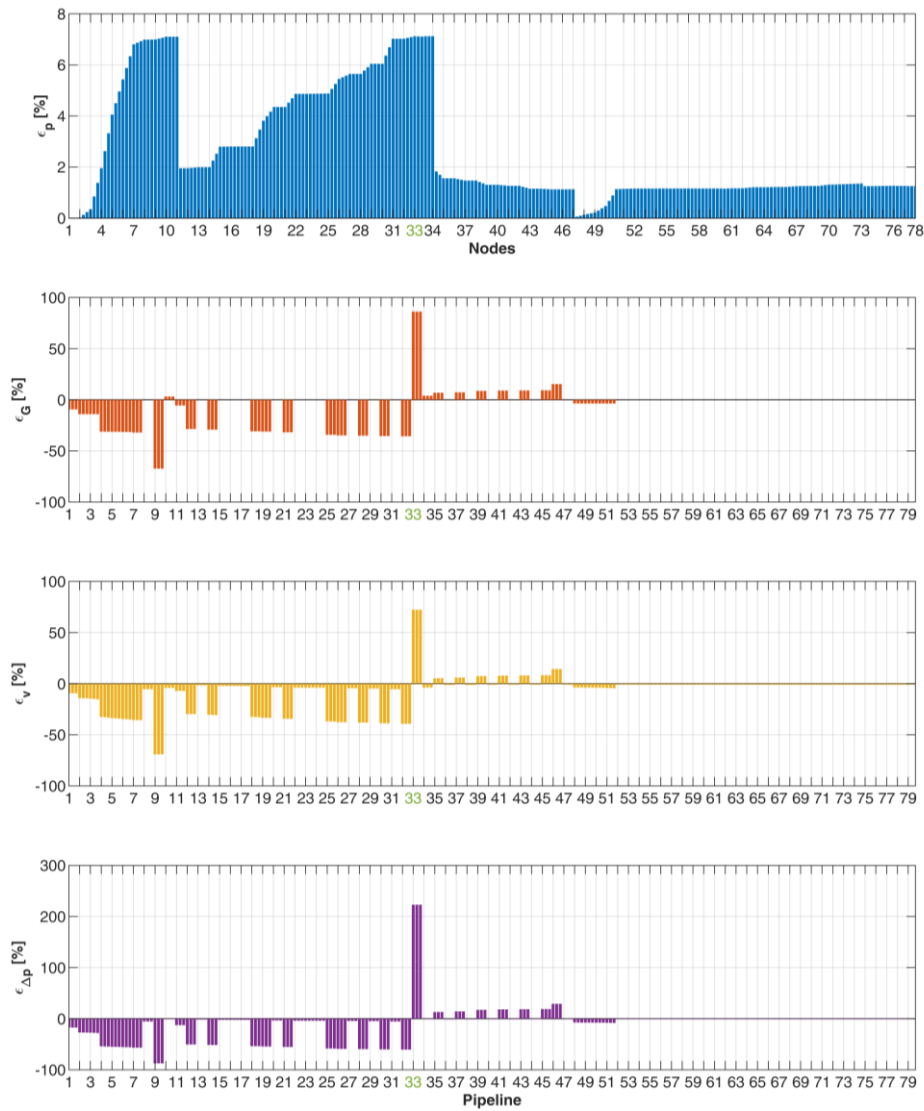
Figure 31 – Relative deviations between injection case and base case of the main fluid-dynamic quantities of the network referred to a specific time ($t = 20:00$ h) for all the nodes or pipes.
Starting from the top: blue bar plot: nodal pressure deviation; orange bar plot: mass flow deviation for each pipeline; yellow bar plot: velocity deviation for each pipe; purple bar plot: pressure drop deviation for each pipeline.

As a final remark, it is worth noting that the different behavior of the different sections of the network originates from the presence of two loops, which, in fact, are topological solutions in order to generate a self-balancing infrastructure. In contrast with this dynamic, it is possible to consider the behavior of the tree-shaped section of the network rooted to one of the two main loops (in node 51): for this set of pipelines, the fluid-dynamic impact of biomethane injection is homogeneous and no compensations can be observed.

Impact of the choice of the injection node

To provide a complete discussion about the hydraulic implications of the activation of a distributed injection of biomethane, the simulation just discussed was repeated changing the position of the injection node. In particular, the injection node was moved upstream towards the traditional gas receiving station (node 2). In a further trial, the injection was moved downstream and in particular at the root node of the tree-like portion of the network (node 46). The main results of this analysis are displayed in Figure 32.
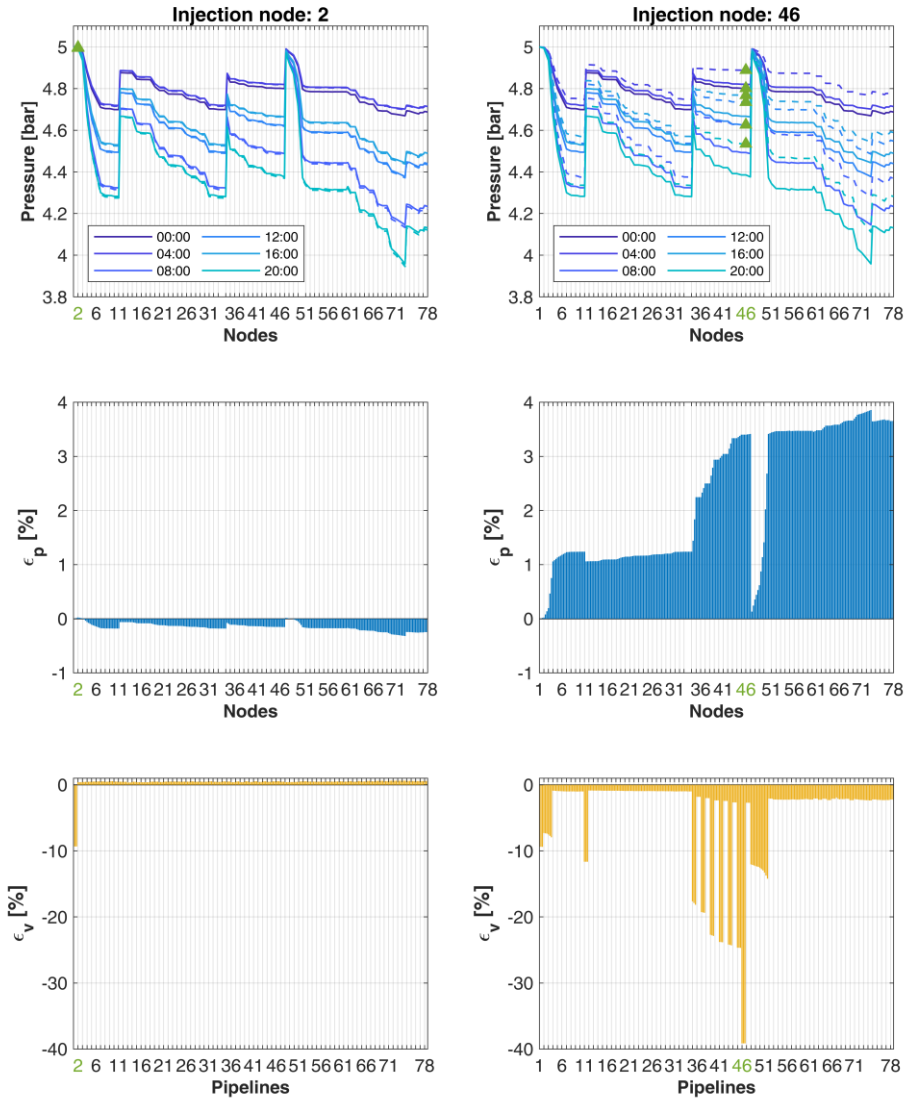
Figure 32 – Impact of the choice of biomethane injection point on nodal pressure profiles and velocity in the pipeline.
First line: comparison of the complete nodal pressure sequences between non-injection and injection scenario, for a selection of hours (every 4 hours). Solid lines: non-injection scenario; Dashed lines: injection scenario. The green triangle highlight the nodal pressure of the injection node.
Second line – blue bar plot: nodal pressure relative deviations between injection case and base case of the dynamic quantities of the network referred to a specific time (t = 20:00 h).
Third line – yellow bar plot: velocity deviation for each pipe.

In Figure 32, results of the two injection cases are summarized following the scheme of the previous paragraph: first, the nodal pressures for selected hours (every 4 hours) are given for both the non-injection and the injection case, in order to have a graphical comparison of the variations introduced by the injection practice. Subsequently, the relative variations of the main hydraulic quantities are computed and reported in the figure. In this case, only the nodal pressure relative variation and the gas velocity relative variation are represented. Of course, the reference case is considered to be the non-injection case.

The different distribution throughout the network of the relative deviations for each of the three injection scenarios indicates the impact that the choice of the injection point has on the hydraulic asset of the network.

Considering the case of injection at node 2, it is possible to note that it is the case introducing the smallest perturbations in terms of gas velocity through the pipes and thus in terms of nodal pressures. The velocity has a considerable decrease in the first pipeline, the one connecting the fossil-gas entry point to node 2 where the biomethane injection is located. This happens because the fossil natural gas request is lower as it is partially substituted by biomethane. Except for the first pipeline, all the other pipes, which are located downstream the biomethane injection, undergo very little increase of the velocity, caused by the slightly higher amount of mass flow requested. In fact, the biomethane has a lower heating value than the one of traditional natural gas. Consequently, all the nodal pressures have decreased in a quite homogeneous way.
It is worth highlighting that the behavior of the network in this case is monotonic and homogeneous: all the nodes have their pressure reduced by 0.2 ÷ 0.4 % because of the biomethane injection at node 2.

Moving the injection downwards, it is possible to note uneven pattern of nodal pressure variations and pipeline velocity variations, similar to what happen in the case of injection at node 33 (Figure 31). Both in the case of injection at node 33 and injection at node 46, the nodal pressures undergo an increment, differently than what observed in the case of injection at node 2. The area upstream the injection preserve a higher-pressure field because less natural gas flows through these pipes. The nodes downstream the injection point display furtherly higher nodal pressures because they are affected by the higher-pressure level at the injection point originated from the observation before and the pressure is maintained by the decentralized injection. In addition, these are the nodes of the network that have the lowest pressure levels in the non-injection case, thus the ones that shows the highest variation in relative terms.

It is worth noting that the injection point is the root of a tree-shaped portion of the grid as well as a part of one of the two loops of the grid. Thus, all the downstream nodes, belonging to the tree topology reacts in the same way while

the upstream nodes are affected differently according to their position in the loops with respect to the injection point. The major pressures rearrangement can be observed in the loop where the injection node is located, in which the portion from node 35 to node 47 where the nodal pressure progressively grow with respect to the base case scenario, as long as they are nearer to the injection point. The other portion (node 48 to 50) rearranges accordingly. The other loop appears instead to react with an even pressure increase. This behavior is similar to what observed in the case of injection in node 33.

Thus, the choice of the injection node has an impact on the nodal pressure throughout the whole network as the gas flows are modified (and so the velocities). As a general consideration, the closest the injection point gets to the traditional gas receiving station, the least influent will be the impacts on the pressure field. Under these circumstances, in fact, the fluid-dynamic organization of the infrastructure is not substantially changed and the pressure deviation (evenly distributed) will be related to the change in the gas quality rather than other reasons. Conversely, when the injection is in a more peripheral point, then gas flows are modified because part of the network is required to distribute less gas, given the presence of an additional source. In general, the pressure field will be increased.

Impact on gas quality

The natural gas that is considered for this simulation is characterized by a molar fraction of methane equal to 98.3 % and, together with the other compounds, it has a higher calorific value of 54.68 MJ/kg. The biomethane is instead assumed as composed of 97% of methane and 3% of CO_2, thus having a calorific value of 51.23 MJ/kg. This type of biomethane is complying the gas quality requirements for injection set in [34] for the Italian context. However, its injection within the network has a non-negligible impact on the gas quality of the network. In fact, a complete substitution of the natural gas by the biomethane would cause a reduction of the calorific value provided to each costumer of the network equal to 6.3 %, if invariant gas consumption (mass based) are considered. Under the assumption (made in these simulations) to consider the thermal energy demand at each node rather than the mass flow request, the difference in the energy content reflects on the amount of gas flowing in the network instead.

Nevertheless, the condition of complete fuel switching for the whole network cannot be reached under the assumption of network double feeding (traditional gas receiving station always feeding the network together with the biomethane). The gas quality perturbations will then be a more or less local occurrence and its magnitude depend on a time and a space variable, which together contributes to define the blending of the biomethane within the fossil natural gas. The blending magnitude is time-dependent by means of the variation of gas consumption rate of

the whole users of the network. It is also space-dependent, changing according to the location of the injection node. The position of the injection node highly influence the size of the influenced area.

In Figure 33, a screenshot of the network status is given for the three cases concerning the injection point choice, referred to the same moment in time (h 20:00). Among the other variables depicted, the gas quality is given in terms of higher heating value of the gas that is flowing within each portion of the pipes. It is displayed by the color of the inner part of each pipe. The orange color indicates 100% of fossil natural gas, while the dark green one stand for 100% biomethane.
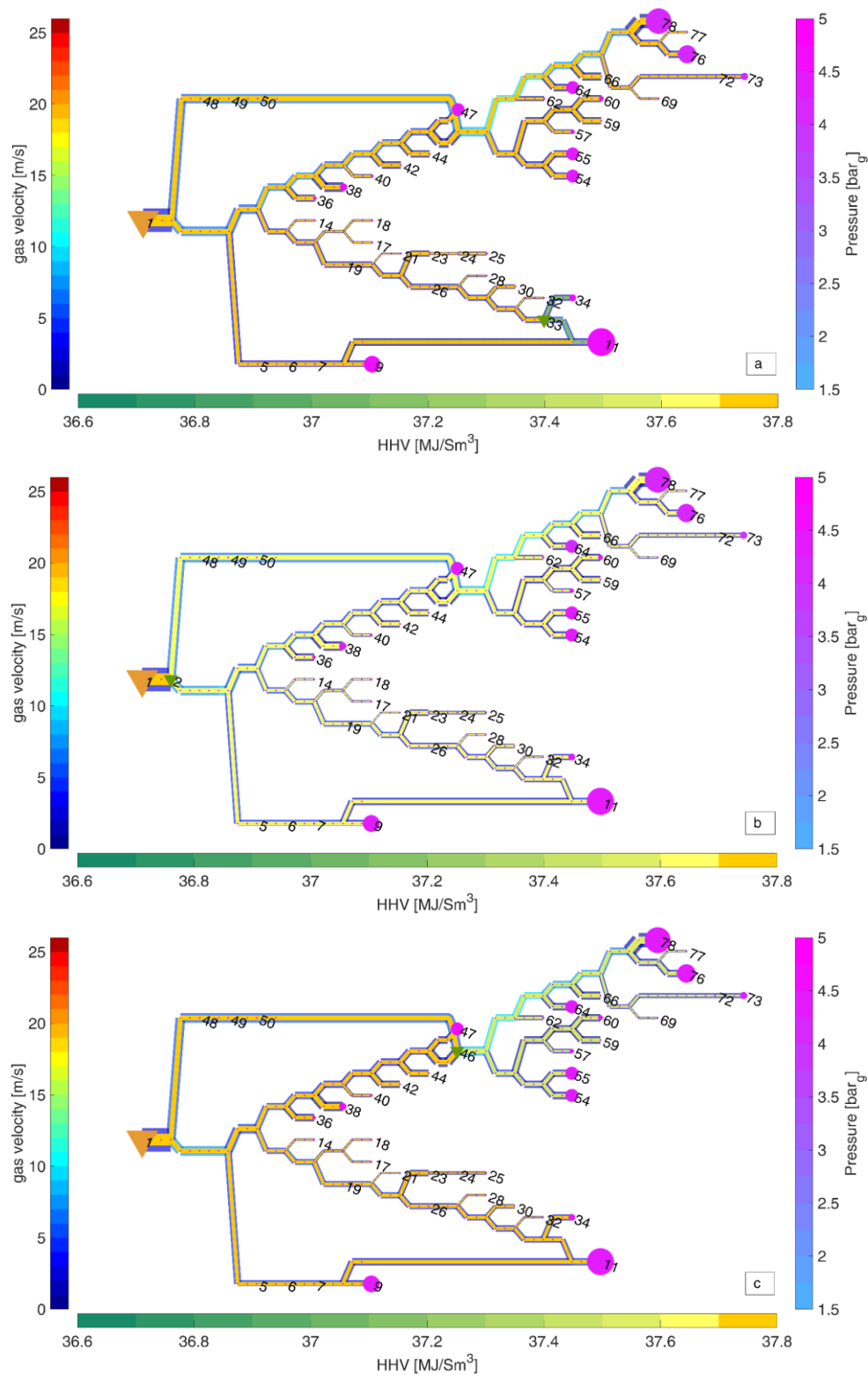
Figure 33 – Screenshots of the network status referred to h 20:00 for the three injection cases addressed. a) injection point: node 33; b) injection point: node 2; c) injection point: node 46. The injection point is highlighted with a green triangle; the natural gas entry point is indicated by an orange triangle. The figures display all the hydraulic quantities throughout the network and the gas quality within each pipe (in terms of higher heating value)

As it is possible to note, when injecting in node 33 (Figure 33.a), the gas quality perturbation is the greatest in terms of deviation of the higher heating value from the fossil natural gas one (– 4.1 % on average). On the other hand, in this case the perturbation affects the smallest number of final users.

Interestingly, the further blending potential of a meshed network is highlighted considering the gas quality that reaches node 11, as compared to the one reaching node 34. A closer look is given by Figure 34, where the quality variation over the time is given for both the mentioned nodes.
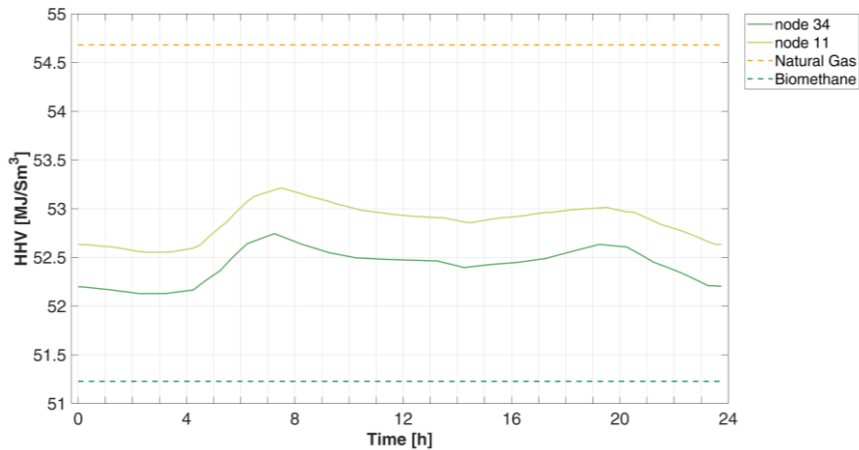
Figure 34 – Quality perturbation profile in terms of higher heating value variation in time for the two consumption nodes that are nearest to the injection point (node 33). Effect of gas blending at the injection and inside the network.

It is possible to see that already at the injection node (node 33) the biomethane is mixed with the natural gas. In fact, node 34 – that is directly connected to the injection point – receives the quality pattern shown in figure in terms of higher heating value. The dashed lines represent the higher heating value of the biomethane (green line) and of the natural gas (yellow line) as benchmarks. Concerning node 11, its higher heating value pattern results always higher than the one of node 34 of about 0.9 %. The reason for this difference it its location. It is in fact located downstream a junction connecting a pipeline that is adjacent to the injection node (33) and another pipeline, in which only fossil natural gas flows. Thus, a further blending inside the network occurs at this junction and the resulting gas is detected by node 11, which is the nearest consumption point.

Back to Figure 33, when the injection is set at node 2 (case b) it is possible to note that the whole network is affected by a drop in the higher heating value of the distributed gas, even though this drop is very little (– 0.8 % on average). In Figure 35 the quality perturbation is given in function of the time. As it is possible to draw from a comparison with the previous Figure 34, the higher heating value of the resulting gas mixture is much higher (and closer to the one of the natural gas) than in the previous case, showing that in that injection point, the network has an higher blending potential. Since the perturbation affects almost the whole

network, it is of interest to track the quality perturbation traveling along the network and assessing the time it takes to reach the farthest node of the network. In Figure 35, the quality perturbation at node 78, one of the farther from the injection point, is also given, showing a lagging between the two of about 1h30min.
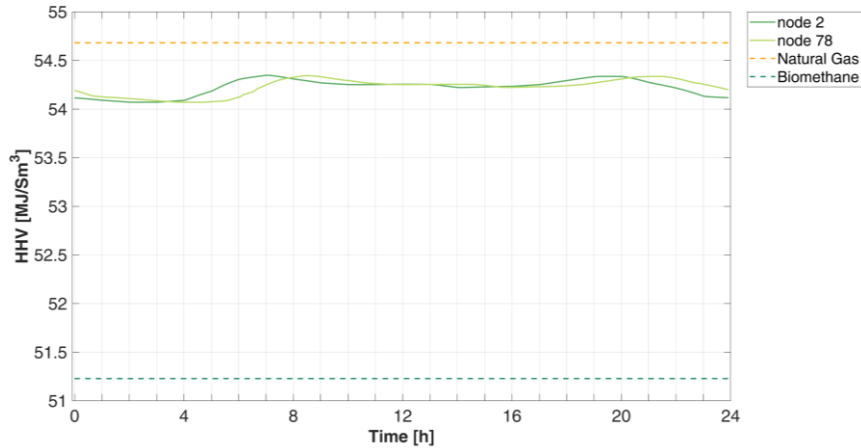
Figure 35 – Quality perturbation profile in terms of higher heating value variation in time for the injection node (node 2) and for consumption node 78, one of the farthest. Effect of the quality transportation.

The case c of Figure 33 shows that the injection at node 46 implies that any perturbations is limited to the downstream portion of the tree-like network, provided that the downstream overall consumption are always exceeding the injection. When this condition is verified, the quality perturbation will be evenly spread throughout the tree, with no further mixing phenomena as the ones observed in case a. The observed perturbation in this case is – 1.5 % on average. In this situation, the DSO has to deal with a portion of the network that is affected by a quality perturbation that is stable from the point of view of the localization. However, it may vary according to the balance between the overall consumption of the network subsection and the injection rate, similarly to what observed in the previous figures.

In Table 11, a summary of the quality perturbation results obtained for the different injection point is given. Minimum and maximum deviations are also indicated in order to account for the variability of this perturbation that is caused by the variation in the overall thermal load demand.

Table 11 – Variation of the higher heating value because of biomethane blending within the natural gas depending on the injection node. Summary of the results with related ranges of deviation with respect to the higher heating value of the fossil natural gas (54.68 MJ/kg).

Injection case	HHV$_{mean}$	Min.	Average	Max.
Node 33	52.4 MJ/kg	– 3.5%	– 4.1%	– 4.7%
Node 2	54.2 MJ/kg	– 0.6%	– 0.8%	– 1.1%
Node 46	53.9 MJ/kg	– 1.1%	– 1.5%	– 2.1%

3.6 Improving biomethane injection acceptability by means of linepack storage

When trying to execute the fluid-dynamic network verification by running the same simulation on the day with minimum consumption, unacceptable results are obtained very soon in the simulation timeframe, since the production-consumption mismatch is remarkable.

The network has been simulated with a pressure set point at the city-gate reduction station of 5 bar$_g$, as in the previous case. Gas consumption boundary conditions have been updated to the profiles of a summer weekend day (August 18th), corresponding to the day of minimum consumption of the whole year.

When production-consumption mismatch occurs, one possible solution of the network simulation is to have a reverse flow of gas at the pressure-controlled inlet node. This is in fact the only possible solution in order to have the pressure boundary condition respected. However, this occurrence does not reflect the real operation of a traditional gas reduction station: in fact, upstream the inlet node there is a portion of the network with higher pressure, thus a compression station would be needed. Also in this case, the model boundary condition would need to be updated.

For the sake of this current research, it was assumed to operate the network without any re-compression station, considering only the behaviour of a traditional city-gate reduction station, which would stop any gas inlet when the pressure conditions are not compliant the usual operating conditions, avoiding any reverse flow. This behaviour has been modelled and introduced in the network simulation program as a conditional boundary condition as previously described in section 3.2. Thus, under the circumstances of abundant gas injected, gas accumulation occurs, increasing the pressure level of the whole network.

Under these assumptions, the nodal pressure sequence as a function of time is given for both the base case and the injection case in Figure 36 (a) and (b) respectively. As it is possible to see, the blockage of the reverse flows at the city-gate causes a continuous and almost linear increase of the pressure throughout all

the nodes, as a consequence of the biomethane accumulation, reaching extremely high and unacceptable pressure levels. The maximum operating pressure of 5 bar$_g$ is exceeded already after the first time step (15 min).
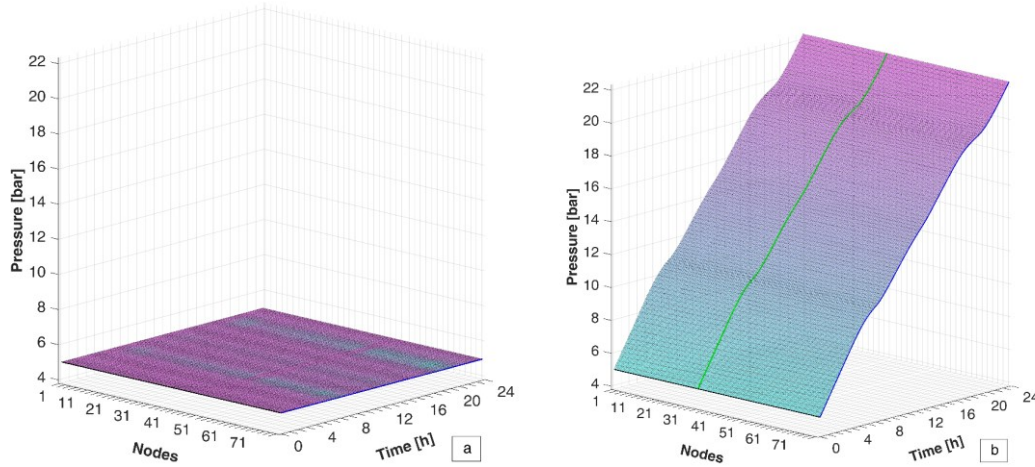
Figure 36 – Time evolution of the nodal pressure field throughout the network during the day of minimum consumption (Aug.17th) under the following scenarios: a) baseline scenario: no injection of biomethane; b) biomethane injection at node 33 with forbidden reverse gas flows at the city gate reduction station and continuous injection. The pressure evolution at the injection node is highlighted in green. The nodal pressure field is represented following the numbering sequence of the nodes. Along the perpendicular direction (y-axis), the time dependence is reported.

This immediate saturation of the network happens because its pressure level is already very close to the operational limit during the base case scenario: the pressure set point is in fact at 5 bar$_g$ and the gas demand during the day is so little that pressure drops are infinitesimal. A comparison between the nodal pressure sequence of the winter base case and of the summer base case is given in Figure 37.
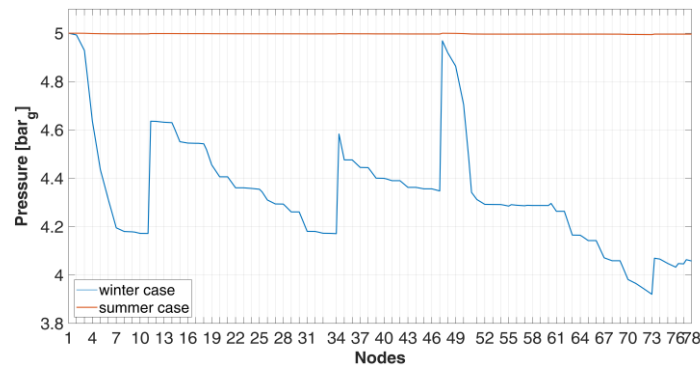
Figure 37 – Comparison between the nodal pressure sequence of the winter base case (no injection) and the summer base case (no injection).

In the summer case, the maximum overall pressure drop is in the order of millibars, while in the winter case this value is about 1 bar.

Consequently, in the summertime case, the pressure of the network can be considered equal to 5 bar$_g$ throughout the network thus implying that the linepack of the gas network is always at its limit. This means that the gas network is not able to accept any additional inlet gas flows that is not counterbalanced by a suitable consumption. That is to say that the storage capacity of the network is already at its limit. In Figure 38, the linepack evolution associated to the two summertime cases simulated before (non-injection and injection case) is given.
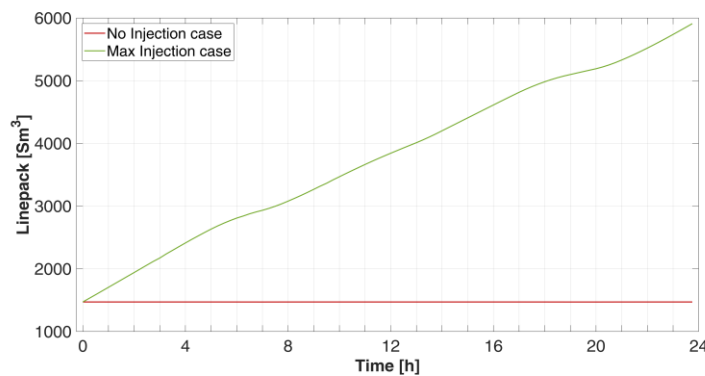
Figure 38 – Summertime linepack evolution in the case of no-injection (red line) and maximum injection (green line).

The red line, associated to the non-injection case, is to be considered as the storage limit of the network: it is the hourly amount of gas that is stored within the geometrical volume of the network when it is operated with the pressure set point equal to the maximum operating pressure. The monotonic increasing line is instead the linepack evolution in the "virtual case" of constant injection of the whole biomethane production and forbidden reverse flows at the city-gate gas entrance. It shows the continuous accumulation of the gas within the geometrical volume of the network, which however, needs to reach unacceptably high pressures.

3.6.1 Unlocking of the linepack storage by pressure modulation

The analysis of the "virtual" injection case of the previous paragraph defines the limits of the biomethane acceptability when the gas network is operated in the simplest business-as-usual way. On the other hand, it is also a useful starting point in order to investigate innovative solutions to increase the biomethane receiving capacity of the network.

From the analysis of the nodal pressure trends as shown in Figure 37, it is possible to infer that for the summer case, the pressure set point at 5 bar$_g$ is much higher than the needs. This observation may lead to question the opportunity to

keep this set point this high or whether it is possible (and even convenient) to lower the pressure set point when consumptions are considerably lower, thus decreasing the overall operating condition of the network. Figure 39.a shows the nodal pressure sequence referred to the maximum consumption hour of the summer day considered before, under different pressure set points, for the case of no distributed injection. Correspondingly, in Figure 39.b the dashed lines represent the linepack under the non-injection case for the different test-pressures.
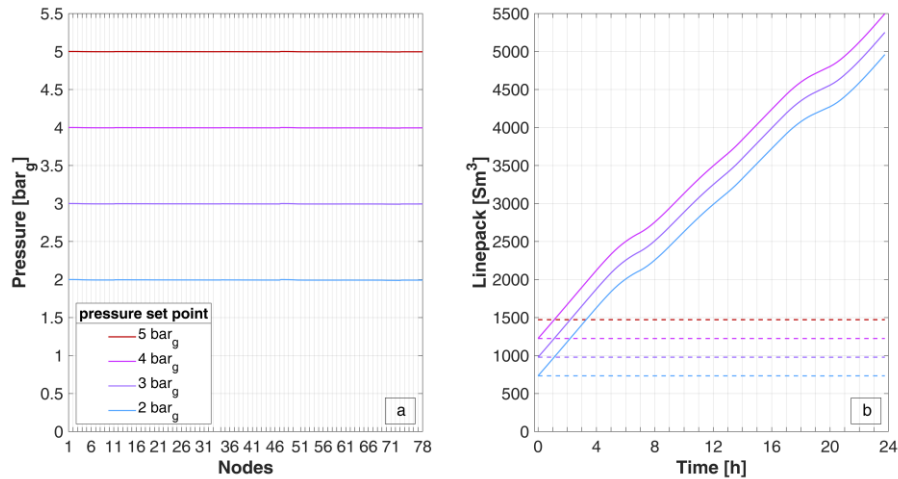
Figure 39 – a) Nodal pressure sequence throughout the network for the different set point pressures; b) Evolution of the linepack for the different set point pressure for both the non-injection case (dashed lines) and the injection case (solid lines); the red dashed line corresponding to the linepack at 5 bar_g is to be considered as the maximum possible linepack.

From this analysis it is possible to draw, on the one hand, that even at very low pressure set points, the network can guarantee proper operating conditions. On the other hand, lowering the pressure set point allows for the unlocking of a linepack storage capacity. The difference between the amount of linepack when the network is operated at 5 bar_g (red dashed line) and the linepack at lower pressure indicates the hourly amount of gas that is virtually storable within the geometrical volume of the network, while keeping the pressure level below the maximum acceptable pressure. Figure 39.b shows that, under these working conditions, the linepack decrease is linear with the decrease of the operating pressure of the network. The rate of linepack decrease for each bar is 33 %, corresponding to an additional storage capacity of about 245 Sm^3 each hour. This allows the network to be more flexible in accepting imbalances between inflows and outflows so to have an accumulation of the gas within the lines.

The gas accumulation function are depicted in Figure 39.b by the solid lines. They are obtained from the time integral of the inlet-outlet mass flow balance of the whole network as follows:

$$LP(t) = LP_0 + \int_{t=0}^{t_{end}} \Delta \dot{M}(t) \; dt \tag{3.4}$$

Where:

$$LP_0 = \left. \sum_{j=1}^{\# \, pipes} \frac{\bar{p}_j}{c_j^2} \, V_{geom_j} \right|_{t=0}$$

is the initial value of the total network linepack, obtained as a summation of all the single pipeline linepack as calculated in Eq.(2.49). It depends on the choice of the pressure set point of the network.

$$\Delta \dot{M}(t) = \left. \sum_{i=1}^{\# \, nodes} -\dot{m}_{ext_i}(t) \right|_{\forall t}$$

is the gas accumulation term, resulting from the balance between inlet and outlet gas flows. According to the convention of sign assumed in Chapter 2, a minus sign is needed in order to consider the inlet flows as positive, so to have an accumulation in fact. Linepack and accumulation terms may be expressed in standard cubic meters rather than kilograms by considering the local density at standard reference conditions (here: $T=15$ °C and $p=1$ atm).

From Figure 39.b, it is possible to measure the increase of the storage capacity of the network as a consequence of the lowering of pressure set point. The intersection between the solid lines and the dashed red line, which corresponds to the maximum acceptable linepack, indicates the time when the network is saturated by the constant injection of the whole production of the biomethane. Results are summarized in Table 12, where the network saturation times are given for the addressed cases. The lower is the starting pressure set point, the higher the accumulation capacity of the network and the longer is the time before the network is saturated.

Table 12 – Network accumulation capacity of biomethane generated with the decreasing of the pressure set point for each pressure level analysed and related saturation time of the network under the case of complete injection of biomethane

Pressure set point	4 bar$_g$	3 bar$_g$	2 bar$_g$
Saturation time	1h 7'	2h 12'	3h 18'
Accumulation capacity	247 Sm³/h	493.3 Sm³/h	738.6 Sm³/h

It is possible to conclude that, concerning this case study, each bar of decrease allows the network to gain slightly more than 1 h of line storability, thus providing flexibility to the system as well as improving renewable gas acceptability.

Of course, this result is specific for the case study addressed: it depends on the total geometric volume of the network and the balance between gas consumption and biomethane injection flow rate. Form this first investigation towards the exploitation of linepack gas storage it has been observed that operating the network at lower pressure is useful to unlock the linepack storage potential. However, this newly created flexibility may not be enough to counterbalance the mismatch between production and consumption. It can only provide some lagging time before the injection cut-off happens. In order to avoid this circumstance, a reduction of the biomethane inlet flow rate is to be imposed.

3.6.2 Biomethane injection partialization

The effects of the reduction of the biomethane injection on the gas accumulation function are depicted in Figure 40, for each of the pressure reduction scenario discussed before. Each graph refers to one inlet pressure set point (p_{set} = 4 ÷ 2 bar$_g$ from the top to the bottom), which defines the linepack for the non-injection case and gives the initial linepack condition LP_0 for the calculation of the accumulation trajectories under different injection reduction scenarios. These scenarios consists in a progressive reduction of 10% of the inflows of biomethane, thus producing ten possible linepack evolutions, under the assumption that the city-gate entry point is not exchanging any mass flow. The analysis depicted in figure, gives the complete set of possibility of biomethane acceptability improvement by the combination of the pressure decrement and injection limitations, in order to avoid the cutting-off solution.
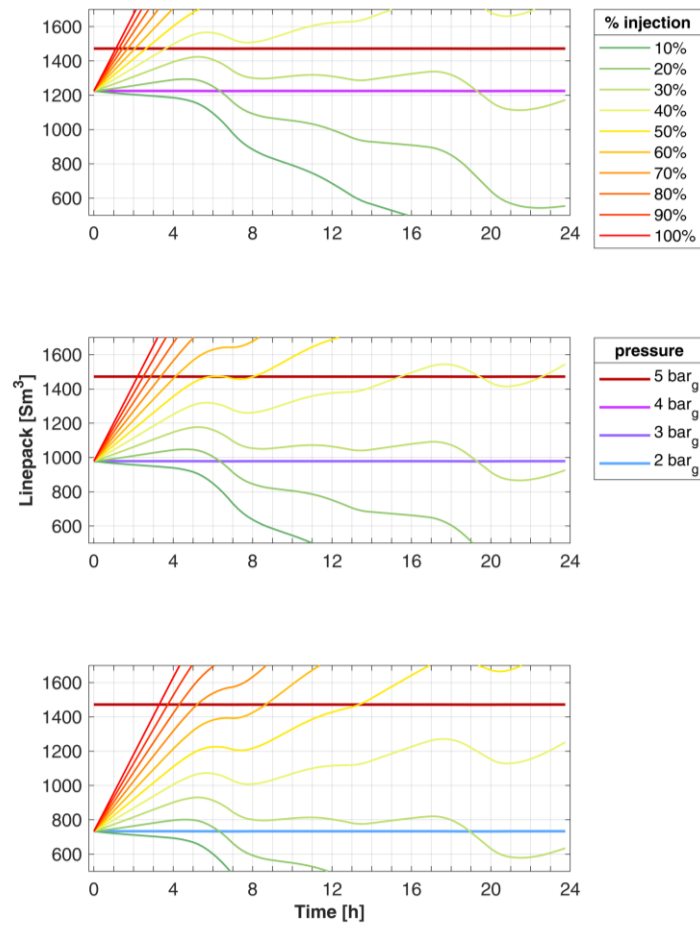
Figure 40 – Variation of the gas accumulation within the network (i.e. linepack evolution) in function of the % reduction of the biomethane injection rate. The multicolor solid lines represent the different injection cases by step of 10% reduction. Each graph refers to a different lowered pressure set point: form the top to the bottom: 4 bar_g ,. 3 bar_g , 2 bar_g . The maximum acceptable linepack (corresponding to 5 bar_g) is indicated on every graph as maximum limit (dark red line).

From the figure, it is clear that in the case of a network at 4 bar_g (upper plot), the reduction of the biomethane injection to 40 % of the biomethane production is still not sufficient to avoid overpressures. It is necessary to drop the injection down to 31.8 %. Turning the network to 3 bar_g (middle plot) allows the injection of the 37.1 % of the biometane production. At last, the network set point to 2 bar_g (lower plot) grants the acceptability to the 42.5 % of the produced biomethane (the 40% line lies in fact completely within the acceptability range of linepack volumes). Thus, in the context of limiting the biomethane injection, lowering the pressure set point allows for a higher fraction of the production allowable in injection, with an almost linear increase between 4 bar_g and 2 bar_g gaining about +5.3% per bar_g in the fraction of injectable biomethane.

As a side comment, it can be noted that at percentages of biomethane injection up to 30%, the linepack evolution drops down the linepack level corresponding to the non-injection scenario at the desired pressure set point. This is possible under the

assumption of the deactivation of the city-gate reduction station. In this situation, the biomethane is the only gas source of the network and, at too low injection percentage, it starts to be insufficient thus emptying the linepack of the network. In the real case, this would not be the case since the city-gate would provide fossil natural gas as fast as the pressure of the network drops lower that its set point.

It is worth saying that this acceptability scenario is tailored for a one-day long low-consumption status of the network. Results are different if the consumption-production mismatch would last longer. This is the common situation for a summer weekend, when industrial gas usage is lower and heating systems are turned off. Predictions on the duration of the possible mismatch are important to set-up the most profitable strategy. In fact, in the context of biomethane injection reduction, what concluded by the analysis of Figure 40 may lead to over-accumulation during the next day. Specifically, considering the case of 2 bar$_g$ set point and the maximum possible injection rate of 42.5 %, it can be noted that the evolution of the linepack is increasing and already at its maximum. A repetition of a consumption pattern similar to the one of the day before, with no modification on the injection side, would soon lead to overcome the linepack limit, as shown in Figure 41. It is then necessary to further decrease the acceptable biomethane in injection.
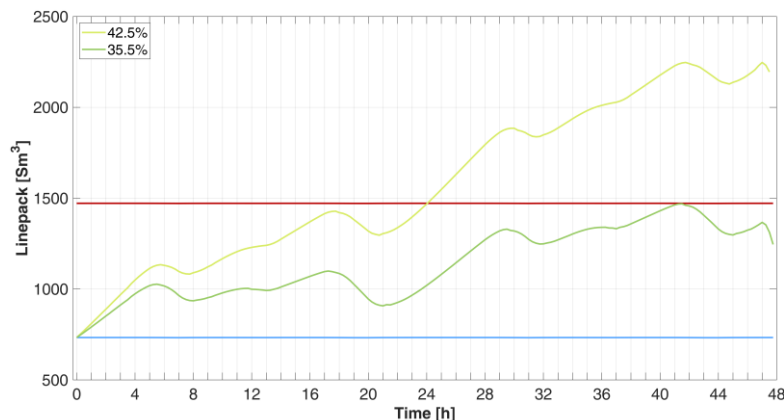
Figure 41 – Linepack evolution in case of persistency of the mismatch condition for a whole day (case of a summer weekend). The linepack trend under the reduction case tailored over 24 hours only (light green line) is compared to the linepack trend adapted for the 48 hours packing (dark green light). The red line represents the maximum acceptable linepack; the light blue line represents the linepack of the 2-bar$_g$ case without injections.

Considering the whole time of critical operating condition of the network (i.e. the two days of a summer weekend), it results that, in the case of pressure set point already lowered to the minimum, the biomethane injection has to be limited to the 35.5 % of the total production. In this way, the storage potential of the linepack, unlocked by the modulating pressure measure, it is fully exploited without any violation of the operating conditions.

3.6.3 Verification of the measures for linepack storage exploitation

The measure taken so far in order to maximize biomethane injection should, at last, be verified in the transition towards an higher consumption day, in which the linepack storage is no needed anymore because consumptions are greater than biomethane production. With higher consumptions on the one hand and a low-pressure set point, pressure drops may increase and nodal pressure should be verified. Furthermore, the impact of restoring the biomethane injection to 100% of the production should also be evaluated.

In Figure 42, different scenarios for the transition to the third day (a weekday) are considered under the point of view of the variation of the linepack and the nodal pressure at the farther node (node 73).
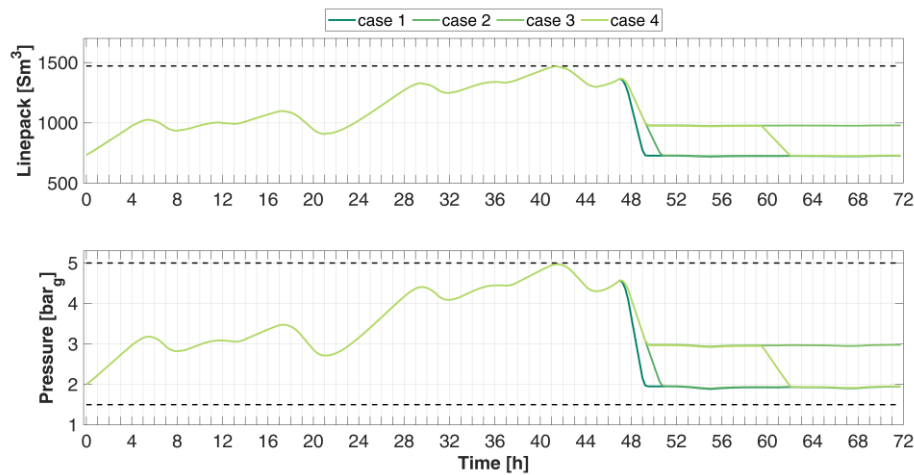
Figure 42 – Linepack (above) and pressure (below) evolution over a three days simulation in which different strategies for the transition to normal operating conditions are compared. For the first 48 hours, the network is operated at a pressure set point at the city-gate of 2 bar_g and the injection is reduced to the 35.5 %. Then: case 1) "nothing changes": the pressure set point at the city gate is maintained at 2 bar_g and the injection is kept reduced. Case 2) restoring the injection: the pressure set point at the city gate is maintained at 2 bar_g and the injection is turned to 100%. Case 3) the pressure set point at the city gate is changed to 3 bar_g and the injection is turned to 100%. Case 4) "modulating pressure": the pressure set point at the city gate is changed to 3 bar_g and after 12 h is linearly decreased to 2 bar_g again while the injection is turned to 100% since the beginning of the third day.

In case 1 and 2, the pressure set point at the city-gate is not changed, thus as fast as the pressure level of the network drops below 2 bar_g, the conventional gas entry point is restored and starts to feed the network again, supporting the biomethane flux. It is worth noting that this occurrence is not instantaneous: it takes over 2 h for the pressure level to decrease due to the increased overall gas consumption, which have overcome the biomethane injection. This dynamics reflects on the linepack value, which decreases until the 2-bar_g linepack line. A similar behavior is observed in case 2, but with slower emptying process, which takes more than 3.5 hours. The difference is due to the different setting for the biomethane

injection: in case 1, the injection is kept reduced while in case 2, the injection of the complete production is restored.

In both the cases, the nodal pressures will be lower than 2 bar$_g$ during the third day. Although the higher consumption rates, higher gas flows thus higher pressure drops, the nodal pressure are still compliant to the minimum values at any time of the simulation, thus no critical conditions are reached. In Figure 42 the nodal pressure variation of the farthest node is given.

To avoid any issues related to possible excessive pressure drops or, in general, to keep the network at a higher pressure level when the need for linepack storage is over, the pressure set point may be changed to a different value than the one for the previous days. This is what is simulated in case 3. Referring to Figure 42, it is possible to see how the linepack (and thus the pressure level of the grid) sets its value to the one corresponding to the pressure set point of 3 bar$_g$.

At last, a proper pressure modulating case is addressed in case 4. In this case, the pressure set point is changed during the third day. The city-gate pressure is first set at 3 bar$_g$ and then, at around noon, it is subsequently reduced from 3 bar$_g$ to 2 bar$_g$, with a linear modulation over 2.5 hours. In Figure 42, the linepack response follows directly the pressure settings changes, which reflect to the nodal pressure of node 73 too. The changing in the pressure set point of the network causes a reduction of the fossil gas inflow at the city-gate, as it is possible to note in Figure 43. In this way, an imbalance between inlet gas flows and gas consumption is generated and the network undergoes and emptying phase in which the pressure level and, consequently, the linepack, are reduced. This phase ends after almost 2.5 hours, when the inward gas flow at the city gate recovers the same value as the previous case, in order to keep the balance of the network (and thus its pressure level).

This 4th case is meant to show how the pressure modulation technique is to be considered in order to prepare the network to improve its flexibility in receiving excess renewable gas production, by means of linepack managing.
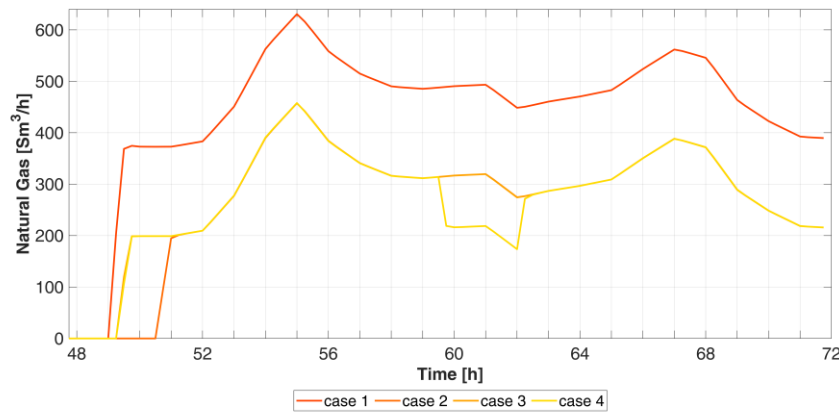
Figure 43 – Restoration of inlet natural gas flow at the city-gate reduction station after the 48 hours of "linepacking" during the weekend. The gas withdrawal profile depends on the control strategies on the pressure set point and about ri-modulation of the biomethane injection.

3.7   Conclusions

The case study considered in this chapter aimed to assess the impact of biomethane injection within the lower pressure level of the gas network, with the constraint of limited receiving capacity. Critical operating conditions have been considered and countermeasures to solve these criticalities in order to minimize the biomethane curtailment have been proposed and tested.

At first, the gas network was tested under a complete injection scenario during the day of maximum consumption (winter case). This can be considered as a "business-as-usual" scenario because the hourly consumption are much higher than the injection rate and so the biomethane may be accepted without particular concerns. However, this case have been addressed in order to test the fluid-dynamic response of the network to the implementation of a further, peripheral injection of a gas with different quality. Different injection points have been tested in order to perform the analysis.

As a general result, the overall pressure level of the network increases when a distributed source of the gas is added in a peripheral point. The additional source, in fact, allows the decrement of the gas flows along the upstream pipes, thus reducing the pressure drops and keeping a higher-pressure level. This pressure gain at the distributed injection point is then maintained along the downstream part of the network as long as the gas quality of the gas resulting from the blending is similar to the one of the previous gas – as for the addressed cases. Conversely, injecting and blending a lower heating value gas (on a volumetric basis) implies an increment of the gas flows downstream the injection point which, in some cases, may cause considerably higher pressure drops, thus counterbalancing the gain in the pressure level obtained by the peripheral

injection. A taste of this occurrence may be found analyzing the injection case at node 2, located at the very beginning of the network: in that case, a full substitution of the distributed gas is in fact obtained, as the biomethane blending affects the whole consumption area, causing a decrement in the higher heating value of the distributed gas. On the other hand, no particular pressure gains are obtained at this stage. It can be seen that the case of injection in node 2 is the only case where an increment in the pressure drop is observed implying a (slightly) lower level of the overall nodal pressures.

As for the impact on the gas quality, it was assessed with reference to the higher heating value of the blend. Of course, the network express its highest blending potential when the injection is nearest to the already existent gas entry points. What is more, in case of constant and continuous injection, the gas quality undergoes variations that depend to the gas consumption pattern: when consumptions lower, the amount of fossil natural gas needed to complement the biomethane delivery lowers, thus the composition of the blend changes.

Already at this stage of this conclusive analysis, it is clear that once distributed injections of renewable gases are accepted, the gas network operating status shift towards a more dynamic ones, which would need proper tools to be managed in the optimal way.

The added value of a dynamic management of the gas network is even clearer when addressing the second part of the model application, devoted to avoid the biometane injection curtailment when consumption levels are too low.

The aim was to exploit the compressibility of the gas in order to store the production in excess within the volume of the network itself (linepack storage). To do so, this storage potential should be unlocked by changing the inlet pressure set point to lower pressure level: in this way, in case of a positive unbalance (i.e. injection higher than consumption), the gas can be stored within the lines without exceeding the maximum operating conditions. On the other hand, the pressure level should be high enough to avoid unacceptable low pressure levels at the farthest nodes. The analysis carried on in this chapter, though referred to a single case study, shows some general trends. When gas consumption are lower and the production-consumption mismatch is more likely, the pressure drops along the network are also lower, thus there is no need to keep the pressure set point at high values. A modulation of the pressure set point on the basis of the gas consumption pattern may give as a consequence a network which is already in the condition to use its linepack to buffer short time mismatch. From the result of this sample case, for each bar of lowered pressure set point, 245 Sm^3 each hour of linepack storage are unlocked, with a +33% linear trend with the pressure. However, the geometric volume of a distribution network is anyways limited, thus this strategy still presents limits. The addressed case, in fact, shows how fast the unlocked linepack may be saturated if the inlet-outlet unbalance is not changed (3h18' in the best situation). On the other hand, when curtailment cannot be avoided, this transient

analysis allows the calculation of the fraction of biomethane to curtail, which depends on the gas consumption pattern and on the duration of the mismatch condition occurrence. The combination of the modulating pressure strategy and the reduction of the biomethane injection during the critical days (summer weekends in this case study) allows recovering the 35.5 % of the total curtailed biomethane in the case of loose constraint (see Table 9). This is equal to roughly 128.000 Sm^3 of recovered biomethane which corresponds to about additional 483.8 equivalent hours of full injection, thus increasing the biomethane injection allowance of +5.7 %, obtaining 89.9% of yearly injection factor.

In order to make this biometane receiving improvement realistic and feasible, a generalized update of the metering systems and the control devices that monitor any gas network is needed, in order to achieve the status of "smart grid". This process is already ongoing at the European level thanks to [131] even though, sometimes, this process lacks of coordination and scope.

Chapter 4

Hydrogen injection cases: simulations and receiving potential assessment

4.1   Introduction

Gas network infrastructure has been considered in the latest years as a possible storage of renewable energy with a remarkable potential and a distributed feature. The storage of renewable sources will be possible by means of power-to-gas processes coupled with distributed injection practices. A key player within this framework is, of course, hydrogen, whose production by means of electrolysis seems to constitute, in the longer term, a viable support for a decarbonized and robust energy system.

Hydrogen is not only considered as the connecting bridge for the complete integration of the power and the gas sectors. From the gas sector perspective only, in fact, it is seen as the crucial molecule to allow the whole value chain to endure its business through the energy transition towards a fully decarbonized energy system.

In this framework, the approaches that the stakeholders of the gas sector are pursuing are sometimes opposite. In Europe only, there are countries such as The Netherlands which are planning a complete shift of portions of their infrastructure from natural gas to hydrogen. A number of pilot projects have been started in the

country during the past few years (2018-2019), ranging from mini-grid test facilities [132] to fuel switching projects at block of buildings [133] and small villages [134]. These initiatives are based on the report [135] financed by *Netbeheer Nederland* (the Dutch association of network operators) which states that the current Dutch infrastructure is suitable to shift from natural gas to hydrogen. It is worth noting that one of the main driver towards these initiatives comes from the sudden change in the political attitude and social perception towards the domestic gas extraction industry, which happened after a series of earthquakes hit the surroundings of Groningen gas fields, one of the main European ones. The government has in fact planned a significant and progressive reduction of the field operations until the complete stop in 2030 [136]. Moreover, some Dutch cities including Amsterdam has introduced a ban for natural gas at urban level where new buildings will be hindered from the natural gas grid connection option thus switching towards an all-electrical building energy supply. Similar to the Netherland approach is the UK one with the H21 project [137], which started with the feasibility study on the hydrogen switching for the city of Leeds [138] that gave a thorough insight on the barriers, the costs and the roadmap to follow to pursue the aim.

Germany, Denmark, France and Italy have undertaken a different approach. In these countries, test cases and pilots plants on hydrogen blending within the natural gas current infrastructure have been put in place. Since 2013, in Falkenhagen (Germany), an hydrogen blending facility powered by excess power from a wind farm have been operated [139] and recently it has turned to a methanation facility within the Store&Go project [140]. Following the same rationale, the French initiative Jupiter1000 by GRTgaz [141] aims at producing either hydrogen and SNG from renewable to be injected at the transportation level. In Schopsdorf (Germany), the distribution level is instead addressed by the power-to-gas plant within the E.ON's Green Gas from Green Power initiative which is planned to raise the hydrogen percentage to 20% [142]. A similar project named HyDeploy is on-going at Keele University (England) [143]. All of these projects are oriented to the distribution level of the gas network in order to demonstrate that gas blends may have minor or negligible impacts on the households' appliances. As for the Danish [144] and the Italian set-ups [145], the target is the transmission level of the network and in particular they both aim at studying the behavior of gas leakages at the regulation and metering stations, at different percentage of hydrogen fraction (up to 10% concerning the Italian case by Snam).

This remarkable number of projects involving hydrogen substitution or blending within the natural gas infrastructure, and the strong increase in their number during the past 2-3 years shows how much the subject of renewable gas and especially hydrogen have gained attention. What is more, they also testify that the blending of hydrogen within the current gas system is not straightforward:

differently from the case of the biomethane inclusion within the value chain, hydrogen has completely different properties than natural gas and its presence within the system has an impact on all the level of the infrastructure. The main issues are the following:

- It may strongly affect the quality management of the gas flows and cross border exchanges,
- it may have a potentially detrimental effects on the materials which constitute the gas network infrastructure itself,
- it may affect the gas leakages arising issues on the usual detection protocols and risk management assessments,
- it may have impacts on the final users' appliances, with different degrees of severity according to the type of appliances themselves.

Before turning to the testing phase, most of these issues were considered in a thorough review from the NREL [43], in which it was concluded that the blending of hydrogen in natural gas up to a concentration of 15 % should not have a severe impact on the overall gas infrastructure. However, a case-by-case analysis is usually required, in particular in the field of the leakage evaluation and safety issues. Other similar studies, however more focused on the effects of the hydrogen blends on the multitude of the different appliances connected to the gas network, were conducted in [146] and general results summarized in [44], the latter as an outcomes from the HIPS-NET initiative form GERG. In this case, particularly stringent limits were imposed by gas turbines and by CNG tanks for the automotive sector, whose steel is not suitable to hydrogen exposition. Finally, a recent and comprehensive summary of the admissible hydrogen for the many different aspect and sectors of the gas infrastructure value chain has been released in a report [147] by Marcogaz, the technical association of the European gas industry. This summary gives a detailed picture of the complexity of the gas system as a strongly interconnected system, which developed on the assumption of a certain gas quality stability, also granted by the national gas quality standards. A change on the fundamental assumption related to the gas quality of the gas, which eventually makes the entire system to evolve into a "multi-gas" one, affects the entire value chain of this complex and interconnected system. In addition, for this change of paradigm to happen, a coordinated effort is needed at all the levels of the infrastructure.

It is under these premises that the case studies presented in this chapter have been developed and executed. The distribution system has been addressed because it is thought to be the first and easiest part from which the gas decarbonization process may start. Thanks to its geographically limited nature, the impacts of any fuel switching or gas blending remain local and affect only a portion of the infrastructure. On the other hand, the same limited feature imposes additional constraints or limitations on the possible decarbonization scenarios. These issues

will also be addressed and analyzed in this chapter in terms of limited hydrogen acceptability and in the following one, in terms of sector coupling feasibility.

This chapter is devoted to simulate scenarios of direct injection and blending of hydrogen within the same gas infrastructure already described in Chapter 3. It is assumed that the production of hydrogen is directly linked to the electricity produced by the renewable energy installations and subsequently injected in the infrastructure. The aim is to assess the impact that the injection of variable flow rates of hydrogen may have on the network, in terms of gas quality perturbations.

4.2 Solar to Hydrogen production and blending within the distribution infrastructure

In this paragraph, the integration of "solar hydrogen" form distributed sources within a gas distribution network is studied following the power-to-gas pathway.

Two photovoltaic power plants of different size (333 kW$_p$ and 500 kW$_p$) are assumed to be coupled with two electrolyzers systems in order to produce hydrogen form 100% renewable source. The hydrogen conversion efficiency of the electrolyzers was assumed to be equal to 65%$_{HHV}$, that is an average value within the common range of alkaline and proton-exchange-membrane (PEM) type [148],[149]. Alkaline and PEM electrolyzers are also the most suitable technology for a coupling with variable renewable energy sources according to the abundant literature [150],[151] and the several projects on these systems [152],[140] . Other technologies, such as high temperature electrolysis by Solid Oxide Electrolysis Cells may give higher efficiencies but they are still at the demonstration phase.

Most of existing studies about power-to-gas systems for hydrogen production address the technical and the operational criticalities emerging from the coupling with the power grid, mostly due to the continuous modulation of the power supply to the electrolyzers and to the possible mismatch between the optimum operation points. These issues affect the hydrogen conversion opportunity, worsening the overall conversion efficiency process thus shrinking the amount of potential hydrogen production.

However, for the sake of the analysis presented hereafter, a simple input-output model of the components of the solar-hydrogen production system is considered.

The solar power production curve is determined as follows:

$$\mathcal{P}_{out}(t) = \mathcal{P}_{nom} \frac{G(t)}{G_{0,AM1.5}} \, PR \qquad (4.1)$$

where

- $\mathcal{P}_{nom}$ is the nominal installed power (expressed in kW$_p$) of the PV plant;

- $G(t)$ is the global irradiance on the panel plane (kWh/m^2) – it is assumed that the power position and orientation is the optimal one;
- $G_{0,AM1.5}$ is the standard global irradiance for air mass AM=1.5 (in kWh/m^2 – it is the standard irradiance for the labeling of PV nominal power);
- PR is the Performance Ratio of the power plant, which is a sort of overall efficiency of the entire installation, taking into account the losses due to operating conditions (temperature, irradiance mainly) which deviates from the standard ones.

The values for $G(t)$ for a northern Italy location have been taken form PV-GIS [153], in which solar irradiance values for average days for each month, with a time resolution of 15 minutes, are available for any specified orientation of the PV panel. Monthly values of Performance Ratios are also available. To be noted that the ratio $\frac{G(t)}{G_{0,AM1.5}}$ can be considered as a normalized solar curve for the average day of the considered month. In Figure 44 the solar power output for the average day of each month is given for the two plants.
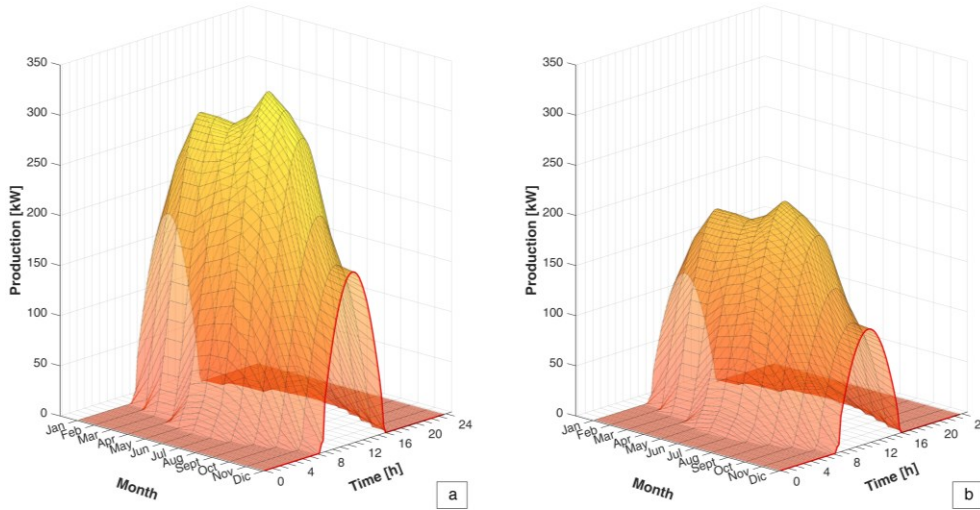
Figure 44 – Solar energy production profiles for the average days throughout the year for the two PV plants: case a) P_{el} = 500 kW$_p$; case b) P_{el} = 333 kW$_p$;

Considering the simplifying assumptions mentioned before, the hydrogen production rate is consequently determined by the application of the electrolyzer conversion efficiency:

$$\dot{m}_{H_2}(t) = \frac{\mathcal{P}_{el}(t)}{HHV_{H_2}} \, \eta_{HHV} \tag{4.2}$$

This allows obtaining a hydrogen production curve which is assumed equal to the injection pattern into the network. In Figure 45 the hydrogen production for the two plants is given for an average day of each month.
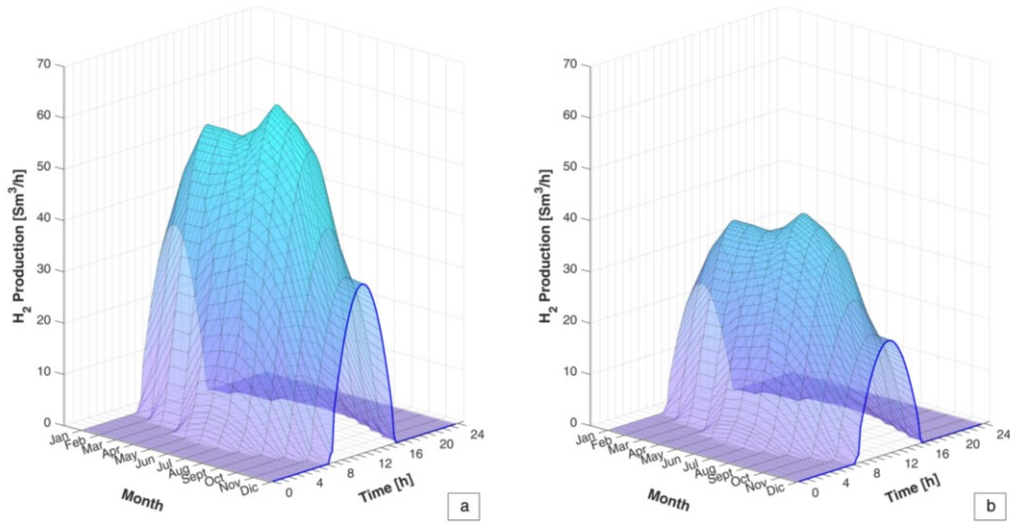
Figure 45 – Hydrogen production profiles from the coupled solar PV – electrolyzer plants for the average days throughout the year. Case a) $\mathcal{P}_{el} = 500$ kW$_P$; case b) $\mathcal{P}_{el} = 333$ kW$_P$;

Differently from the case of distributed injection of biomethane, this case is characterized by an intraday variation of the injection curve that will influence the network in a more complex way, since the magnitude of the perturbation is an interplay between solar energy availability and the intraday variation of the overall gas consumption. The case study presented hereafter aims at determine these aspects. What is more, the seasonality effect is amplified by the seasonality of the hydrogen production linked to the solar energy availability which is counterphased with gas demand
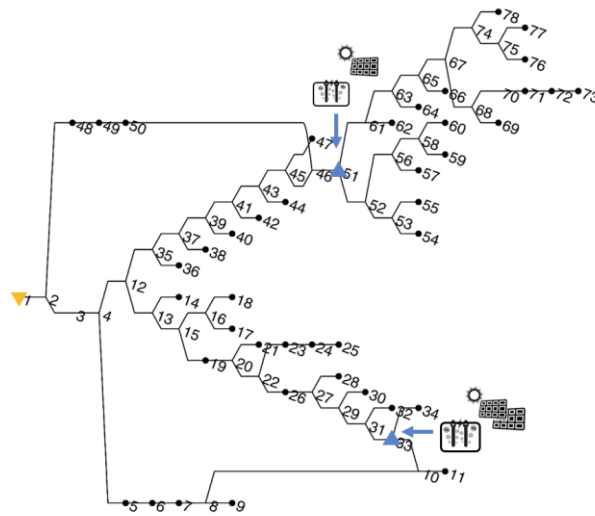
Figure 46 – Network topology scheme with hydrogen injection points highlighted. At node 33, the 500-kW$_P$ plant is connected and virtually injecting; at node 51, the 300-kWp plant is connected.

The hydrogen is injected in two peripheral and non-adjacent nodes of the network in order to assess the local impact that each injection generates and to check whether occurrences of interference between the two injections takes place. In Figure 46 the network scheme is depicted and the two PV+Electrolyzer plants are reported.

4.3   Network simulations

4.3.1 Winter case

The day of maximum gas consumption of the network is chosen for the winter case analysis. The comparison between the profile of the natural gas overall consumption during the day and the injection pattern at the two nodes is given in Figure 47. While the gas consumption are the highest of the year, the solar production and thus the hydrogen production and injection are the lowest.
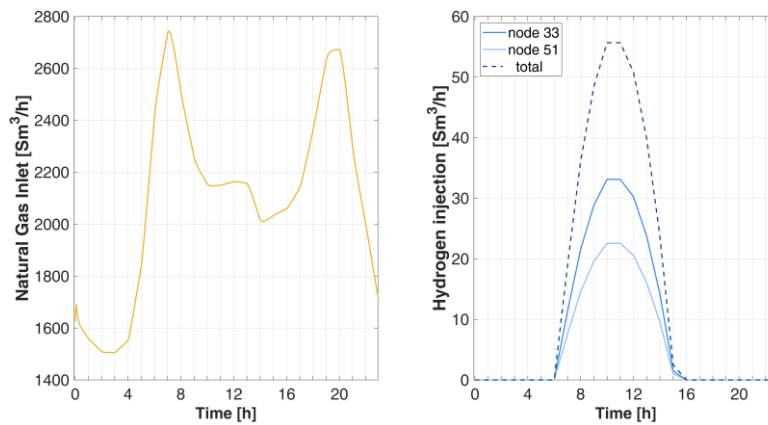
Figure 47 – Inlet gas flows to the network. Left side picture: natural gas inlet flow – for the case of non-injection scenario; right side picture: hydrogen injection sources.

It is worth noting that the inlet natural gas flow refers to the non-injection case, thus it is also equal to the overall gas consumption for the non-injection scenario. When hydrogen is injected, the amount of gas delivered to the costumer will increase while the inlet gas flow at the gas station will reduce.

The evolution of the network when hydrogen is injected is given in Figure 48 for a number of selected moments. The network screenshots are given every two hours for the entire timespan when solar production is active. The inner lines of each pipeline represents the amount of hydrogen within the gas flowing in each pipe while the outer lines indicates the gas velocity. As it is possible to note, the gas consumption rate is high and so are the velocities along the pipelines. This is more evident if a comparison is made with Figure 55, in which the network status is given for the summertime case. The bullets at some ends of the pipelines indicates the major consumption nodes, with the size of the bullet proportional to

the withdrawal gas and the color that gives an indication to the nodal pressure level. The gas entry points are highlighted instead by means of triangles, with the blue ones standing for the hydrogen injection points.

As for the hydrogen tracking, it is possible to note that the modification of gas quality is clearly visible in the surrounding of the injection node 33, where the bigger solar plant is injecting, while is almost visible downstream the node 51, where the network sub-tree originates. Especially for the case of injection node 33, it can be noted that the hydrogen perturbation remains local, investing only the node downstream the injection. The area affected by the injection at node 51 is greater but it is still limited to the downstream portion of the network. What is more, the hydrogen percentage is much more limited.

Gas network at time: 06:00
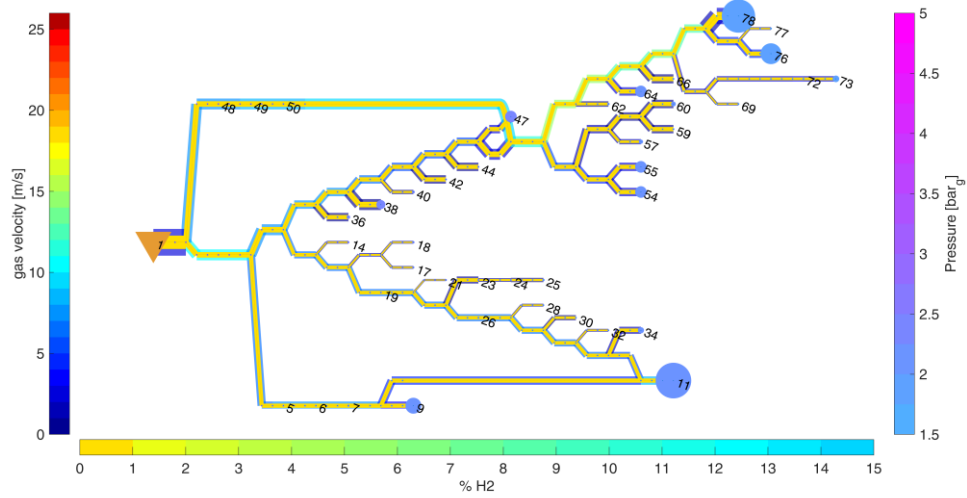
Gas network at time: 08:00

Gas network at time: 10:00

Gas network at time: 12:00

Gas network at time: 14:00
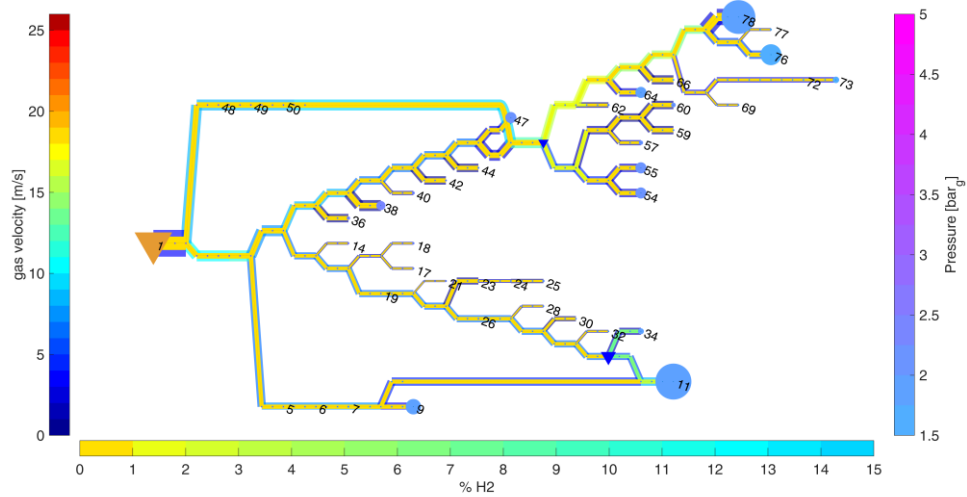
Gas network at time: 16:00
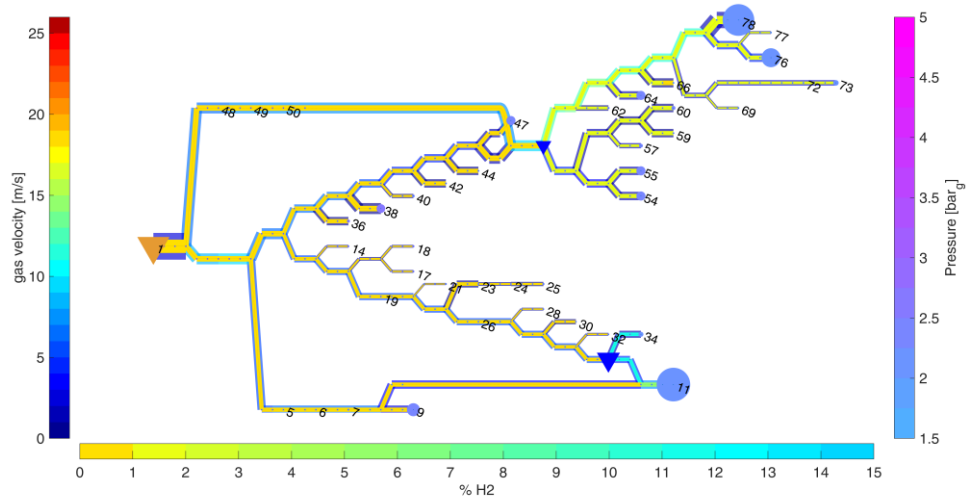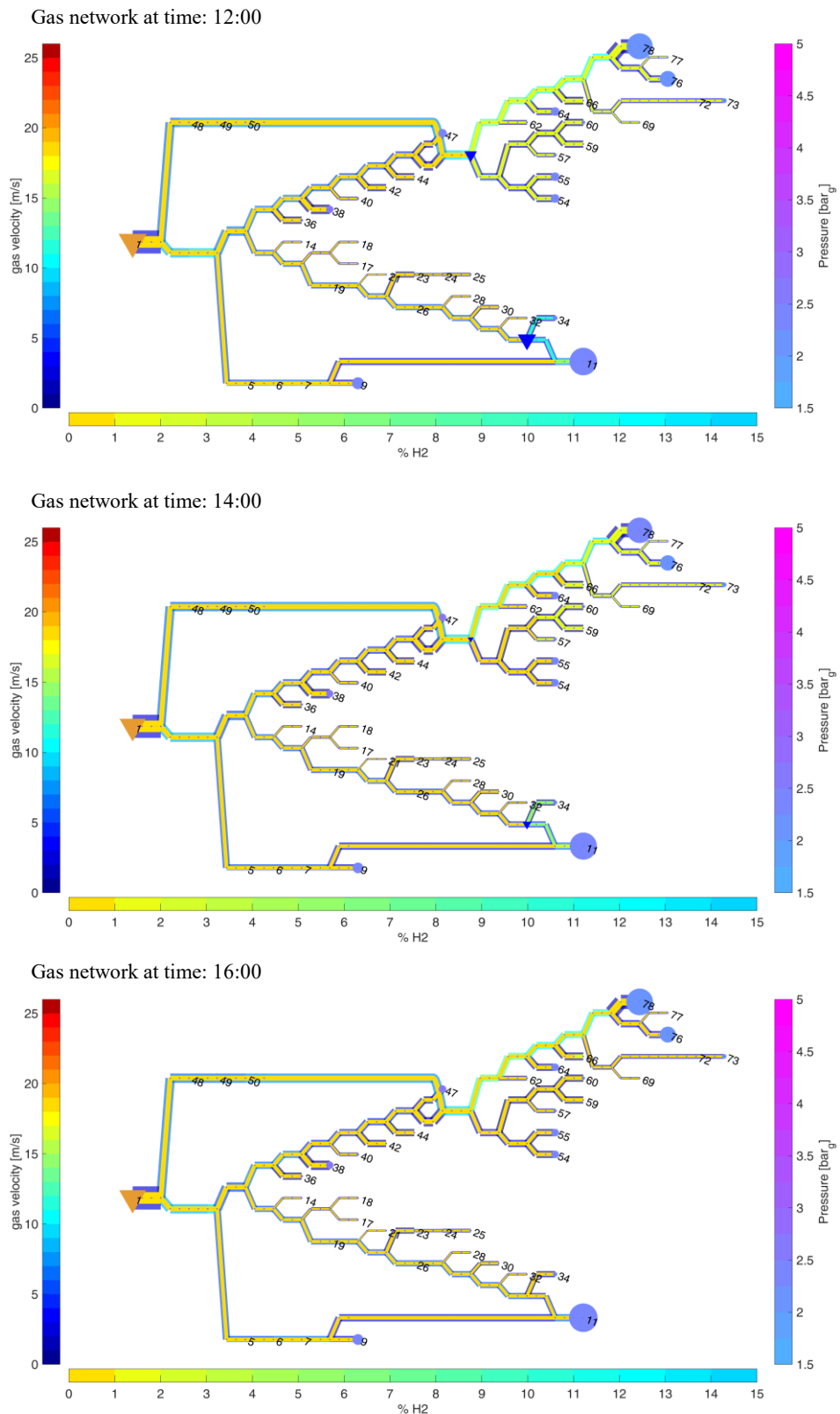
Figure 48 – Screenshots of gas network status during winter injections of solar hydrogen. Triangles highlights the gas entry points (blue triangles for hydrogen), the bullets highlight the main withdrawal points. The color of the bullets indicates the nodal pressure. The size of the symbols are proportional to the amount of gas exchanged. The outlet lines of the pipelines reports gas velocity values; inner lines are colored according to the percentage of hydrogen within the gas flow.

In both cases, hydrogen has a certain propagation time and, especially for the injection at node 51, its presence within the gas of the network persists after the injection has stopped, with a sort of "bubble" of H_2-NG travelling the network. The magnitude of the perturbation is considerably different for the two cases, not only because of the size of the injection, but also because of the blending potential of each point (i.e. the amount of natural gas transiting though each specific node). In Figure 49, the molar fraction of hydrogen for the injection points and some selected downstream nodes are showed.
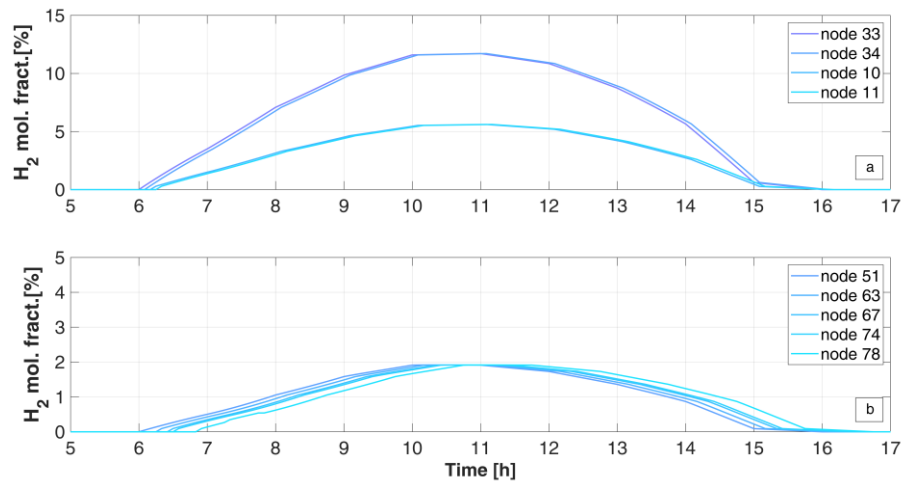
Figure 49 – Intraday evolution of hydrogen molar fraction at the two different injection points and at selection of downstream nodes. Figure a): influence area of injection 33; figure b): node 51 and sequence of node along a branch of the downstream tree, until node 78.

In Figure 49.a, the case for node 33 is depicted. The concentration of hydrogen peaks to almost 12 % following the hydrogen production pattern. The resulting hydrogen-natural gas blend reaches node 34 within a time interval of 5 minutes. Node 11, which also results as a downstream node to the injection point, is also fed by another pipeline of the loop, thus a further blending occurs just before (at junction 10) and the hydrogen is furtherly diluted: the maximum hydrogen presence at node 11 is 5.6 %.

As for the case of node 51 in Figure 49.b, the hydrogen molar fraction still follows the same pattern as the injection, but it reaches only the 2%. With respect to case a), not only is the installed solar power equal to the 2/3 of the plant in node 33, but the amount of gas that flows through node 55 is also higher – see the comparison of the amount of gas that passes through node 55 and 33 in Figure 50.
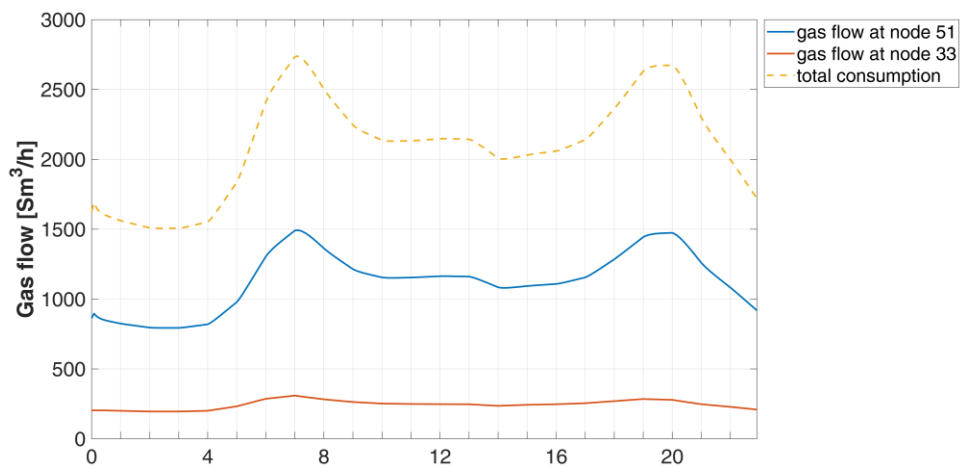
Figure 50 – Profiles of natural gas flow rate at the injection nodes compared to the overall gas consumption of the area (i.e. gas flow at the city gate)

No further blending occurs downstream the injection because the portion of the network has a tree topology thus the mixture formed at the injection node is transported downstream towards the farther exit points, as it is possible to get from Figure 49.b. It takes about 50 minutes for this translation.

The gas network has to deal with at least three different gas quality areas: the area upstream the injections, where traditional natural gas is distributed; and two areas characterized by the variable presence of hydrogen. One of these, in particular, has to face a remarkable gradient of the hydrogen molar fraction.

In the following figures (in Figure 51), the intraday evolution of three relevant fluid-dynamic parameters concerning gas quality variations are given and discussed for the two hydrogen injection nodes (33 and 51) and the consumption node 11, which is subject to further blending. Graphs on the left depicts the molar fraction of hydrogen within the mixture. Correspondingly, the central graphs gives the relative variation of the gas flow rates with respect to the non-injection case, evaluated in terms of standard cubic meters. All the addressed cases displays an increase of volumetric gas flow which follows the hydrogen presence in the mixture. This is because it was assumed that the thermal energy delivery should have remained the same, as boundary condition at the final users. Thus, being the volumetric higher heating value of the hydrogen blend less than the one of natural gas, more gas flow is requested from the users. This is an important aspect to bear in mind when assessing the fossil gas saving potential of the blending practices. In fact, as it is also reported on the graph, the amount of fossil gas that is substituted by the presence of hydrogen does not corresponds to the hydrogen molar faction, but it is less. In Table 13, a summary of the results are given for the three cases addressed in the figures. In particular, the percentage of natural gas substitution stands for the amount of natural gas have been saved calculated on the basis of the hourly gas flow (thus it is variable during the day). The integral of this value is

given later in this paragraph and it indicates the integral of the natural gas substitution curve.

Table 13 – Effect of the hydrogen blending on the gas flow variation and consequent natural gas substitution. Summary of the maximum values obtained for the different quality areas of the network.

node	H_2 molar fraction [%]	Gas flow variation [%]	Natural gas substitution [%]
33	11.7	+8.7 %	4.0 %
11	5.6	+4.0%	1.9 %
51	1.9	1.0%	0.6 %

In order to check on the fluid dynamic impacts downwards the hydrogen injection, the relative variation of the velocity along the pipe that is adjacent to the addressed node (with respect to the non-injection case) is given on the right side graphs. Because of the volume flow rate increase, the velocities will also increase accordingly. In the case study under consideration this does not bring these sections of the network to reach unacceptably higher velocities, but in case of higher amount of hydrogen during times of the year when consumption are higher – or in case the network is operated closer to its limits – this aspect may become an issue.
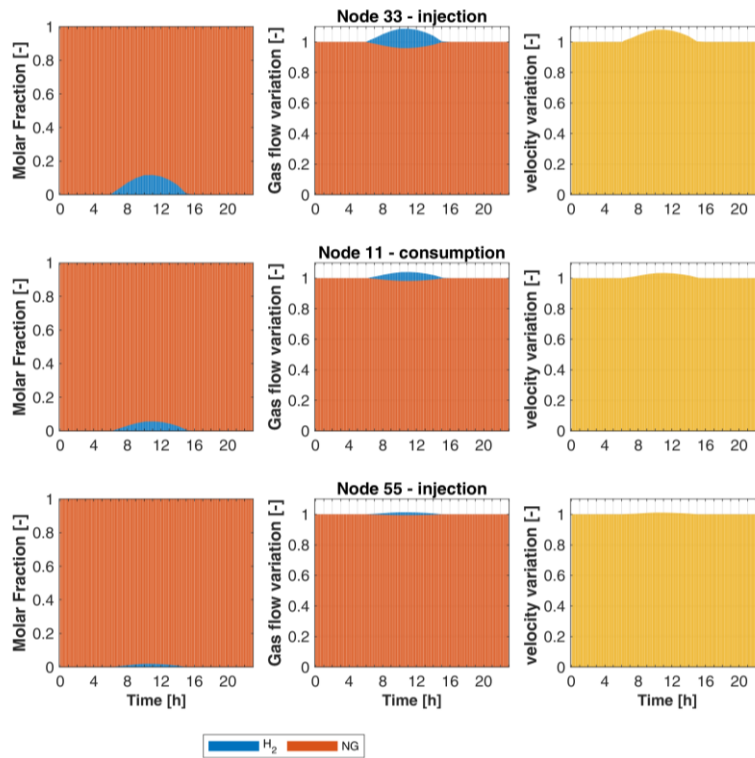
Figure 51 – Effect of the hydrogen blending on the gas flow rates and on the gas velocity at the injection point and at downstream consumption nodes.

Concerning the admissibility of hydrogen within the network and the acceptability of the gas quality of the blend, it should be reminded that the current technical regulation about biomethane injection limits the amount of hydrogen within the acceptable biomethane to 0.5 % [34]. This specific limit is often generalized to the whole Italian infrastructure, even though there are no specific limitations about hydrogen in [154], that is the technical rule setting the gas quality standards in Italy.

Therefore, when considering the 0.5 % limit, none of the considered injections generates a gas blend that is acceptable. Referring to the [154], which sets limits on gas quality parameters, then the situation is different and it is summarized in Figure 52.
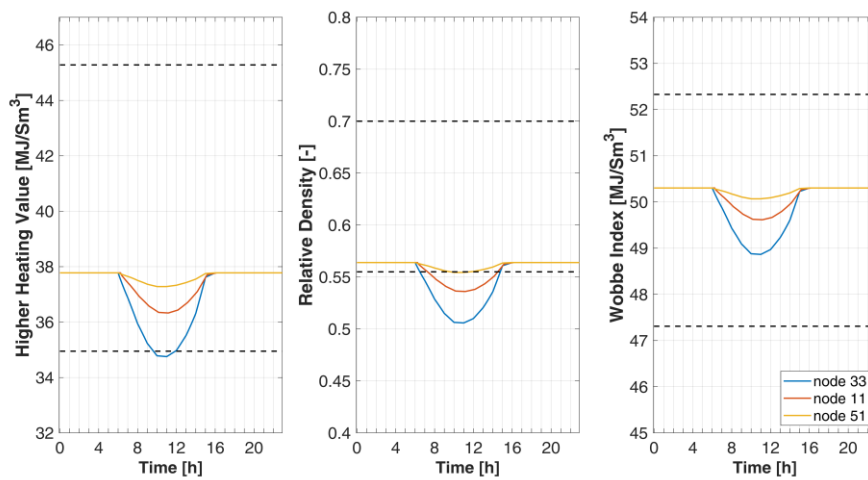
Figure 52 – Intraday variation of the three main gas quality parameters (higher heating value, relative density and Wobbe Index) for three selected nodes of the network: node 33 and 51 as the injection nodes and node 11 as consumption node.

The intraday variation of three main gas quality parameters are displayed for each of the addressed node. Each graphs refers to one of the parameter whose acceptability range are set in the national standards and here reported as dashed black lines. It is possible to infer that, when dealing with hydrogen injection and blending, the most critical value is the relative density of the resulting mixture. In fact, the only case in which the hydrogen blending brings to acceptable values is the one in node 51, where the smaller version of the solar-powered electrolyzers injects its production in a point with relatively high gas flows – it is the root of a tree-shaped portion of the network. Thus, at hydrogen concentration as high as almost 2%, the mixture approaches the minimum acceptable value of relative density. As for the other injection point and the consumption node 11, the hydrogen fraction gets quickly above 2%, thus the gas at those nodes are not compliant with the current regulations. It is worth noting that the critical value for the molar fraction of hydrogen within the natural gas with respect to the relative density depends on the composition of the natural gas itself. Natural gases with

less methane and higher fractions of heavier hydrocarbons may host higher quantities of hydrogen [21,54,155].

When turning to higher heating value and Wobbe Index, the hydrogen impacts appear to be less critical. In fact, even though hydrogen has a lower heating value than natural gas (on volumetric basis), it cause the heating value to exit the acceptability range only for molar fractions of about 12%.

In the end, concerning the Wobbe Index, it appears to be the least sensitive to the presence of hydrogen, given that though a drop is observed, its value is always well within the acceptability ranges. This is a remarkable result considering that the Wobbe Index is the traditional parameter representing the interchangeability of fuel-gases. Two gases having the same Wobbe Index releases the same thermal power output at a burner, with no need to change its valve setting. However, especially when dealing with hydrogen blends, Wobbe Index should not be the only reference criteria to establish whether a certain percentage is acceptable for the safe use of any downstream appliances and the safe management of the network.

At last, an evaluation on the fossil natural gas flow rates at the city-gate reduction station is performed in order to determine the savings of natural gas.
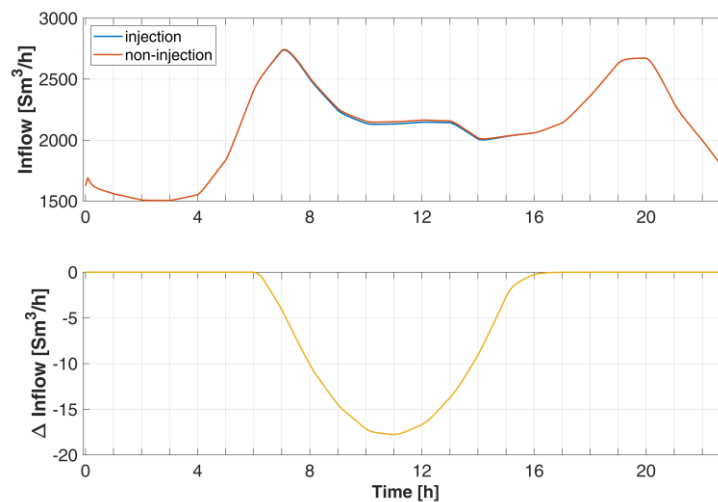
Figure 53 – Natural gas flow variation at the gas reduction station depending on the injection/non-injection scenario. Upper graph: gas flow rate patterns for the two cases; Lower graph: difference between the two-gas patterns above (i.e. saved natural gas)

As it is possible to see in Figure 53 (upper graph), the difference between the inlet flow of natural gas at the reduction station is barely visible. In the lower picture, the difference between the injection and the non-injection case is showed, representing the amount of fossil natural gas that is saved in this scenario. The overall daily natural gas savings are equal to the 0.22% of the daily gas consumption in the non-injection case.

4.3.2 Summer case

The day with minimum gas consumption is chosen for the summer case analysis. The solar hydrogen production is instead one of the highest of the year. The comparison between the profile of the natural gas overall consumption during the day and the injection pattern at the two nodes is given in Figure 54 –Figure 54.
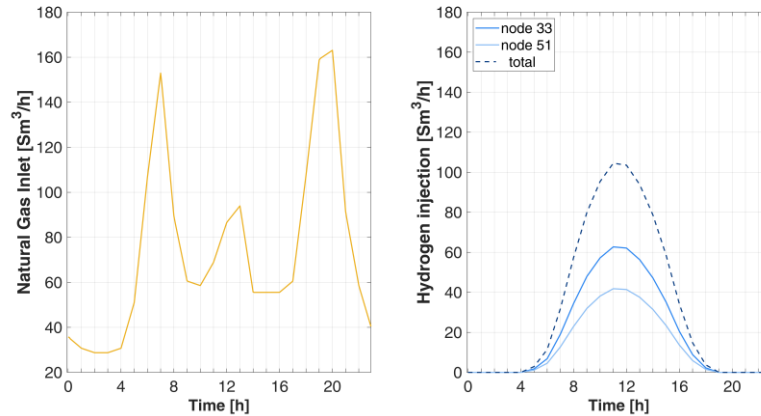
Figure 54 – Inlet gas flows to the network. Left side picture: natural gas inlet flow – for the case of non-injection scenario; right side picture: hydrogen injection sources.

It is worth noting that the gas consumption refers to the non-injection case, thus the amount of delivered gas will increase in case of hydrogen blending scenarios. In addition, in terms of mass balances, the density of hydrogen is about 8 time smaller than the density of natural gas, so the inlet mass flow of the hydrogen is very small compared to the natural gas flows. Furthermore, the energy content of the natural gas and of the hydrogen in volumetric terms is about 3:1, so each standard volume of hydrogen injected will substitute about 0.3 Sm^3 of natural gas under the assumption that the final users' consumptions are accounted in energy terms and no fuel switching effects at the appliances are considered. That is to say that no occurrences of over injection as observed for the biomethane case will happen.

The evolution of the network when hydrogen is injected is given in Figure 55. Differently than the previous winter case, the screenshots of the network are given with a time step of 4 hours in order to cover almost the whole time span in which relevant quality perturbations are visible throughout the network. In fact, as it is possible to see, the hydrogen presence within the network remains even after the injections have ended. In general, the dynamic of the network during particularly low summer time conditions is slow. This is clear referring to the gas velocity within the pipes (outer lines of each pipeline in figure), which are much lower than the ones depicted in Figure 48. Velocities are determined by the gas consumption rates that are also considerably lower in this case with respect to the winter consumptions. The size of the bullets are proportional to the gas

consumption level. However, it has been necessary to change the dimension scale to make summertime consumptions visible on the figures.

Gas network at time: 05:00
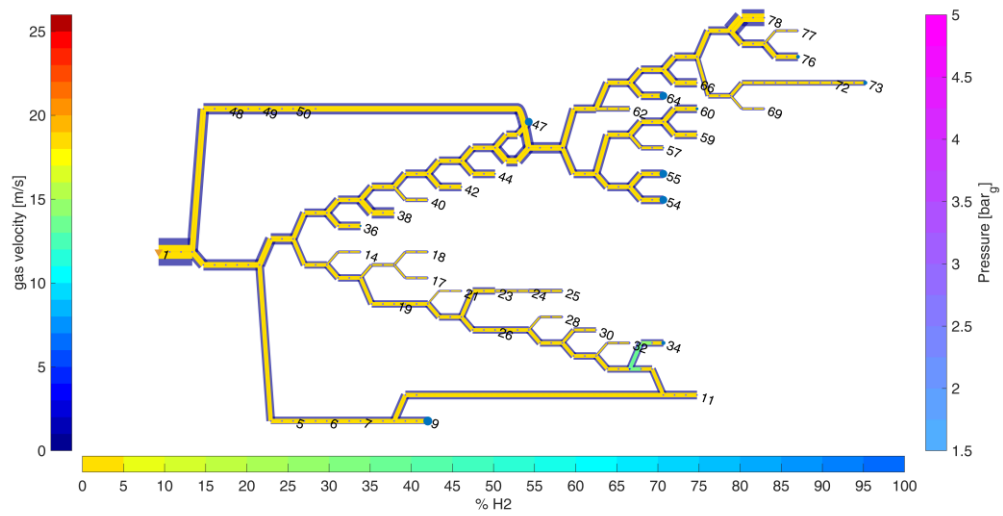
Gas network at time: 09:00
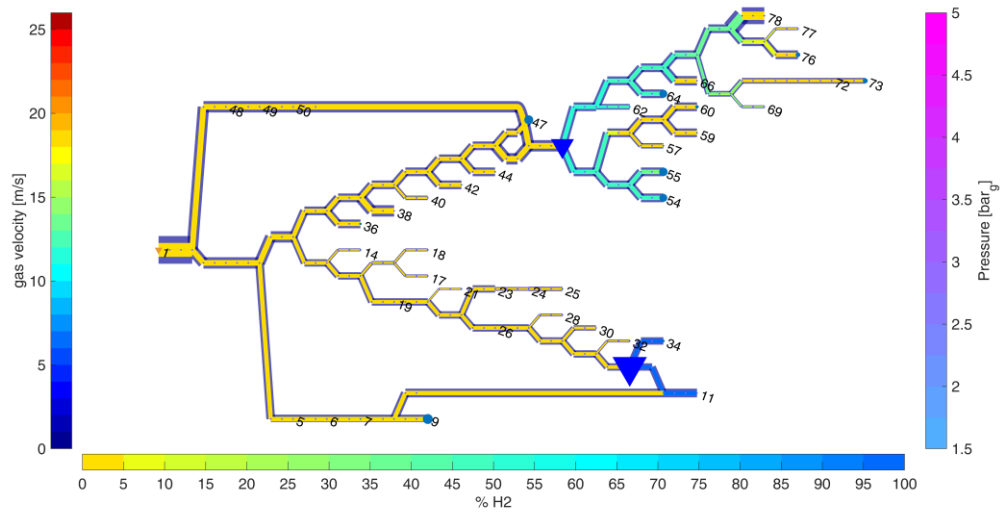
Gas network at time: 13:00
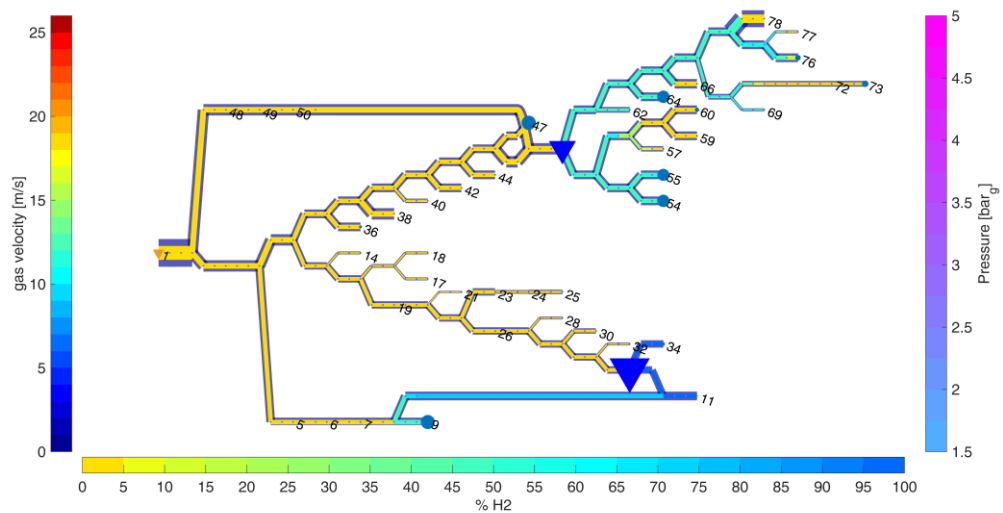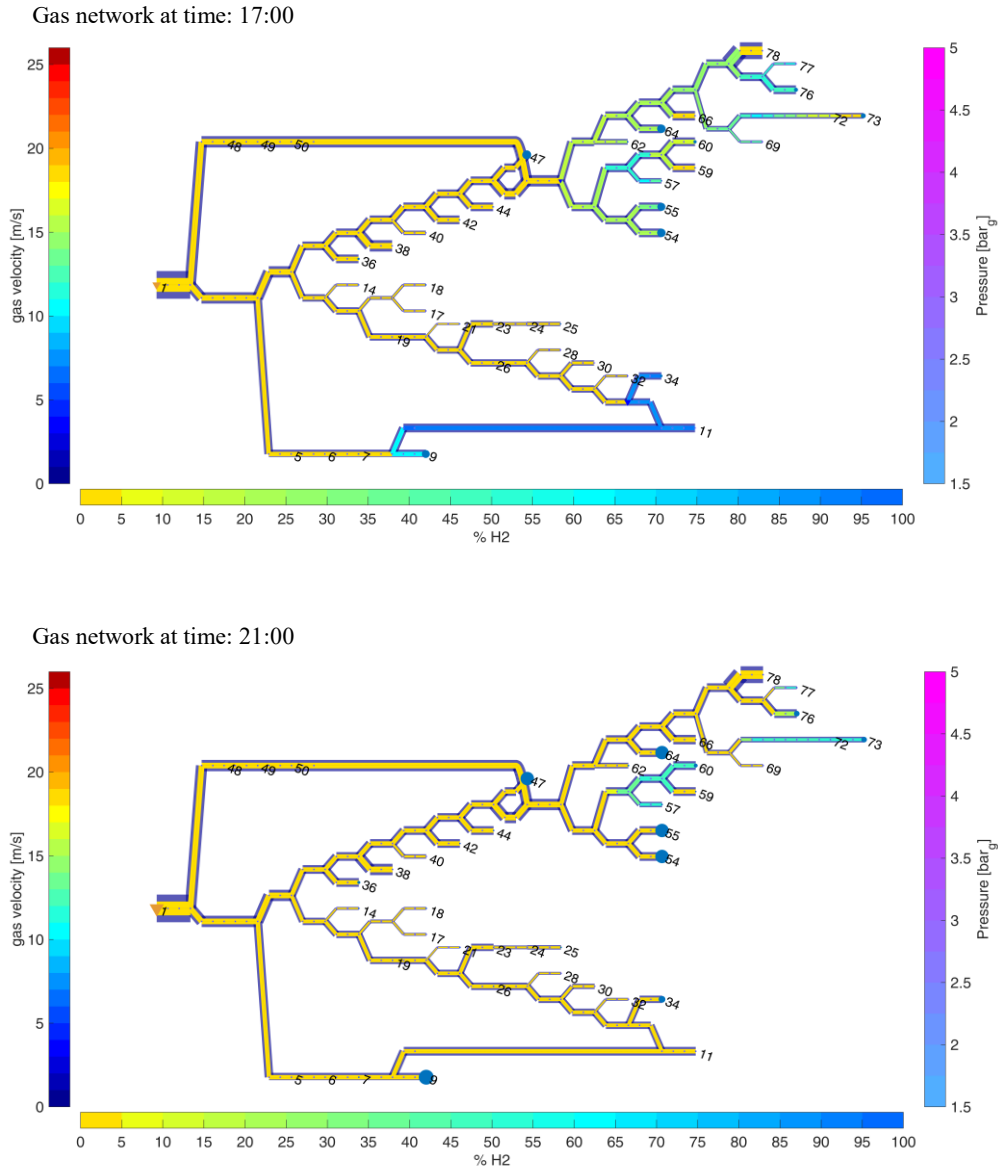
Figure 55 – Screenshots of gas network status during summer injections of solar hydrogen. Triangles highlights the gas entry points (blue triangles for hydrogen), bullets highlights the main withdrawal points. The color of the bullets indicates the nodal pressure. The size of the symbols are proportional to the amount of gas exchanged. The outlet lines of the pipelines reports gas velocity values; inner lines are colored according to the percentage of hydrogen within the gas flow.

The slower dynamics are clearly visible in the following graphs that represent the variation of the hydrogen concentration during the day at contiguous nodes. In Figure 56.a, the case for node 33 and its contiguous consumption node 34 is depicted. The concentration of hydrogen grows during the morning until it peaks 100%, obtaining thus a total substitution of the natural gas, replaced by hydrogen (under the assumption of maintaining the same energy output to the users).

Interestingly, the growth of the hydrogen fraction does not follow exactly the solar curve. This is an effect of the blending process within natural gas flow which varies according to the gas consumptions. Considering the hydrogen evolution at node 34, it is possible to note a lag in the hydrogen transport towards the exit node in the early morning, linked to the consumption pattern of the users at node 34. It takes about 1h35' for the hydrogen to get to the consumption node 34. Then the lag reduces until it almost disappears.
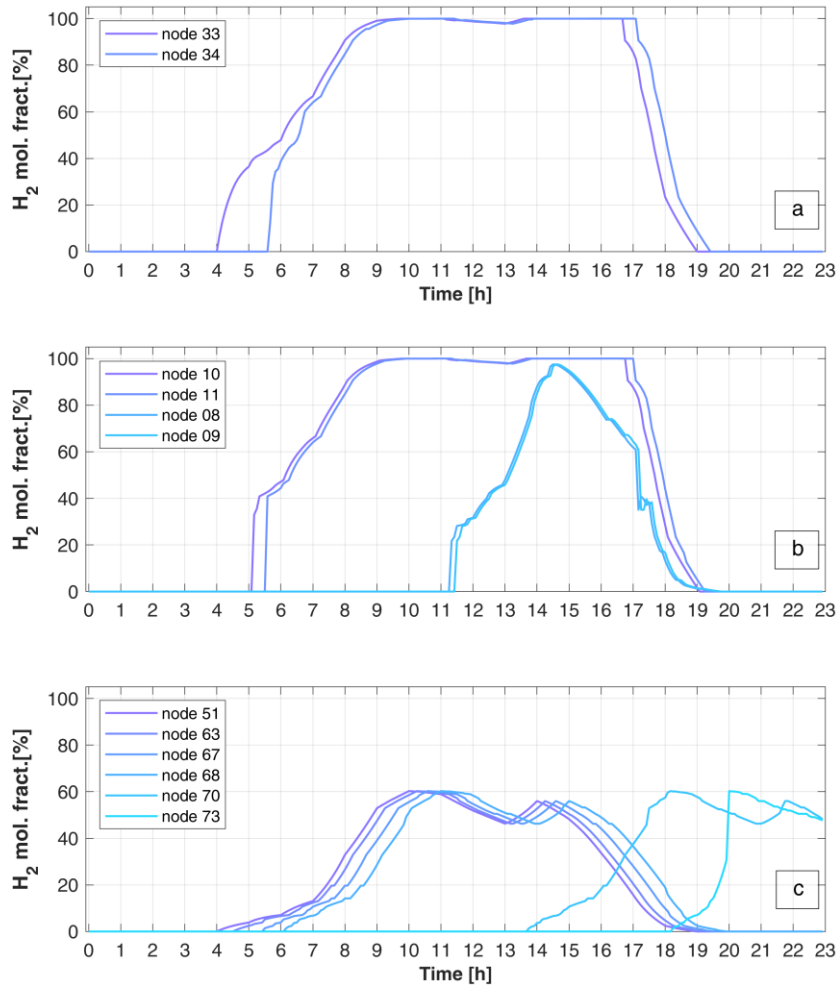
Figure 56 – Intraday evolution of hydrogen molar fraction for three different groups of nodes. Figure a): Injection 33 and contiguous consumption node 34; figure b) influence area of injection 33; figure c): node 51 and sequence of node along a branch of the downstream tree, until node 73.

A more peculiar situation is depicted in Figure 56.b, where the hydrogen fraction evolution of further nodes influenced by the injection at node 33 is given. The molar fraction at nodes 10 and 11 is given in order to perform a comparison with the previous winter case. In Figure 49.a, their hydrogen evolution pattern was given in order to show a further blending occurring within the network itself.

As of the summer case, nodes 10 and 11 undergo almost the same hydrogen evolution pattern of the injection node, slightly anticipating the transport time with respect to node 34, but then following the same pattern of the other nodes already commented. The further injection phenomena happens this time further away from the injection node, at node 8, the junction before consumption node 9. This junction is part of one of the two loops of the network so it can receive gas from both sides of the loop. This situation happens when hydrogen reaches the node and blends further. The result of this mixing process reaches almost instantaneously the consumption node 9. To be noted that the hydrogen reaches these node after about seven hours, generating at first a H_2-NG blend at around 30%, and then growing up to 97.5 % of hydrogen. These interactions at nodes 8 and 9 shows that and inversion of the gas fluxes happens along the connecting pipelined during the day.

A less complex blending scenario develops around the injection at node 51 (Figure 56.c) even though more peculiar dynamics of the hydrogen fraction evolution may be observed if compared to the winter case of Figure 49.b. In terms of profiles, what happens to the injection point is more or less translated to all the downstream nodes, with higher transport times with respect to the winter case. No further blending occurs downstream the injection because the portion of the network has a tree topology. Hydrogen concentration peaks 60 % but then the hydrogen pattern is influenced not only by the solar production but also by the consumption pattern, thus giving to the hydrogen molar fraction curve a different shape than the one it displayed in the winter case. In that case (see Figure 49.b, the curve followed the solar production thanks to the consumption pattern of the area which were quite stable – see Figure 50). It worth noting the persistence of hydrogen within the network under summertime gas consumptions: node 70 and 73 starts registering hydrogen presence when the solar production is almost over.

As observed for the winter case, the gas network has to deal with at least three different gas quality areas: the area upstream the injections with traditional natural gas and two areas characterized by the variable presence of hydrogen. During summer operating conditions, both the areas have to face a remarkable gradient of the hydrogen molar fraction, but the injection at node 33 results critical. Hydrogen in fact saturates the downstream lines in terms of complete gas substitution: there are thus nodes that will undergo a complete fuel switching (from 100% natural gas to 100% hydrogen) in a matter of a single day. What is more, the area influenced by injection at node 33 is wider under summertime network conditions.

In the following figures (in Figure 57), the intraday evolution of three relevant fluid-dynamic parameters concerning gas quality variations are given and discussed for the two hydrogen injection nodes (33 and 51) and two consumption nodes (11 and 9). Graphs on the left depicts the molar fraction of hydrogen within the mixture. Correspondingly, the central graphs gives the relative variation of the gas flow rates with respect to the non-injection case, evaluated in terms of

standard cubic meters. Because of the assumption that the thermal energy delivery to the users should have remained the same, all the addressed cases displays an increase of volumetric gas flow, which follows the hydrogen presence in the mixture. Of particular interest is the cases in which hydrogen substitutes completely the natural gas. As it is possible to see, the gas flow relative variations is coherent with the ration between heating values of natural gas and hydrogen on standard cubic meters basis (3:1). Thus, as the percentage of hydrogen grows within the blend, the total volume of the mixture should grow in order to carry the same amount of energy.
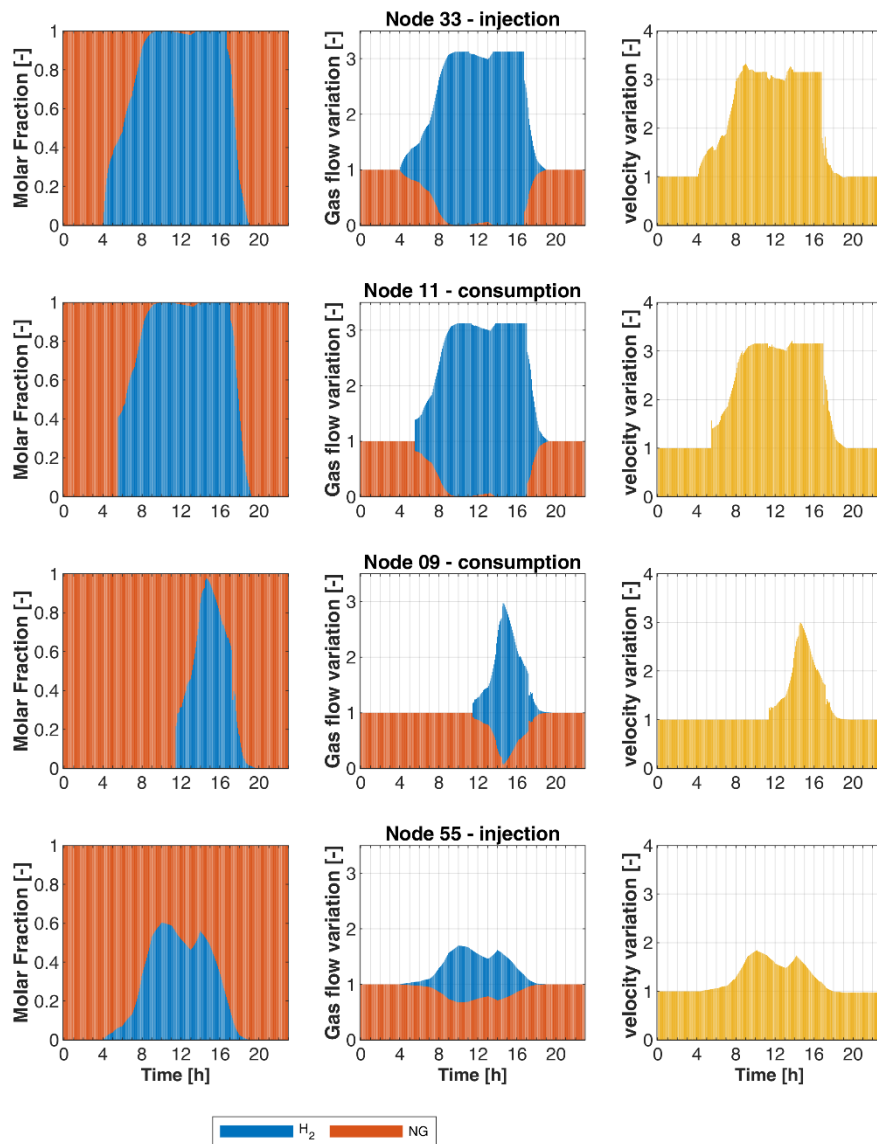
Figure 57 – Effect of the hydrogen blending on the gas flow rates and on the gas velocity at the injection point and at downstream consumption nodes.

The aspect of a non-linearity between the hydrogen fraction within the gas flow and the natural gas substitution provided that the same amount of energy is contained within the gas mixture, has already been addressed in the past sub-

section, where smaller amount of hydrogen where considered. In this case, the trajectory of a complete fuel switching can be analyzed. In Table 13, a summary of the results are given for the four addressed cases. It is worth noting the case of node 51 in which when the hydrogen molar fraction reaches 60% the amount of natural gas that has been substituted is 32.6%.

Table 14 – Effect of the hydrogen blending on the gas flow variation and consequent natural gas substitution. Summary of the maximum values obtained for the different quality areas of the network.

node	H_2 molar fraction [%]	Gas flow variation [%]	Natural gas substitution [%]
33	100	+212.7	100
11	100	+212.7	100
09	97.5	+196.7	92.6
51	60.3	+69.6	32.6

On the right side of Figure 57, the relative variation of the velocity along the pipe that is adjacent to the addressed node is given. Even though the velocity increase follows the same behavior of the gas flow increase, thus growing up to three times, it does not bring the addressed sections of the network to reach unacceptably high velocities. However, it is still a non-negligible variation, which is already remarkable for the case of 60 % hydrogen blends. This aspect is to be taken into account for scenarios in which hydrogen-rich blends are to be employed during the whole year or for those networks that are closer to their operational limits.

Besides the velocity potential issue, a more critical aspect regards the strong variations on the gas quality parameters. In Figure 58 the intraday variation of higher heating value, relative density and Wobbe Index is given for the four nodes addressed in the previous figure. The limits for each parameter are also given in each graph, according to [154]. As opposite to the previous case, no parameters are compliant with the standard limits under any of the circumstances. In fact, besides the relative density, which is already very near to the lower acceptability limit when 100% natural gas is considered, the higher heating value and the Wobbe index too drops under the respective acceptability limits with very sharp profiles, following the quick increase of hydrogen fraction within the gas flow.

In particular, the critical value of hydrogen molar fraction that causes the drop of the higher heating value is 12.4 %, which is reached within the first 30 minutes of injection for the case of injection at node 33. As for the Wobbe Index, the critical threshold within this case is 24.1%, which is reached just 10 minutes later. As for injection at node 55, the limits are reached later: after 2h40' of injection for the higher heating value and after 7h40' for the Wobbe Index. Of course blending a

smaller amount of hydrogen in a network node where higher amount of gas flows makes the practice less impactful and more acceptable.
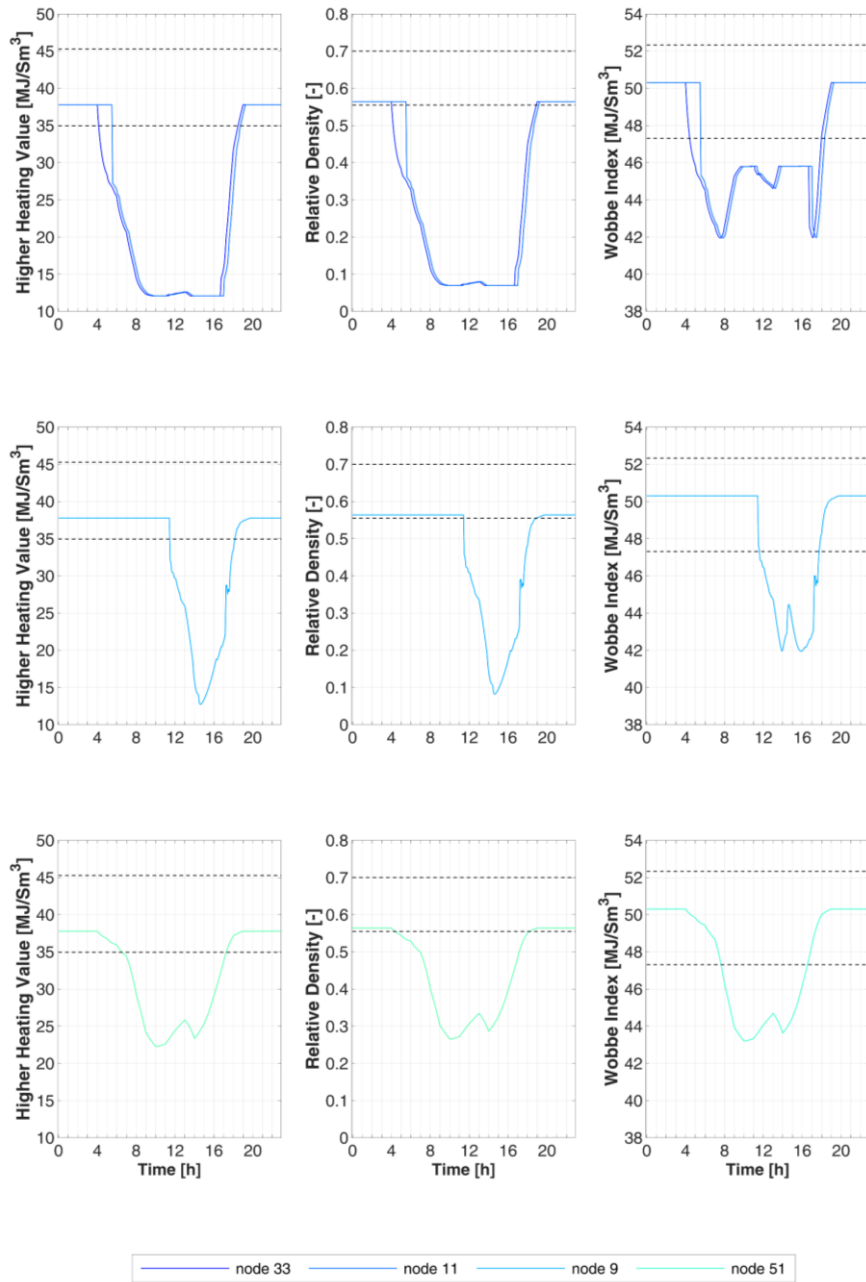
Figure 58 – Intraday variation of the three main gas quality parameters (higher heating value, relative density and Wobbe Index) for four selected nodes of the network: node 33 and 51 as the injection nodes and node 11 and 09 as consumption nodes.

It is worth noting the different behavior of the Wobbe Index variation displays with respect to the other parameters, especially when very high levels of hydrogen are approached. In correspondence of these cases, the Wobbe Index increases again after a sharp drop. This happens when hydrogen fraction exceeds the 80 % and it is linked to the formula for the calculation of Wobbe Index, which have a strong non-linearity given by the square root of the relative density of the gas at

the denominator. This causes the Wobbe Index of a hydrogen-natural gas mixture to grow again when hydrogen fraction approaches 100%.

The comments just made about the gas quality perturbations in the summer case raise critical issues on the direct injection of hydrogen within the gas network in the context of integration between renewable energy and renewable gas, thus making the case study just addressed a "virtual" case. This is not only due to the non-compliance with the quality standard, but also for the sudden fuel switching (natural gas – hydrogen) which some areas of the network undergoes within a very short time span (hours). This may probably have too strong impacts on the final users' appliances.

Nonetheless, in order to complete the analysis following the scheme of the winter case, the flow rates of fossil natural gas at the city-gate are compared for the two cases of injection/non-injection in order to evaluate the savings of natural gas.
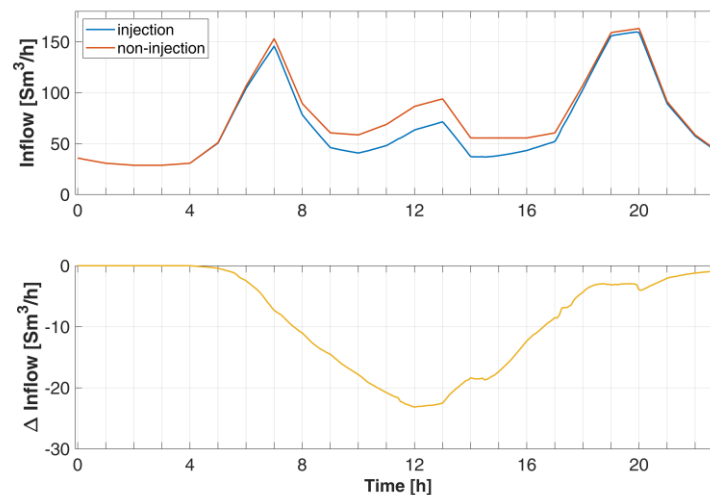
Figure 59 – Natural gas flow variation at the gas reduction station depending on the injection/non-injection scenario. Upper graph: gas flow rate patterns for the two cases; Lower graph: difference between the two-gas patterns above (i.e. saved natural gas)

In Figure 59 (upper graph), the entry gas flow rates under the two scenarios are displayed. Differently form the case of Figure 53, the difference between the inlet flows of natural gas is clearly visible. In the lower picture, the difference between the injection and the non-injection case is showed, representing the amount of fossil natural gas that is saved in this scenario. The overall daily natural gas savings are equal to the 11.7% of the daily gas consumption in the non-injection case.

4.4 Hydrogen admissibility

The case studies and the analysis from the previous sections showed that the critical parameters for the hydrogen acceptability within the gas network are the ones related to the gas quality. This often translates into a set of maximum acceptable percentages of hydrogen in the H_2-NG mixture, according to the quality parameter taken into account.

The previous analysis showed that the impact of the hydrogen injection within the network is a combination of the following different factors:
- hydrogen production curves,
- gas consumption rates,
- choice of the injection point.

Two out of three of these factors are directly related to gas network and the amount of gas that flows throughout each pipe.

The gas consumption rates, strongly influenced by the season, determines the overall amount of gas entering the infrastructures and, to some extent, the way the gas distributes within the network. The partition of gas fluxes among each pipeline is a complex interplay between intraday consumption patterns of costumers or clusters of costumers and network topology. Some examples of a similar complex network behavior have been observed when reverse gas flows occurred during the summertime case scenario of solar-hydrogen injection. The amount of gas flowing through each pipeline of the network at any moment of the infrastructure operational activity is an essential information in order to determine the amount of hydrogen that is acceptable in injection by each node of the network.

4.4.1 Methodology

By means of the gas network model presented and applied in this work, it is possible to determine the hydrogen receiving potential throughout any network, once the topology and gas consumption patterns are given.

In this section, this evaluation has been carried out for the infrastructure already considered in the previous cases, under the two operating conditions of winter maximum consumption and summer minimum consumption.

The hydrogen acceptability is a preliminary analysis, in the sense that the hydrogen receiving potential is assessed, but no injections are performed. Thus, knowing the amount of gas that passes through each node, the amount of hydrogen that is possible to inject and to blend within the gas flux is calculated on the basis of the choice of the hydrogen fraction limit. The procedure that leads to the problem formulation is here illustrated.

First, it is necessary to know the amount of gas which flows through each node. When solving the fluid-dynamic problem, the gas mass flows are referred to the pipelines in which they transit rather than to the nodes they pass through. Thus, the allocation of pipeline mass flows to corresponding node is to be performed by means of the following formula:

$$\mathbf{G_n} = \mathbf{A} \,(\mathbf{I}\,\boldsymbol{G})\, \mathbf{A^+} \tag{4.3}$$

Where the term $(\mathbf{I}\,\boldsymbol{G})$ is equal to a $b{\times}b$ diagonal matrix with all the gas flow values on the diagonal. Equation (4.3) generates an $n{\times}n$ matrix whose diagonal corresponds to the nodal allocation of the branch gas flows. Therefore, it is possible to extract the following $n{\times}\,1$ vector:

$$\boldsymbol{G_n} = diag(\mathbf{G_n})$$

In order to obtain a formulation for the assessment of hydrogen acceptability, the "gas substitution rule" must be expressed in the form of equation. Throughout this work, the assumption of preserving the amount of energy within the gas flow has been considered as the condition for the obtained hydrogen-gas blend. In mathematical form, it can be written as follows:

$$\boldsymbol{G_n} \circ HHV_{NG} \;=\; \boldsymbol{G_{n_{H_2}}} \circ HHV_{H_2} + \; \boldsymbol{G'_n} \circ HHV_{NG} \tag{4.4}$$

Where the mathematical operator ∘ stands for the "element-by-element" product. Equation (4.4) sets the condition for which the energy content of the gas flow through each node in the situation of no-injection must be equal to the energy content of the hydrogen and natural gas mixture obtained after the possible injection of the gas flow $\boldsymbol{G_{n_{H_2}}}$. The energy content of the ex-post blend is expressed as a sum of the two main components: hydrogen and natural gas, keeping in mind that for the natural gas part, a new vector $\boldsymbol{G'_n}$ is to be considered since a partial substitution of natural gas by the injected hydrogen will occur, as already commented in the previous sections

Thus, Equation (4.4) has two unknowns that are the amount of hydrogen $\boldsymbol{G_{n_{H_2}}}$ and the updated value of the nodal natural gas fluxes $\boldsymbol{G'_n}$. These two values are interdependent by means of the definition of hydrogen fraction $\boldsymbol{y}_{H_2}$:

$$y_{H_2} = \frac{G_{n_{H_2}} \circ \rho_{H_2}^{(STD)}}{G_{n_{H_2}} \circ \rho_{H_2}^{(STD)} + G'_n \circ \rho_{NG}^{(STD)}} \tag{4.5}$$

that is expressed in vol/vol terms, applying the standard densities to each mass gas flows.

In this analysis, the hydrogen fraction y_{H_2} is the independent variable: the amount of the hydrogen receiving potential of each node is determined according to the choice of the desired hydrogen fraction. This choice can be made so that the resulting blend is compliant with one of the gas quality parameters discussed before or any other imposed hydrogen limit.

From Eq. (4.5) it is possible to obtain an expression for G'_n . This expression is to be used in Eq. (4.4) in order to obtain the following formula for the assessment of the hydrogen injection potential of each node, as a function of the hydrogen fraction y_{H_2}:

$$G_{n_{H_2}} = \frac{G_n}{\dfrac{HHV_{H_2}}{HHV_{NG}} + \dfrac{1 - y_{H_2}}{y_{H_2}} \dfrac{\rho_{NG}^{(STD)}}{\rho_{H_2}^{(STD)}}} \tag{4.6}$$

in which all the operations among vectors are to be intended as element-by-element operations.

By means of Equation (4.6), once the target hydrogen y_{H_2} is set and the fluid-dynamic of the gas network is solved, the amount of hydrogen that can be blended within each node is obtained so to get the desired H$_2$-NG mixture.

If a time evolution of the network is considered, then the profile of the maximum amount of acceptable hydrogen can be determined. This kind of information may be useful in order to check the mismatch between production profiles and hydrogen receiving potential ones.

The information about the acceptable hydrogen profiles can also be converted in terms of electrical power that is necessary to provide to an electrolyzer in order to produce the same amount of hydrogen by means of this formula:

$$\mathcal{P}_{el}(t) = \frac{\dot{m}_{H_2}(t) \, HHV_{H_2}}{\eta_{HHV}} \tag{4.7}$$

where η_{HHV} is the conversion efficiency of the electrolyzer. In case the electrolyzer is directly coupled with a renewable energy source, then the storability of renewable electricity within the gas network is obtained.

In any case, in the context of sector coupling and integration between electricity and gas infrastructure, this amount of "equivalent electricity" gives a measure of the actual flexibility that the gas network may provide to the power sector.

4.4.2 Results

The methodology illustrated in the previous subsections has been applied to the two case studies already addressed, in order to highlight the seasonality that affects any gas distribution infrastructure.

A target value for the hydrogen molar fraction needs to be chosen. From the previous analysis it emerged that the natural gas feeding the network is already very light in terms of relative density, being its value very close to the lower limit set by Italian standards. In fact, already when the hydrogen fraction exceeds 2%, the relative density of the obtained mixture gets outside the ranges. However, under the higher heating value and the Wobbe Index perspective, the hydrogen acceptability margins are wider. Considering the higher heating value, the critical hydrogen fraction for this case is around 12% while for Wobbe Index the value turns to be 24%. For the sake of this analysis, the critical values of hydrogen molar fraction for the cases of relative density and for higher heating value have been considered and results are given in the following figures. In Figure 60 and Figure 61, the hydrogen acceptability maps are given for the two network conditions (summer and winter respectively). In the figures, the values of hydrogen acceptability are already translated in equivalent amount of renewable power that is necessary to employ in order to produce hydrogen by means of the power-to-hydrogen pathway, by the application of Equation (4.7) and considering an electrolyzer efficiency of 65%$_{HHV}$. They are referred to a single time step: noon (12:00).

Renewable hydrogen admissibility map – $y_{H_2} limit = 2\%$ – summer case
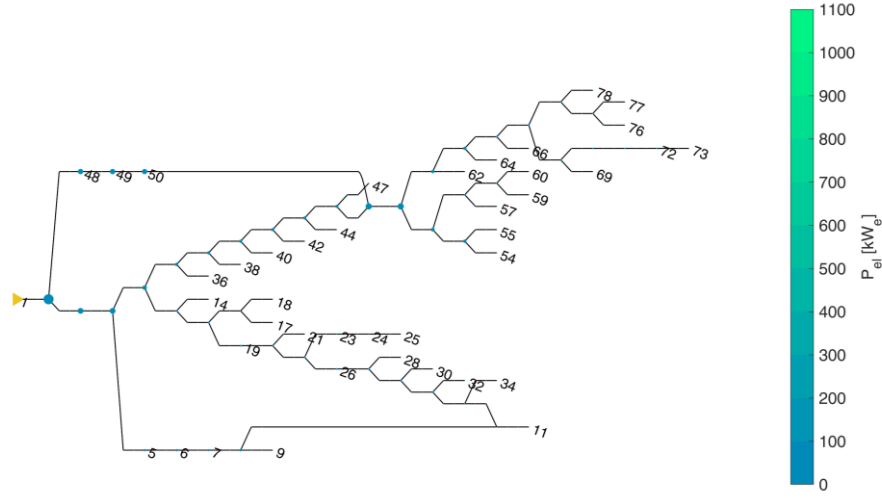
Renewable hydrogen admissibility map – $y_{H_2} limit = 12\%$ – summer case
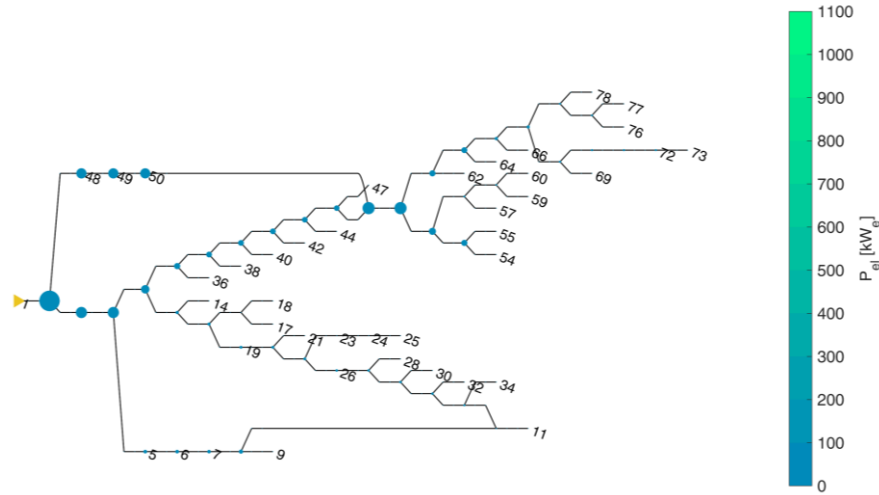
Figure 60 – Hydrogen admissibility maps for the two considered hydrogen limits, referred to the timeframe 12:00. Summer case.

Concerning the summer time – minimum consumption – gas load conditions, the bottlenecks that the gas network shows in the framework of the hosting capability of renewable gas are clearly visible from these admissibility maps. If the most strict hydrogen limit is to be observed ($y_{H_2} limit = 2\%$), then, referring to the 12:00 timeframe, only around 1.7 Sm³/h of hydrogen is injectable at the city-gate node, which corresponds to around 8.9 kW$_e$ of renewable power requirement as input to the chosen electrolyzer. The number changes if the hydrogen limit of $y_{H_2} limit = 12\%$ is considered, but in terms of required power, the number is still well below 100 kW addressing the city-gate node, as it is possible to infer from Figure 60 ($\mathcal{P}_{el}$ = 58.3 kW$_e$ corresponding to a hydrogen production of 11.1 Sm³/h).

Renewable hydrogen admissibility map – $y_{H_2} limit = 2\%$ – winter case
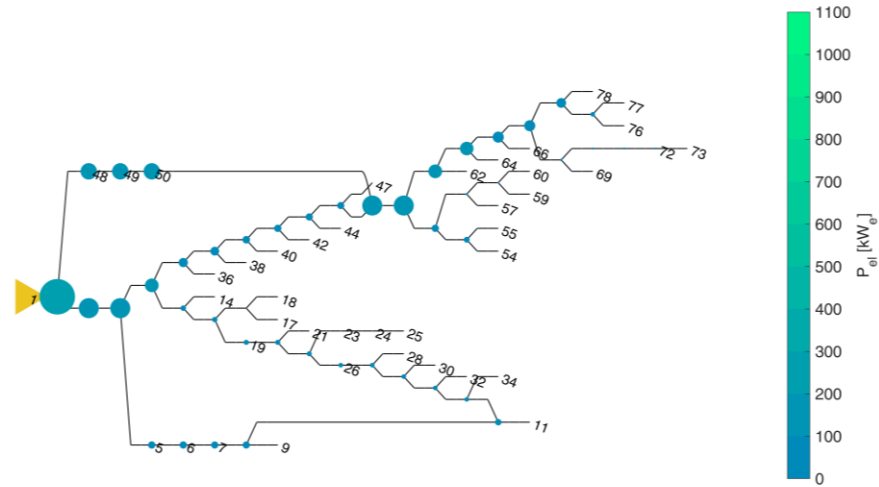
Renewable hydrogen admissibility map – $y_{H_2} limit = 12\%$ – winter case
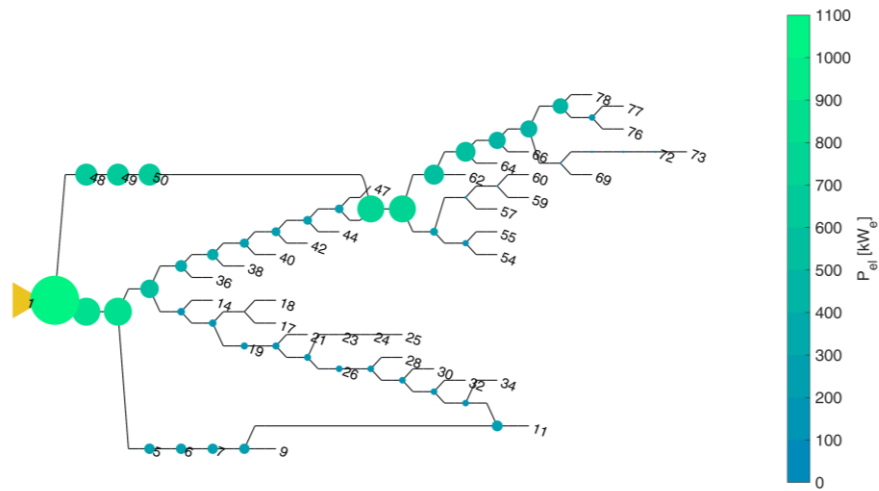
Figure 61 – Hydrogen admissibility maps for the two considered hydrogen limits, referred to the timeframe 12:00. Winter case.

More significant results are displayed in Figure 61 where the winter case condition is addressed, referring to a gas network screenshot at 12:00. A distributed hydrogen injection potential is visible throughout the network already for the case of hydrogen fraction limit sets at 2%. In this case, the receivable hydrogen at the city-gate node at noon grows to 43.8 Sm^3/h, which corresponds to an electrolyzer power input of around 226 kW$_e$. On the basis of Equation (4.6), these values grows linearly with the amount of gas flowing through each node.

With respect of the increase of hydrogen fraction limit, the acceptable hydrogen growth is instead non-linear, as it is possible to infer again from the Equation (4.6). As it is possible to observe from Figure 61, the amount of acceptable

hydrogen has a significant increase when the composition limits is raised to 12% . This allows in fact receiving a hydrogen injection flow of 282.6 Sm^3/h corresponding to 1.46 MW$_e$ of power to be provided to the electrolyzer system.

The comments are all referred to the city-gate node because, of course, it is always the node with the maximum blending capacity, since the gas flow for the whole consumption area pass through this point and given the gas flows magnitude of certain cases; it is the only node that allows a fair comparison of the results. The network visualization of the hydrogen acceptability results under a given hydrogen fraction limit are useful to extend these analysis to the other nodes of the network in view of distributed injection scenarios (similar to the ones addressed in 4.2). It emerges, for example, that the nodes with relevant blending potential turns to be node 46 and 51, as well as the group of node 48-49-50. Less potential is instead displayed by the bottom section of the network, where also node 33 is located.

To complete the analysis of the hydrogen admissibility case study, the two hydrogen admissibility curves obtained for the two hydrogen limits are given in Figure 62 and Figure 63 for the summer and the winter days respectively, referred to the case of node 51.

For both cases, it is possible to observe the remarkable variability of the admissible hydrogen pattern (blue lines), which follows the gas consumptions profiles. Comparing the two figures, it is also possible to see the different order of magnitude on the y-axis scale, which is linked to the seasonality of the consumptions. This difference is exacerbated by the fact that the maximum and the minimum consumption days have been compared. However, these are relevant cases because represent the extreme case scenarios one should expect from the gas network behavior.
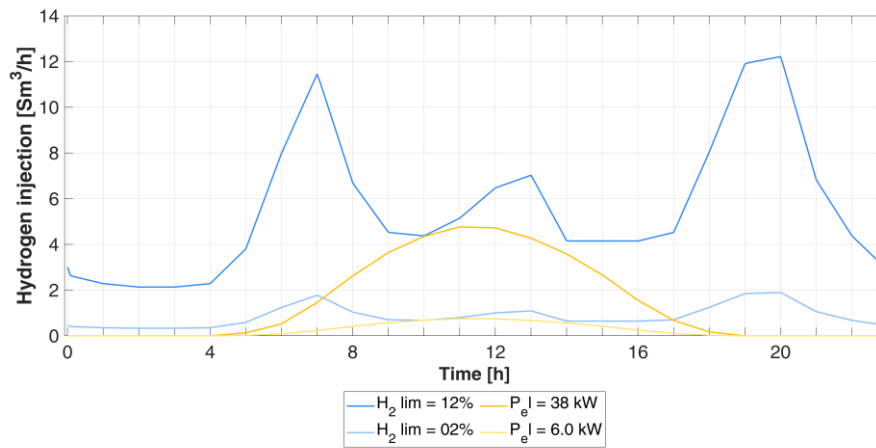
Figure 62 – Hydrogen admissibility profiles at node 51 for the two investigated hydrogen fraction limits (2% and 12%) referred to the summer time case, compared to the calculated maximum acceptable hydrogen profiles produced by solar source.
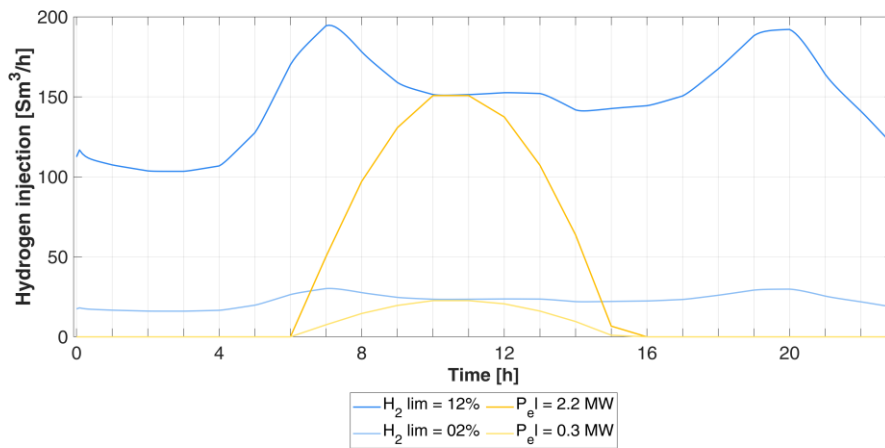
Figure 63 – Hydrogen admissibility profiles at node 51 for the two investigated hydrogen fraction limits (2% and 12%) referred to the winter time case, compared to the calculated maximum acceptable hydrogen profiles produced by solar source.

Given the profiles of the network, constraints just commented, on the same graph, the maximum solar hydrogen production profiles that match with the hydrogen admissibility ones is given and the rated power of the solar PV system is calculated. Concerning the summertime case of Figure 62, the solar panel rated power referred to the 12% hydrogen limit scenario must be limited to 38 kW. Turning to the homologous case within the winter scenario of Figure 63, this value grows up to 2.2 MW as a combined effect of increased hydrogen admissibility and decreased solar energy productivity. These observations pose

questions on the mismatch between gas sector and the power sector, at least concerning the solar energy coupling by means of hydrogen from power to gas.

At last, not only the seasonal variation, but also the intraday mismatch between hydrogen admissibility and hydrogen production may undermine affect the solar hydrogen coupling, as it is possible to see from the two figures: hydrogen admissibility peaks are not aligned with solar production one.

4.5   Conclusions

In this chapter the gas network model is employed for the simulation of a gas distribution network under hydrogen blending from two distributed sources, whose injection profiles varies according to a production profile. With respect to the biomethane case, in this application the multi-gas features of the model has been best highlighted, showing the quality tracking capability in complex network conditions as well as the capability to account for the fuel switching by computing higher amount of gas flowing through the pipes affected by hydrogen blending.

The results obtained from the network simulation cases showed that the direct injection of a gas that is completely different form the usual natural gas may have critical impacts on the fluid-dynamic of the network (especially the section that is downstream the injection). Under the assumption that the final users' thermal energy demand remains constant as not affected by the fuel switching, then the amount of distributed gas, in volumetric terms, must grow in order to compensate the loss in the volumetric higher heating value caused by higher fraction of hydrogen. The peculiar trend of natural gas substitution by hydrogen has been observed and commented, being non-linear with respect to the hydrogen fraction. In Figure 64 this trend is reported for the whole spectrum of possible hydrogen fraction within a H_2-NG blend, under the assumption that hydrogen is progressively substituting natural gas in order to obtain a gas mixture that have the same energy content as the starting natural gas. It is possible to see that the trend of the hydrogen contribution in energy terms to the overall energy content of the mixture is not linear with the hydrogen molar fraction, as already noted during the simulations. This is an important aspect to bear in mind when evaluating the benefits of hydrogen injection within the gas system: as it is possible to infer from Figure 64, to obtain a 10 % substitution, the hydrogen fraction within the blend should be higher than 20%.

The red line indicates instead the linear volume growth caused by the hydrogen, following the 3:1 ratio of the higher heating values.
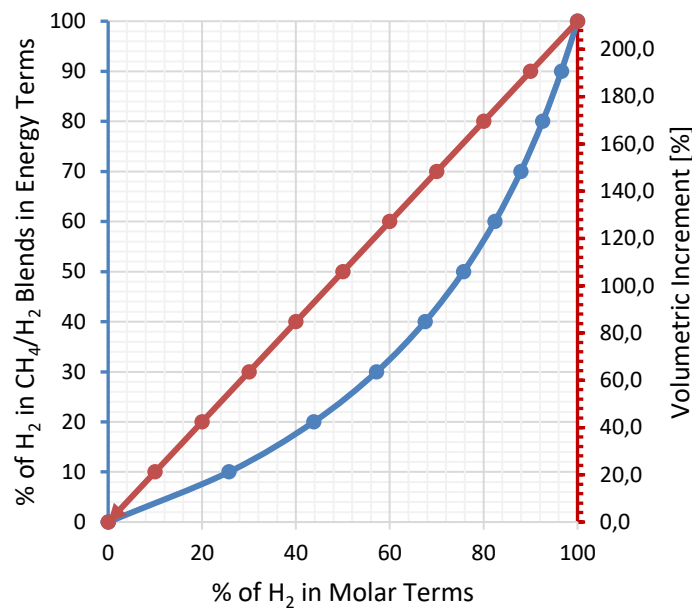
Figure 64 – Impact of the growing hydrogen fraction within the natural gas-hydrogen blends. Left axis is referred to the blue line that displays the contribution of the hydrogen fraction to the energetic content of the blend; Right axis is referred to the red line that displays the volumetric increment of the overall natural gas mixture caused by hydrogen substitution of natural gas. These values are referred to mixture with constant energy content.

It is worth noting that the assumption of constant thermal energy output, especially at final users' appliances level, may not represent the exact reality of their behavior. This in fact depends very much on the combustion control and regulation systems of the final appliances. The ones that are not equipped with self-regulating systems may be affected in their thermal output release as a consequence of the different density of the hydrogen-natural gas mixture. However, in the context of the assumptions made, the higher flow rate implies higher velocity, which have been registered not to be critical in the observed cases, but it may turn to be a critical parameter in those networks working near their limits. This aspect depends on the rationale behind the planning of the infrastructure itself and the subsequent evolution of the amount and of the type of connected users. This is one of the reason why generalization of results about the feasibility of similar practice on large scale are difficult to be inferred. A case-by-case analysis is still needed to check local and peculiar possible barriers.

By means of the network simulation tools, the impact of the hydrogen blending is evaluated on a broader level, the network infrastructure one. The distributed nature of renewable energy sources may express in the future the need of distributed injections of renewable gases throughout the infrastructure, with possible multiple injection points as the one that has been simulated. Having a global picture of the network behavior is important to assess the magnitude of the quality perturbations, their size in terms of influenced network area and its

evolution under different working condition of the network. These dynamics may also end to generate possible interferences between the different sources. This is not an occurrence that was observed within the sample case studies presented here, but it may be a possible scenario consequent to the choice of different injection points or depending on the network topology or the interplay between gas consumptions profiles, injection profiles and flow distribution.

The major impacts are observed in terms of quality perturbation of the natural gas. If the current Italian ranges of higher heating value, relative density and Wobbe Index are to be applied, the presence of hydrogen may quickly cause unacceptable deviation of at least one of these: the relative density. However, this is strongly influenced by the conditions of the natural gas in which the blending is practiced, adding a further terms of peculiarity to the general discussion about hydrogen blending in natural gas. It is worth to be also reminded that gas quality regulation are still not homogeneous throughout Europe, even though the gas network infrastructure is highly interconnected. This to say that gas quality ranges are good indicators but does not establish the acceptability or not of a hydrogen blend, as it is also proven by the several pilots initiatives described in the introduction.

Thanks to the different scenarios that have been simulated, it is more relevant to put in comparison the different gas quality impacts under different gas network and hydrogen production working conditions. In fact, while during the winter operation mode the blending may be considered acceptable throughout the network as does not exceed 12%, in the summer case the hydrogen availability may be so high that areas of 100 % of hydrogen may originates, creating full hydrogen district. Even though this is a "virtual" scenario, this draws the attention on the flexibility limits the natural gas distribution infrastructure may offer to the electricity system. This aspect is especially critical addressing the case of solar power production coupled to the sector integration by means of hydrogen. In fact, the times of the year of maximum production corresponds to the times of minimum consumption of the gas network.

This aspect has led the author to set up the assessment of the hydrogen admissibility map and the determination of the admissibility profiles that set the hydrogen injection limits to prioritize the constraints required by the gas network in the framework of greening the gas and coupling the sector. The evidence from this exercise is that the strong seasonal variation may be a non-negligible bottleneck towards the sector coupling, at least at the level of distribution level where the infrastructure manage limited amount of gas.

So, while the gas distribution level may offer promising case studies to exercise the hydrogen blending practice (with quality impacts limited on a confined and well defined area with no need of higher level harmonization efforts on the quality standard regulations), the magnitude of the allowable hydrogen, especially coming from variable renewable source may be significantly reduced

by the limited capacity they have. A possible option to avoid similar issue may come from the production of SNG from renewable hydrogen and then, injecting it into the gas infrastructure. The value chain would be even more improved if the necessary CO_2 for the methanation would come from a previous sequestration from biogas upgrading.

Chapter 5

Electric and Gas infrastructure

combined simulation

5.1 Introduction

Hydrogen production and injection within the gas network is often considered as an alternative way to store surplus energy produced by the renewable sources and which may be otherwise curtailed in order to avoid unbalances on the electrical infrastructure.

In this section, a sample case study of sector integration is given, for the case of distribution infrastructures, which are nowadays characterized by a certain amount of distributed generation. A different urban case study has been addressed with respect to the previous model applications. In this case, both electric and gas infrastructures are known and the main features of the area and of the infrastructures are presented in the following sections.

The case study investigates, on the one hand, the impacts on the electricity distribution infrastructure of a progressively high penetration of solar distributed generation. On the other hand, whenever the electrical infrastructure reaches critical or unconventional operating situations, the excess of the solar production is assumed to be converted into hydrogen by means of a suitable power-to-gas system and subsequently injected into the gas distribution grid.

5.2   Interlink between the infrastructure models

The integrated modeling framework consists of the sequential simulation of the electricity and the gas network infrastructures. According to the case study here addressed, there is no need to set up a modeling framework capable to solve numerically power and gas flows within the same time iteration, because the tested scenario is sequential. In fact, the impacts of higher amount of PV on the power grid are shifted to the gas sector, whose operating condition will not affect the power system anymore.

At first, all the data about the energy infrastructures and the energy consumption profiles are collected. The topology of the networks and the useful technical features of the branches (cables and pipelines) are provided to the model as parameters. Being the medium voltage and medium pressure level of the energy grids the focus of the model, the majority of the consumption nodes are composed of clusters of users. The composition of each consumption clusters in terms of types of final users is also a relevant information to be given. The data acquisition phase ends with the input of the power and gas consumption curves for each user type. In this specific case, these data are obtained from users' consumption profiles expressed as a fraction of the installed electrical power and the daily gas flow rates.

The RES penetration scenario is then tested on the electricity infrastructure. A RES penetration rule is decided so that distributed generation is progressively installed. For each installation step, the electric power flow is performed for a typical day by means of the electrical network model. Solar production curves for a typical day of each month, taken from PV-GIS database [156] are also provided as input to the model. In fact, to take into account the seasonality of the solar production, a further month-by-month iteration is carried out.

In order to check the operating conditions of the electric infrastructure, specific key performance indicators are calculated and their compliance with the normal operation limits are checked. Table 15 summarizes the key performance indicators considered for the electrical case, together with their operational limits.

Table 15 – Summary of the electricity network constraints to be verified during the simulations

Parameter	Units	Limits
Nodal Voltage	[p.u.]	0.95 ÷ 1.05
Max Line Current	[p.u.]	< 1
Reverse Power Flow	[MW]	0

Thus, possible deviations of the key performance indicators are assessed and a system integration strategy is developed in order to solve the issues emerged.

A P2G solution is adopted, consisting of the production of hydrogen from an electrolyzer in order to store in molecular form the fraction of solar production that causes issues to the electrical distribution grid. Furthermore, the produced hydrogen is injected directly in the gas distribution infrastructure, so that it is blended within the natural gas stream.

A solar overproduction curve may be produced whenever a deviation from normal operating condition occurs. This curve is an input to the electrolyzer model, which converts it into a hydrogen production rate that will be provided as additional input to the gas network model. Once a location for the electrolyzer is chosen, the gas network model is run and the effects of the variation of gas composition in time and in space are evaluated. Also for the gas case, the operating conditions of the infrastructure are checked. Fluid-dynamic indicators and its compliance with the normal operation limits are evaluated. Furthermore, the three main parameters for the evaluation of the gas quality are also considered. These parameters are the most common throughout all the European regulations and standards [157]. Table 16 summarizes the indicators considered for the evaluation of the gas network case, together with their operational limits referred to the Italian case [154].

Table 16 – Summary of the gas network constraints to be verified during simulations: fluid-dynamic operational limits for medium pressure distribution network and Italian national gas quality ranges according to [154].

Parameter	Units	Limits
Pressure	[bar_g]	$1.5 \div 5$
Gas Velocity	[m/s]	< 25
Higher Heating Value	[MJ/Sm^3]	$34.95 \div 45.28$
Relative Density	[-]	$0.55 \div 0.7$
Wobbe Index	[MJ/Sm^3]	$47.31 \div 52.31$

The sample urban area is built around the available data for an urban electric grid, coming from the *ATLANTIDE* project [158]. Starting from those data and through additional assumptions, the electrical scheme was shaped in a topographical form covering an area of 4.4×5 km^2. The spatial distribution of the users, together with the estimation of their gas consumption rates, allowed designing a possible gas network layout, consistent with the urban framework associated to the electrical case. A detailed explanation may be found in [159]. In the following sections, the main features of the two infrastructures as well as the related consumption localization and profiles are given.

5.2.1 Electrical infrastructure

The grid is operated at medium voltage (15 kV) and it consists of 96 nodes and 96 lines; however, one of the lines is kept open in order to operate the grid in radial mode. Figure 65 shows the schematization of the topology of the grid. As it is shown, the electrical infrastructure is composed of 11 feeders. All the lines are fully described in terms of linear resistance, capacitance, inductance, length and maximum current. Each node may be either a final user or a cluster of users. No distributed generation is present in the base case.
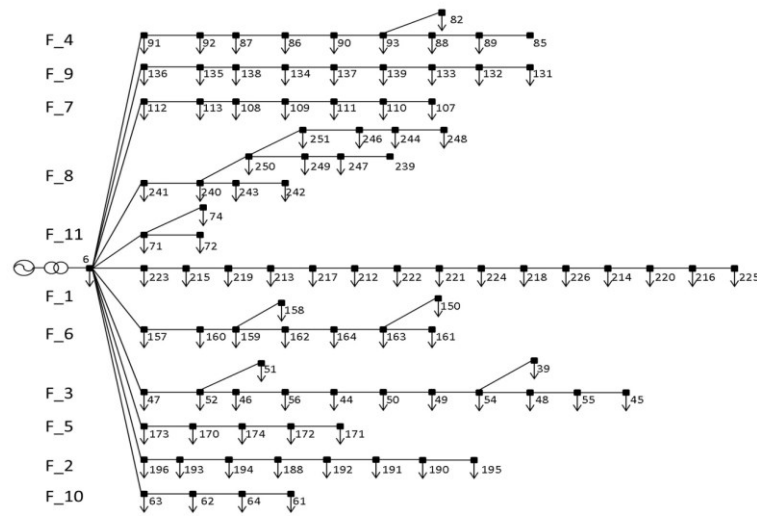
Figure 65 – Schematic topology of the urban distributed electric network.

5.2.2 Electrical user types, rated power and profile

Four categories of users are considered in this framework: residential, industrial, commercial and offices. The nodes along each feeder may be either industrial users directly connected to the medium voltage or MV/LV substations clustering the other types of users. For each of them, the total installed rated power for each category is known. A set of reference nominal powers for each users' counter was assumed in order to calculate the number of users for each category as well as to estimate the number of inhabitants. The total installed power (for consumption) is 25.6 MW_e and based on the assumptions made, the inhabitants are about 11,500. The pie charts of summarize the main electricity statistics of the area, in terms of the allocation of the installed power among the four categories of final users and their share over the total number of users (electric meters).
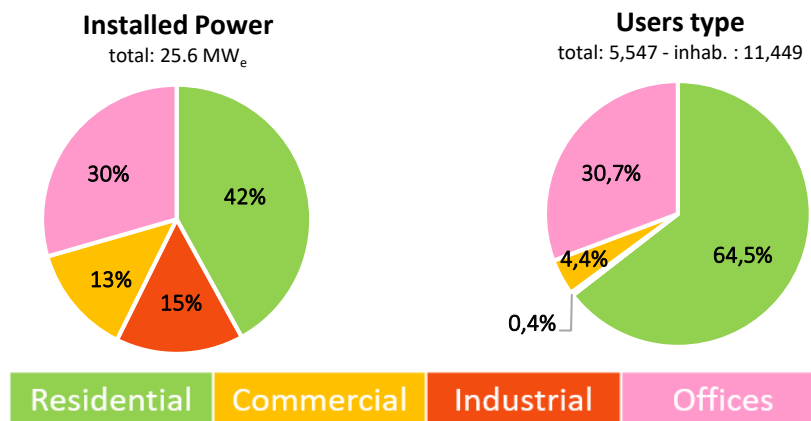
Figure 66 – Electricity statistics of the urban area according to users' type. Left: distribution of the installed nominal power; Right: users' type distribution.

Concerning the users' profiles, four load curves were available from [158], one for each category, with a time step of 15 min. Figure 67 shows the profiles expressed in per unit (p.u.) with respect to the installed power.
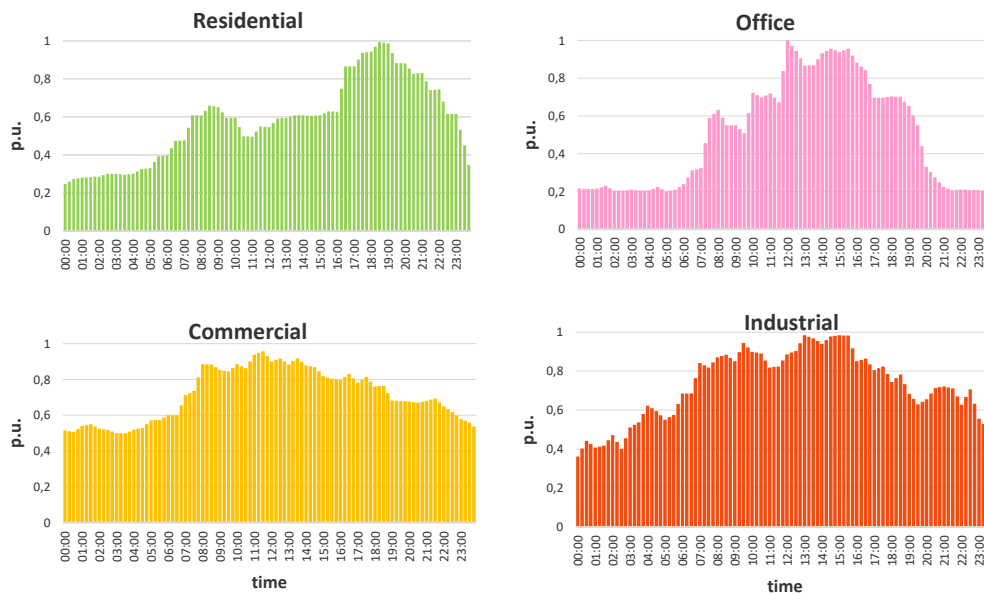
Figure 67 – Electricity consumption profiles for each user type.

As the last step towards the characterization of the sample urban area, a topographic shape of the scheme in Figure 68 is proposed by choosing a set of users' densities. In this way, a gas network may be designed accordingly, after having estimated the gas consumption of the scattered users. On the left side the topography of the urban area is shown, while on the right side the layout of the gas network is presented accordingly.
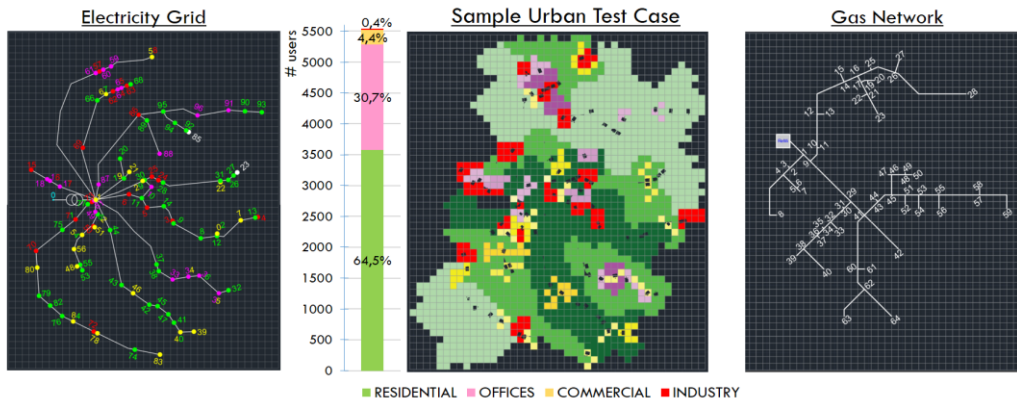
Figure 68 – Urban case electricity grid, topography and proposed gas network layout.

5.2.3 Natural gas infrastructure

The natural gas infrastructure was designed on purpose, starting from the available data and information from the electrical case. The complete methodology is described in [159]. Following the approach of the electrical case, the addressed gas network is the medium pressure one, operated at $p_{max} = 5\ bar_g$. It has a tree-shaped topology, consisting of 64 branches and 63 nodes, a fraction of which are consumption ones. Among them, 22 nodes consist of industrial users directly connected to the medium pressure network and 12 nodes are final reduction stations (FRSs), feeding non-industrial areas of consumption. As shown in Figure 68, the network starts from a single metering and reduction station (M/R station), also called city-gate, located outside the urban context limits, in which gas from transmission level is withdrawn. It is composed of a central feeder supplying five other sub-feeders to the FRSs or industrial users. All the pipe sections are described in terms of inner diameter, length and inner roughness.

5.2.4 Natural gas user types, rated power and profiles

Gas consumption data have also been estimated starting from the electrical case. As a fundamental assumption, it was decided that for each single electrical user, a gas meter is installed, so to have an equivalence between electrical and gas users, keeping the distinction among the four categories as in the previous case. For each users' category, the natural gas consumption estimation was carried out through semi-empirical methodologies [160], commonly used within the gas sector. Daily gas consumption per unit of building covered area (or covered volume) were available from handbooks [161] so the daily consumption was calculated assuming covered areas and volumes for each user category. The daily consumption of natural gas is the starting value both for the calculation of the maximum gas flow (useful to size the gas network) and for the gas consumption

profiling (in order to run the simulations). Detailed information may be found in [159]. Concerning natural gas uses for the industrial activities, the allocation of the consumption was carried out arbitrary on the basis of yearly data.

According to this methodology, a characterization of the area under natural gas consumption may be given: the total consumption of natural gas on yearly basis is about 100.3 MSm^3/y shared among the different users' types as depicted in Figure 69.
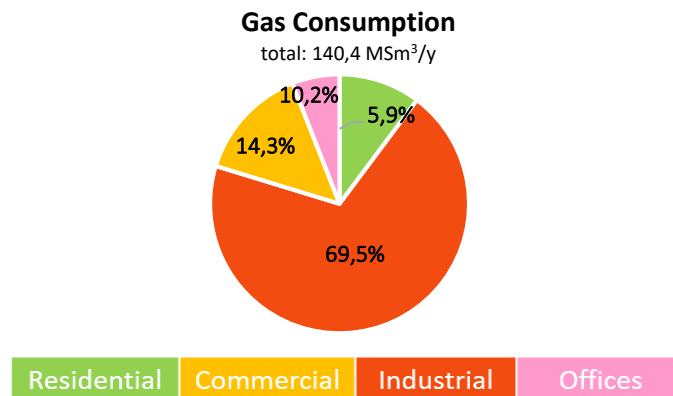
Figure 69 – Composition of the yearly gas consumption of the urban area according to the different user types.

To finalize the characterization of the area under the natural gas consumption point of view, the users' profiles need to be defined. Based on the four electrical load curves already presented and other available consumption patterns in [161] and [160], the profiles in Figure 70 are proposed as own elaboration. The time step is equal to 15 min, and the entries in the vertical axis are expressed as a percentage of the daily consumption.
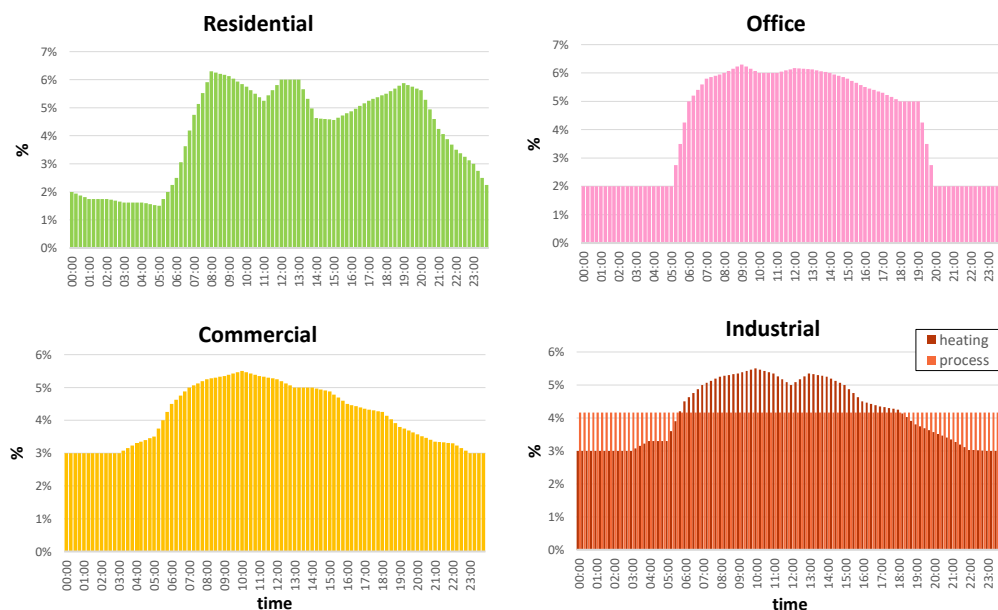
Figure 70 – Natural gas consumption profiles for each user type.

5.3   Electric network model

The electricity network can be represented by a directed graph, similarly to what has been described in section 2.3 referring to the gas networks. In the electrical case, the set of nodes represents the connection points between two or more electrical components, also called "bus", while the set of edges mainly represents the electricity lines connecting the nodes or an electrical transformer. For the sake of the addressed analysis, the edges will represent only the distribution lines of the network.

Differently than the gas network, the dynamic of the electricity networks is so fast that the power flow analysis are simulated by means of steady state equations, thus the temporal evolution of the system is obtained as a sequence of steady states.

It is also assumed that the AC three-phase distribution system is balanced and thus it can be modeled referring to its single-phase equivalent, referring to a single line (out of the three).

Electric lines are represented by the so called "π-line lumped-parameter model" as represented in Figure 71.
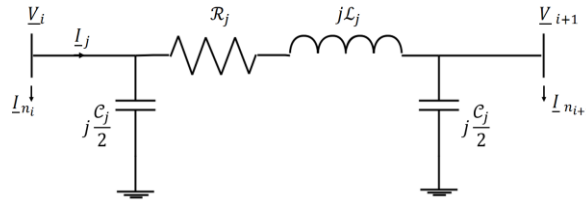
Figure 71 – Generic representation of the electric line according to the π-circuit lumped-parameter model.

The features of the conductors of a network such as line resistance $\mathcal{R}_j$, inductance $\mathcal{L}_j$ and capacitance $\mathcal{C}_j$, are usually given as distributed parameters (r_j, ℓ_j, c_j) with unit of measurements expressed in per unit length of the line. The lumped-parameter model consists of representing these features as if they were concentrated within the single elements of an ideal circuit (that has the shape of a π) where:

$$\mathcal{R}_j = r_j \cdot l \; ; \qquad \mathcal{L}_j = \ell_j \cdot l \; ; \qquad \mathcal{C}_j = c_j \cdot l \; ;$$

These lumped-parameters allow, in turn, determining the line impedance $\underline{Z}_j$, which allows expressing the generic line equation as follows:

$$\underline{\Delta V}_j = \underline{V}_i - \underline{V}_{i+1} = \underline{Z}_j \underline{I}_j \tag{5.1}$$

The nodes of the electrical network are the locations where the generators or the loads are located. As for the loads, different models may be applied depending on the type of load considered. They differ according to the control variable used to set the operating point. In fact, loads may be:

a) Power driven: the absorbed active power $\mathcal{P}$ and the reactive power $\mathcal{Q}$ are assigned;
b) Current driven: the magnitude of current I and the power factor $cos\varphi$ are assigned;
c) Impedance driven: the magnitude of $\mathcal{Z}$ and the power factor $cos\varphi$ are assigned;
d) Generic, with absorbed active power $\mathcal{P}$ and the reactive power $\mathcal{Q}$ given by the following relations:

$$\mathcal{P} = \mathcal{P}_n \left(\frac{V}{V_n}\right)^{\alpha} \qquad\qquad \mathcal{Q} = \mathcal{Q}_n \left(\frac{V}{V_n}\right)^{\beta}$$

This is the most generic way to describe the loads. In fact, according to the value of the exponent, all the previous cases may be obtained.

Generation buses are instead usually of two types:

a) $\mathcal{P}V$: where active power $\mathcal{P}$ and the voltage magnitude $|V|$ are given, while the reactive power $\mathcal{Q}$ and the voltage phase are calculated
b) $\mathcal{P}\mathcal{Q}$: similar to case a) of the load so that the generated active power $\mathcal{P}$ and the reactive power $\mathcal{Q}$ are assigned; to be noted that the active power $\mathcal{P}$ will have an opposite sign with respect to the case of $\mathcal{P}\mathcal{Q}$ loads.

The difference of the two generator types depends on whether the voltage control is present (or feasible) or not.

A convention of sign must be decided to indicate the direction of the power flows at the boundary nodes. The exchanged power towards a bus is positive in case of a load at the bus while it is negative in case of a generation bus. The sign of the current is determined accordingly.

When performing power flow simulation it is necessary to consider a third type of node, where the magnitude and the phase of the voltage are set (with phase equal to zero since it is the reference node) and the active power $\mathcal{P}$ and reactive power $\mathcal{Q}$ are calculated instead. In radial distribution networks, this node is often the exit node of the High-Voltage/Medium-Voltage transformer and so the bus which is connected to the higher voltage level of the network. This node is called "slack-bus" or reference node and it is the root of the tree-shaped topology of the network. The calculated values of power correspond to the total amount of active and reactive power consumed by the whole network.

Power flow simulations are aimed to determine the voltages at every node and the currents in every branch, thus making possible to evaluate the electrical power distributed throughout the network, to determine the line losses and to perform

checks on the operating constraints such as maximum acceptable losses, maximum line currents or nodal voltage levels.

In the field of power system analysis, it is common to perform power flow calculations referring the units of measurement of the electrical quantities to the per-unit system. This system consists of expressing all the quantities as fractions of a defined reference quantity (base unit). In case of power flow simulation, it is common to choose the rated power and the rated voltage of the slack node to generate the reference values for the impedances and for the currents and thus obtaining the reference base for the per unit system. All the electrical quantities related to the analysis of the distribution system will be expressed in reference to the chosen base, this including the computed results and the constraints set on the network.

For the case of tree-shaped (also defined as radial) network, in which no loops are present, a suitable method is the Backward/Forward Sweep (BFS) that is an iterative method. Iterations are needed because, in general, the equation at the buses may be not linear. In fact, when power driven buses are present, the nodal expression equation linking the nodal current and the nodal voltage is:

$$\underline{S}_i = \mathcal{P}_i + jQ_i = \underline{V}_i \, \underline{I}_{i_{ext}}^* \tag{5.2}$$

that is nonlinear. It can be underlined that most of the load buses in a distribution network infrastructure are modeled as power driven.

The BFS owes its name to the structure of each iteration, which is composed of a first computation step in which line currents are determined starting from the nodal equations and assuming a tentative initial value for the nodal voltages:

$$\underline{I}_{i_{ext}}^{(k)} = \left(\frac{\underline{S}_i}{\underline{V}_i^{(k)}} \right)^* \qquad \forall \; i^{th} \; bus \tag{5.3}$$

where $\underline{V}_i^{(k)}$ is the tentative value of the nodal voltage coming from the previous iteration or the initial guess $\underline{V}_i^{(0)}$.

This step is called "backward step" because calculations originates from the end nodes of the radial network and line currents are then computed moving backwards to the slack bus, where the total current is obtained, applying the Kirchhoff's current law (KCL):

$$\underline{I}^{(k)} = \mathbf{A^{mod}}^{-1} \, \underline{I}_{ext}^{(k)} \tag{5.4}$$

where $\mathbf{A^{mod}}$ is the modified version of incidence matrix as defined in section 2.3, in which the row corresponding to the slack node has been removed so to obtain, in case of tree shaped networks, a square matrix.

Once the line currents $\underline{I}^{(k)}$ are all known, the forward sweep is executed by using the line equation (5.1) in its matrix form in order to determine the voltage drops and then, moving forward form the slack node to the end buses, the nodal voltages are determined. The resulting equation may be written as follows:

$$\underline{V}^{(k+1)} = V_{slack}\,\mathbf{1} - \mathbf{A^{mod}}^{\mathbf{t}}\,diag(\underline{Z})\underline{I}^{(k)} \tag{5.5}$$

or, referring directly to the nodal currents vector $\underline{I}^{(k)}_{ext}$:

$$\underline{V}^{(k+1)} = V_{slack}\,\mathbf{1} - \mathbf{A^t}\,diag(\underline{Z})\mathbf{A}^{*-1}\,\underline{I}^{(k)}_{ext} \tag{5.6}$$

where $\mathbf{1}$ is a column vector with all unity components.

Of course, the computed voltages $\underline{V}^{(k+1)}$ are not coincident with the tentative initial value, thus based on the new nodal voltages vector, an updated line currents vector should be obtained, starting the Backward/Forwards procedure again, until convergence is reached.

This procedure can be merged within a single expression:

$$\underline{V}^{(k+1)} = V_{slack}\,\mathbf{1} - \mathbf{A^t}\,diag(\underline{Z})\mathbf{A}^{*-1}\left(\frac{\mathbf{S}}{\underline{V}^{(k)}}\right)^{*} \tag{5.7}$$

that is the iterative equation of the method.

The convergence criterion is set on the nodal voltages by means of this expression:

$$\max\left(\frac{\left|\underline{V}_i^{(k+1)} - \underline{V}_i^{(k)}\right|}{\left|\underline{V}_i^{(k)}\right|}\right) < toll \qquad \forall\, i^{th}\, node \tag{5.8}$$

Once the power flow of the network is solved, the line losses are calculated by means of this equation:

$$\mathcal{P}_{loss} = \mathcal{R}\,I^2 \tag{5.9}$$

The checks on the constraints is also performed verifying that nodal voltages and branch currents comply with the following conditions

$$0.95 \text{ p. u.} < \underline{V}_i < 1.05 \text{ p. u.} \qquad \forall \; timestep \; t \qquad (5.10)$$

$$\underline{I}_j < \underline{I}_{j_{max}} \; . \qquad \forall \; timestep \; t \qquad (5.11)$$

In the framework of an increasing penetration of energy form solar distributed sources, a further check is considered: active power flow at the slack node should not be positive (in accordance with the sign convention), meaning that the power should not be exported towards higher levels of electricity infrastructure.

$$\mathcal{P}_{slack} < 0 \qquad \forall \; timestep \; t \qquad (5.12)$$

These conditions should be tested for any time step.

5.4   Simulations and Results

5.4.1   Increasing of solar distributed generation

In order to study the effects of an increasing penetration of solar power plants on the electrical distribution system, a penetration rule must be decided. In this case study, the RES penetration is progressive, meaning that the installations are incremental. For each installation step, a 0.1 kW of photovoltaic output was installed at each residential and office type users. Thus, installations result evenly distributed throughout the nodes and linearly increasing. Figure 72 depicts the installation trajectory: on the vertical axis, the percentage of the total installed PV power over the total load is given while on the horizontal axis the percentage of PV energy production over the total energy consumption (on an annual basis) is presented. Each bullet represents the installed power of a single power plant, located at residential and office users (with a step of 0.5 kW).
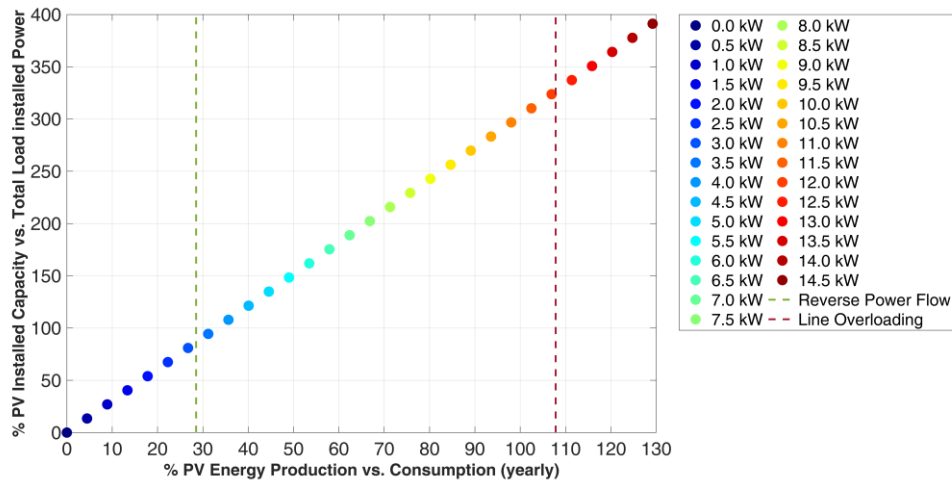
Figure 72 – RES penetration trajectory according to the distributed PV installation rule. Vertical-axis: percentage of the total installed PV power over the total installed load; Horizontal-axis: percentage of PV energy production over the total energy consumption (on an annual basis).

For each installation case, the electrical network is simulated over the whole year considering 12 representative days (one for each month). The performance indicators are checked for the whole time period and the results are reported in Figure 72 (dashed lines). As it can be noted, the thermal limit is exceeded for the first time in the case of 12.1 kW of solar power plant installed at each residential and office user, corresponding to a scenario of an annual solar energy production equal to 106.7% of the total energy consumption. More specifically, the saturation period lasts just for a single time step (15 min), taking place only in July and the saturated line is line 1 – the branch collecting all the feeders towards the HV/MV transformer. Conversely, the voltage at each node is always maintained within the operational limits. The reverse power flow condition occurs for the first time when the solar penetration corresponds to 27.6% (3.2 kW installed each users) of

total energy consumption. The first occurrence is recorded for one hour during the month of July, for a total energy surplus of 244 kWh with maximum surplus power of 344 kW. In order to observe reverse power flows all year round, the solar penetration must have reached 53.5%. (6.1 kW installed each users). In this case, occurrences range from 30 minutes for a typical day of December to 8 hours 15 minutes in July. In Figure 73, the evolution of the occurrence of the reverse flow condition is given as a function of months and of the penetration of solar energy on the total consumptions of the area. In this case reverse flow occurrences are evaluated in terms of percentage of hours in which the reverse flow takes place over the whole year (vertical-axis values).
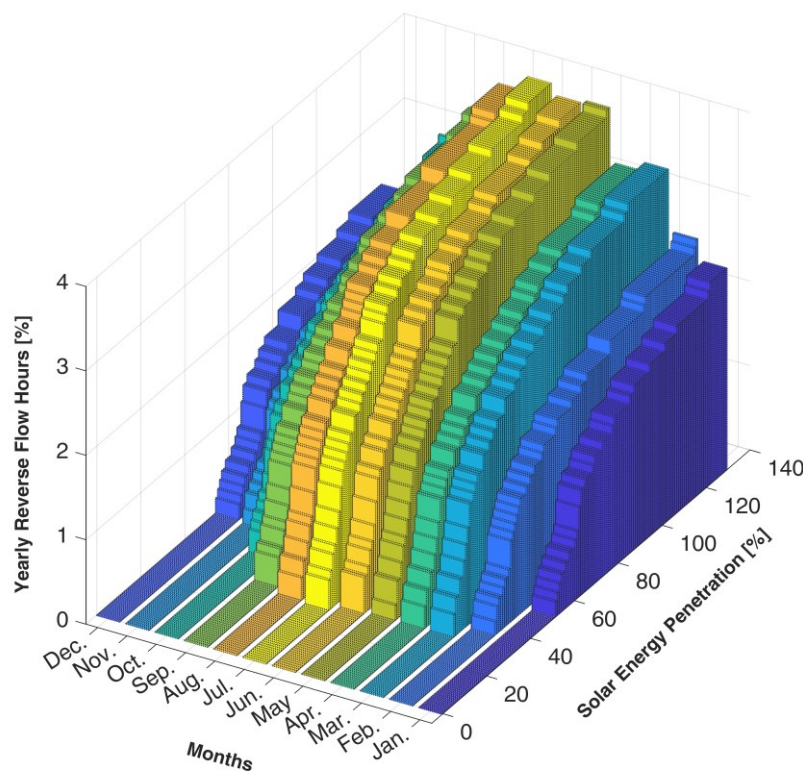
Figure 73 – Occurrences of the reverse flow condition is given as a function of months and of the penetration of solar energy over the total consumptions of the area. Reverse flow occurrences are evaluated in terms of percentage of hours in which the reverse flow takes place over the whole year (z-axis values).

5.4.2 Electricity and gas sector coupling

The electrical simulation above shows that the main deviation from the normal operating condition consists of the occurrence of reverse power flows, whose frequency and intensity increase as the solar energy contribution increases. Even though it is not as critical as a deviation of nodal voltages or the saturation of the lines, it implies, with respect to the higher voltage levels of the network, the

transformation of a passive hub to an active one, providing energy rather than consuming it. In order to avoid this situation, energy surplus may be stored locally. A strategy of sector coupling is here proposed by considering a power-to-gas solution based on electrolyzer, which produces hydrogen whenever a surplus of power is available from the grid. A power to hydrogen efficiency is assumed equal to 70%$_{HHV}$ as commonly reported in literature [148], [162]. The hydrogen production profile is then calculated accordingly. Solid lines in Figure 74 shows the hydrogen production patterns for three different stages of solar energy penetration (30% 40% 50%), both for the summer case (July) and for the winter case (February). In view of the injection of hydrogen within the natural gas stream it worth mentioning that the seasonality affects also the gas network, being the gas demand tightly related with the space heating needs. To consider this, the gas consumption profiles in the summer case have been reduced to the 15% of the winter case (with the exception of the process-related industrial gas consumption profile).
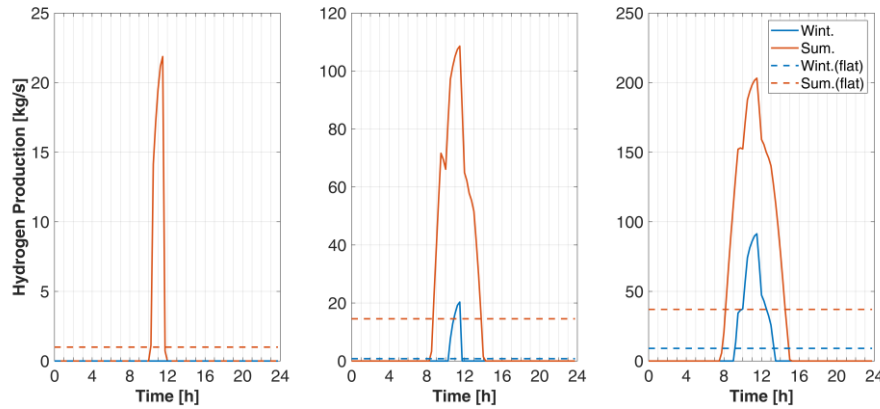
Figure 74 – Hydrogen production patterns for three different stages of solar energy penetration (30% 40% 50% from left to right). Orange lines: summer case (July); Blue lines: winter case (February). The dashed lines are the corresponding flat injection profiles

5.4.3 Hydrogen injection scenarios

A wide range of variability characterizes hydrogen injection scenarios depending on several parameters. In the framework of hydrogen blending within the gas network infrastructure, two additional terms of variation may be considered: 1) the "direct injection" versus the "flat injection"; 2) the choice of the injection node.

The first term considers the possibility to decouple the hydrogen production profiles with the injection ones by means of a suitable buffer system. Thus, for each of the five injection profiles in Figure 74 a corresponding "flat profile" over the whole day is generated (dashed lines). These profiles will be used to run the simulations of distributed injection on the network infrastructure in order to test the impact of this type of sector coupling. Concerning the choice of the injection node, all the hydrogen production profiles are tested on two different injection

nodes. In the first case, a median node (node 30) is chosen, following a proximity criterion between the HV/MV station and the gas network. In the second case, the hydrogen injection is assumed to be localized right after the gas city gate (node 2).

For each of the three stages of solar energy penetration, four injection profiles have been generated, considering the seasonal variation (summer or winter) and the injection mode (direct or flat). Additionally, these injection scenarios have been tested on two different injection nodes, thus generating a total of 24 hydrogen injection scenarios.

In this paragraph, the results of the fluid-dynamic simulations of the 24 hydrogen injection scenarios are reported and compared. Hydrogen injection within the gas infrastructure has an impact both on the fluid-dynamic of the gas flowing within the pipelines and on its composition and quality. Furthermore, dealing with network systems and distributed injections, the gas properties vary throughout the network and the magnitude of the introduced perturbation varies according to the injection point.

Fluid-dynamic results

For each injection scenario and for each modeled time step, both the gas velocity along each pipeline and the pressure level at each node have been compared with their operational limits in order to check the fluid-dynamic impacts of blending hydrogen within the natural gas.

Results show that gas velocity may become critical in a few branches during a few hours of the winter case, when the hydrogen injection rate is one of the highest. The critical cases refer to the highest solar penetration stage (50%) when considering the direct injection mode. However, they do not correspond to the highest injection rate, since the maximum amount of hydrogen is produced during the summer season. This means that the overcoming of the gas velocity limit is not only linked to the amount of hydrogen injected, but it has to deal with the gas consumption level and the network design too, as it will be clarified afterwards. Concerning pressure levels, no criticalities emerge.

Concerning the impact on the velocity field, the daily velocity profiles within branch 49 are given in Figure 75, since it results to be the most critical pipe. Each graph is referred to one of the two injection node scenarios. The profiles are given for all the cases of direct injection during different seasons. The cases regarding the flat injection have not been considered since they do not cause major variations.

Figure 75 helps to clarify the combined effect of hydrogen abundance and higher natural gas consumptions that leads to the exceeding gas velocity within branch 49. While gas velocity perturbation is smaller among the winter cases than the summer ones due to the smaller hydrogen production rate, in absolute terms, the winter gas velocity is sensibly higher because of the higher gas consumption.

Furthermore, by the comparison of the two injection-node cases of Figure 75, it can be noted that injecting hydrogen in node 30 (median node) has a higher impacts on the velocity than injecting at node 02 because the same amount of hydrogen is injected within a smaller amount of natural gas stream. This will also have an impact on gas quality perturbation, as it will be commented below.
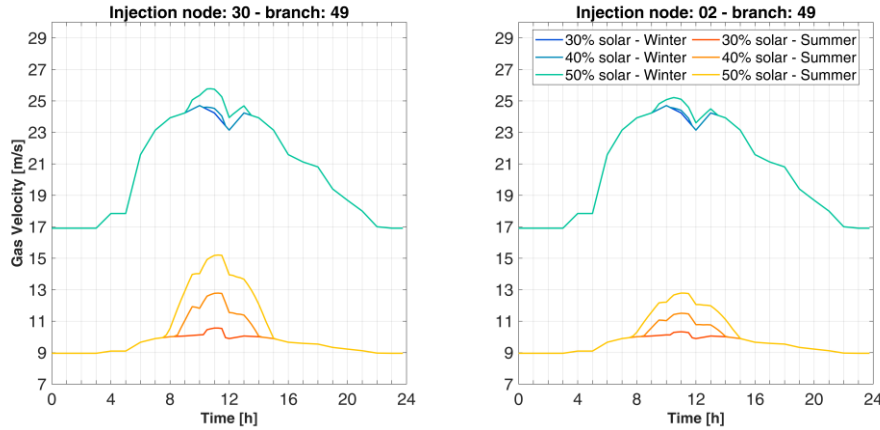
Figure 75 – Daily velocity profiles within branch 49. Left: injection node 30 – right injection node 02.

A quantification of the velocity perturbation induced by the distributed injection of hydrogen at different branches of the network and for the different seasons is given in Figure 76. The branch selection follows a continuous path form the city-gate to node 60, the farther node of the network (see the scheme in Figure 68).

The variation is calculated in relative terms with respect to the base case (gas network operated with no distributed injections). Data are referred to the time step characterized by the maximum hydrogen injection rate (t=11:30). All the three hydrogen injection profiles coming from the three stages of solar penetration are reported, as well as the related flat injection cases (bars in lighter color). To be noted that for the 30% solar penetration case, no hydrogen is produced during the winter months, so no perturbations are detected. It is also worth noting that scales are different between the upper part of the figure (winter cases) and the lower part (summer cases); thus, in the case of 50 % of solar penetration, the velocity increase downstream the injection nodes ranges between almost 4 % in the winter case to more than 50 % for the summer case. The highest perturbations occur for the summer cases and for median injection node (node 30). The same behavior is to be found for the flat injection cases, even though the perturbations are sensibly lower: from less than 1% to slightly more than 5%. As a final remark, Figure 76 also depicts a difference in the sign of the velocity variation. Gas velocities increase downstream the injection and decrease upstream the injection as a result of the substitution of an amount of natural gas with an unconventional fuel gas

(hydrogen) that has a smaller calorific value on a volume basis (HHV_{H2} = 12.07 MJ/Sm^3 ; HHV_{CH4} = 37.09 MJ/Sm^3).
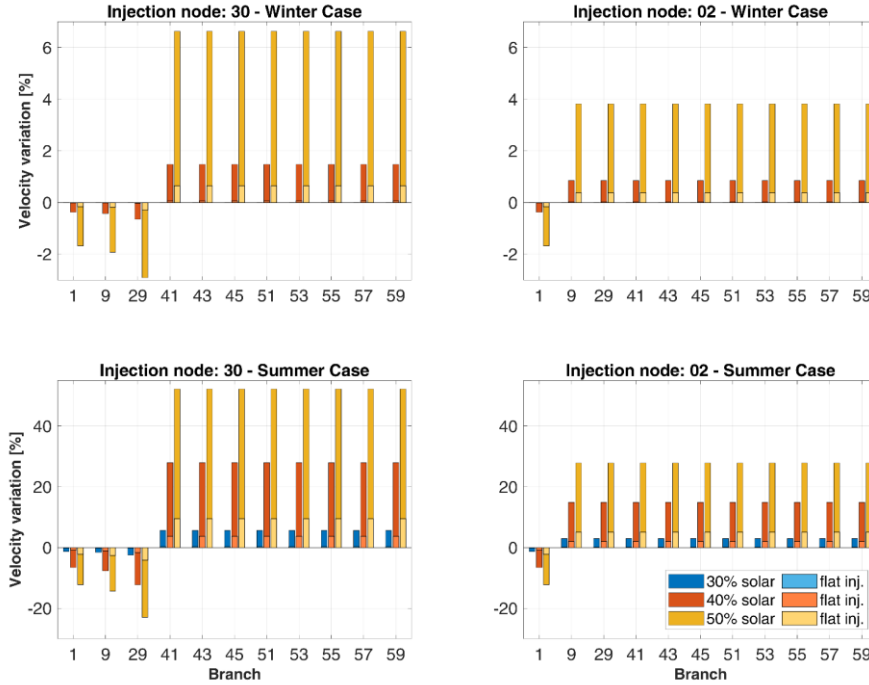
Figure 76 ─ Velocity perturbation induced by the distributed injection of hydrogen with respect to the no-injection case (base case) along the longest branch of the network. Left: injection node 30 – right injection node 02; upper part: winter cases, lower part: summer cases; lighter colors: flat injection cases.

The variation of volume gas flows has also an impact on the pressure drops along the pipelines. Figure 77 shows the pressure drops variation with respect to the base case along the same sequence of branches as in Figure 76 and referring to the same time. All the three hydrogen injection profiles coming from the three stages of solar penetration are reported, as well as the related flat injection cases (bars in lighter color). Pressure drops variations follow the same trends as the velocities ones. However, the impact on the pressure levels at each node is negligible, as it can be inferred from Figure 78, where the pressure profile along the selected sequence of branches is given.

Nodal pressures are given with respect to the distance from the starting node (city gate) so to picture the pressure profile as a function of the cumulative length. For each node-injection case, pressures profiles are given for the direct injection case for all the three stages of solar penetration, both for the winter and for the summer case. It is evident that pressure levels are negligibly affected for any of the addressed scenarios.
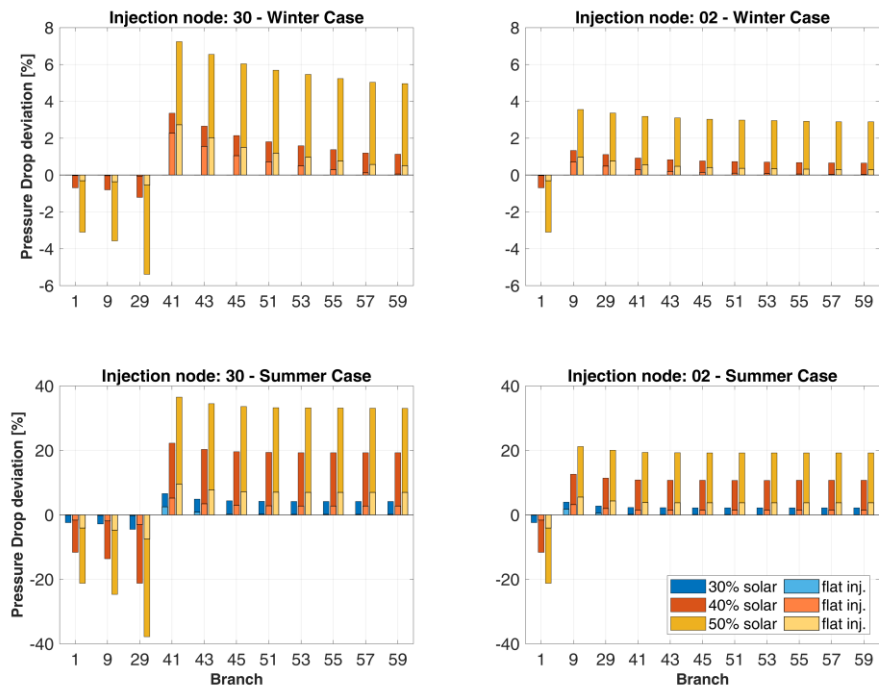
Figure 77 – Pressure perturbation induced by the distributed injection of hydrogen with respect to the no-injection case (base case) along the longest branch of the network. Left: injection node 30 – right injection node 02; upper part: winter cases, lower part: summer cases; lighter colors: flat injection cases.
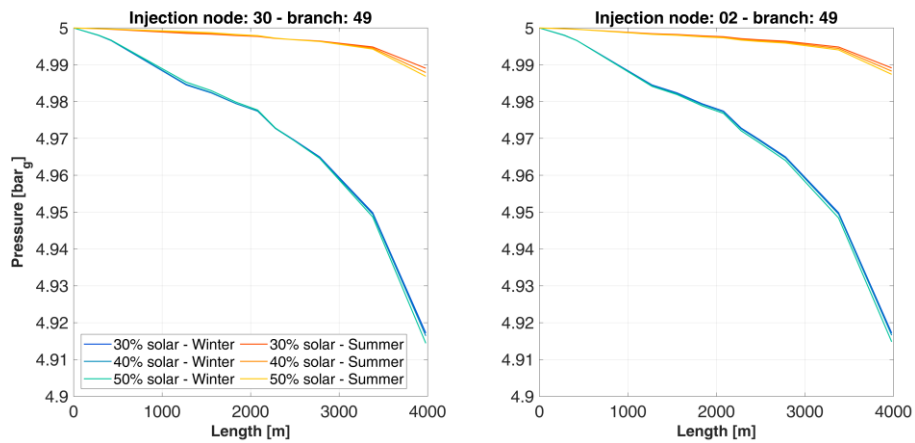
Figure 78 – Nodal pressure along the longest branch of the network. Left: injection node 30 – right injection node 02; blue curves: winter cases, orange curves: summer cases.

Gas quality results

The major impact of hydrogen injection practice within natural gas infrastructure is on gas quality parameters. The three main parameters, together with the hydrogen molar concentrations are presented in Figure 79 and Figure 80 for all the addressed case studies. Since each single case study is based on a dynamic simulation, the graphs display the variation of the quality parameters for the whole day and for all the injection cases related to a specific solar penetration stage. Figure 79 shows the direct injection cases while Figure 80 refers to flat injection ones. Orange curves refer to summer cases while the blue ones to the winter season. For each season, the injection cases at node 30 and at node 02 are given, thus resulting in four curves for each graph. Concerning the higher heating value, the relative density and the Wobbe index graphs, the higher and the lower limits of acceptability, as expressed in the Italian Standards system [154], are also depicted, delimiting the acceptability area (colored area).
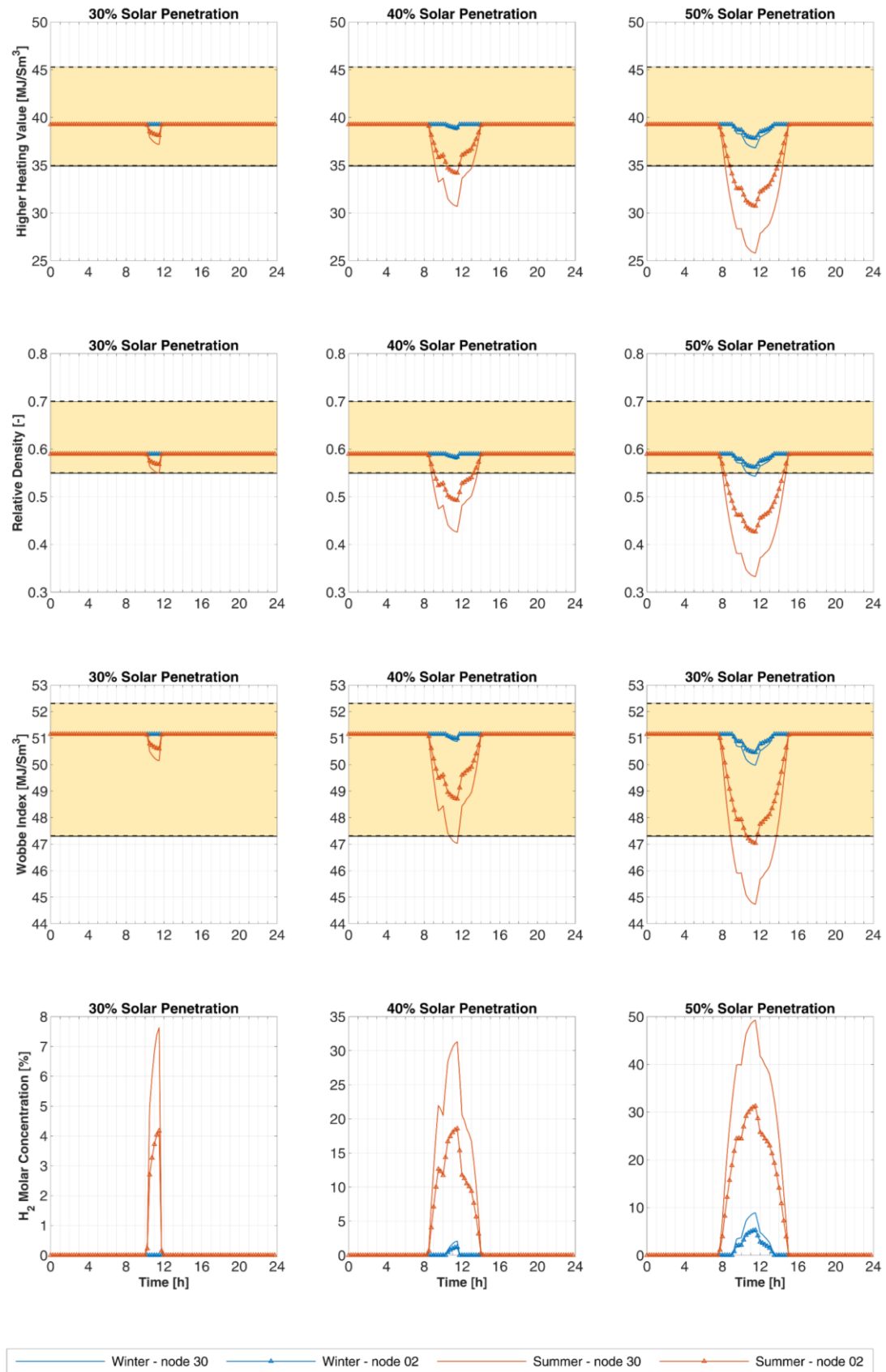
Figure 79 – Daily variation of gas quality parameters and hydrogen molar concentration for the complete set of injection scenarios, under the assumption of direct injection.
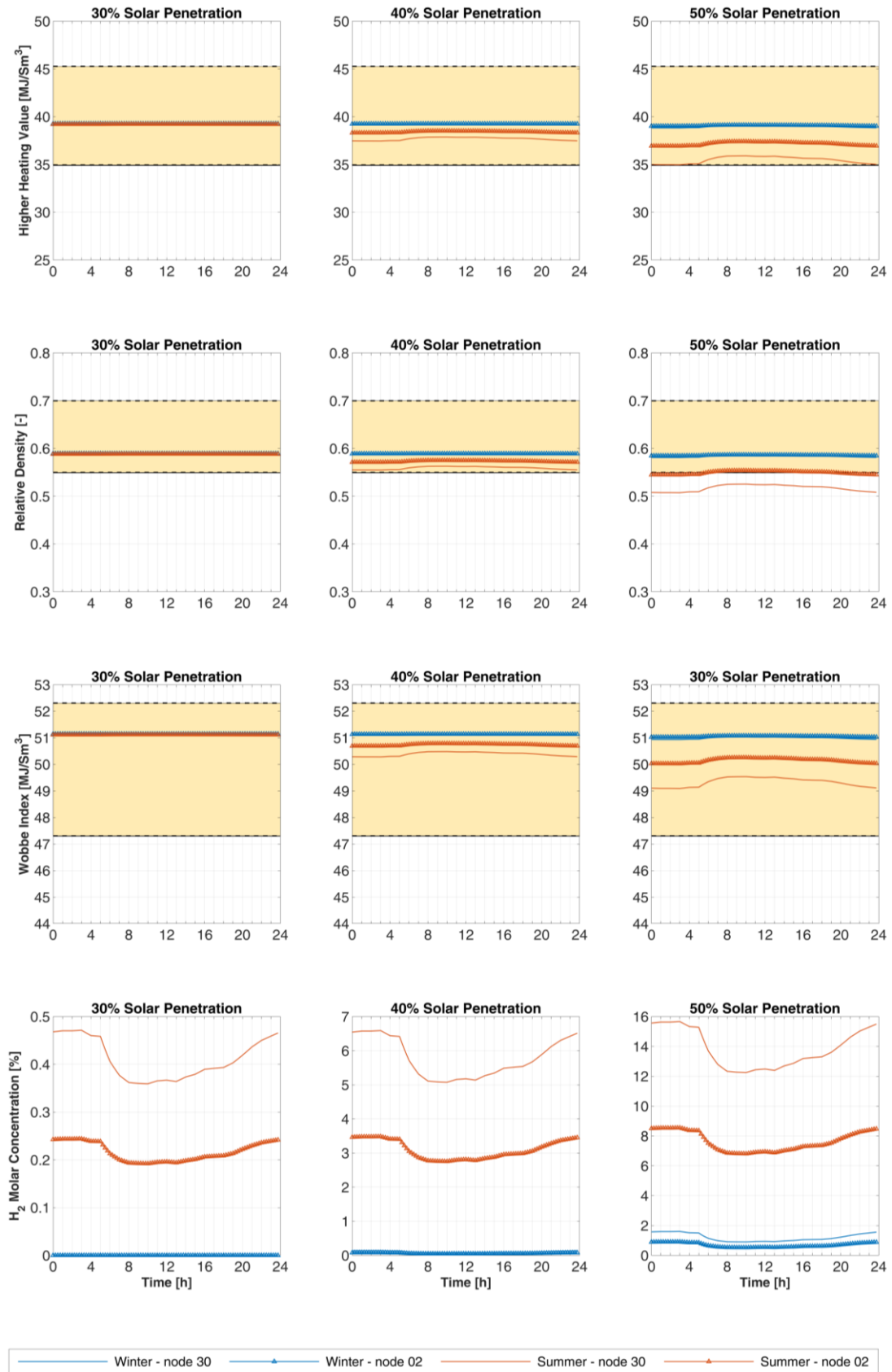
Figure 80 – Daily variation of gas quality parameters and hydrogen molar concentration for the complete set of injection scenarios, under the assumption of flat injection.

Concerning the graphs of the molar concentration of hydrogen, it is worth noting that vertical axis scale changes through the different solar penetration cases. As the magnitude of the hydrogen injection increases (both in term of timespan and in term of peak), the hydrogen presence within natural gas increases, ranging from 7.6% to 49.3% with reference to the maximum values. These maximum values of hydrogen concentrations are obtained for the summer cases and for the case of injection at node 30.

To reduce the peaks, injecting hydrogen at an upstream node (towards the city gate) is an effective solution. As it can be seen from the picture, the maximum hydrogen concentration is reduced to 4.2%, 18.6% and 31.2% for the three stages of solar penetration when moving the injection to node 02. Moving the injection node can thus lead to halve the hydrogen percentage peak. Similar reduction results are obtained also for the winter cases and for all the cases related to the flat injections.

Flat injection patterns are more effective, by even out the peaks and spreading the injection throughout the day. The achievements in the reduction of the hydrogen percentage peaks are considerably higher: the hydrogen concentration at the maximum injection time drops to 0.4%, 5.2% and 12.5% for injection at node 30 or to 0.2%, 2.8% and 6.9% for injection at node 02 (summer case), with the hydrogen composition decrease ranging from 20 times to 4 times.

It is worth noting that flat injections do not mean a flat concentration of hydrogen. In fact, it also depends on the withdrawal rate of natural gas from the city gate, in which a constant flux of hydrogen is to be blended, and so ultimately, it depends on the gas consumption profiles. Interestingly, in the framework of flat injections, the fluctuations of hydrogen concentration have an opposite behavior with respect to the direct injection case: hydrogen concentration is higher overnight when natural gas demand is lower. However, the variation is slow throughout the day and limited to ± 1.7%.

Concentration of hydrogen within the natural gas has a direct effect on the three gas quality parameters, as it is clear from the overall analysis of Figure 79 and Figure 80. Hydrogen blending has the effect of lowering down both relative density and higher heating value (volume based). Consequently, the Wobbe index undergoes a reduction too. As it can be observed, relative density is the most critical parameter, as the lower limit is reached already at 30% of solar penetration, in the summer case and for direct injection at node 30. In terms of hydrogen concentration, the lower limit is reached exceeding 6.7%. Nonetheless, even at the maximum concentration for this specific case (7.6%), the Relative Density of the blend is less than 1% lower than the limit. Moving to higher solar penetration stages, the perturbation on gas quality becomes more prominent, with all the three parameters exceeding the lower limit in the summer cases, with direct injection. Relative density is usually lower than the limits during the injection period, while higher heating value drops down to unacceptable level when the

hydrogen concentration becomes higher than 15.5%. The Wobbe index instead results as the less impacted parameters, with the lower limit reached only when hydrogen concentration exceeds 29%.

Of course, the hydrogen composition limits obtained from the previous discussion depend on the quality of the natural gas at the entry point. Heavier natural gas and/or natural gas having a higher calorific value can acceptably blend more hydrogen within their stream.

From Figure 79, it is also clear how critical the direct injection of hydrogen can be in terms of gas quality acceptability and management. When performing flat injections instead (see Figure 80), all the scenarios corresponding to 30% and 40% solar penetration are acceptable. Criticalities emerge just for the summer cases at 50% of solar penetration, both of them providing gas blends with relative density slightly lower than the lower limit, for the whole day. For injections at node 02 relative density is –1.8% of the lower limit and for injection at node 30 it is –8.5%.

5.5   Discussion

The results presented in the previous sections show that hydrogen injection practice have a minor impact on the fluid dynamics of the network, while it may be critical with respect to natural gas quality.

On a fluid-dynamic point of view, the substitution of a portion of natural gas with hydrogen, having a lower density and a lower calorific value on volume basis, implies an increase of volume flow rates through the pipeline downstream the injection. This have an impact on velocities, pressure drops and pressure levels at each node. For what concerns the case study here addressed, pressure levels are negligibly affected by all the injection scenarios even though pressure drops undergoes significant relative variation with respect to the non-injection base case. This aspect may become more significant on gas networks with greater geographical extension and complexity, since the impact of hydrogen injection on the pressure drops is not negligible and it is strictly related to the technical features of the pipelines. The consequent variation on pressure levels may become relevant in case of networks with higher pressure drops and areas with lower pressure levels already at the base case.

A similar discussion may be drawn concerning the velocity. Velocity variation is higher as the percentage of hydrogen within the gas network grows. However, the velocity limits are exceeded when hydrogen concentration is lower than the maximum possible one (within the case: 50% solar penetration), and consequently, the velocity relative deviation is smaller. It is evident that the base case condition of the gas network (on a fluid-dynamic point of view) has a fundamental role in the acceptability of hydrogen blending practice. To blend smaller amount of hydrogen within a network that operates at high level of saturation of pipeline flow capacity is more critical than blending higher amount of hydrogen within a network operating with lower saturation level. This consideration may be applied to cases of hydrogen blending at transmission system level too.

In the context of electricity and gas sector integration, the coupling of solar energy production and hydrogen production and injection from power-to-gas results in a positive match under a fluid-dynamic point of view of the gas network, with higher availability of hydrogen when gas networks are less utilized and vice versa.

However, the same cannot be concluded from the analysis of gas quality results. In fact, gas quality parameters are very sensitive to hydrogen concentration variation, with relative density exceeding the lower limit already when hydrogen molar concentration reaches 6.7%. Thus, under the gas quality point of view, the seasonality effect of hydrogen abundance and lower gas consumption brings to a negative superposition, with the gas network being challenged by the excess of renewable energy in the form of unacceptable amount

of renewable gas, according to the current regulatory framework. This is evident comparing the winter and the summer cases: critical concentration of hydrogen are reached already for the 30% solar penetration stage at the worst summer injection case (injection at node 30), while for the winter case the critical concentration is reached at the analogous case but for the 50% solar penetration stage. From an overall analysis of the results, it can be inferred that moving upstream the injection node has a slightly beneficial effect both on gas quality acceptability an on fluid-dynamic impacts. However, it is with the flat injection mode that most of the injection scenarios gain acceptability as it can be inferred from the comparison of the two acceptability matrices given in Table 17.

Table 17 – Hydrogen injection acceptability matrices: comparison between direct injection case and flat injection case, detailed for each gas parameter and the two possible injection nodes. Green: parameter within the regulatory limits; Red: parameter exceeding the regulatory limits; Limits set by [154].

Summer Case								
Direct injection profile					Flat injection profile			
Quality parameter	Solar penetration stage			Injection node	Quality parameter	Solar penetration stage			Injection node
	30%	40%	50%			30%	40%	50%	
HHV	🟩	🟥	🟥	30 / 02	HHV	🟩	🟩	🟩	30 / 02
RD	🟥 / 🟩	🟥	🟥	30 / 02	RD	🟩	🟩	🟥	30 / 02
WI	🟩	🟩 / 🟥	🟥	30 / 02	WI	🟩	🟩	🟩	30 / 02

It is worth adding that flat injections have the minimum impact on the fluid dynamics of the gas network. Flat injections are also crucial in minimize the gas quality fluctuations. In fact, the sharp variations of gas quality corresponding to the direct injection of hydrogen (following the solar overproduction) may be even less tolerable than the exceeding of one (or more) quality parameters, in terms of grid management and appliances functionality.

5.6   Conclusions

The case study presented here aimed at clarify the impacts of electricity-gas sector coupling by means of power-to-hydrogen and grid injection at urban level. A simulation algorithm able to model both the electricity and the gas network status was built for the purpose of testing the behavior of the infrastructures under different scenarios of renewable energy penetration and hydrogen injection cases. Specifically, a consequential simulation strategy was followed. Electricity network was first simulated so to test the impacts of increasing penetration of distributed solar production, to evaluate critical network status (namely: determination of the power surplus) and then to provide as output a set of hydrogen production profiles. These profiles were used to test the impact of distributed hydrogen blending on the local gas grid, under different cases.

Under the electrical point of view, results showed that the electricity network does not encounter operational criticalities in terms of nodal voltages deviations or line saturations. Nonetheless, mismatches between consumption and solar production lead to surplus energy production and consequent reverse power flows at the HV/MV station already at 28% of solar energy penetration (over the yearly consumption). The energy surplus grows in magnitude and becomes more frequent (both over the single typical day and over the year) as the solar energy penetration increase. This power surplus gave the motivation to the sector coupling strategy by means of local hydrogen production and its injection within the gas network infrastructure of the same urban area. This sector coupling could have a twofold benefit: on the one hand, it offers an energy storage option that contributes to increase the flexibility of the electrical system; on the other hand, it contributes to the decarbonization of the natural gas sector.

Several injection cases were analyzed in order to test the seasonality effect, the choice of the injection node and the injection pattern. Results showed that, in general terms, the injection of increasing amount of hydrogen has a strong impact within the gas network management, both under fluid-dynamic and gas quality point of view. This is mainly due to the fact that hydrogen has a considerably lower density and volumetric calorific value: the same energy output at the users is obtained with higher flow rates, implying higher velocities and pressure drops along the pipelines. On a fluid-dynamic point of view, when pipelines are operated near to the maximum flow capacity they may undergo exceeding velocity, even in case of smaller amount of hydrogen. These fluid-dynamic results imply that in view of the implementation of hydrogen blending practice, the fluid-dynamic verification should be carried out case by case on the existing networks.

In the context of sector coupling between solar overproduction and hydrogen injection, the seasonal effect insisting both on the electrical side and on the gas infrastructure has a positive superposition, with less hydrogen injection when natural gas is at its maximum utilization rate.

On the contrary, the seasonal effect has a detrimental effect on the impact of hydrogen injection on the gas quality. To be underlined that the choice of the injection node and the hydrogen injection pattern have a prominent role in the preservation of gas quality parameters within the limits. However, the hydrogen fraction within natural gas has different impacts on the different quality parameters. For instance, according to the case study presented here, while the maximum acceptable hydrogen concentration with respect to relative density is about 6.7%, according to the Wobbe index it goes up to 29.1%. Considering that throughout Europe, the regulation on gas quality is different, both in terms of limits and in terms of parameters, a revision of the gas quality parameters and their limits should be extensively addressed, taking into account all the interconnected elements of the natural gas sector (users' type, appliances, materials…). Thus, even though the gas quality undergoes major impacts anyways, with sharp variations in the cases of direct injection, an open discussion on gas quality and hydrogen-natural gas blends may move further the acceptability limits.

In conclusion, the results of this case study highlights that the integration of electricity and gas sector through power-to-hydrogen and hydrogen blending at local level is not straightforward. The impacts on the gas network are non-negligible and further studies on the acceptability of higher molar concentration of hydrogen within the natural gas as well as its possible sharp variations needs to be carefully addressed.

With this work, the potentialities of the consequential simulation algorithm for the electricity and gas sector coupling have been highlighted by means of a sample case study. However, the algorithm can easily be applied to real and more complex case studies, in order to evaluate different network topologies, different renewable penetration strategies and dynamics so to contribute to gain knowledge on the actual impacts of sector coupling.

Chapter 6

Conclusions

The fluid-dynamic network simulation tool for transient and multi-gas operations of the natural gas infrastructure has been applied to a number of case studies related to possible future scenarios of renewable gas distributed injections.

Among the many levels of the gas infrastructure, the local, lower pressure, distribution one has been addressed in order to contribute to the progress of the studies on renewable gases integration and on sector coupling on that area, which is not as much covered as the higher pressure transmission infrastructure, to the author's knowledge. The distribution level may gain more and more importance as the energy transition proceed further and more decentralized energy systems' schemes and business case will develop. In fact, a push towards this scenario is coming from the European Directives on Energy Communities [7,163]. What is more, most of the renewable energy sources have a distributed feature that, inevitably, may reflect on the way the energy infrastructures are operated and managed. Even though local energy infrastructures have the advantage to be widespread on the territory and thus proximate to plants; on the other hand, they may exhibit some specific criticalities and bottlenecks, related to their limited extension.

These issues become known very clearly when dealing with injection of biomethane within a network with limited capacity as performed in Chapter 3. The author had the chance to have a confirmation about the factual nature of these circumstances when visiting a real biomethane production and injection plant and during meetings with gas sector employee at the attended international conferences. The DSO's common concerns about the biomethane injection is how to manage a continuous production when consumption varies during the day and, most crucially, with the season. The case study presented is thus quite common

and it is, nowadays one of the main driver which leads the biomethane producers to avoid the distribution infrastructure nearer and at lower pressure (meaning lower compression costs), preferring the transmission one. In a sector that is geared towards rural areas, and featured with a considerable number of small-sized biogas producers scattered around the territory, this aspect may undermine a deep commitment towards the biomethane production and, as a consequence, it may shrink the estimated potential of biomethane contribution to the greening of the gas sector.

A thorough investigation on the critical occurrences of biomethane injection, employing advanced modelling tool which are not the traditional ones used to run nowadays networks helps to gain insights on possible countermeasures, possibly pushing forwards the current network limits or helping the definition of new technological solution. In fact, once verified the non-critical impacts on the fluid-dynamic behaviour of the network of distributed biomethane source, a scenario with modulating pressures has been set-up in order to assess the potential of the linepack storage. In fact, when running the gas distribution system during low consumption periods, lower pressure levels may still be accepted thanks to the reduced gas flows. Lowering the level of line pressure is beneficial in a biomethane injection scenario because it unlocks a certain amount of potential gas storage within the line, as it has been illustrated along the case study. Thus, knowing the balances between biomethane production and users' consumptions, it is possible to operate the network in a more dynamic way, thus optimizing the amount of the injectable biomethane. According to the addressed case, the 33% of linepack capacity were unlocked for each bar of decrease. This added capacity gave a time span of 3h18' before the network was saturated. Otherwise, by balancing the injection with the consumption trends generating an accumulation curve, it has been possible to define a partial curtailment of the biomethane injection, thus avoiding total curtailments. On aggregated terms, this innovative management of the distribution network tested with the gas network model allowed an increase of the biomethane injection allowance of +5.7 %, obtaining a final value of 89.9% of yearly injection factor.

On the other hand, similar management of the gas network would be possible if a strong digitalization of the metering systems is pursued accordingly.

In the framework of renewable gases, biomethane is of course much easier to integrate within the current system and, to some extent, it is already a reality thanks to the almost identical chemical nature as the fossil natural gas one.
A truly "multi-gas" system would instead be achieved if hydrogen is to be allowed within the pipes.

The cases of hydrogen injection and blending within the distribution infrastructure have been simulated and analyzed in Chapter 4 with a focus on the impacts on both fluid-dynamic and quality perturbations and in Chapter 5 setting

up a proper sample case for a combined simulation of an electrical and gas infrastructure simulation by means of power-to-gas.

If hydrogen production has to follow the renewable energy availability, to be granted with its renewable origin, a first remarkable difference with respect to the biomethane case has to be considered: the production curve is not as steady as the biomethane one; it has marked intraday variation and potentially significant difference throughout the year. This patterns are particularly true (and somehow regular) if the solar energy production is considered, as in the addressed cases.

In Chapter 4, a double injection of hydrogen has been presented in order to show the potentiality of the model in managing multiple injection points, with variable injection rate and injecting a gas that differs from the one within the pipes. Thus, the quality tracking features have also been highlighted.

The first stage of quality perturbation caused by hydrogen blending within the natural gas is reflected on the variation of the fluid-dynamic main quantities downstream the injection. Under the assumption that the energy transported or distributed through the pipe to the final user has to be kept constant, then, as the hydrogen molar fraction increases, the volume flow rates downstream the injection point increase as well. This has an effect of the calorific value of hydrogen that is about 3 times lower than the natural gas one on volumetric basis. Consequently, gas velocities downstream the injection points increase. A different situation is observed upstream the injection point where the natural gas flows are reduced as an effect of partial substitution by hydrogen. However due to the ratio between the calorific values, the substitution of natural gas by hydrogen is very slow and less than linear as it has been showed in the conclusion of Chapter 4. This is something is worth reminding especially when trying to assess the amount of greenhouse gas emissions avoided. In this context, the natural gas substitution potential of biomethane is, of course, higher, thanks to its very similar calorific value. What is more, the assumption of constant energy delivery is widely used throughout the literature but should be more precisely assessed and verified by an experimental based comparison, given that it is determined by the end-of-the-pipe appliances reaction to changing burning properties of fuel gas.

The case study also highlights the strong rate of variations that the gas quality undergoes throughout the day when hydrogen is injected. Besides the summertime case, in which a smaller portion of the network finds itself relying on 100% hydrogen thus undergoing a complete fuel switching, in the wintertime case as well the gas quality parameters undergo a significant variation which may be difficult to handle by the common (or older) households and industrial appliances. The aspect of hydrogen presence within the natural gas and its effect on existing connected appliances is being deeply addressed by most of the gas stakeholders with industrial based research. The case studies here addressed showed that form the final appliances point of view, not only is it a question of being able to efficiently burn gas-hydrogen blends, but also to be prepared to manage varying

concentrations at steep rates. Whether it is technically feasible or convenient is to be evaluated with wider techno-economic analysis. The output of this research, together with outputs from appliances-based investigation may be of use to the definition of an innovative gas quality regulation framework or gas burners design & control. It may be devoted to set constraints on the rate of variation of gas quality rather than setting quality limits or allow the definition of considerably different qualities areas through the different levels of the network (transmission vs distribution) or within the same infrastructure. Of course, this is a process within a process: the direction of regulatory framework evolution will depend on the evolution opportunities within the gas infrastructure itself.

A further term of variation is the geographical spreading of the gas quality. It has been highlighted by the modelling activities that the complex interconnections between pipelines that commonly compose a network may act as additional blending points, contributing to generate further different-qualities areas.

When injecting and blending hydrogen within a portion of the gas infrastructure (the distribution one) the choice of the injection location has an important role in the subsequent fluid-dynamic and quality impacts. From the opposite point of view, different locations throughout the network have different availability in receiving and blending hydrogen, provided that a quality constraint is given. This aspect has been tackled by applying the gas network model in a reverse way than the usual one, pre-defining a maximum hydrogen molar fraction an thus evaluating the amount of renewable power that is was possible to blend in form of hydrogen, according to the fluid-dynamic status of the network. Thus, not only have injection potential maps been obtained, but also acceptable renewable power injection profiles. This kind of evaluation is devoted to the assessment of the amount of flexibility a natural gas distribution network may provide in each of its point and at any of its operational timeframe. Once more, the seasonality of gas consumption strongly determines the availability of flexibility from the gas network side, unless gas storage facilities are to be planned.

A complete example of sector integration between power and gas is given at last in Chapter 5. A different sample urban area was considered, endowed with a medium voltage power distribution network too. The case study is specifically devoted to the analysis of potential synergies coming from the integration by means of power to gas technology in a scenario of increasing penetration of distributed solar energy. As the distributed photovoltaic plants grows in number and size throughout the area, the electricity network may get to unconventional operating point. For instance, mismatches between production and consumption may happen, ending with a local over production. It has thus been assumed to allocate this amount of energy on to the gas network in the form of hydrogen, and to evaluate the impacts under different injection scenarios.

The main message from this activity is that, once more, the direct coupling between the solar-based production and gas network is not so much promising:

the seasonality of both renewable production and gas consumption negatively interfere. Of course, if the daily amount of overproduced energy is to be stored and released throughout a wider timespan, then most of the criticalities on the gas network side are solved, with also a stabilization of the gas quality downstream the injection point.

The final considerations that may be drawn from all these sample case studies is that the gas network may indeed (and should) undertake a process of greening the gas with an evolutionary trajectory towards a multi-gas system. Figures or numbers out of the results of these few case studies (or additional similar ones) cannot be (yet) generalized into synthetic numbers to be spent on scenarios studies for future outlooks. On the other hand, the methodologies set up and applied may indeed be replicated easily on further cases, either real or built for the purpose. The gas network model may be also applied to transmission systems and complemented with non-pipeline elements such as compressors and reduction stations in order to widen the field of analysis and provide simulations for innovative management strategies which may highlight further potentialities ad opportunities and detecting criticalities to be tackled, either in a technical or in an institutional-regulatory base.

References

[1]   International Energy Agency. IEA Data and Statistics. IeaOrg 2020. https://www.iea.org/data-and-statistics?country=WORLD&fuel=Electricity and heat&indicator=Heat generation by source (accessed April 26, 2020).

[2]   Oxford Martin School, University of Oxford. Electricity Share by fuel source 1960-2015. OurworldindataOrg 2020. https://ourworldindata.org/grapher/world-electricity-by-source?country=European Union (accessed April 26, 2020).

[3]   BP. BP Statistical Review of World Energy, 68th edition 2019:1–69.

[4]   UNFCCC COP. Paris Agreement. COP Rep No21 2015.

[5]   Unruh GC. Understanding carbon lock-in. Energy Policy 2000;28:817–30. https://doi.org/10.1016/S0301-4215(00)00070-7.

[6]   Seto KC, Davis SJ, Mitchell RB, Stokes EC, Unruh G, Ürge-Vorsatz D. Carbon Lock-In: Types, Causes, and Policy Implications. Annu Rev Environ Resour 2016;41:425–52. https://doi.org/10.1146/annurev-environ-110615-085934.

[7]   The European Parliament and the Council of the European Union. Directive (EU) 2018/2001 of the European Parliament and of the Council on the promotion of the use of energy from renewable sources. Off J Eur Union 2018.

[8]   European Commission. Energy Roadmap 2050. vol. 2. 2012. https://doi.org/10.2833/10759.

[9]   Winkler J, Breitschopf B, Ragwitz M, Mistre M, Cail S, Harmelink M. Renewable energy directive target - Study for the ITRE Commitee. 2018.

[10]   Després J. Modélisation du développement à long terme du stockage de l'électricité dans le système énergétique global. Grenoble Alpes, 2015.

[11]   AEMO. Black System South Australia 28 September 2016. 2017.

[12]   Mancarella P, Puschel S, Zhang L, Wang H, Brear M, Jones T, et al. Power system security assessment of the future National Electricity Market. 2017.

[13]   OFGEM. Ofgem's Future Insights Series: The Decarbonisation of Heat. 2016.

[14]   KPMG. 2050 Energy Scenarios: The UK Gas Networks role in a 2050 whole energy system. 2016.

[15]   The heat is on. Nat Energy 2016;1:16193 https://doi.org/10.1038/nenergy.2016.193.

[16]   IEA. World Energy Outlook 2019. 2019.

[17]   ENTSOG. Ten-year network development plan 2018 executive summary. 2018.

[18]   EDSO. FLEXIBILITY IN THE ENERGY TRANSITION - A Toolbox for Electricity DSOs. 2018.

[19]   eurogas. FLEXIBILITY IN THE ENERGY TRANSITION - A Toolbox for Gas DSOs. 2018.

[20]   ENTSOG, ENTSO-E. TYNDP 2020 Scenario Report. 2020.

[21]   Pellegrino S, Lanzini A, Leone P. Greening the gas network – The need for modelling the distributed injection of alternative fuels. Renew Sustain Energy Rev 2017;70:266–86. https://doi.org/10.1016/j.rser.2016.11.243.

[22]   Rotunno P, Lanzini A, Leone P. Energy and economic analysis of a water scrubbing based biogas upgrading process for biomethane injection into the gas grid or use as transportation fuel. Renew Energy 2017;102:417–32. https://doi.org/10.1016/j.renene.2016.10.062.

[23]   Giglio E, Lanzini A, Santarelli M, Leone P. Synthetic natural gas via integrated high-temperature electrolysis and methanation: Part II—Economic analysis. J Energy Storage 2015;2:64–79. https://doi.org/10.1016/j.est.2015.06.004.

[24]   Ecofys. Gas for Climate: How gas can help to achieve the Paris Agreement target in an affordable way. 2018.

[25]   Pöyry. Fully decarbonising Europe's energy system by 2050 Decarbonising Europe's energy system. 2018.

[26]   ewi Energy Research & Scenarios gGmbH. The energy market in 2030 and 2050 – The contribution of gas and heat infrastructure to efficient carbon emission reductions. 2018.

[27]   Bothe D, Bongers T, Ahlert M, Kuhn J. The importance of the gas infrastructure for Germany's energy transition. 2018.

[28]   Speirs J, Balcombe P, Johnson E, Martin J, Brandon N, Hawkes A. A greener gas grid: what are the options? 2017.

[29]   Abbess J. Renewable Gas - The Transition to Low Carbon Energy Fuels. London: Palgrave Mamillan; 2015. https://doi.org/https://doi-org.ezproxy.biblio.polito.it/10.1057/9781137441805.

[30]   European Biogas Association. EBA Statistical Report 2019. Annu Rep 2019:68. https://doi.org/10.1139/e11-014.

[31]   Directorate-General For Energy and Transport. Mandate to CEN for standardisation in the field of gas qualities 2007.

[32]   Directorate-General for Energy. Mandate to CEN for Standards for Biomethane for Use in Transport and Injection in Natural Gas Pipelines 2010.

[33]   UNI/EN. UNI 16723:2016 2016.

[34]   UNI/TR. UNI/TR 11537:2016 2016.

[35]   GSE. Contatore DM 2 Marzo 2018 (biometano). GseIt 2020. https://www.gse.it/contatore-biometano (accessed April 26, 2020).

[36] GSE. Procedure applicative - DM 2 marzo 2018 (GSE). 2018.

[37] DVGW. DVGW-Arbeitsblatt G685, Gasabrechnung 2008.

[38] Quality G, Supports T, Gases R, Schley P, Hielscher A, Sc CFM, et al. Development of a new method for gas Quality Tracking 2018:1–15.

[39] Hydrogen on the rise. Nat Energy 2016;1:16127. https://doi.org/10.1038/nenergy.2016.127.

[40] Staffell I, Scamman D, Velazquez Abad A, Balcombe P, Dodds PE, Ekins P, et al. The role of hydrogen and fuel cells in the global energy system. Energy Environ Sci 2019;12:463–91. https://doi.org/10.1039/c8ee01157e.

[41] ENTSOG. Innovative Projects Platform. EntsogEu/Hydrogen n.d. https://www.entsog.eu/hydrogen?page=1 (accessed April 26, 2020).

[42] Mazza A, Bompard E, Chicco G. Applications of power to gas technologies in emerging electrical systems. Renew Sustain Energy Rev 2018;92:794–806. https://doi.org/10.1016/J.RSER.2018.04.072.

[43] Melaina MW, Antonia O, Penev M. Blending Hydrogen into Natural Gas Pipeline Networks : A Review of Key Issues. 2013.

[44] Altfeld K, Pinchbeck D. Admissible hydrogen concentrations in natural gas systems. Gas Energy 2013:1–12.

[45] The European Parliament and the Council of the European Union. Regulation (EU) 2016/426 of the European Parliament and of the Council on appliances burning gaseous fuels. Off J Eur Union 2016;L 81:99–145. https://doi.org/http://eur-lex.europa.eu/pri/en/oj/dat/2003/l_285/l_28520031101en00330037.pdf.

[46] UNI/EN. UNI EN 437:2019 - Test gases -Test pressures - Appliance categories 2019.

[47] UNI/EN. UNI EN 437:2009 2009.

[48] CEN/TC 234. Gases from non-conventional sources — Injection into natural gas grids — Requirements and reccomendations 2011:1–37.

[49] UNI/EN. UNI 16726:2018 2018.

[50]   Osiadacz A. Simulation of transient gas flows in networks. Int J Numer Methods Fluids 1984;4:13–24. https://doi.org/10.1002/fld.1650040103.

[51]   Fiebig Hielscher A. Span R. Gulin A. Rickelt S. Schley P. C. Gas Quality Tracking in Distribution Grids with SmartSim - Application in Complex and Meshed Grids. Int. Gas Union Res. Conf., 2014.

[52]   Abeysekera M, Wu J, Jenkins N, Rees M. Steady state analysis of gas networks with distributed injection of alternative gas. Appl Energy 2015;164:991–1002. https://doi.org/10.1016/j.apenergy.2015.05.099.

[53]   Guandalini G, Colbertaldo P, Campanari S. Dynamic Quality Tracking of Natural Gas and Hydrogen Mixture in a Portion of Natural Gas Grid. Energy Procedia 2015;75:1037–43. https://doi.org/10.1016/j.egypro.2015.07.376.

[54]   Guandalini G, Colbertaldo P, Campanari S. Dynamic modeling of natural gas quality within transport pipelines in presence of hydrogen injections. Appl Energy 2017;185:1712–23. https://doi.org/10.1016/J.APENERGY.2016.03.006.

[55]   Chaczykowski M, Zarodkiewicz P. Simulation of natural gas quality distribution for pipeline systems. Energy 2017;134:681–98. https://doi.org/10.1016/j.energy.2017.06.020.

[56]   Chaczykowski M, Sund F, Zarodkiewicz P, Hope SM. Gas composition tracking in transient pipeline flow. J Nat Gas Sci Eng 2018;55:321–30. https://doi.org/10.1016/j.jngse.2018.03.014.

[57]   Pambour KA, Sopgwi RT, Hodge BM, Brancucci C. The value of day-ahead coordination of power and natural gas network operations. Energies 2018;11:1–23. https://doi.org/10.3390/en11071628.

[58]   Clegg S, Mancarella P. Integrated Modeling and Assessment of the Operational Impact of Power-to-Gas (P2G) on Electrical and Gas Transmission Networks. IEEE Trans Sustain Energy 2015;6:1234–44. https://doi.org/10.1109/TSTE.2015.2424885.

[59]   Clegg S, Mancarella P. Storing renewables in the gas network: modelling of power-to-gas seasonal storage flexibility in low-carbon power systems. IET Gener Transm Distrib 2015;10:566–75. https://doi.org/10.1049/iet-gtd.2015.0439.

[60]   Langelandsvik LI. Modeling of natural gas transport and friction factor for large-scale pipelines. NTNU, 2008.

[61]   Abdolahi F, Mesbah A, Boozarjomehry RB, Svrcek WY. The effect of major parameters on simulation results of gas pipelines. Int J Mech Sci 2007;49:989–1000. https://doi.org/10.1016/j.ijmecsci.2006.12.001.

[62]   Prandtl L. The Mechanics of Viscous Fluids. vol. 3. 1935.

[63]   Nikuradse, J. Stromungsgesetze in rauhen Rohren [Laws of flow in rough pipes]. Ver Dtsch Ing Forschungsh 1933;361:1.

[64]   Colebrook CF. Turbulent Flow in Pipes, with particular reference to the Transistion Region between the Smooth and the Rough Pipe Laws. J Inst Civ Eng 1939;11:133–56. https://doi.org/10.1680/ijoti.1939.13150.

[65]   Hofer P. Beurteilung von Fehlern in Rohrnetzberechnungen (error evaluation in calculation of pipelines). GWF Gas/Erdgas 1973;114:113–9.

[66]   Langelandsvik LI, Postvoll W, Svendsen P, Overli JM, Ytrehus T. An Evaluation of the Friction Factor Formula Based On Operational Data. PSIG Annu Meet 2005:16.

[67]   Langelandsvik LI, Kunkel GJ, Smits AJ. Flow in a commercial steel pipe. J Fluid Mech 2008;595:323–39. https://doi.org/10.1017/S0022112007009305.

[68]   Cheng NS. Formulas for friction factor in transitional regimes. J Hydraul Eng 2008;134:1357–62. https://doi.org/10.1061/(ASCE)0733-9429(2008)134:9(1357).

[69]   Brkić D, Praks P. Unified friction formulation from laminar to fully rough turbulent flow. Appl Sci 2018;8:1–13. https://doi.org/10.3390/app8112036.

[70]   Modisette JL. Equation of State Tutorial. Proc. PSIG—The 32nd Annu. Meet. Savannach, Savannach: PSIG; 2000, p. 1–21. https://doi.org/10.1007/978-3-662-44185-5_1506.

[71]   Peng D-Y, Robinson DB. A New Two-Constant Equation of State. Ind Eng Chem Fundam 1976;15:59–64. https://doi.org/10.1021/i160057a011.

[72] Redlich O, Kwong JNS. On the Thermodynamics of Solutions. V. An Equation of State. Fugacities of Gaseous Solutions. Chem Rev 1949;44:233–44. https://doi.org/10.1021/cr60137a013.

[73] Soave G. Equilibrium constants from a modified Redlich-Kwong equation of state. Chem Eng Sci 1972;27:1197–203. https://doi.org/10.1016/0009-2509(72)80096-4.

[74] Mohamadi-Baghmolaei M, Azin R, Zarei Z, Osfouri S. Presenting decision tree for best mixing rules and Z-factor correlations and introducing novel correlation for binary mixtures. Petroleum 2016;2:289–95. https://doi.org/10.1016/j.petlm.2016.05.003.

[75] Jaeschke M, Audibert S, van Caneghem P, Humphreys AE. High accuracy compressibility factor calculation for natural gases and similar mixtures by use of a truncated virial equation. VDI-Verlag; 1989.

[76] Jaeschke. M, Humphreys AE. The GERG Databank of High Accuracy Compressibility Factor Measurements. 1990.

[77] ISO. ISO 12213-3:2006 - Natural Gas: Calculation of compression factor - Part 3: Calculation using physical properties 2006.

[78] Benedict M, Webb GB, Rubin LC. An empirical equation for thermodynamic properties of light hydrocarbons and their mixtures. J Chem Phys 1940;8:334–45. https://doi.org/10.1063/1.1750658.

[79] Benedict M, Webb GB, Rubin LC. An Empirical Equation for Thermodynamic Properties of Light Hydrocarbons and Their Mixtures II. Mixtures of Methane, Ethane, Propane, and n-Butane. J Chem Phys 1942;10:747–58. https://doi.org/10.1063/1.1723658.

[80] Starling KE. Fluid thermodynamic properties for light petroleum systems. Gulf Pub. Co; 1973.

[81] AGA. AGA 8 - Compressibility Factors of Natural Gas and Other Related Hydrocarbon Gases. AGA; 1992.

[82] ISO. ISO 20765-1:2005 - Natural Gas: Calculation of thermodynamic properties - Part 1: Gas phase properties for transmission and distribution applications 2005.

[83]   Chaczykowski M. Sensitivity of pipeline gas flow model to the selection of the equation of state. Chem Eng Res Des 2009;87:1596–603. https://doi.org/10.1016/j.cherd.2009.06.008.

[84]   Kunz O, Klimeck R, Wagner W, Jaeschke M. The GERG-2004 Wide-Range Equation of State for Natural Gases and other mixtures. VDI-Verlag; 2007.

[85]   Kunz O, Wagner W. The GERG-2008 wide-range equation of state for natural gases and other mixtures: An expansion of GERG-2004. J Chem Eng Data 2012;57:3032–91. https://doi.org/10.1021/je300655b.

[86]   ISO. ISO 20765-2:2015 - Natural gas: Calculation of thermodynamic properties - Part 2: Single-phase properties (gas, liquid, and dense fluid) for extended ranges of application 2015.

[87]   Uilhoorn FE. A comparison between PSRK and GERG-2004 equation of state for simulation of non-isothermal compressible natural gases mixed with hydrogen in pipelines. Arch Min Sci 2013;58:579–90. https://doi.org/10.2478/amsc-2013-0040.

[88]   Helgaker FJ. Modeling Transient Flow in Long Distance Offshore Natural Gas Pipelines. NTNU - Norwegian Uiversity of Science and Technology, 2013.

[89]   Helgaker JF, Oosterkamp A, Langelandsvik LI, Ytrehus T. Validation of 1D flow model for high pressure offshore natural gas pipelines. J Nat Gas Sci Eng 2014;16:44–56. https://doi.org/10.1016/j.jngse.2013.11.001.

[90]   Herrán-González A, De La Cruz JM, De Andrés-Toro B, Risco-Martín JL. Modeling and simulation of a gas distribution pipeline network. Appl Math Model 2009;33:1584–600. https://doi.org/10.1016/j.apm.2008.02.012.

[91]   Osiadacz AJ. Different Transient Flow Models - Limitations, Advantages, And Disadvantages. PSIG Annu Meet 1996:26.

[92]   Osiadacz AJ, Chaczykowski M. Comparison of isothermal and non-isothermal pipeline gas flow models. Chem Eng J 2001;81:41–51. https://doi.org/10.1016/S1385-8947(00)00194-7.

[93]   Menon ES. Gas Pipeline Hydraulics. CRC Press; 2005. https://doi.org/10.1201/9781420038224.

[94] Kiuchi T. An implicit method for transient gas flows in pipe networks. Int J Heat Fluid Flow 1994;15:378–83.

[95] Abbaspour A, Chapman KS. Nonisothermal Transient Flow in Natural Gas Pipeline. J Appl Mech 2008;75:1–8. https://doi.org/10.1115/1.2840046.

[96] Pambour KA, Bolado-Lavin R, Dijkema GPJ. An integrated transient model for simulating the operation of natural gas transport systems. J Nat Gas Sci Eng 2016;28:672–90. https://doi.org/10.1016/j.jngse.2015.11.036.

[97] van der Hoeven T. Math in Gas and the art of linearization. University of Groningen, 2004.

[98] Ferziger JH, Perić M. Computational Methods for Fluid Dynamics. 3rd ed. Springer, Berlin, Heidelberg; 2002. https://doi.org/10.1007/978-3-642-56026-2.

[99] Patankar S V., Spalding DB. A calculation procedure for heat, mass and momentum transfer in three-dimensional parabolic flows. Int J Heat Mass Transf 1972;15:1787–806. https://doi.org/10.1016/0017-9310(72)90054-3.

[100] Sciacovelli A, Verda V, Borchiellini R. Numerical Design of Thermal Systems. Turin: CLUT; 2013.

[101] Karki KC, Patankar S V. Pressure based calculation procedure for viscous flows at all speedsin arbitrary configurations. AIAA J 1989;27:1167–74. https://doi.org/10.2514/3.10242.

[102] Raithby GD, Schneider GE. Numerical solution of problems in incompressible fluid flow - Treatment of the velocity-pressure coupling. Numer Heat Transf 1979;2:417–40.

[103] Roberts RC. Molecular diffusion of Gases. In: McGraw-Hill, editor. Am. Inst. Phys. Handb., 1972.

[104] Ryan MJ, Mailloux RL. Methods for performing composition tracking for pipeline networks. Proc. 18th PSIG Annu. Meet., Pipeline Simulation Interest Group; 1986.

[105] Hager T, Bentaleb A, Wehrmann E. Simulation System with Calorific Value Tracking for Gas Distribution Grids With an Incomplete Measurement Infrastructure. Proc. XX IMEKO World Congr. Metrol. Green Growth, International Measurement Confederation; 2012.

[106] Helgaker JF, Müller B, Ytrehus T. Transient flow in natural gas pipelines using implicit finite difference schemes. J Offshore Mech Arct Eng 2014;136:1–11. https://doi.org/10.1115/1.4026848.

[107] Chorin AJ. Random Choice Solution of Hyperbolic Systems. J Comput Physcs 1976;22:517–33.

[108] Modisette JL. Lagrange - A pipeline flow model based on points moving with the fluid. Proc. 36th PSIG Annu. Meet., 2004, p. 1–5.

[109] Osiadacz AJ. Simulation and Analysis of Gas Networks. E. & F.N. SPON; 1987.

[110] Ke SL, Ti HC. Transient analysis of isothermal gas flow in pipeline network. Chem Eng J 2000;76:169–77. https://doi.org/10.1016/S1385-8947(99)00122-9.

[111] Behbahani-Nejad M, Bagheri A. The accuracy and efficiency of a MATLAB-Simulink library for transient flow simulation of gas pipelines and networks. J Pet Sci Eng 2010;70:256–65. https://doi.org/10.1016/j.petrol.2009.11.018.

[112] Wang H, Liu X, Zhou W. Transient flow simulation of municipal gas pipelines and networks using semi implicit finite volume method. Procedia Eng 2011;12:217–23. https://doi.org/10.1016/j.proeng.2011.05.034.

[113] Alamian R, Behbahani-Nejad M, Ghanbarzadeh A. A state space model for transient flow simulation in natural gas pipelines. J Nat Gas Sci Eng 2012;9:51–9. https://doi.org/10.1016/j.jngse.2012.05.013.

[114] SIMONE - Solution for simulation and optimisation in gas industry n.d.

[115] Pápay J. A termeléstechnológiai pararnéterek változása a gáztelepek müvelése során. OGIL Müsz Tud Közl 1968:267–73.

[116] Snam. Snam - Portale Misura. MisuraSnamIt n.d. https://misura.snam.it/portmis/coortecDocumentoController.do?menuSelect ed=4300.

[117] EBA 2018. Statistical Report of the European Biogas Association 2018. Brussels, Belgium: 2018.

[118] Scarlat N, Dallemand J-F, Fahl F. Biogas: Developments and perspectives in Europe. Renew Energy 2018;129:457–72. https://doi.org/10.1016/J.RENENE.2018.03.006.

[119] Italian Ministry of Economic Development. Decreto interministeriale 18 dicembre 2008 - Incentivi produzione energia 2008.

[120] GSE. Energia da Fonti Rinnovabii in Italia - Rapporto Statistico 2017. 2018.

[121] Eurostat. Renewable energy statistics 2019. https://ec.europa.eu/eurostat/statistics-explained/index.php/Renewable_energy_statistics.

[122] Daniela Thrän EB, Tobias Persson, Mattias Svensson , Jaqueline Daniel-Gromke, Jens Ponitka MS, Baldwin J. Biomethane Status and Factors Affecting Market Development and Trade. 2014.

[123] Graf F, Ortloff F, Kolb T. Lessons learned in Germany. Proc. 26th World Gas Conf., vol. 16, 2015, p. 142–5. https://doi.org/10.15252/embr.201440011.

[124] DVGW. DVGW G 265-2:2012-01 - Anlagen für die Aufbereitung und Einspeisung von Biogas in Erdgasnetze - Teil 2: Fermentativ erzeugte Gase - Betrieb und Instandhaltung 2012.

[125] Anigas, Assogas, Utilitalia. Immissione diretta di biometano in rete. 2016.

[126] Energinet. System Plan 2018 - Electricity and gas in Denmark. 2018.

[127] Agency Danish Environmental Protection. Decision to establish biogas pipeline between St. Andst and Pottehuse and a compressor station at St. Andst: EIA is not required (in Danish) 2017. https://mst.dk/service/annoncering/annoncearkiv/2017/maj/vvm-screening-biogasledning-ml-st-andst-og-pottehuse/ (accessed April 14, 2020).

[128] Cavana M, Leone P. Towards Renewable Gases Distribution Networks: the Importance of a Transient and Multi-component Fluid-dynamic Gas Model 2019. https://doi.org/10.5071/27theubce2019-5bo.4.5.

[129] ARERA. 229/2012/R/GAS - Testo integrato delle disposizioni dell'Autorità per l'energia elettrica e il gas in ordine alla regolazione delle partite fisiche ed economiche del servizio di bilanciamento del gas naturale (Settlement) 2012:1–17.

[130] CIG. UNI 9165:2004 - Gas distribution networks. Pipeworks with maximum operating pressure up to 5 bar 2004.

[131] European Parliament and the council of the European Union. Directive 2004/22/EC of the European Parliament and of the Council of 31 March 2004 on measuring instruments. Off J Eur Union 2004;2003:1–80. https://doi.org/10.1016/j.amjmed.2009.09.004.

[132] The Green Village. WATERSTOFSTRAAT - Hydrogen Street: Natural gas grid for transporting hydrogen 2020. https://www.thegreenvillage.org/projects/waterstofstraat (accessed April 26, 2020).

[133] Stedin. Power2Gas - Waterstof in Rozenburg. StedinCom 2020. https://www.stedin.net/over-stedin/duurzaamheid-en-innovaties/een-nieuw-energiesysteem/power2gas.

[134] Kiwa, Stedin. Dutch village Stad aan 't Haringvliet can switch to green hydrogen. KiwaCom 2020. https://www.kiwa.com/en/media/news/2019/study-by-kiwa-and-stedin-dutch-village-stad-aan-t-haringvliet-can-switch-to-green-hydrogen/.

[135] Kiwa, Netbeheer Nederland. Toekomstbestendige gasdistributienetten. 2018.

[136] Sterling T. Dutch government to halt gas production at Groningen by 2030. ReutersCom 2018. https://www.reuters.com/article/netherlands-groningen-gas/dutch-government-to-halt-gas-production-at-groningen-by-2030-idUSA5N1O601N (accessed April 26, 2020).

[137] Northen Gas Networks, DNV-GL. H21 project. H21 n.d. https://www.h21.green/ (accessed April 26, 2020).

[138] Sadler D, Cargill A, Crowther M, Rennie A, Watt J, Burton S, et al. H21 Leeds City Gate Report 2016:1–382.

[139] Hydrogeneurope. WindGas Falkenhagen. HydrogeneuropeEu n.d. https://hydrogeneurope.eu/project/windgas-falkenhagen.

[140] Horizon 2020 project. Store&Go n.d. https://www.storeandgo.info/.

[141] GRTgas. Jupiter1000. Jupiter1000Eu n.d. https://www.jupiter1000.eu/english.

[142] E.ON. Hydrogen levels in German gas distribution system to be raised to 20 percent for the first time. EonCom 2019. https://www.eon.com/en/about-us/media/press-release/2019/hydrogen-levels-in-german-gas-distribution-system-to-be-raised-to-20-percent-for-the-first-time.html.

[143] Isaac T. HyDeploy: The UK's First Hydrogen Blending Deployment Project. Clean Energy 2019;3:114–25. https://doi.org/10.1093/ce/zkz006.

[144] Bruun J, Graf T, Iskov H, Koch B. Energy Storage – Hydrogen Injected into the Gas Grid via Electrolysis Field Test. Int. Gas Union Res. Conf. 2014, Copenhagen: 2014.

[145] Lanzi D, Clavenna A, Crespi M, Rozzi E, Leone P, Lanzini A. Impact of natural gas-hydrogen blend on the emission of atmospheric pollutants from an industrial pre-heating burner. Int. Gas Union Res. Conf. 2020, vol. 2020, Muscat: n.d., p. 1–9.

[146] de Vries H, Mokhov A V., Levinsky HB. The impact of natural gas/hydrogen mixtures on the performance of end-use equipment: Interchangeability analysis for domestic appliances. Appl Energy 2017;208:1007–19. https://doi.org/10.1016/j.apenergy.2017.09.049.

[147] Marcogaz. Overview of Available Test Results and Regulatory Limits for Hydrogen Admission into Existing Natural Gas Infrastructure and End Use. 2019.

[148] Ferrero D, Gamba M, Lanzini A, Santarelli M. Power-to-Gas Hydrogen: Techno-economic Assessment of Processes towards a Multi-purpose Energy Carrier. Energy Procedia, vol. 101, 2016, p. 50–7. https://doi.org/10.1016/j.egypro.2016.11.007.

[149] Holladay JD, Hu J, King DL, Wang Y. An overview of hydrogen production technologies. Catal Today 2009;139:244–60. https://doi.org/10.1016/j.cattod.2008.08.039.

[150] Mazza A, Bompard E, Chicco G. Applications of power to gas technologies in emerging electrical systems. Renew Sustain Energy Rev 2018;92:794–806. https://doi.org/10.1016/j.rser.2018.04.072.

[151] Sterner M. Bioenergy and renewable power methane in integrated 100% renewable energy systems. kassel university, 2009.

[152] Gahleitner G. Hydrogen from renewable electricity: An international review of power-to-gas pilot plants for stationary applications. Int J Hydrogen Energy 2013;38:2039–61. https://doi.org/10.1016/j.ijhydene.2012.12.010.

[153] JRC. PVGIS. Eu Sci Hub n.d. https://ec.europa.eu/jrc/en/pvgis.

[154] Italian Ministry of the Interior. D.M. 18/05/2018 - Regola tecnica sulle caratteristiche chimico fisiche e sulla presenza di altri componenti nel gas combustibile 2018.

[155] Cavana M, Lanzini A, Leone P. Hydrogen blending into the gas distribution grid: the case study of a small municipality 2018:11–9.

[156] JRC. PV-GIS n.d. http://re.jrc.ec.europa.eu/pvgis/.

[157] Marcogaz, eurogas, GERG. Gas Bridges : the natural gas network as key partner of the energy transition. 2017.

[158] Pilo F, Pisano G, Scalari S, Dal Canto D, Testa A, Langella R, et al. ATLANTIDE - Digital archive of the Italian electric distribution reference networks. CIRED 2012 Work. Integr. Renewables into Distrib. Grid, IET; 2012, p. 165–165. https://doi.org/10.1049/cp.2012.0783.

[159] Mazza A, Cavana M, Mercado Medina EL, Chicco G, Leone P. Creation of Representative Gas Distribution Networks for Multi-vector Energy System Studies. 2019 IEEE Int Conf Environ Electr Eng 2019 IEEE Ind Commer Power Syst Eur (EEEIC / I&CPS Eur 2019:1–6. https://doi.org/10.1109/EEEIC.2019.8783701.

[160] Sabatini F. Criteri di progettazione di reti ed impianti per la distribuzione del gas naturale. Edizioni Consiag; 1990.

[161] Tarenzi V, Cerè A, Caimo F. Calcolo del regime stazionario di una rete di trasporto e di distribuzione del gas (bassa, media ed alta pressione). open source; 2015.

[162] Schmidt O, Gambhir A, Staffell I, Hawkes A, Nelson J, Few S. Future cost and performance of water electrolysis: An expert elicitation study. Int J Hydrogen Energy 2017;42:30470–92. https://doi.org/10.1016/j.ijhydene.2017.10.045.

[163] European Parliament, Council of the EU. Directive (EU) 2019/944 on Common Rules for the Internal Market for Electricity and Amending Directive 2012/27/EU. Off J Eur Union 2019:18. https://doi.org/http://eur-lex.europa.eu/pri/en/oj/dat/2003/l_285/l_28520031101en00330037.pdf.

List of Publications

Peer-Reviewed Journal Papers

2019 **Biogas blending into the gas grid of a small municipality for the decarbonization of the heating sector.**

Marco Cavana, Pierluigi Leone

in: Biomass & Bioenergy (August 2019) - ISSN: 0961-9534

Conference Papers

2019 **Assessment of the Hydrogen Receiving Potential of a Distribution Gas Network using a Multi-Component and Transient Gas Network Model**

Marco Cavana, Pierluigi Leone

in: Proceedings of the European Fuel Cell Conf. and Exhib. - ISBN 978-88-8286-386-9

2019	**Creation of Representative Gas Distribution Networks for Multi-vector Energy System Studies** A. Mazza, M. Cavana, E. L. Mercado Medina, G. Chicco, P. Leone in: Proceedings of the Int. Conf. on Environment and Electrical Engineering Organization: IEEE doi.org/10.1109/EEEIC.2019.8783701
2019	**Towards Renewable Gases Distribution Networks: The Importance of a Transient and Multi-Component Fluid-Dynamic Gas Model** Marco Cavana, Pierluigi Leone in: 27th European Biomass Conference and Exhibition Proceedings - ISSN 2282-5819 Organization : ETA-Florence Renewable Energies doi.org/10.5071/27thEUBCE2019-5BO.4.5
2017	**Hydrogen Blending into the Gas Distribution Grid: The Case Study of a Small Municipality** Marco Cavana, Andrea Lanzini, Pierluigi Leone in: Proceedings of 6th European PEFC & Electrolyser Forum - ISBN 978-3-905592-21-4 Organization : EFCF - European Fuel Cell Forum 2017 www.efcf.com/index.php?id=2675

Others

2018 on line blog (in Italian)	**Gas Italia 2044: 100 candeline a gas rinnovabile** Pierluigi Leone, Marco Cavana, Chiara Delmastro, Romano Borchiellini. in: Rienergia (n°85) - ISSN 2531-7172 Organization : Rie-Ricerche Industriali ed Energetiche, Staffetta Quotidiana. rienergia.staffettaonline.com/sommario/407/

Awards

2019   Selected finalist at 9th GERG Young Researcher Award
            at: EGATEC 2019: European Gas Technology Conference by
            Marcogaz and GERG (Groningen – NL)

2018   PhD Day Poster Award 2018
            at: Energetics PhD Day of PoliTo (Turin)

2017   8th GERG Young Researcher Award for Best 3-min speech
            at: Annual Eurogas Conference 2017 (Brussels)
            Selected on the basis of an abstract among the six finalists
            and voted as the best presenter of a 3-min pitch.

2017   Best Poster Award
            at: EUBCE 2017: 25th European Biomass Conference and
            Exhibition (Stockholm)
            Selected among 71 posters within the same subject.